Fluorescent cannabinoids: Strategies towards the synthesis of fluorescently labelled CB_2 receptor ligands

Andrew Stephen Yates
BPharm MRPharmS AMRSC

School of Pharmacy, The University of Nottingham
Nottingham
UK

Thesis submitted to the University of Nottingham for the degree of Doctor of Philosophy

November 2004

“A chemist dabbling in his lab
Felt his project was a little drab

So embarked to discover fluorescent weed
Citing a greater scientific need

Soon had friends with glowing lips
Funded his life on their grateful tips

Checked his spectra, in disbelief
When his friends got no relief

He made an error in his reaction
That gave his friends no satisfaction

In desperation he hid away
Improving his creation day by day

His project done, his girlfriend’s plea
Was to write it up as a PhD

This is what I submit to you
To read, to marvel, to hold as true”

- A. S. Yates

Table of contents

Index of fluorescent ligands

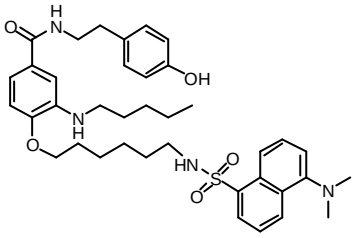

I.D name -Dansyl-JTE2-6 **99**
Design and synthesis - Chapter 2 page 67
Chemistry – Section 2.3 page 84
Pharmacology – Section 2.4 page 90
Chemical analysis Chapter 8 page 194

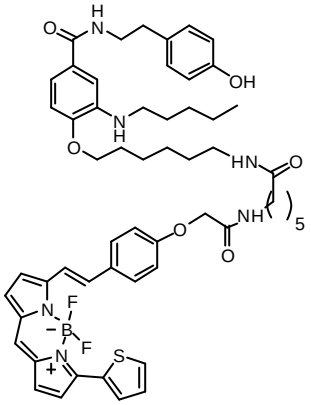

I.D name -Bodipy-JTE2-6 **100**
Design and synthesis - Chapter 2 page 67
Chemistry – Section 2.3 page 84
Pharmacology – Section 2.4 page 90 & section 5.3 page144
Chemical analysis Chapter 8 page 195

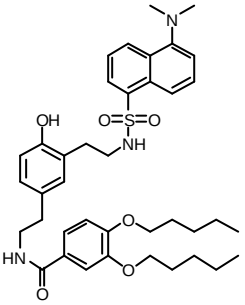

I.D name -Dansyl-JTE2-3 **120**
Design and synthesis - Chapter 4 page 124
Chemistry – Section 4.3 page 129
Pharmacology – Not tested
Chemical analysis Chapter 8 page 212

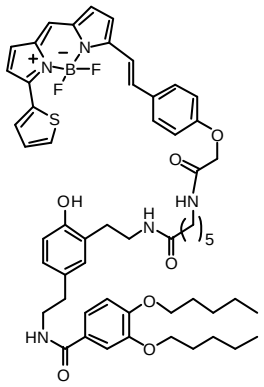

I.D name -Bodipy-JTE2-3 **121**
Design and synthesis - Chapter 4 page 124
Chemistry – Section 4.3 page 129
Pharmacology – Section 4.4 page 132 & section 5.3 page144
Chemical analysis Chapter 8 page 211

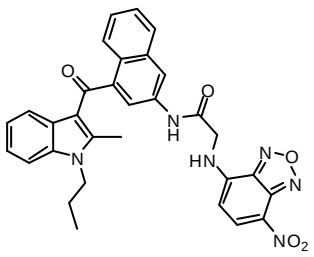

I.D name -3-Gly-NBD-JWH015 **132**
Design and synthesis - Chapter 6 page 154
Chemistry – Section 6.4 page 166
Pharmacology – Section 6.5 page 168
Chemical analysis Chapter 8 page 220

Abstract

An increased understanding of the peripheral cannabinoid receptor (CB_2) is required due to the CB_2 receptor's emerging involvement in a number of disease states. New fluorescent technologies are capable of generating information about the CB_2 receptor systems that has been unachievable using existing pharmacological methods *i.e.* radioisotope techniques.

Our work, to develop fluorescently labelled CB_2 receptor ligands, will provide cannabis researchers a unique pharmacological tool to use in conjunction with these emerging fluorescent technologies. This will aid the understanding of cellular actions of cannabinoids and accelerate the discovery of novel CB_2 selective drugs.

We report on the design, synthesis, and biological evaluation of novel fluorescent ligands targeted towards the CB_2 receptor. The fluorescent ligands were designed and synthesised by conjugating recognized high affinity selective CB_2 ligands (JTE2-3, JTE2-6 & JWH015) to appropriate fluorescent dyes via a chemical linker. Positioning of the fluorescent dye upon the pharmacophore was guided using established SAR data and supplemented by in-house molecular modelling experiments.

Our results showed that modification of JTE2-3 and JTE2-6 with dansyl and BODIPY® fluorophores resulted in fluorescent ligands which displayed poor affinity to the CB_2 receptor and consequently were unsuccessful when used in fluorescent confocal microscopy experiments. Furthermore, our studies revealed important species selectivity, associated with JTE2-3, which was previously unrecognised.

Using *de novo* drug design on JWH015, we synthesised and tested a 3-naphthyl modified fluorescent conjugate, 3-Gly-NBD-JWH015. The compound retained limited affinity to the CB_2 receptor, but fluorescent confocal microscopy did not reveal specific receptor membrane binding. Further experiments using 3-naphthyl precursor compounds, displaying less bulky 3-substituents, demonstrated that limited modification to the 3-naphthyl position of JWH015 was tolerated and provided a first insight to the SAR at this position.

Acknowledgements

Many thanks to my supervisors Barrie Kellam, David Kendall, Weng Chan and Stephen Doughty for their invaluable advice and support throughout this work.
For specific contributions, I would particularly like to thank Stephen Briddon for his guidance on confocal microscopy and fluorescence matters, Tim Self who was able to give up his valuable time to help me in the practical aspects of microscopy and Diane Hall who cultured all of the CHO cells used within these experiments.

To all the people who have given their time, their knowledge and their resources in the chemistry, pharmacology and molecular modelling laboratories, I extend my deepest gratitude. In particular I would like to mention Richard Middleton (chemistry), Paul Smith (chemistry), Rudesh Toofany (molecular modelling), Paul Millns (pharmacology) and James Leggett (pharmacology), without whom I could not have submitted this thesis.

I would also like to acknowledge the help and resources received from Professor Debra Kendall and her group in the University of Connecticut, Storrs, USA, who conducted all of the experiments in human embryonic kidney cells expressing the hCB_2 receptors.

Thanks Mum for pulling a haemorrhagic stroke out of the bag in my final year of studies (by the way I asked her if she minded this going in!). The six week break from the lab certainly left me feeling refreshed!

Finally a big thank-you to my eagle-eyed proof-reader, and long suffering girlfriend Katrina T. Bird.

This work was gratefully funded by the BBSRC.

Abbreviations

AC	adenylate cyclase
AAI	aminoalkylindole
ABNR	Adopted-Basis set Newton-Raphson
AcCl	acetyl chloride
Ala	alanine
Arg	arginine
Asp	aspartic acid
AP-MS	atmospheric pressure mass spectrometry
Atm	Atmospheres
B_{max}	binding site density
BMS	Bristol Myers Squibb
Bn	benzyl
Boc	*tert* butoxycarbonyl
BR	Bovine Rhodopsin
BSA	Bovine serum albumin
cAMP	adenosine 3',5'-cyclic monophosphate
Calcd.	calculated
Cbz	benzyloxycarbonyl
CC	classical cannabinoid
CDI	*N*, *N*'-Carbonyldiimidazole
CHO	Chinese Hamster Ovary
CNS	central nervous system
conc.	concentrated
COSY	correlation spectroscopy
CPA	N^6-cyclopentyladenosine
D_2O	deuterium oxide
DC-FCCS	dual colour fluorescence cross correlation spectroscopy
dec.	decomposition
DCM	dichloromethane
DCC	*N*, *N*-dicyclohexylcarbodiimide
DEAD	diethylazodicarboxylate
dil.	dilute

DMAP	dimethylaminopyridine
DMEM	Dulbecco's modified Eagle's medium
DMF	*N*, *N*-dimethylformamide
DMSO	dimethylsuphoxide
DPAT	2-dipropylaminotetralin
EC_{50}	concentration of drug evoking half maximal effect
EDTA	ethylenediaminetetraacetic acid
EL	extracellular loop
ES-MS	electrospray mass spectrometry
ESP	electrostatic surface potential
EtOAc	ethyl acetate
EtOEt	diethylether
EtOH	ethanol
FAB-MS	fast atom bombardment mass spectrometry
FCS	fluorescence correlation spectroscopy
FIDA	fluorescence intensity distribution analysis
FGI	functional group interconversion
FTIR	fourier transform infra-red
fs	femtosecond
GDP	guanosine diphosphate
Glu	glutamic acid
Gly	glycine
GPCR	Guanosine binding protein coupled receptor
GTP	guanosine triphosphate
GTP-γ-S	guanosine 5'-[γ-thio]triphosphate
h	hours
hCB_2	human CB_2
HEK	human embryonic kidney
His	Histidine
HPLC	high pressure liquid chromatography
HTS	high throughput screening
Ile	isoleucine
K	Kelvin

Kcal	kilocalorie
K_d	equilibrium dissociation constant
K_i	equilibrium affinity constant
KJ	kilojoule
Lit	literature
Lys	lysine
λ_{abs}	wavelength of maximum absorption
λ_{em}	wavelength of maximum emission
M	molar (mol L^{-1})
M+	molecular ion (+ vely charged)
M-	molecular ion (- vely charged)
MeCN	acetonitrile
MD	molecular dynamics
MEK	methyl ethyl ketone
MeOD	deuterium labelled methanol
MeOH	methanol
Mesyl	methanesulphonyl
min	minutes
MH+	protonated molecular ion
MHRA	Medicines and Healthcare Products Regulatory Agency
MMFF	Merck Molecular Forcefield
mL	milliliter(s)
mmol	milli moles
mol	moles
m.p.	melting point
MRC	Medical Research Council
MS	Multiple Sclerosis
NAH	northern aliphatic hydroxyl
NBD	7-nitrobenzofurazan
NCC	non-classical cannabinoid
NECA	5'-(*N*-ethylcarboxamido)adenosine
nm	nanometer
nM	nanomolar

NMR	nuclear magnetic resonance
NSB	non-specific binding
OMs	methanesulphonate (mesylate)
OSu	succinimidyl ester
PBS	phosphate buffered saline
PCR	polymerise chain reaction
PET	photoinduced electron transfer
Pd/C	Palladium on charcoal (10%)
PG	protecting group
Phe	phenylalanine
PKA	protein kinase A
ps	picosecond
Pro	proline
q	quantum yield
Q.S.	quantity sufficient
rCB_2	rat CB_2
RMSD	root-mean-square-derivative
rt	room temperature
RTF	rich text format
SAH	southern aliphatic hydroxyl
SAR	structure activity relationship
sat.	saturated
SEM	standard error of the mean
Ser	serine
SMD	single molecule detection
SPAP	secreted placental alkaline phosphatase
TBAF	tetra-*n*-butylammonium fluoride
TBDMS	*t*-butyldimethylsilyl
Δ^9-THC	Δ^9-tetrahydrocannabinol
THF	tetrahydrofuran
Thr	threonine
TLC	thin layer chromatography
TM	transmembrane

Trp	tryptophan
Tyr	Tyrosine
VDW	Van Der Waals

1. Introduction

There are currently a limited number of *in-vitro* assays available to study receptor-ligand interactions. The techniques that are used, such as radioligand binding and reporter-gene assays, are not ideal due to the speed, cost and technical implications associated with these assays. We are interested in developing an emerging technique which can be used to study receptor-ligand interactions using fluorescent-labelled ligands. Fluorescent ligands with specificity towards GPCRs are promising to be extremely useful tools in the field of pharmacology and drug discovery[1-3]. They offer advantages to most of the problems associated with existing techniques; however few fluorescent GPCR ligands are known, which presently restricts the use of this technique. Our group is interested in studying the peripheral cannabis receptor (CB_2), which is a member of the GPCR class of receptors. We aim to develop novel fluorescent ligands that act at the peripheral cannabis receptor (CB_2), for use in both fluorescent-based biological experiments and in the screening of novel synthetic cannabinoids from combinatorial chemical libraries. Thus potentially providing data on both the cellular actions of cannabinoids and providing a tool to enhance the opportunity of discovering new selective cannabinoids.

Cannabis and the active pharmacological agents acting at the cannabis receptors, the cannabinoids, have long been of interest to scientists who wished to use the compounds in alleviating suffering caused by human disease. From its beginnings as a crude preparation used in China 2000 B.C., through to its current clinical trials in the United Kingdom by the company GW Pharmaceuticals, the use of cannabis for medicinal purposes has long been the subject of controversy. Primarily, this has been the result of an association of cannabis with a 'drug of abuse', compounded by the lack of scientific data available on how cannabis elicits its effects. The recent discovery in 1993 of the peripheral cannabis receptor (CB_2)[4], which is unrelated to the psychoactive effects of cannabis, in conjunction with a general softening of societies' attitudes to the use of cannabis[*], has provided cannabis research groups a unique opportunity of providing quality scientific data and novel synthetic cannabinoid compounds which may provide relief to suffering patients.

[*] The licensing of UK clinical trials for cannabis medicines and the downgrading of cannabis to a class C drug under the Misuse of Drugs Act 1971 are viewed by the author as a 'softening of attitudes' towards the use of cannabis.

1.1 Fluorescent labelled ligands as a tool to study G-protein coupled receptors

G-protein coupled receptors (GPCR) are widely expressed in the body and play a fundamental role in the physiology and the pathophysiology of disease (see section 1.3.1 for further details of GPCRs). Agonists and antagonists towards the GPCRs are the most successful class of drugs, in terms of therapeutic benefit and commercial sales, with GPCR ligands accounting for 50% of the modern drug arsenal[5], and approximately 9% of total global pharmaceutical sales worth $23.5 billion dollars in 2000[6]. An example of some of the best selling therapeutics targeted at GPCRs, demonstrating the diversity in receptors and indications that GPCR agonists and antagonists can be used to treat are shown in Table 1-1.

Trade name (generic name)	GPCR targeted	Agonist or Antagonist	Indication	Company
Claritin® (Loratidine)	Histamine H_1	Antagonist	Rhinitis or allergy	Eli Lilly
Imigran™ (sumatriptan)	Serotonin 5-$HT_{1B/1D}$	Agonist	Migraine	Glaxosmithkline
Cozaar® (Irbesartan)	Angiotensin AT_2	Antagonist	Hypertension	Merck and Co.
Serevent® (Salmeterol)	β_2 Adrenoreceptor	Agonist	Asthma	Glaxosmithkline
Singulair® (Montelukast)	Leukotriene BLT_1	Antagonist	Asthma	Merck and Co.

Table 1-1 Selection of the best selling therapeutics targeted at GPCRs in 2000. Adapted from reference 6.

Despite their importance as drug targets, techniques to investigate the pharmacology surrounding the ligand-receptor interactions are limited to studying the interactions of the receptor with radioactively labelled receptor-specific-ligands or analyzing 'downstream processes' of receptor activation, such as reporter genes, GTP-γ-S and cAMP assays.

Studying the receptor using a radioactively labelled ligand has been the primary and most established method for studying ligand-receptor interactions. Use of a ^3H or ^{125}I radioactive ligand specific to the receptor of interest can be used to determine the dissociation constant (K_d) of the radioactive ligand and the binding site

density (B_{max}) when saturation binding experiments are used[7]. Alternatively competition experiments are capable of determining the equilibrium constant for a competitive inhibition of the receptor (K_i) when studying the displacement of the radiolabelled ligand by a non-radioactive ligand[7]. The technique can be extended to mapping the distribution of receptors in a section of tissue by using a technique called autoradiography (see section 1.3.4.1). Use of radioligand techniques suffer from a number of problems. The technique relies on equilibrium between free ligand and receptor bound ligand and is not capable of easily studying binding kinetics. Equilibration takes time to achieve and this is mirrored in the relatively long assay times associated with radioligand binding techniques. Separation of the bound and free ligand, using filtration or centrifugation, is another time consuming step in the assay, and finally the filtered matter (representing the bound ligand component) must be allowed to incubate with scintillation fluid long enough for the tritium to diffuse out and interact with the scintillator. Therefore the process of using a radioligand to study ligand-receptor interactions takes a significant amount of time which is a serious problem for users of this technique wishing to perform thousands (high throughput screening (HTS)) and up to a one hundred thousand (ultra highthroughput screening (uHTS)) assays a day screening new chemical entities for receptor affinity[8,9]. Finally the assay produces significant quantities of radioactive and flammable scintillation effluent which has an associated high cost for its disposal. Other techniques using radioactive reporter elements, such as intracellular cAMP and GTP-γ-S binding, are able to give information on the efficacy of a ligand upon binding to a GPCR. These techniques, specifically GTP-γ-S binding, have been developed into a HTS assay format *i.e.* Scintillation proximity assay (SPA) beads or Flashplates®[10]. However the technique still employs radioactive substances and suffers from sensitivity problems discussed in section 1.3.4.3.

Development of non-radioactive, homogenous, miniaturized assays for GPCRs has been slow[11]. Recently, however, reporter-gene systems for the study of GPCRs have offered an alternative to biochemical and binding assays[12]. The reporter-gene is a sequence of DNA whose product is synthesized in response to a cellular change occurring within the cell, *i.e.* an increase in cAMP. Examples of the reporter elements produced include enzymes, and Luciferase (a luminescing compound)[12]. By choosing the correct promoter and reporter elements the assays can; allow the ligand-

receptor interaction to be studied and quantified in living cells, can elucidate signalling pathways associated with the receptor and can be used in HTS applications[12]. However the assays' drawbacks are the need to stably transfect a cell line with the appropriate genetic code, and the 4-6 hour incubation required to express the reporter gene product[12]. Therefore new techniques to study ligand-receptor interactions avoiding some of the problems stated above would be a welcome development in the pharmacology and HTS laboratories.

The use of fluorescent ligands to study GPCRs interactions promises to be a valuable addition to the techniques discussed above in the field of pharmacology and drug discovery[1-3]. Fluorescence assays offer the advantages of high sensitivity, reduced sample volumes, low effluent disposal costs, fast assay times and an ability to detect a wealth of biological phenomena in a real time aqueous environment[1-3,13]. The development of fluorescent ligands with affinity towards a specific GPCR of emerging importance, the CB_2 receptor (see section 1.3.4), will allow this system to be interrogated with all of the advantages fluorescence assays offer.

1.1.1 Principles of fluorescence

Fluorescence is described as the emission of light energy as a molecule relaxes from an excited electronic state to a lower energy state[14,15]. A fluorescent dye is capable of absorbing a discreet package of energy (E_{abs}), in the form of electromagnetic radiation, which can promote an electron from the ground state (S_0) up to a first excited singlet state (S_1). The emission phase of fluorescence is represented by the loss of energy from S_1 to S_0 (E_{em}), typically over a lifetime of 10^{-8}s. Due to loss of energy within the S_1 state, via non-radiative pathways, the emitted fluorescence will be of lower energy and hence longer in wavelength than that of the electromagnetic energy absorbed. This phenomenon is described as the red or Stoakes shift and allows the user to detect the emitted light over the background of the light source used to excite the fluorescent dye[14].

Competing with emission is a number of other mechanisms which are capable of transferring the energy from S_1 to S_0 through non-radiative pathways.

- **Internal conversion** occurs from the S_1 of one molecule to the S_1 of another molecule. Quenching of fluorescence by this mechanism can occur over relatively long distances of up to 10 nM[14-16].
- **Intersystem** crossing involves the formation of a triplet state. Magnetic perturbations caused by environmental factors such solvent, paramagnetic ions and atoms with a large atomic radius (heavy atom effect) are capable of changing the direction of spin of the electron in S_1[14]. The resulting triplet state is of lower energy than the corresponding S_1 and possesses a much longer lifetime (10^{-2}-10^{2} s)[15]. This stability makes it vulnerable to loss of energy through non-radiative processes such as collisions with solvent and the quenching of triplet states in the solution phase is always observed.
- **Photobleaching** may occur in susceptible dyes if a high energy excitation light source (i.e. Laser) is used. The flurophore undergoes a chemical reaction, which is usually initiated from the triplet state and is free radical in nature, to yield a non-fluorescent product[17,18].

These quenching effects are measured as the fluorescent dyes quantum yield (q), and are important factors when choosing the fluorescent dye that will be conjugated to the biological ligand. Many of the sensitive fluorescent techniques used with fluorescent ligands are negatively affected if the dyes are subject to these quenching mechanisms.

1.1.2 Fluorescent techniques

We intend to use our novel fluorescent CB_2 ligand in a number of different fluorescent applications which will be considered briefly below.

1.1.2.1 Confocal microscopy

Fluorescent labelled ligands have found use in confocal microscopy experiments reporting on biological functions such as intra-cellular binding events[19], uptake mechanisms and subsequent cell storage[20], and receptor localization, internalization and density measurements[21-25]. The optical principles are outside the scope of this report but for futher information readers are directed towards two excellent

references[16,26]. Confocal microscopy confers advantages over conventional wide field light microscopy by only reporting on a small percentage of the total fluorescence observed. Thus confocal microscopy is capable of providing information on thin slices (0.5 μm) of a cellular structure under investigation resulting in increased resolution compared to wide field microscopy whose depth of field is between 2-3 μm[16]. An important consideration in designing fluorescent ligands for confocal application is that due to the optical principles behind the technique large excitation energies from laser sources must be used which can increase the photobleaching of the ligands used[26]. Visualization of fluorescent derivatives of the α_1 adreno-receptor agonist prazosin[21], the D_1 dopamine antagonist SCH 23390[22], the β-adrenorecptor antagonist CGP 12177[23], the adenosine antagonist XAC[24] and the adenosine agonist N^6-aminobutyladenosine[25] by confocal microscopy have been used by researchers to comment upon the localization, distribution and internalization of receptors at the single cell level.

1.1.2.2 Single molecule detection

Single molecule detection (SMD) is a term used to describe a number of different techniques, which are capable of distinguishing fluorescence bursts caused by a molecule of interest and background fluorescence. In contrast to bulk fluorescent techniques (such as confocal microscopy) which studies the average values generated from a system over time, SMD techniques are capable of studying fluctuating systems under equilibrium by generating very small detection volumes (sub-femtolitre (10^{-15} L)) and using small concentrations of fluorophore (sub-nanomolar ($<10^{-9}$ M))[27,28]. SMD is therefore an ideal approach to reducing the amounts of scarce and expensive materials used in biomedical research (such as enzymes, receptors, cells, solvent and ligands) which makes it a powerful tool in both biological assays and HTS[28].

There are several different methods for studying time-dependant fluorescence fluctuations and the following is a brief introduction concerning their application in studying fluorescent receptor ligands.

1.1.2.2.1 Fluorescence correlation spectroscopy

The philosophy and experimental realisation of fluorescence correlation spectroscopy (FCS) was first published in the early 1970s[29,30], but it is only recently through advantages in laser technology and confocal microscopy that the technique is gaining influence in biological chemistry[28]. The in-depth principles of FCS are outside the scope of this thesis and readers are directed to comprehensive reviews on this topic[28,31,32]. In brief, however, FCS is capable of generating information on the rotational and translational diffusion and the life time of the excited state of a flurophore by deciphering the random fluctuations of fluorescence observed using autocorrelation mathematics[28,32]. FCS can therefore give information upon the binding state of a fluorescent ligand without the need for physical separation. FCS has been used in conjunction with fluorescent derivatives of the $5HT_3$ receptor antagonist GR119566 to show the binding constants of the fluorescent ligand, the stoichiometry of the ligand-receptor interaction and the mass of a $5HT_3$ receptor [33]. This methodology has also been used to demonstrate that $5HT_3$ receptors are found in different environments within a cell membrane[34]. It has subsequently been shown by our research group that the interactions of a fluorescent adenosine agonist and antagonist with the adenosine A_1 receptor can be studied using FCS to provide data on receptor environment within the membrane [24,25]. Taken together it is clear that FCS can provide useful biological information on receptor-ligand interactions occurring dynamically upon live cells when combined with a fluorescent ligand specific to the receptor being studied. The experimental conditions and the process of autocorrelation mathematics used in FCS demand that the fluorescent dyes used have a high quantum yield[33], high photostability[34], do not form triplet states easily[33] and exhibit an emission wavelength which is far separated from the background cellular autofluorescence[34].

1.1.2.2.2 Other single molecule detection techniques

The application of other SMD methods for biological monitoring is beginning to be used; however most of these techniques have not yet been used with fluorescent receptor ligands to date. The following SMD methods have been reported to have the potential to be used to study ligand-receptor interactions using a fluorescent labelled ligand.

- **Dual colour fluorescence cross-correlation spectroscopy** (**DC-FCCS**) is a technique designed to study two spectrally separated fluorophores (i.e. green and red dyes) interacting in the same confocal detection volume[35]. Thus, we can envisage labelling the CB_2 receptor with Green Fluorescent Protein[36] and labelling a CB_2 ligand with a red fluorescent dye and detecting the binary species, as would occur in ligand-receptor binding. DS-FCCS confers advantages over FCS as the simplified data analysis of this technique allows for high confidence millisecond determination of a binary species, occurring within the detection volume making it highly suitable as a high throughput screening assay[37,38].

- **Image correlation spectroscopy** combines confocal scanning microscopy with FCS measurements. This method generates high-resolution images, which can be used to characterize a variety of cell features of both dynamic and structural nature. Thus, the numerical data extracted from FCS measurements can be overlaid onto a real image of the structure under study to allow easier interpretation of the data[39].

- **Fluorescence intensity distribution analysis** (**FIDA**) is a technique that discriminates between different fluorescent species according to their specific molecular brightness. It is a development of the analysis performed on the data from a classical FCS experiment. In classical FCS, the system under investigation requires large changes in the molecular weight of the fluorescence species to influence the observed diffusion coefficient (a doubling of the diffusion coefficient requires an 8-fold increase in molecular weight). The diffusion coefficient can then be used to determine parameters

such as bound *versus* unbound ligand concentrations. However the emission characteristics of the fluorophore can also change upon binding or when several ligands aggregate together giving rise to bright species which dominate the autocorrelation curves. These problems are overcome when using FIDA analysis, which is capable of distinguishing fluorescent molecules on the basis of their molecular brightness. FIDA analysis has been used successfully to study the binding of a fluorescent 5HT receptor ligand to an unspecified 5HT receptor over expressed in *E. Coli* [40]. This method was capable of demonstrating that the addition of the high affinity $5HT_{1A}$ ligands 8-hydroxy-DPAT (agonist) and NAN-190 (antagonist) inhibited the binding of the fluorescent ligand, shown as a reduction in the number of "bright spikes" observed[40]. Thus, FIDA appears capable of generating "yes" or "no" decisions on whether an unlabelled ligand is capable of competing with a fluorescent ligand for occupancy at a receptor, something that is of great interest to researchers in high throughput screening laboratories looking to discover new receptor ligands.

1.1.2.3 High throughput screening applications

One of the main aims of this research was to design a fluorescent CB_2 ligand which could be used in a fluorescent-based HTS assays, enabling screening of new lead compounds with affinity to the CB_2 receptor. HTS is the primary engine driving lead discovery in most pharmaceutical companies and currently involves performing several million assays per year[1]. The testing of vast numbers of synthetic and natural compounds against a receptor target of therapeutic interest imposes great demands for both faster and smaller volume assays without compromising data quality[1,11]. SMD based HTS addresses each of these requirements by offering fast (0.2 – 0.4 seconds per scan) and low volume (often limited by liquid handling capabilities) assays, which are still capable of being highly sensitive and quantitative[13,41]. The low assay volume required allows cost savings on the amounts of test compounds, biological materials and solvent required for each assay. The non-radioactive nature of the tests also reduces the cost per assay due to the decreased cost of waste disposal. Various research groups have demonstrated SMD to be applicable to HTS[1,13,33,37,38,40,42].

1.2 Cannabis

Cannabis is a collective term for a series of preparations derived from the plant *Cannabis sativa.* There are many regional or colloquial names for the preparations of cannabis but the two most commonly referred to in the United Kingdom are marijuana and hashish (cannabis resin). Marijuana consists of the dried leaves and female flower heads and hashish is the plant secretions compressed into blocks. These preparations can either be heated and the vapour inhaled, or eaten to afford adsorption of the active pharmacological agents present within cannabis; the cannabinoids.

The term cannabinoid was originally used to describe the family of approximately sixty, 21-carbon structures present within the preparations of cannabis. Of these, the most significant in terms of both quantity and psychoactive efficacy, is the compound Δ^9-tetrahydrocannabinol (Δ^9-THC **1**, Figure 1-1)[43]. Recently the term cannabinoid has been used to describe any compound that has activity at the cannabis receptors including synthetic and endogenous compounds.

1.2.1 Historical overview of cannabis

Cannabis, and hence, the cannabinoids have enjoyed a long history of use as a medicinal agent. Cannabis had its first entry in the worlds oldest Pharmacopoeia, the Chinese *Shen-nung pen-ts'ao ching* which was compiled in the first or second century *A.D*). The list of over 100 ailments which *ma* (cannabis) was used to treat includes many which cannabis is currently prescribed or undergoing clinical trials for *i.e.* anti-emetic, pain relief, and rheumatism[44]. Following its first recorded use in China approximately 5000 years ago, cannabis has enjoyed many centuries of medicinal use; which have included the treatment of pain, asthma and dysentery, the promotion of sleep, the suppression of nausea and vomiting and the abolition of convulsions and spasms[45]. Within the United Kingdom doctors could legally prescribe cannabis until 1971, and cannabis still had an official entry in the Pharmaceutical Codex until 1949.

Cannabis cannot be introduced without considering its potential use as a 'drug of abuse'. Although a thorough review of this subject is outside the scope of this work, the reader is directed to a review of cannabis misuse[46]. The fact that cannabis is

used as an intoxicating drug has been a factor in its prohibition as a medicinal agent. Within the United Kingdom cannabis is the most widely used of the illicit drugs with an estimated 1,503,000 users between 16-24 years old using the drug in 1999[47]. Cannabis is used recreationally because of the euphoria it produces. The adverse physiological effects it produces include psychomotor and cognitive impairment, anxiety, panic attacks, acute psychosis and paranoia. In 1971 this led to its reclassification as a controlled drug, placing it within Schedule 1 of the Misuse of Drugs Act 1971 (drugs without therapeutic value), where it still remains today, hampering its use or evaluation as a medicine.

A thorough scientific understanding regarding cannabis as a drug has only recently started to be compiled. The following discoveries have been fundamental to the current understanding of how cannabis exerts its pharmacological actions.

- **1964** Gaoni and Mechoulam first elucidated the structure of the major psychoactive compound (Δ^9-THC **1**, Figure 1-1) in cannabis resin[43].
- **1982** Pfizer Central Research synthesised and patented CP 55, 940 **2** (Figure 1-1)[48]. This compound demonstrated that the core three ring structure (A, B & C) of the natural cannabinoids could be simplified to two rings (A & C) and still retain potent cannabinoid pharmacology[49].
- **1990** Matsuda *et al.* provided the first definitive poof of a central cannabinoid receptor (CB_1) by isolating the cDNA of a cannabinoid receptor from a rat brain and expressing it in Chinese Hamster Ovary (CHO) cells[50]. The central CB_1 receptor has been shown to be responsible for the euphoric and psychotropic effects of Δ^9-THC **1** [51].
- **1991** Stirling Research Group discovered a new chemical class of cannabinoid ligand, the indole cannabinoids[52]. These compounds showed no chemical resemblance to the tri or bicyclic classical cannabinoids. The potent cannabinoid Win 55212-2 **3** (Figure 1-1) was developed through this research program[53].
- **1992** Devane *et al.* isolated and characterised the first endogenous ligand to the cannabis receptor. Anandamide **4** (Figure 1-1) was extracted from the lipophillic fraction of porcine brain extracts and was shown to bind to

membranes derived from rat brain homogenate (the standard test for CB_1 receptor binding)[54].

- **1993** Munro *et al.* discovered a second cannabinoid receptor which was isolated from human myeloid cells[4]. The finding of a second cannabinoid receptor named the peripheral CB_2 receptor was evidence that some of the beneficial therapeutic uses of cannabis are derived from a non-psychoactive pathway.
- **1994** Sanofi introduced the first selective CB_1 antagonist SR141716 **5** (Figure 1-1) which has proved a useful investigative tool into the *in vivo* and *in vitro* functions of the endogenous cannabinoid system[55,56]. Under the trade name Rimonabant® it is now under investigation as a drug in a number of medical conditions.
- **1998** Sanofi introduced the first selective CB_2 antagonist SR144528 **6** (Figure 1-1) which has proved to be a powerful tool in investigating the *in-vitro* and *in-vivo* actions and effects of the CB_2 receptor[57].

This selected chronology showing the major scientific discoveries associated with cannabis highlights that it has only been in the last decade that scientists have been able to relate cannabis pharmacology to two different receptor sub-types (CB_1 and CB_2), each capable of binding a diverse range of chemical ligands. Researchers are now beginning to exploit this information in developing new treatment strategies for disease. It is envisaged that the addition of a fluorescent labelled ligand, selective to the CB_2 receptor, will give scientists a new tool capable of exploring the less well characterized CB_2 receptor, at a level of detail which is not available using current pharmacological ligands. The renaissance surrounding the use and testing of cannabis in the United Kingdom has arisen since positive recommendations towards medicinal cannabis were made in reports by the House of Lords select committee on Science and Technology[58,59]. The committee, after studying the available literature and taking statements from eminent scientists, were favourable towards medicinal cannabis as long as a careful scientific approach to its use was adopted. A key conclusion from the 1998 report was that "clinical trials of cannabis for multiple sclerosis (MS) and chronic pain should be mounted as a matter of urgency"[58]; a reflection of the potential benefits that are being ignored by cannabis's continued prohibition.

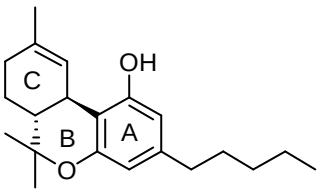

Δ^9-tetrahydrocannabinol **1** (Dronabinol)

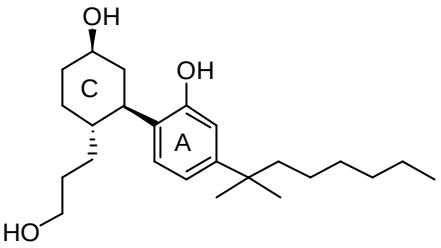

CP 55, 940 **2**

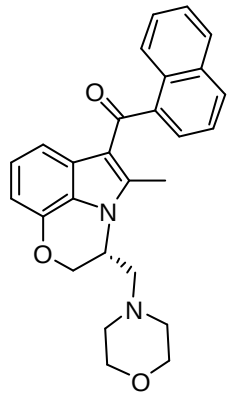

Win 55212-2 **3**

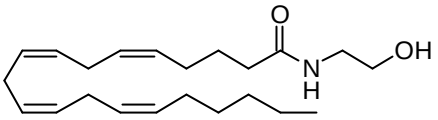

Anandamide **4**

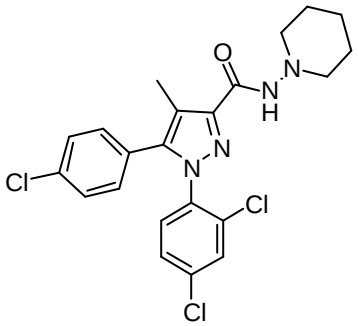

SR141716 **5**

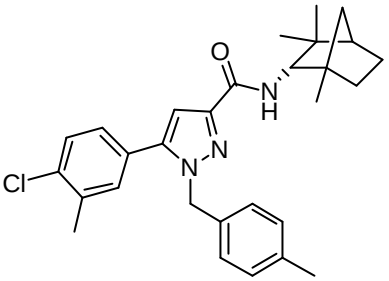

SR144528 **6**

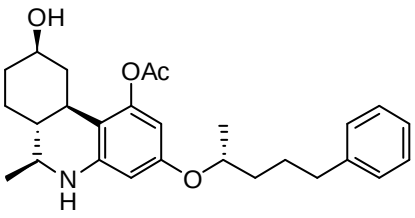

Levonantradol **7**

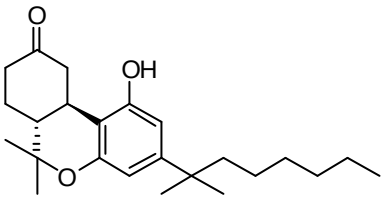

Nabilone **8**

Figure 1-1 The chemical structure of a number of selected cannabinoid ligands.

This recommendation has led to both the Medical Research Council (MRC) and a privately owned company, GW Pharmaceuticals, being granted Home Office licenses enabling them to conduct a large clinical trial into cannabis based medicines for the relief of symptoms in MS and pain control. The full results of these trials are still awaited. However, GW Pharmaceuticals have already made their first submission to the UK's regulatory authority, the Medicines and Healthcare Products Regulatory Agency (MHRA), for their standardised cannabis extract product Sativex® to be used in patients with MS and neuropathic pain[60].

One of the key reasons cannabis has returned to a status as a drug of medicinal value has been that quality scientific evidence, amassed by cannabis researchers over the last half a century, has become impossible for governmental bodies to ignore. However, further research into cannabis and its actions is essential, if cannabinoids are to find approval with politicians, regulatory authorities and the general public, as an effective therapeutic agent.

1.2.2 Therapeutic use of cannabis

Cannabis's use as a "cure all" for nearly 5000 years has led to it being evaluated as a medicine in literarily hundreds of diseases. Thus, cannabis has been used as an analgesic, anti-spasmodic, anticonvulsant, anti-emetic and hypnotic throughout ancient China, the Middle East, Southern Africa and South America, and was still advocated up until the 19th century by eminent doctors such as W. B. O'Shaughnessy (the medic who discovered the pathology of Cholera) and Russell Reynolds (Queen Victoria's personal physician)[61]. Indeed Reynolds wrote "Indian hemp, when pure and administered carefully, is one of the most valuable medicines we possess"[62].

In recent years the evidence base to support cannabis as a medicinal product has grown and the prospect of a cannabis-based product is now real. Following the House of Lords Committee report in 1998, cannabis trials are currently underway and reporting on the use of standardized cannabis preparations or synthetic Δ^9-THC **1** (Figure 1-1) for use in MS and pain. Cannabinoids have also been evaluated in a number of other conditions and the individual conditions that cannabis is currently being used for as a potential therapy will now be considered.

1.2.2.1 Multiple Sclerosis

Multiple Sclerosis (MS) is the most common disabling nervous system disease of young adults, with an estimated 85,000 people suffering with the condition in the United Kingdom. MS is a progressive, degenerative disease, in which the brain and spinal cord nerves are damaged by the gradual destruction of myelin, the protective insulating layer of fatty tissue that normally coats nerve fibres. Although the precise cause of the disease is unknown, it is thought to represent an auto-immune condition whereby the body's own defences attack and break down the myelin leading to the major symptoms of muscle spasticity (90%), urinary tract dysfunction (90%), tremor (80%) and pain (50%)[63]. Anecdotal reports of the beneficial use of cannabis to alleviate the suffering caused by MS have arisen primarily because individuals with MS constitute the biggest users of illicit cannabis for medicinal purposes[64]. Controlled clinical trials have tried to establish a product license for cannabis medicines by showing them to be efficacious and safe.

A review of the literature up until 1997 indicates that there have been 15 reported trials conducted into cannabis usage and MS [45]. The total number of subjects in the trials however was extremely low; a total of approximately 174 people throughout all the trials. The trials broadly showed that cannabis was generally well-tolerated and patients showed improvement in the subjective assessment of their symptoms, but did not show improvement in their objective assessment of spasticity and tremour. A summary of the details and results of the three largest clinical trials are shown in Table 1-2.

More recently two larger trials using orally dosed Δ^9- THC **1** (Figure 1-1) or cannabis extract have also proved inconclusive in their support for use of cannabis based medicines in MS[65,66]. Both trials showed that there was significant improvement in subjective spasticity and pain but there was no significant difference when analysis of the objective assessment of disease markers, such as spasticity, was considered. In both trials cannabis side effects caused by the medication where rated as mild and well-tolerated. In summary, cannabis has not been shown to conclusively provide measurable benefit in MS when trialed in humans. However, patients did report a perceived benefit from the cannabis-based medicines, and many more regularly use illicit forms of cannabis to self-medicate. A major problem in the trials is that the Δ^9- THC **1** or cannabis extract have been dosed orally. Cannabis absorption

from the gut is variable and slow and this is problematic when finding a correct dose within its small therapeutic window, which if exceeded, results in psychotropic side effects[45]. GW Pharmaceuticals appear to have overcome this problem by formulating the cannabis extract into a sublingual spray. Their medicinal product, Sativex®, is now awaiting regulatory approval for use in MS.

Another approach to avoiding the psychotropic side effects of cannabis is to target the non-psychotropic CB_2 receptor. It has recently been established that the peripheral cannabis receptor (CB_2) is responsible for some of the therapeutic actions of cannabinoids in animal models of MS, possibly through an immunoregulatory pathway[67-69]. If this evidence of CB_2 receptor involvement can be shown in human MS patients it would enable the development of a non-psychoactive therapy, targeted to the CB_2 receptor, which may be suitable for long-term use.

1.2.2.2 Analgesia

Pain is one of the most common medical symptoms requiring drug treatment. Although the arsenal of analgesics available is extensive, there are certain painful conditions for which conventional analgesics fail to treat effectively. Chronic neuropathic pain arising from damage to neural tissue is usually unresponsive to established analgesic medication. A need for a new effective analgesic to combat neuropathic pain is therefore needed[70]. The results from trials involving pain are mixed. A systematic review by Campbell *et al.* of nine human trials involving cannabis as an analgesic concluded that cannabinoids are no more effective than codeine in controlling pain, but with the disadvantage of increased central nervous system (CNS) side-effects[71]. A summary of the three largest trials are shown in Table 1-2. It was proven that Δ^9-THC **1** and the synthetic cannabinoid levonantradol **7** (Figure 1-1) had an analgesic effect, but at the expense of drowsiness and CNS side-effects. The authors do however concede that new and effective agonists at the cannabinoid receptors could reduce the CNS side-effects and that these should be evaluated as an analgesic in neuropathic pain and spasticity. A recent discovery that the CB_2 receptor is implicated in neuropathic pain pathways has made the idea of a cannabinoid analgesic, free from CNS side effects, more of a reality[72,73]. It is interesting to note that GW Pharmaceuticals product Sativex® is currently awaiting licensing for use in neuropathic pain. A recently published trial using Sativex®

showed that the sublingual formulation was able to significantly reduce pain in patients suffering from a mixture of intractable neurogenic symptoms when assessed by Visual Analogue Scoring assessment[74]. Although the cannabis treatment group had significantly increased side effects the authors concluded that these were generally well-tolerated.

1.2.2.3 Nausea and vomiting

Nausea and vomiting are the only indications that presently have a cannabinoid containing medicine available to patients. These are the orally administered synthetic cannabinoids Dronabinol (Marinol®) and Nabilone **8** (Cesamet®, Figure 1-1). Dronabinol is the trade name for synthetic Δ^9-THC **1** and is licensed in the United States for nausea and vomiting associated with cancer chemotherapy and as an appetite stimulant to overcome the devastating cachexia often observed in AIDS and cancer patients. For a thorough analysis on the uses, efficacy and side effects of Dronabinol, readers are directed to the clinical review by Plasse *et al.*[75].

Nabilone **8** is a synthetic cannabinoid that was developed by scientists at the Eli Lilly Company, who were looking to modify the natural cannabinoids (i.e. Δ^9-THC **1**) to have improved separation of the desired therapeutic effects from the psychotropic side effects. Although it still possessed a psychotropic side-effect profile, it was thoroughly tested in clinical trials and received a license in the United Kingdom for use in nausea and vomiting caused by cytotoxic chemotherapy unresponsive to conventional anti-emetics. A thorough review of the clinical trials involving Nabilone **8** was conducted by Ward and Holmes[76].

1.2.2.4 Appetite modification

Anecdotal evidence and early published work on the effects of cannabis have reported that users show an increase in appetite[77]. Cannabis agonists such as Δ^9-THC **1** (Dronabinol, Figure 1-1) are used as an appetite stimulant and can significantly reverse the weight loss observed in cancer and AIDS, with 47% of the patients trialed reporting a subjective increase in appetite[75]. Recent evidence has shown that the

endogenous cannabinoid system e.g. anandamide **4** (Figure 1-1) may tonically activate the CB_1 receptor, maintaining food intake[78]. The same authors of this study showed that if the CB_1 receptor antagonist SR141716 **5** (Figure 1-1) was administered to mice it reduced their food intake. This has led the company, Sanofi-Synthelabo, to trial SR141716 **5** (Rimonabant®), which is currently in worldwide phase III trials, as an anti-obesity agent. This is the first example that we are aware of where a cannabis antagonist is undergoing a clinical evaluation and demonstrates that synthetic cannabinoids are beginning to find uses in clinical settings

1.2.2.5 Other therapeutic areas

Cannabis has also been evaluated as a medicine in a number of other disease states. For example, epilepsy, glaucoma, asthma, mood disorders and as a sedative. These conditions are likely to derive their benefit from activation of CB_1 receptors, and there is no current evidence to suggest any CB_2 receptor involvement and readers are directed to some excellent reviews on the trials already conducted[45,61,79]. As the scope of this thesis wishes to examine the usefulness in directing research towards the peripheral CB_2 receptor these therapeutic areas will not be examined in any further detail.

Indication	Number of subjects	Drug and dose	Type of study	Results[i]	Reference
MS	13 patients with MS	Oral Δ^9-THC **1** 2.5-15mg once or twice a day	Double blind, placebo controlled	Significant subjective improvement in spasticity at doses of 7.5mg Δ^9-THC **1** and above, but no change in objective measurements of weakness, spasticity, coordination, gate or reflexes. Side effects in 12 patients on Δ^9-THC **1** and 5 patients on placebo.	77
MS	10 patients with MS 10 normal controls	Smoking cannabis. 1.54% Δ^9-THC **1** per cigarette single dose	Double blind, placebo controlled	Cannabis impaired posture and balance in all subjects, causing greater impairment in MS patients. No other objective neurological changes but subjective improvement in some patients. "High" experienced with cannabis.	78
MS	112 patients with MS	Smoking cannabis - dosage not known	Questionnaire survey	Improvement in muscle spasms and pain, depression, tremor, anxiety, paraesthesiae, weakness, balance and constipation. No information on adverse effects.	79
Pain	10 patients with cancer pain	Oral Δ^9-THC **1** 5, 10, 15, 20mg in random order	Double blind, placebo controlled	Significant pain relief with 15 and 20mg Δ^9-THC **1** compared to placebo. Drowsiness and mental clouding common	80
Pain	36 patients with cancer pain	Oral Δ^9-THC **1** 10 and 20mg vs oral codeine	Double blind, placebo controlled	Δ^9-THC **1** 20mg and codeine 120mg gave equivalent and significant pain relief compared with placebo. Δ^9-THC **1** caused sedation and mental clouding.	81
Pain	56 patients with post-operative pain	Intra-muscular levonantradol **7** (a synthetic cannabinoid) 1.5-3mg	Double blind, placebo controlled	Significant pain relief with both doses of levonantradol **7** compared with placebo. Drowsiness common with levonantradol **7**.	82

Table 1-2 A summary of some of the major human clinical trials involving MS or pain symptoms. i) summary of results was taken from reference 45.

1.3 The cannabis receptors

Two cannabis receptors have been identified and cloned, the central CB_1 and the peripheral CB_2 receptor [80]. Both of these receptors belong to the larger super family of the Guanosine Binding Protein Coupled Receptors (GPCR). In order to appreciate the complexity and importance of the cannabinoid receptor, it is important to understand the nature and workings of the GPCR family to which it belongs.

1.3.1 GPCR receptors

The GPCR super family has a common protein structure embedded within the phospholipid membrane. The distinguishing feature of the GPCR is that the protein chain winds back and forth through the membrane seven times - hence GPCRs are also know as seven transmembrane (TM) receptors. The receptor comprises of 7 α-helices that are lipophilic on their outside face, which transverse the lipid membrane, connected by intra-cellular and extra-cellular loops (Figure 1-2). The α helices are numbered from 1 (I) through to 7 (VII) and are clustered together in a barrel type structure.

GPCRs are difficult to study at the molecular level due to their intrinsic association with the cell membrane. They are difficult to purify due to the reliance upon the lipid membrane encasing the receptor to stabilize their structure and hence cannot be crystallised. These difficulties have partially been overcome recently by using a 2.8 Å X-ray crystal structure of a related 7-TM protein called Bovine Rhodopsin (BR) as a template for the individual amino acid sequence of the GPCR[81]. Evidence that the crystal structure of BR is a satisfactory model for the GPCRs has been generated by a number of researchers[82-84].

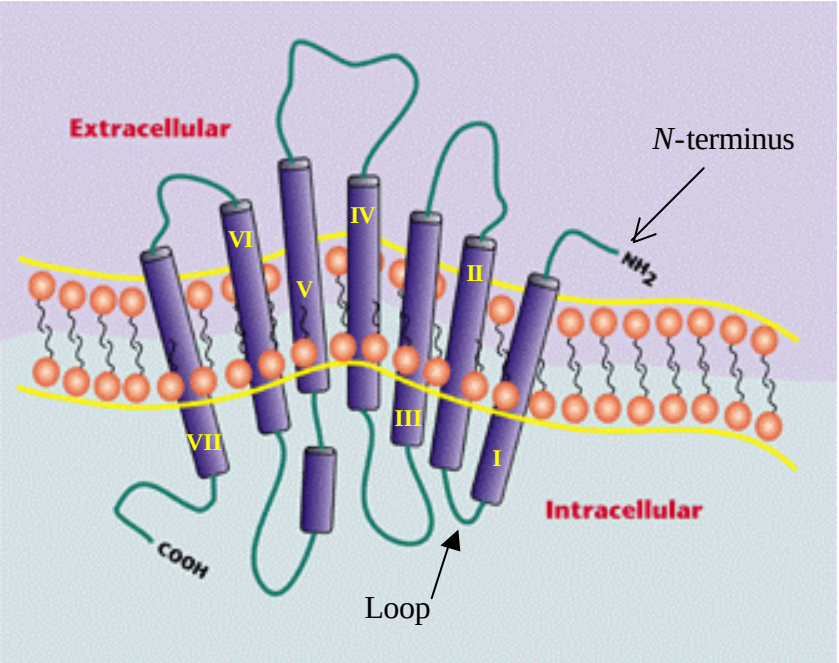

Figure 1-2 A cartoon description of a GPCR receptor.

The 3D structure of the GPCR is important as it dictates how an external ligand interacts with the receptor and how the receptor translates this stimulus into a cellular event. Ligand binding to the GPCR can occur either in a deep binding pocket within the TM regions (type A); to the top of the TM regions (type B); or involve interaction with the extra-cellular loops (type C)[85].

When a ligand binds to the GPCR a cascade of events are initiated that result in a signal being passed from the extra-cellular surface to the intra-cellular domain where cell processes can be regulated. Upon activation with an agonist ligand the GPCR undergoes a conformational change allowing a membrane bound protein, called a G-protein, to bind to the receptor ligand complex. G-protein coupling is the first level in the signalling cascade (see Figure 1-3). The coupling event is able to propagate the signalling process due to the heterotrimeric structure of the G-protein which consists of three separate subunits (α, β, and γ). When un-coupled from the receptor the α subunit binds guanosine diphosphate (GDP **9**, Figure 1-4). Upon ligand induced receptor coupling, the α subunit changes conformation and its guanyl binding pocket now preferentially binds guanosine triphosphate (GTP **10**, Figure 1-4) instead of GDP **9**. The expulsion of GDP **9** by GTP **10** causes further conformational changes in the G-protein trimer and causes it to separate into an α subunit binding

GTP **10** and a βγ complex. The activated receptor-ligand complex is capable of activating several G-proteins in this way, leading to signal amplification.

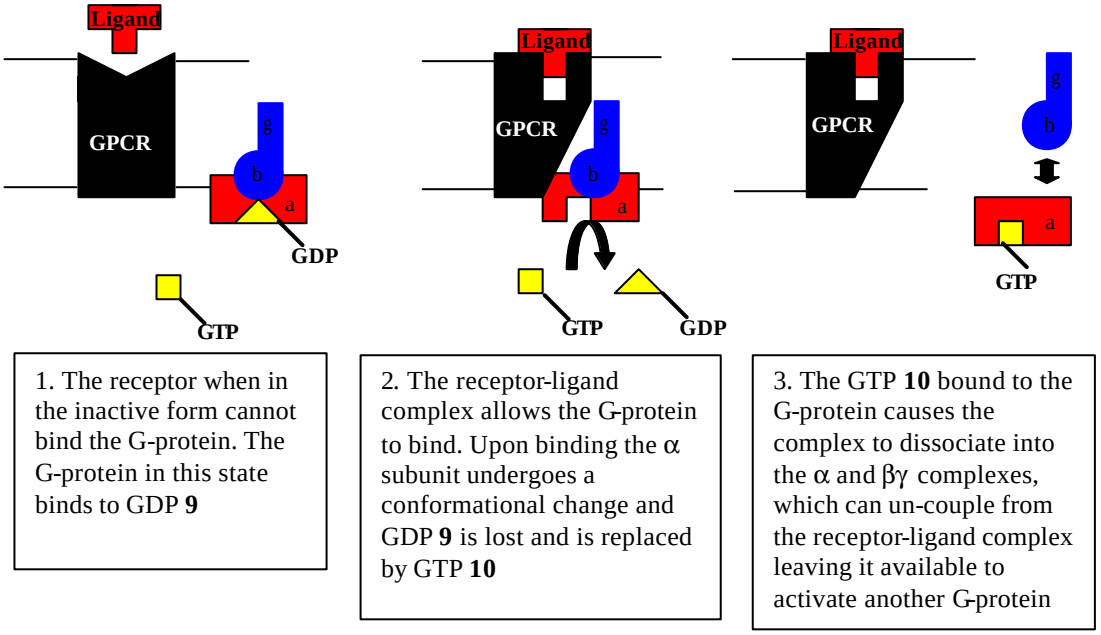

Figure 1-3 A cartoon description of the events following the agonist stimulation of a GPCR.

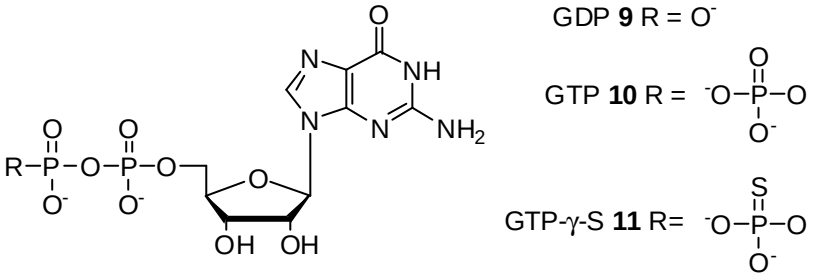

Figure 1-4 Guanyl nucleotide analogues GDP **9**, GTP **10**, and GTP-γ-S **11**

A further consequence of receptor activation of a GPCR, which adds to the difficulty in studying these receptors in any intimate depth, is the possibility that activation of the receptors leads to desensitisation or internalization, via the action of a cellular protein β-Arrestin[86]. As a consequence of this there may be decreased receptor availability or desensitisation of the receptor to the ligand, resulting in the reduction of the signal amplification process.

However for a functioning GPCR, activation yields both an α-GTP complex and a βγ complex which form the second level in the signalling cascade. The α, β, and γ subunits are not homogeneous in any single cell system. There are at least twenty different α (i.e. α_s, $\alpha_{i/o}$, α_q,), five β, and six γ subunits that have been described[87]. A receptor can only couple to certain G-proteins available within the cell, and thus activate specific α, β, and γ subunits exclusive to the receptor type. It is the type of subunit which is activated that determines the cellular effect of the receptor. The effects of G-protein cell signalling is an extremely large field of biology and will not be explored in depth, instead readers are directed towards excellent reviews on this topic[87-89]. However an example will be given of the mechanisms by which the α_i subunit affects cell function in-order that the reader has an understanding of the cellular actions of activation of the cannabinoid receptor which couples to $\alpha_{i/o}$ G-proteins ($G_{i/o}$)[80,90].

1.3.2 $G_{i/o}$ Cell signalling

The active $\alpha_{i/o}$ subunit, formed, by the GTP **10** replacing bound GDP **9**, has a finite lifetime in which it can carry out signalling duties[91]. This is due to an intrinsic GTPase activity of the α subunit which cleaves the terminal phosphate group of GTP **10** generating GDP **9** which returns the α subunit to its inactive form in which it can recombine with a βγ unit to form the original trimeric G-protein (see Figure 1-3 and Figure 1-5). An interesting observation, that forms the basis of a functional GPCR assay, is that when synthetic GTP analogues, such as GTP-γ-S **11** (Figure 1-4), are present the GTPase function within the α subunit is unable to hydrolyse the guanyl analogue and the α unit is trapped in the active state [89] (Figure 1-5). Within the lifetime of its activation, the $G_{i/o}$ protein is capable of eliciting a number of responses within the cell. The action of the α subunit with secondary effector systems has been studied in the greatest depth and it is these effects that will be considered further. Free βγ subunits are also emerging as possessing an important role in the cell signalling following GPCR activation but will not be considered in this report[92].

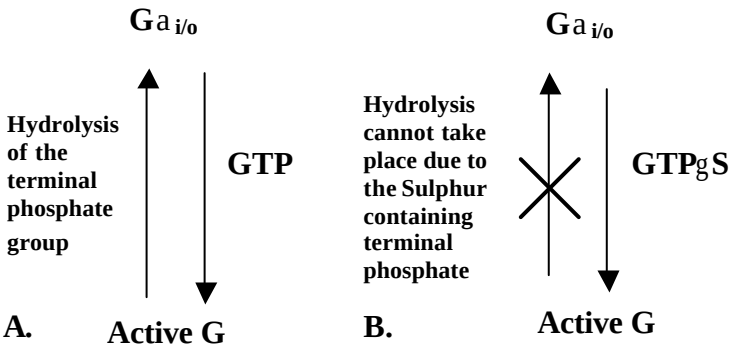

Figure 1-5 (A) Cycling of $G\alpha_{i/o}$ with GTP. (B) Incomplete cycling of $G\alpha_{i/o}$ with GTP-γ-S

The first discovered and most studied response of the $\alpha_{i/o}$ subunit was its ability to inhibit the membrane bound enzyme Adenylate Cyclase (AC), which catalyses the conversion of adenosine triphosphate (ATP) to cyclic adenosine monophosphate (cAMP). Thus activation of an $\alpha_{i/o}$ protein leads to a decrease in the intra-cellular cAMP levels in the cell (Figure 1-6). The secondary messenger cAMP is responsible for the activation of another cellular enzyme, Protein Kinase A (PKA), which causes phosphorylation of further cell specific enzymes leading to a cellular response. The $\alpha_{i/o}$ unit is also capable of attenuating ion channels located within the cell membrane causing an increase in K^+ (via GIRK channels) and a decrease in Ca^{2+} entry (via N-type channels) into the cell [89,93] (Figure 1-6). This leads to a reduced neurotransmitter release through reduced intra-cellular Ca^{2+} and a hyperpolarized membrane potential resulting in a higher depolarizing stimulus required for the cell to "fire". Thus the overall effect of activating a GPCR which is coupled to a $G\alpha_{i/o}$ protein is to apply a biochemical "brake" to the functions of the cell.

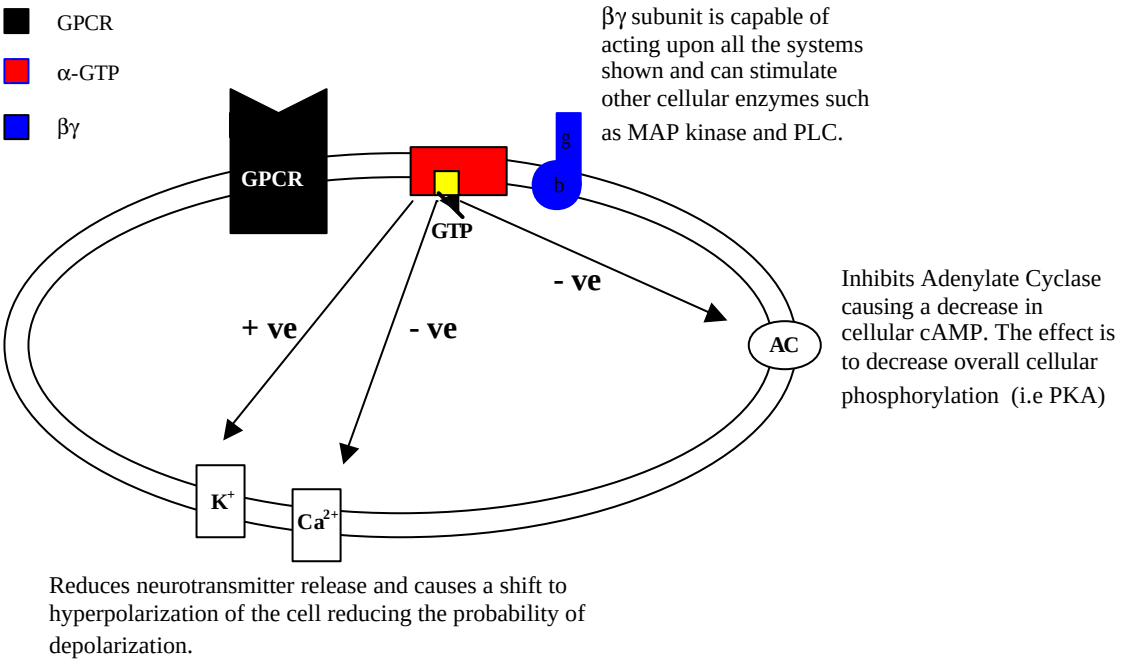

Figure 1-6 The main cellular effects of activation of a GPCR linked to an $\alpha_{i/o}$ containing G-protein. AC adenylate cyclase, cAMP cyclic adenylate monophophate, PKA Protein Kinase A, MAP Mitogen-Activated Protein, PLC Phospholipase C.

1.3.3 The CB_1 receptor system

As the focus of our work is dedicated to the development of CB_2 selective fluorescent ligands only a brief introduction, regarding the role of the CB_1 receptor system will be given. Readers who wish to understand the CB_1 receptor system in further depth are directed to two excellent reviews on the subject[51,80]. The central cannabis receptor was the first cannabis receptor to be discovered in 1990[50]. It is named the central receptor as it is mainly located within the central nervous system (CNS), although Northern blot analysis of CB_1 mRNA has found evidence of the receptor in many peripheral tissues, including the heart, liver, kidney, spleen, small intestines, testes and ovaries[51]. The distribution of the CB_1 receptor in the CNS is not homogenous and is most densely located within the cerebellum, basal ganglia, hippocampus, and the cerebral cortex[80]. The CB_1 receptor is a type A GPCR receptor which couples to $G\alpha_{i/o}$ proteins leading to the expected cellular responses explained in section 1.3.2. (*i.e.* a decrease in cellular cAMP etc). The human CB_1 receptor contains 472 amino acids[94] and the mouse and rat CB_1 receptor contains 473 amino acids[50,95]. Overall these three receptors have a high amino acid sequence homology of between 97-99%.[80]. The

pharmacology of the CB_1 receptors has been extensively studied. *In-vitro* assays can be performed on membrane homogenates derived from rat or mouse whole brain and on transfected cell lines expressing the CB_1 receptor (human or rat). It is noteworthy to comment that when using a transfected cell line, the preparation will only contain the CB_1 receptor, however this is not necessarily the case when using primary tissues that express dense populations of the CB_1 receptor such as the brain. This is because the CB_2 receptor, expressed on microglia[73,96], and possibly a new type of cannabinoid receptor yet to be identified may also be present within the brain[97]. The different *in vitro* assays available for CB_1 receptors are also the same tests used to investigate the CB_2 systems and will be covered in section 1.3.4.3.

The complex array of behavioral effects exhibited by the cannabinoids acting at the CB_1 receptor have been characterized in numerous animal species, including humans. Drug discrimination tests, dog static ataxia, mouse tetradmodels and many others have been used in order to demonstrate the psychoactive effects of the CB_1 cannabinoids. Table 1-3 describes the main observations and outcomes of the *in-vivo* bioassays used in CB_1 pharmacology. These assays are evidence that the CB_1 receptor is responsible for the bizarre and complex psychoactive effects of the cannabinoids as blockade using the CB_1 antagonist SR141716 **5** negates the effect.

It is notable that the bulk of the cannabinoid literature has focused ultimately on the CB_1 receptor and its pharmacological responses[51,80]. This has been a result of a number of factors. Primarily since the discovery of Δ^9-THC **1** in 1964 the activity of cannabis has been associated with the psychoactive effects it produces. With the discovery of the CB_1 receptor in 1990 and its expression throughout the CNS, scientists were able to quantify the effects of cannabis to this receptor and much work was, and still is, being undertaken on this system. The discovery in 1993 of the CB_2 receptor gave scientists a new avenue of exploration in cannabinoid research. Since the discovery of the CB_2 receptor, the literature has remained heavily biased towards the understanding and exploitation of the CB_1 receptor. For example, an ISI Web of Science database search under the search terms “CB1” or “CB2” afforded results from 1993-2003 of 1570 and 569 papers respectively[†]. This bias towards CB_1 research is despite the fact that the CB_1 receptor by its very nature gives rise to the detrimental

[†] Web of Science search (http:wok.mimas.ac.uk) conducted on 22nd December 2003

psychoactive side effects which have caused problems in the use of cannabis medicines as detailed in section 1.2.2.

Name of test	Description	Observations	Evidence of CB_1 receptor involvement	Reference
Dog static ataxia	A range of cannabinoids and other CNS acting drugs are administered	Psychoactive cannabinoids produce an effect where the dog weaves to and fro whilst remaining in one spot. This is not repeated when other CNS active drugs are used.	SR141716 **5** a potent CB_1 antagonist blocks ataxia effects of Δ^9-THC **1**.	98
Mouse tetradmodel	A range of cannabinoids and other CNS acting drugs are administered. The test is also know as the Billy Martin test after the Professor who discovered the response.	Psychoactive cannabinoids produce sedation, hypothermia, anti-nociception and catalepsy. Other CNS acting drugs produce these effects but not in the same dose range.	SR141716 **5** blocks the tetrad effect for most cannabinoids indicating CB_1 involvement.	99
Rat drug discrimination	Rats are trained to press a lever for a food reward when under the influence of a psychoactive cannabinoid (Δ^9-THC **1** etc). They are then administered a range of cannabinoids and other CNS acting drugs.	If fed an investigational drug that is perceived by the animal to be a psychoactive cannabinoid the animal pushes the lever to indicate this to the investigator.	When rats trained on CP 55,940 **2** or Δ^9-THC **1** were co-administered SR141716 **5** and a psychoactive cannabinoid the lever pushing reaction was blocked.	100
Human assay	Humans volunteers are administered cannabinoids and asked to rate how they feel under the influence of the drug (i.e using visual scale analogues)	Pyscoactive cannabinoids such as Δ^9-THC **1** were described as giving a"drug high", getting them "stoned" and volunteers were able to assess the "drug strength" and distinguish placebo.	Doses of 90mg of oral SR141716 **5** produced ~40% reduction in the visual analogue ratings of the high experience using inhaled cannabis.	101

Table 1-3 A summary of *in vivo* bioassays used to determine the activity of compounds at the CB_1.

1.3.4 The CB_2 receptor system

The peripheral CB_2 receptor was discovered in 1993 by Munro *et al.* [4] and is the second and last cannabinoid receptor discovered to date. Being the newest of the cannabinoid receptors the CB_2 receptor system has been subject to less investigation than the CB_1 system. However the CB_2 system is emerging as an attractive target for drug therapy [102,103].

The peripheral CB_2 receptor was discovered by accident during work to identify novel GPCRs expressed in human myeloid cells (human promyelotic leukaemic line HL60). One of the receptors discovered was 44% homologous (rising to 68% in the transmembrane regions) to the previously discovered CB_1 receptor[4]. The sequence identity although significantly lower than the usual 70-80% homology observed in other GPCR families, was enough to lead to the discovery of the second cannabinoid receptor. The receptor is mainly located in the peripheral cells of the immune system and has led to the speculation that the CB_2 receptor is implicated in immunological control[4,51,80]. The cellular distribution (and the methods used to determine this) of the CB_2 receptor will be discussed in section 1.3.4.1. Following its discovery in human tissue, the CB_2 receptor has been cloned from the mouse (mCB_2)[104] and the rat (rCB_2)[105 106]. The sequence homology between the mouse and human CB_2 is only 82% and the homology between rat and human is lower at 81%[105], or 57%[106] in the more recent model. There is obviously a discrepancy between these two rCB_2 receptor clones. The differences are believed to be derived from the different primers used in the Polymerise Chain Reaction (PCR) amplification step used to generate the cDNA. Griffin *et al.* generated a receptor that contained 360 amino acids (the same number as in the human CB_2 receptor and 81% homologous) which when cloned in Human Embryonic Kidney (HEK) cells bound the specific CB_2 antagonist SR144528 **6**, and other non-specific agonists (*i.e.* Win 55212-2 **3** and Δ^9-THC **1**) and showed a decrease in cAMP production upon agonist stimulation[105]. The other receptor generated by Brown *et al.* contained 410 amino acids (and was 57% homologous to human CB_2 receptor) and when transfected in CHO cells was stimulated by Win 55212-2 **3** to produce an increase in MAP Kinase[106] (Figure 1-6).

They further demonstrated that their cloned receptor was expressed in native rat spleen. Brown explained the discrepancy between the two cloned rat receptors was due to Griffin using a PCR primer that was expressed from an intron piece of rat cDNA. As a result the receptor expresses 18 amino acids not actually present, and is missing 54 amino acids that arise from an exon piece of DNA located upstream. The disparity between the two rat sequences occurs in the carboxyl tail of the receptor which is not involved in ligand binding; hence both receptors are capable of binding cannabinoids. The carboxyl tail of the human CB_2 receptor is involved in the process of receptor desensitisation through a mechanism of phosphorylation of a terminal serine residue (residue 352) promoting β arrestin internalisation[107].

From this observation it was noted that the rat receptor having a different carboxyl tail may act differently to the human receptor and researchers should be wary of extrapolating data from a rat model to human systems. Indeed, we report in chapter 5 that we found large differences in binding affinity between the rat and human CB_2 towards a particular cannabinoid ligand.

1.3.4.1 The distribution of the CB_2 receptor

The original work of Munro *et al.* assayed different organs of the rat for the CB_2 receptor and showed the presence of a cannabinoid receptor that was located on cells and tissues of the immune system. Their techniques involved Northern blot analysis of the mRNA expressed within a tissue and in-situ hybridisation of CB_2 DNA. The hybridisation was achieved using a β emitting radioactively labelled oligonucleotide (containing ^{35}S-dATP) complementary to CB_2 receptor DNA, followed by autoradiography (exposure of the tissue slice to a β sensitive film). Both of these experiments showed that the CB_2 receptor is located in the spleen; the autoradiography gave spatial information identifying CB_2 receptors in the macrophage containing marginal zone of the spleen. Just after Munro *et al.* published their ground breaking work, Lynn and Herkenham published work confirming the presence of a cannabinoid receptor in multiple lymphoid organs of the rat immune system including the spleen[108]. The technique they used was to equilibrate a β emitting radioactively labelled non-selective cannabinoid ligand [^{3}H] CP 55,940 with a tissue of interest. The tissue was then subjected to autoradiography which highlighted areas of lymphatic tissue that bound CP 55,940 **2** in a dose responsive and blockable manner.

The conclusion of their work was that binding was confined to organs that were rich in B lymphocyte cells *i.e.* the marginal zone of the spleen, lymph nodes and Peyers patches. These techniques and other similar published experiments[106,109] are extremely useful in establishing the presence of the CB_2 receptor and its location within a piece of tissue. However, in order to examine the location of the CB_2 receptor on individual immune cells, fluorescent based immunocytochemistry experiments have been conducted[96,110,111]. In these experiments antibodies were raised in rabbits against the carboxyl terminus end (intra-cellular) of the rCB_2 receptor (known as rabbit anti-rat CB_2 antibodies). These antibodies were then labelled with a fluorescently labelled secondary antibody raised against the primary rabbit antibodies, and fluorescent confocal imaging (section 1.1.2.1) was used to visualise and quantify the CB_2 receptors (Figure 1-7).

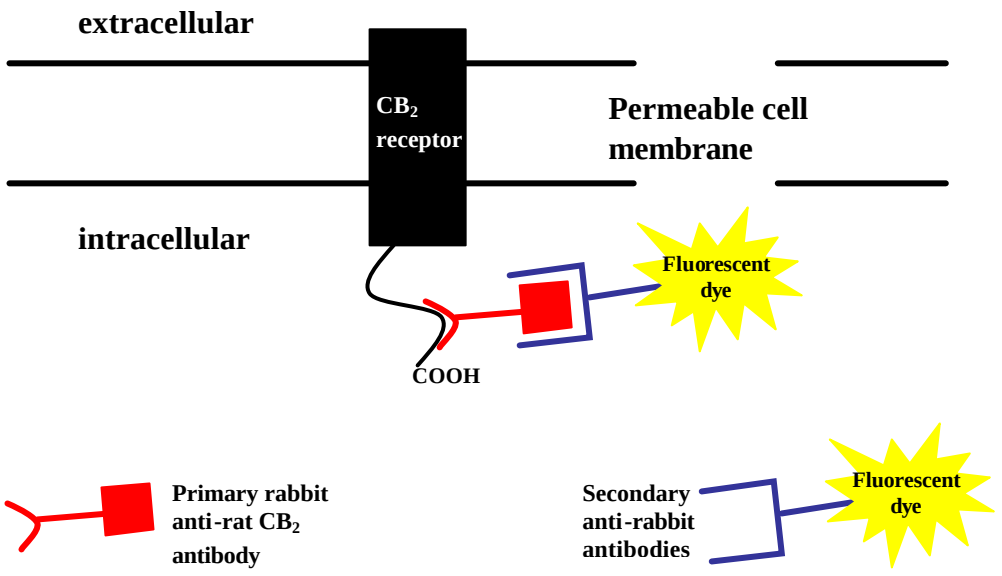

Figure 1-7 Immunocytochemistry to visualize the rat CB_2 receptor. Cells are permeabilised to allow the large Mw antibodies to gain access to the intracellular side of the receptor. CB_2 receptors are visualized by using primary antibodies raised against the rat CB_2 receptor terminal carboxylic acid sequence (these antibodies are collected by injecting rabbits with a peptide sequence corresponding to the terminal carboxyl amino acid sequence) and secondary labelling using fluorescently conjugated antibodies raised against a rabbit.

Using this immunocytochemistry approach Carayon *et al*. were able to identify that the CB_2 receptor was located in tonsil tissue and was restricted to areas of the tonsil that expressed B-cells. They were also able to estimate (from the fluorescence per cell) that there were approximately two thousand CB_2 receptors per B-cell[110]. Walter *et al*. demonstrated, using the same technique, that CB_2 receptors were located in the

lamellipodia of activated microglial cells (an immune cell) of the CNS which was the first reported detection of CB_2 receptors within the CNS[96]. It has been shown by both authors that the use of fluorescence visualization of the CB_2 receptor can give much more detailed information on the location and abundance of the receptor than can be obtained using any other technique.

The disadvantage of this technique is that the antibodies against the CB_2 receptor are difficult to produce. Rabbits must be injected with the carboxyl tail antigen for many months before they produce the CB_2 receptor antibody. The other disadvantage of using antibodies is that they are large molecular weight immunoglobulins (IgG) and cells must be fixed and permeablised in-order for them to gain access to the carboxyl terminus of the receptor. Therefore the technique is unable to detect real time processes (such as receptor re-location or internalisation) in living cells.

Our approach of designing a fluorescent ligand to the CB_2 receptor would overcome these problems and would combine the same ease of conducting an autoradiography experiment using [^{3}H] CP 55, 940 "out of a bottle", with the sensitivity of immunocytochemistry experiments on living cells/tissue.
Many different techniques have been used to determine the location of the CB_2 receptor. A summary of CB_2 receptor tissue distribution is shown in Table 1-4 and it can be seen that the locations are exclusively cells and tissues involved in immune regulation.

Cell type/Tissue	Species	Reference
B lymphocytes	Human	110,111
Macrophages	Human	111
Microglia	Rat	96
Natural Killer cells	Human	111
Peripheral mononuclear cells	Human	111
CD4 lymphocytes	Human	111
CD8 lymphocytes	Human	111
Lymph nodes	Human	111
Peyer's patches	Rat	108
Spleen	Human, rat	4,108,111
Tonsils	Human	111
Thymus	Human	111

Table 1-4 Location of the CB_2 receptors in immune cells and tissues.

The immune distribution of the CB_2 receptor has lead to its immunological effects being studied and will be discussed in the following section.

1.3.4.2 Immune functions of the CB_2 receptor

Having established that the CB_2 receptor is located on the cells and tissues of the immune system it is hardly surprising that many investigations into the immune effects of the cannabinoids have been conducted. It is outside the scope of this report to detail the exact mechanisms involved in CB_2 immune regulation, other than to comment that many authors have concluded that the action of cannabinoids acting at the CB_2 receptor induce changes in the levels of important signalling molecules. Thus cytokines (TNF-α, IL-2 etc), nitrous oxide and prostanoid production have all been shown to be attenuated by the action of cannabinoids and this results in downstream changes in immune function[102,103].

Three selected examples from the literature demonstrate the link between the CB_2 system and immune regulation.

- **CB_2 knockout mice** have been used to show that CB_2 receptors are involved in immuno-regulation. It was demonstrated that the non-specific agonist Δ^9-THC **1** (Figure 1-1) inhibited helper T-cell activation in wild type mice, but did not inhibit T-cells derived from the CB_2 knockout mice[109].
- **Increased cytokine levels in human MS patients being treated with cannabis extract** and Δ^9-THC **1** has been reported[112]. The likely mechanism of action of cannabinoids in treating MS is via attenuating immune function (MS is an autoimmune disease – see section 1.2.2.1). A small study of 16 patients demonstrated that cannabis based treatment significantly increased levels of TNFα and IL-12 in whole blood and plasma respectively compared to control. Although no direct involvement of the CB_2 system was shown (i.e. using CB_2 selective antagonists) it was suggested by the authors that changes in cytokine levels observed were due to cannabinoid activation of the CB_2 receptors located on immune cells[112]. This evidence is supported by other investigations using murine models of MS. These investigations show CB_2 selective agonists alter immune function by altering cytokine production,

immune cell recruitment and pathohistology, all direct markers in MS disease control[68,69].

- **CB_2 selective agonists are effective in reducing pain**[72,113]. The mechanism of action remains unclear but it is postulated that it is dependant upon the ability of CB_2 agonists to alter inflammatory states, such as Nerve Growth Factor induced mast cell degranulation, neutrophil accumulation in inflammatory models[113], and cytokine release from activated microglia in neuropathic pain[73]. This evidence is included to draw the reader's attention towards a common problem – the lack of any definitive mechanisms available for CB_2 mediated immune regulation. Both Zhang *et al.* [73] and Nackley *et al.* [113] make reference to exploring the phenotype of cells expressing the CB_2 receptor as crucial to elucidating the mechanism of action. However "due to the low CB_2 mRNA levels and the lack of specific CB_2 antibodies, it is not possible to perform double labelling experiments to identify conclusively the phenotype of nerve injury-induced CB_2 expressing cells"[73]. A selective CB_2 fluorescent ligand would allow researchers to achieve CB_2 labelling and generate further evidence on the mechanism in which CB_2 receptors participate in immune function.

1.3.4.3 *In-vitro* bioassay systems

A number of well established and defined *in-vitro* assays are available to test experimentally whether a compound has affinity and activity at the CB_2 receptor.

1.3.4.3.1 Binding assays

The classical displacement binding assay is capable of determining to what degree a know concentration of a test compound is capable of displacing a know concentration of radiolabelled cannabinoid from a preparation containing CB_2 receptors. The most widely used commercially available radiolabelled cannabinoid is [^{3}H] CP 55, 940 (Figure 1-13) and has approximately equal affinity for both CB_1 and CB_2 receptors (it is also the probe of choice in CB_1 binding assays)[80]. It is noteworthy that there is no radiolabelled CB_2 selective agonist or antagonist currently commercially available. Due to the unspecific nature of CP 55, 940 **2** the membrane used for binding must

contain only CB_2 receptors. For this reason the spleen (see 1.2.4.1) is chosen when using primary tissue or transfected cell lines can be used that express a specific species (i.e. rat or human) of CB_2 receptor. Common cell types for this purpose are Human Embryonic Kidney (HEK)[105,114] or Chinese Hamster Ovary (CHO) cells[106].

1.3.4.3.2 [^{35}S] Guanosine-5'-O-(3-thiotriphosphate) binding

The [^{35}S] Guanosine-5'-O-(3-thiotriphosphate) ([^{35}S] GTP-γ-S) bioassay exploits the coupling of CB_2 receptors to G-proteins (section 1.3.1). It relies on the increase in G-protein affinity for GTP **10** (and hence GTP-γ-S **11**, Figure 1-4) that is triggered by agonist occupation of the CB_2 receptors. The measured response is the net agonist-stimulated [^{35}S] GTP-γ-S **11** binding to the G-protein[10]. The assay, when investigating CB_2 receptors, is performed on membrane homogenates from transfected cells (CHO or HEK) expressing high levels of receptor. GTP-γ-S **11** binding for the CB_1 receptor can be performed on brain homogenate[115] or using whole brain tissue sections (giving spatial information of receptor localization via autoradiography)[116] to determine CB_1 receptor activation in primary tissue. However, there are no documented literature examples where spleen (or any immune tissue) membrane homogenate or tissue sections have been used to determine GTP-γ-S binding for the CB_2 receptor in primary tissue.

1.3.4.3.3 Inhibition of cyclic AMP production

The decrease in cellular cAMP production can be exploited for the quantitative, functional bioassay of cannabinoids *in-vitro*[51]. CB_2 receptor assays are performed using transfected cell lines expressing the CB_2 receptor clone. Cells expressing CB_2 receptors naturally (e.g. mouse spleen cells and human lymphocytes) are relatively insensitive to cannabinoid induced inhibition of cAMP production[80].

1.3.4.3.4 Practical difficulties

One practical difficulty in conducting assays using cannabinoid compounds is their high lipophillicity and low water solubility. As such compounds first have to be dissolved in either ethanol or dimethyl sulphoxide (DMSO) to give a stock solution, which can be diluted in the final aqueous test solutions containing Bovine Serum

Albumin (BSA) which acts as a solubilising agent and reduces non-specific binding of the cannabinoids.

1.3.4.4 Therapeutic indications of the CB_2 receptor

As previously discussed in section 1.2.2 the CB_2 receptor has emerging importance in a number of disease states. These disease states and the evidence of CB_2 involvement will be briefly introduced.

1.3.4.4.1 Pain

It is well documented that cannabinoid agonists exert antinociceptive effects (section 1.2.2.2 and Richardson *et al.*[117]). The majority of these effects are thought to be mediated by CB_1 receptors as the effect can be blocked by CB_1 selective antagonists[117]. Recently, new experiments have shown that analgesic nociception is additionally mediated via CB_2 receptors. Mice deficient in CB_1 receptors display a hypoalgesic state when treated with Δ^9-THC **1** (Figure 1-1)[118] and the analgesic effects of the endogenous cannabinoid ligand Palmitoylethanolamide can be blocked using the CB_2 selective antagonist SR144528 **6** (Figure 1-1)[119]. The work on CB_2 participation in pain control has recently been accelerated by the discovery of the selective CB_2 agonist AM1241 **58**, (Figure 1-21). This agonist has been demonstrated to inhibit experimental neuropathic pain (spinal cord ligatures)[72,73], and experimental inflammatory pain (carrageenan evoked thermal and mechanical stimuli)[113,120] without producing the problematic CNS effects associated with non-specific cannabinoids[120].

1.3.4.4.2 Multiple Sclerosis

As discussed in chapter 1.2.2.1 cannabinoids are being trialed for the treatment of multiple sclerosis (MS). Two recent discoveries have indicated that by selectively targeting the CB_2 receptor system disease symptoms and underling pathology may be controlled. The debilitating symptoms of MS, such as tremor and spasticity, were shown to be decreased in an autoimmune disease model of MS by using the CB_2 selective agonist JWH 133 **27** (Figure 1-12)[121] and increased when the animals were

treated with SR144528 **6** (which indicated that the endogenous cannabinoid system has tonic activity in MS)[67]. Using a different autoimmune model of MS, Arévalo-Martin *et al.* demonstrated that the selective CB_2 agonist JWH015 **53** (Figure 1-21)[122] was able to significantly improve neurological defects in a long lasting manner[69]. Improvements in the neurological defects observed were mirrored in an improvement in motor function.

1.3.4.4.3 Immunomodulation

The location of CB_2 receptors on immune cells combined with evidence that cannabinoids can suppress the immune system serve as strong indicators that they may be a useful target for novel immunomodulatory drugs[103]. Direct evidence of non-specific cannabinoids (i.e. Δ^9-THC **1**) causing immunosuppression has been demonstrated by the increased susceptibility towards the herpes simplex virus in mice[123,124]. Whilst susceptibility to herpes virus is not a positive effect, there are many disease states that do require management using immunosuppressive therapy e.g. rheumatoid arthritis, psoriasis, organ transplant patients etc. Recent evidence has shown that the CB_2 receptor can be targeted to give clinical effects of immunosuppression. A key paper that demonstrated the link between immune regulation and CB_2 receptors described the use of CB_2 receptor knockout mice previously discussed in section 1.2.4.2. The use of CB_2 selective ligands for investigating clinically relevant immune regulation has been lacking. However, Iwamura *et al.* has recently shown that the CB_2 selective ligand JTE 907 **66** (Figure 1-22) and SR144528 **6** were capable of reducing the swelling associated with carrageenan-induced mouse paw edema in a dose dependant manner[125]. Furthermore many of the patents protecting novel CB_2 selective ligands are purported to be useful as anti-inflammatory, anti-allergic and immunoregulator agents[126-129].

1.3.4.4.4 Cancer

Following the discovery that anandamide **4** inhibits the proliferation of human breast cancer cell lines *in vitro,* via a CB_1 receptor mediated mechanism[130], researchers have become interested in exploiting cannabinoids as novel anticancer agents. The first reported CB_2 mediated anti-tumor activity was reported by Sánchez *et al.*[131]. They

were able to show that the highly aggressive glioma tumor could be inhibited by intra-tumourally administered JWH 133 **27** (Figure 1-12), and this effect was blocked by SR144528 **6** but not by SR141716 **5**. They also demonstrated a correlation of the severity of biopsied human tumours with CB_2 receptor expression within the tumor, using immunofluorescence techniques discussed in 1.3.4.1. The authors comment that that the CB_2 receptor might serve as a diagnostic marker of glial cell proliferation/malignancy. Hence any fluorescent ligand generated via our own research could be evaluated for this role. Further work using the selective CB_2 agonist JWH015 **53** (Figure 1-21) in treating cancers of the immune system (i.e. leukemia and lymphomas) has shown that it was effective at causing significant apotosis in these immune cell lines[132]. The non-specific agonist Δ^9-THC **1** (Figure 1-1), which also caused apotosis, was partially blocked by the co-administration of SR144528 **6** (Figure 1-1) adding evidence that the effect was mediated at least partially via CB_2 receptors. Others have demonstrated that the over expression of the CB_2 receptor in leukemic cell lines acts as an oncoprotein and postulate that further work into the role of the CB_2 receptor may open new ways into the treatment of acute myloid leukemia[133]. Although the evidence is sparse and the mechanisms unclear the potential of the CB_2 receptor mediated anticancer actions is an area worthy of further exploration.

1.4 Ligands for the cannabis receptors

In considering a suitable CB_2 selective ligand that can be successfully labelled with a fluorescent dye it is necessary to consider the cannabinoids that already exist, and review them in terms of their suitability for conjugation with a large molecular weight fluorescent dye. The final construct should also retain a high affinity to the CB_2 receptor, retain selectivity towards the CB_2 over the CB_1 receptor, and be chemically suitable in terms of the conditions employed in the *in-vitro* biological environment. The consideration for the fluorescent dye will be considered in section 2.2.4.

To fit these criteria the CB_2 selective ligands were considered for their following properties.

- High affinity towards the CB_2 receptor (i.e. $K_i \leq 20$ nM)
- High CB_2/CB_1 selectivity (≥ 20)
- Chemically stable to hydrolysis, light and enzymatic degradation
- Structure Activity Relationship (SAR) that provides evidence that the ligand can tolerate molecular extension and bulky substituents
- Structure that allows its synthesis outside the Misuse of Drugs Act

There are a number of different chemical types of ligands that have affinity towards the cannabinoid receptor and some of these chemicals have been mentioned previously (**1** –**8**, Figure 1-1). For the purposes of this review it is useful to segregate cannabinoids into one of five chemical classes using a method modified from Khanolkar *et al.*[134] which is illustrated in Figure 1-8 using some examples of drugs already discussed.

For each class of compound the principal ligands will be introduced, general SAR will be discussed and the CB_2 selective ligands will be considered in greater detail with a view for modification with fluorescent dyes. For a more thorough review of CB_1 selective ligands cannabinoid readers are directed towards some excellent review articles[134-140].

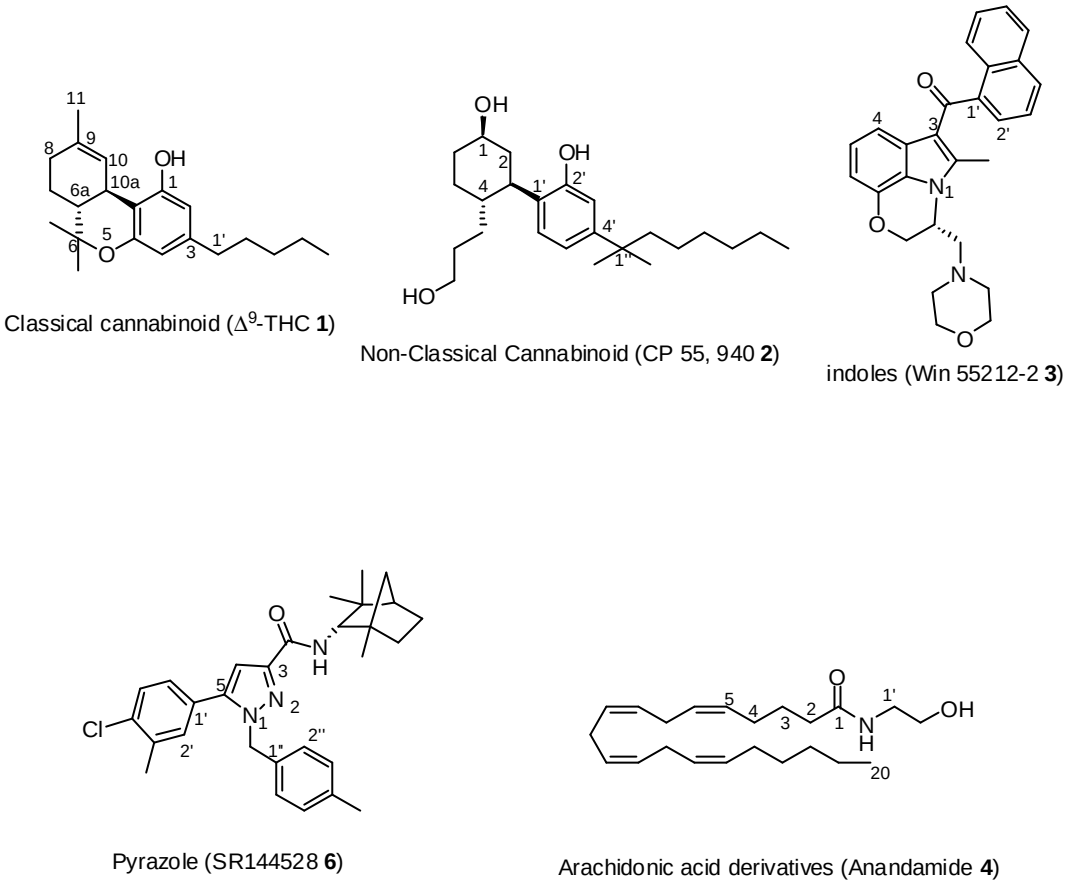

Figure 1-8 Chemical classes of cannabinoids showing the numbering systems employed.

1.4.1 Nomenclature

The naming of cannabinoid compounds can be extremely confusing, as often historical trivial names are used over the systematic IUPAC[‡] names and many of the chemical ligands with biological activity are known by codes (i.e SR144528 **6**) given by their discovering inventor/company.

The naming of compounds in this report will use the common trivial and code names most often found in the majority of the scientific literature, as even the IUPAC itself concedes that trivial names "…are useful, and in many cases indispensable"[141]. Some examples of the complexity of the systematic name and their trivia/code name equivalent are given in Table 1-5.

[‡] International Union of Pure and Applied Chemistry.

Trivial/code name	IUPAC name
Δ^9-THC **1**	(6a*R*)-6,6,9-trimethyl-3-pentyl-(6a*r*,10a*t*)-6,7,8,10a-tetrahydro-6*H*-benzo[*c*]chromen-1-ol
Win 55212-2 **3**	(*R*)-(+)-{2,3-dihydro-5-methyl-3[(4-morpholinyl)methyl]pyrrolo(1,2,3-de)-1,4-benzoxazin-6-yl}(1-naphthalenyl)methanone
SR144528 **6**	*N*-[(1*S*)-endo-1,3,3-trimethyl bicyclo[2.2.1] heptan-2-yl]-5-(4-chloro-3-methylphenyl)-1-(4-methylbenzyl)-pyrazole-3-carboxymide

Table 1-5 Examples of trivial and code names and their systematic equivalent. The systematic name was obtained by searching for the structure of the compound in the Beilstein database BS0304AE and using the systematic IUPAC name found.

The similarity between abbreviated coded names only relates to the discovering inventor/company and not to the chemical or pharmacological class of compound. Thus JWH015 (**53**, Figure 1-21) is a member of the indole class whilst JWH133 **27** (Figure 1-12) is a member of the classical cannabinoid class. Similarly SR141716 **5** is a CB_1 antagonist whilst SR144528 **6** is a CB_2 antagonist. A list of the common abbreviations and their origins are given in Table 1-6.

Abbreviation	AM	CP	HU	JTE	JWH	O	SR	Win
Description	**A**lexandros **M**akriyanis, University of Connecticut, Storrs, USA	**C**entral **P**fizer	**H**ebrew **U**niversity, Jerusalem, Israel	**J**apan **T**obacco Inc. Japan	**J**ohn **W**. **H**uffman, Clemson University, South Carolina, USA	**O**rganix Inc. USA	**S**anofi **R**echerche. Later Sanofi Winthrop now Sanofi-Synthelabo	Stirrling **Win**throp Inc. Later Sanofi-Winthrop now Sanofi-Synthelabo

Table 1-6 Common abbreviations used to name cannabinoid compounds and the explanation of the abbreviation.

The numbering of cannabinoid compounds is shown in Figure 1-8 and is used as an important descriptor when describing the SAR of a compound. In this report a semi systematic approach is taken when dealing with derivatives of known compounds. For example the addition of a nitro group to the 3' of Win 55212-2 **3** would result in a compound named 3'-nitro-Win 55212-2 **12** (Figure 1-9).

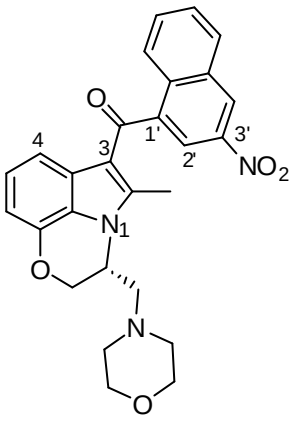

3'-nitro-Win 55212-2 **12**

Figure 1-9 Example of a semi-systematic approach to nomenclature

Finally in cannabinoid medicinal chemistry a term which is frequently employed in the literature and within this report in discussing compounds, is the notion of North (being at the top of the page) and South (being at the bottom of the page) to describe certain functional groups or ring systems within a compound. Thus in CP 55, 940 **2** (Figure 1-13 A) the secondary hydroxyl at position 1 is known as the North Aliphatic Hydroxyl (NAH) and the primary hydroxyl terminating the propyl chain is known as the Southern Aliphatic Hydroxyl (SAH)[137].

1.4.2 Classical cannabinoids

The classical cannabinoids (CC) are based around the core tricyclic dibenzopyran structure, shown by the rings A B and C of Δ^9-THC **1 (**Figure 1-10). Other common examples of CC compounds include Δ^8-tetrahydrocannabinol (Δ^8-THC **13)** and HU210 **14** (Figure 1-10).

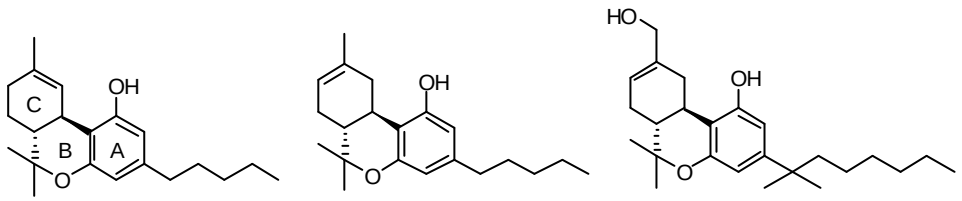

		Δ^9-THC **1**	Δ^8-THC **13**	HU210 **14**
Ki (nM)	CB_1 receptor	35 - 80	47	0.06 - 0.73
	CB_2 receptor	4 - 75	39	0.17 - 0.52

Figure 1-10 Structures of common classical cannabinoids and their K_i values (or ranges of K_i values reported)[80].

These CC are not selective ligands and show nanomolar affinity to both CB_1 and CB_2 receptors. Researchers concur that the SAR of the CC can be dealt with by considering three key sites upon the pharmacophore[80,137,138].

- The C3 alkyl side chain domain.
- The C1 phenolic group domain.
- The C9 methyl group domain.

Each will be considered separately with particular reference given to modifications that increase CB_2 affinity or involve a large bulky subsistent (mimicking a fluorescent dye). It should be noted that analogues of Δ^8-THC **13** will be considered due to their ease of synthesis and enhanced stability relative to their Δ^9-isomers[142] which is an important consideration when extrapolating the data for intended synthetic purposes.

1.4.2.1 The side chain

The hydrophobic alkyl side chain is a key pharmacophore in the CC. An alkyl chain of between 3 to 7 carbon units is required for activity[138]. The addition of dimethyl groups (located at position (1',1') or (1',2')) on a heptyl chain is optimal for overall activity, although no selectivity between CB_1 and CB_2 receptors is gained[143]. This is clearly demonstrated in the case of 3-(1',1'-dimethylheptyl)-Δ^8-THC **16** where the K_i falls from 22 to 0.49 for the unsubstituted heptyl compound **15** at the CB_1 receptor[144] (Figure 1-11). Other approaches to modify the side chain are detailed below and in Figure 1-11.

- **Halogenated alkyl chains**, such as a 5'-iodopentyl chain **17** have led to modest increase in affinity to CB_1 receptors[145].
- **Unsaturated bonds and 1' substituents** have been used to conformationally define the alkyl chain. Thus, Papalatis *et al*. have shown that dithiolane at 1' **18**, and later a 1'cyclopropane derivative of 3-heptyl-Δ^8-THC increased the affinity to both the CB_1 and CB_2 receptors but showed no enhancement of selectivity.[146,147]. Dithiolane at position 1' also increased affinity to the cannabinoid receptors when pentyl derivatives of Δ^8-THC were assessed[148].

Although the derivatives were synthesised to impart rigidity to the side chain, the increased cannabinoid affinity observed maybe due to 1' steric bulk interacting with a binding domain present within both receptors[147].

- **Constraining the side chain**, using two or three carbon bridges to lock C1' or C2' of the side chain to C2 or C4 of the phenolic ring, lead to a decrease in activity at both CB_1 and CB_2 receptors and gave no selectivity towards either receptor[149,150].
- **Replacement of the alkyl chain with bulky cyclic groups** has been demonstrated to increase receptor affinity, whilst producing a moderate increase in CB_2 selectivity[148,151]. Use of a cycloheptyl group **19**[148] or a phenyl group **20**[151] gave a 4 fold and 13 fold selectivity towards the CB_2 receptor respectively.

In conclusion, side chain manipulations often result in compounds with enhanced affinity towards both cannabinoid receptors. The most promising modification, with respect to finding a lead compound with CB_2 selectivity, incorporates a bulky substituent (mimicking a fluorescent dye), comes from compounds **19** and **20**. However, to date only simple hydrocarbon groups have been evaluated and not larger heterocycles (of which most fluorescent dyes are chemically similar to – section 2.2.4), and the resulting CB_2 selectivity is not as large as would make the compounds useful for our purposes.

1.4.2.2 The phenolic group

Use of the 3-(1',1'-dimethylheptyl) group provides the "magic bullet"[137] for improving receptor affinity and therefore the majority of phenolic modifications have been conducted upon 1',1'-dimethylheptyl-Δ^8-THC **15** analogues.
Until recently it was thought that the phenol group at C1 was essential for cannabimimetic activity[80]. It is now accepted that the phenol group can be removed (in 1-deoxy analogues) or masked as the ether/ester and still retain an affinity towards the cannabinoid receptors, often with increased affinity towards the CB_2 receptor[137]. Gareau *et al.* demonstrated that the 1-methoxy and 1-deoxy analogues of 1',1'-dimethylheptyl-Δ^8-THC (**21** & **23**, Figure 1-11) displayed less affinity to the

cannabinoid receptors but enhanced selectivity towards the CB_2 receptor (1-methoxy **21** K_i CB_1=16 μM & CB_2=20 nM and 1-deoxy **23** K_i CB_1=250 nM & CB_2=21 nM)[144]. Larger groups such as the diacetoxyphosphate ester **22** (Figure 1-11) however lowered the affinity at the CB_2 receptor. At around the same time Huffman *et al.* reported that 1-deoxy versions of HU210 **14** and 3-(1',1'-dimethylheptyl)-Δ^8-THC **15** also exhibited CB_2 selectivity. Further work by, Song and Bonner, and Huffman *et al.*, used 3D molecular modelling to postulate that the residue Lys192, present in TM 3, of the CB_1 receptor forms important interactions with the phenol group present in CC and non-classical cannabinoids (section 1.4.3) and if this residue is mutated, or the phenol group is removed or masked, then the binding to the CB_1 receptor is reduced[152,153]. The analogous lysine residue in the CB_2 receptor (Lys109) has been shown by mutational analysis not to be involved in important interactions with the phenolic group of the CC and hence the compounds still show high affinity to this receptor[154]. The application of modifying the phenol group to produce selective CB_2 ligands will be discussed in 1.4.2.4. Modifications to the phenol group introducing bulky substituents have been published[155]. Derivatives of Δ^8-THC include biphenyl **24**, aminoalkyl chains **25** and morpholinoalkyl ethers **26** (Figure 1-11). Work was carried out in 1991, before existence of the CB_2 receptor was confirmed and hence the compounds were assayed only against the CB_1 receptor (using rat brain homogenate). All of the compounds suffered large decreases in binding affinity with EC_{50} (concentration of compound capable of displacing 50% of the radiolabelled CP 55, 940 **2**) in the μM range. To the best of our knowledge the compounds have never been assayed in CB_2 receptor assays.

1.4.2.3 The 9-methyl group

The main observation relevant to this report is that when the 9-methyl group present in Δ^9 or Δ^8-THC is oxidized to the hydroxymethyl group (as occurs during human metabolism of Δ^9-THC **1**) the affinity of the resulting compound is increased[80]. The most common demonstration of this effect is with the compound HU210 **14** (11-hydroxy-(1',1'-dimethylheptyl)-Δ^8-THC).

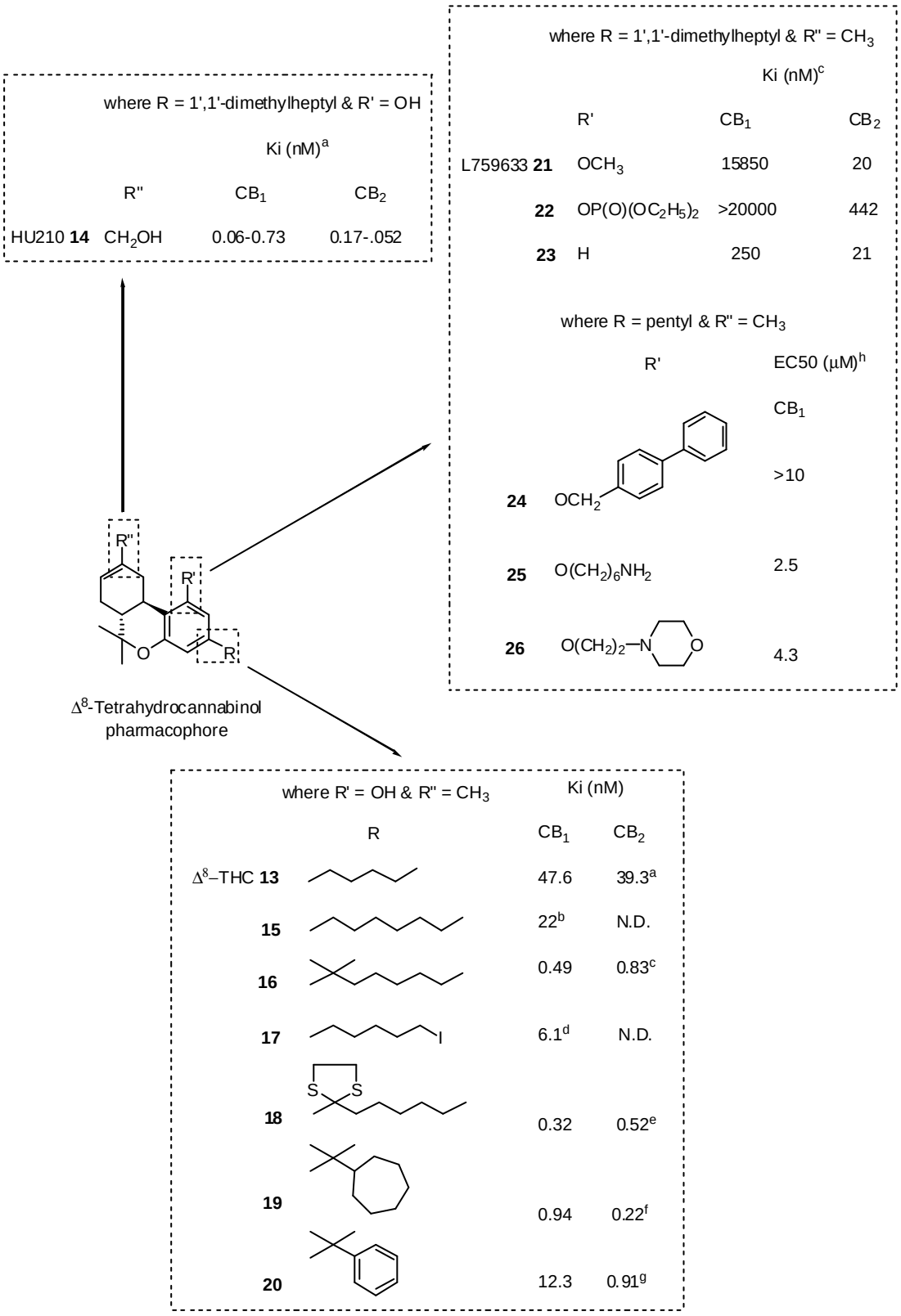

Figure 1-11 SAR of Δ^8-THC analogues modifying the C1, C3 and C9 position. Abbreviations - a ref. 80 b ref. 156 c ref. 144 d ref. 134 e ref. 146 f ref. 148 g ref. 151 h ref. 155 ND not determined.

It incorporates the "magic bullet"[137] of the 1', 1' dimethylheptyl side chain and gains increased affinity to both the CB_1 and CB_2 though the hydroxyl group at C11 (range of reported K_i CB_1 0.06-0.73 & CB_2 0.17-0.52 nM)[137]. Further oxidation of the methylene to the aldehyde abolishes all cannabinoid activity[137].

1.4.2.4 CB_2 selective classical cannabinoids

The work generated by Gareau *et al.* and later by Huffman *et al.* showed that Δ^8-THC analogues devoid of a C1 phenol group led to compounds with high CB_2 selectivity and good CB_2 affinity[144,153]. The compound 3-(1',1'-dimethylheptyl)-1-methoxy-Δ^8-THC (L759633, **21**) (Figure 1-11 & Figure 1-12) displayed the best CB_2 profile with a K_i of 15850 & 20 nM at CB_1 & CB_2 respectively[144]. The actual K_i and large selectivity shown by L759633 **21**, has been disputed by other authors, where lower CB_2 affinity and selectivity have been reported (K_i CB_1 941 & CB_2 65 nM[121] and K_i CB_1 713 & CB_2 57 nM[157]), however they have all demonstrated that it was CB_2 selective compound.

Work by Huffman and co-corkers to further exploit these findings led them to synthesise a number of 1-deoxy-(1',1'dimethylalkyl)-Δ^8-THC analogues to explore the nature of the side chain requirements to improve CB_2 affinity[121]. This study revealed that short alkyl chain lengths decreased CB_1 binding at little or no expense to CB_2 binding affinity whilst the opposite was true for longer alkyl chain lengths[121]. The optimum compound for affinity and selectivity was found to be 3-(1',1'-dimethylbutyl)-1-deoxy-Δ^8-THC (JWH133, **27,** Figure 1-12) which displayed a K_i of 677 & 3.4 nM at CB_1 & CB_2 receptors respectively[121]. In a later study Huffman assessed the effect of introducing C11 hydroxyls (known to increase cannabinoid affinity – section 1.4.2.3) and masking the C1 hydroxyl group of 3-(1',1'-dimethylalkyl)-Δ^8-THC[157]. The resulting 11-hydroxy analogues gave higher affinity compounds at both CB_1 and CB_2 receptors as expected, but with no overall gain in terms of CB_2 affinity versus selectivity[157]. Again side chain SAR demonstrated that shorter alkyl chains were optimum for CB_2 affinity. The optimum compound selected from the 16 different analogues was 3-(1',1'-dimethylpentyl)-1-methoxy-Δ^8-THC (JWH229, **28**, Figure 1-12) which exhibited a K_i at the CB_1 receptor of 3134 nM and at the CB_2 receptor of 18 nM[157].

It was shown that in both of these studies affinity and selectivity for the CB_2 receptor could not be quantitatively assessed by opting for a specific C3, C1 and C9 substituent, but rather each of these groups affected the other. As Huffman himself comments in his thorough review of this topic "…development of preliminary SAR for 1-deoxy-cannabinoids, was achieved, although to a limited extent"[135].

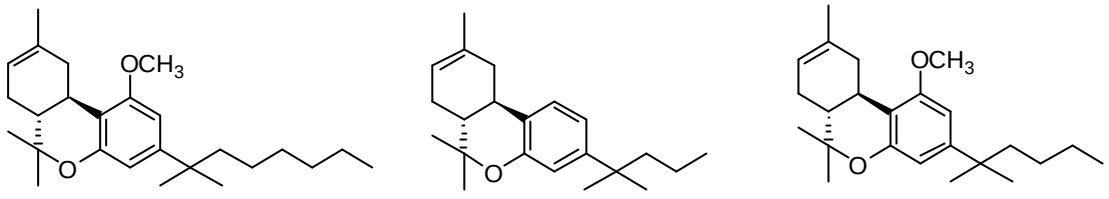

L759633 **21** JWH133 **27** JWH229 **28**

Figure 1-12 The structures of selective CB_2 classical cannabinoids

The evidence presented highlights that CC's attain a high selectivity and affinity towards the CB_2 receptor with analogues containing short C3 alkyl side chains and simple C1 deoxy- or methoxy- motifs. There is little evidence to convince us that a large bulky fluorescent dye could be incorporated onto a CC to produce a CB_2 selective ligand. Combined with the need to acquire a Home Office license (and the associated strict working guidelines) for working with Δ^8-THC it was felt that the CC template would be unsuitable for the initial work into generating fluorescent CB_2 ligands.

1.4.3 Non-classical cannabinoids

The Non-Classical cannabinoids (NCC) are a group of CC like compounds that lack the pyranoid B ring (Figure 1-1). In their quest for improving the analgesic properties of cannabinoid compounds, scientists at Pfizer started to modify the dihydropyran ring of THC type compounds. The resultant compound, Levonantradol (CP 50,556, **7,** Figure 1-1), which entered into human clinical trials (section 1.2.2.2), demonstrated that the pyran ring of THC was not required for cannabinoid activity. Subsequently the Pfizer group synthesized a number of compounds lacking the pyranoid B ring[48]. Two compounds emerged from their endeavors that are of interest; CP 55,940 **2** and CP 47,497 **29** (Figure 1-13 A). CP 47,497 **29** represents the prototypical compound of

the A-C bicyclic series and CP 55,940 **2** (in its tritiated form – see Figure 1-13 B) is the most widely used radiolabelled cannabinoid used to study CB_1 and CB_2 receptor binding.

It is well established that CP 55,940 **2** (and its radiolabelled counterpart) have high affinity at both the CB_1 and CB_2 receptor with K_i values of between 0.5-5.0 and 0.69-2.8 nM respectively[51,80]. However despite extensive SAR studies conducted on analogues of CP 55,940 **2** and CP 47,497 **29** concerning *in-vitro* and *in-vivo* CB_1 pharmacology the ability of the these analogues to interact with CB_2 receptors remains to be established[80,158].

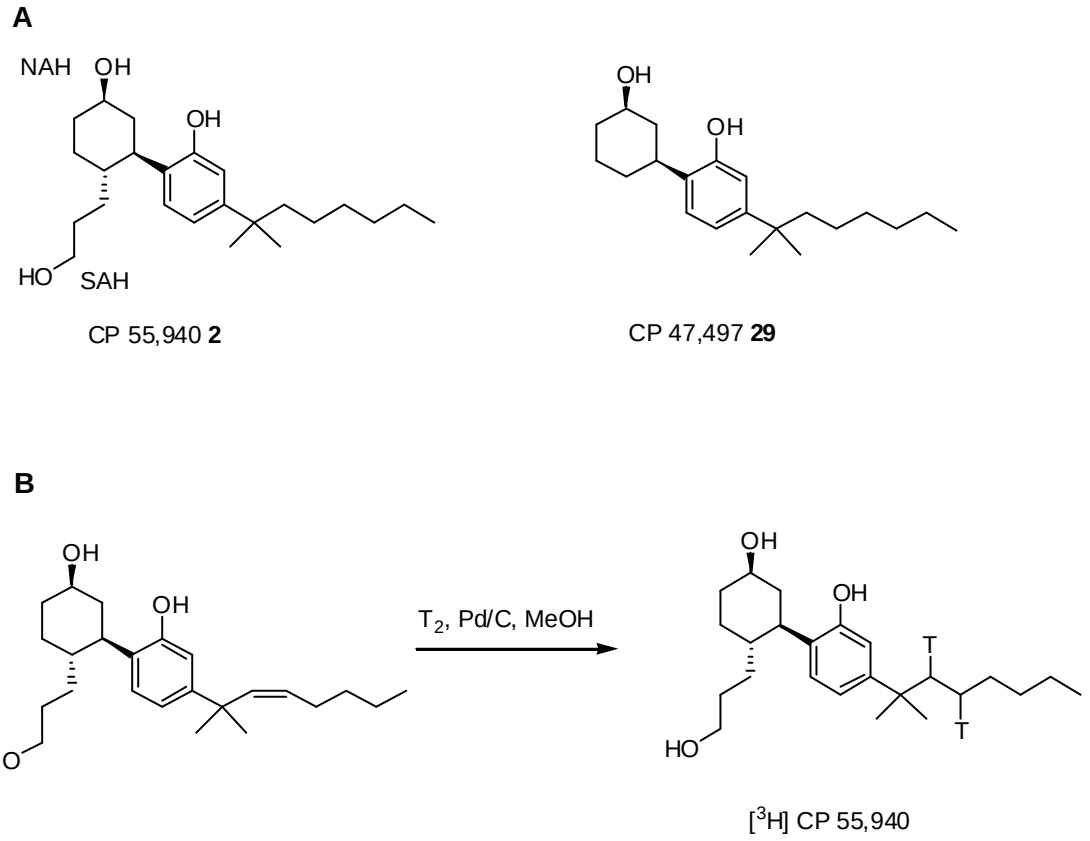

Figure 1-13 (A) The structures of two typical NCC. NAH Northern Aliphatic Hydroxyl. SAH Southern Aliphatic Hydroxyl. (B) The synthesis of tritiated CP 55,940, the most common radiolabelled cannabinoid[159].

The SAR conducted on NCCs for the CB_1 receptor shows very similar trends to those found for CC ligands (see - 1.4.2).

- C4' 1',1'-dimethyl substituted side chain of between 5 and 7 carbon units is optimal for CB_1 binding[158].
- The 2'-deoxy analogues still retain affinity at the CB_1 receptor although it is decreased by ~40 fold[158].
- The NAH at C1 can be removed with the compound retaining cannabinoid activity *in-vivo*[158].
- Other SAR explored the cyclohexanol ring size and the substituent at C4 of CP 47,497 **29** analogues. Of the 26 analogues examined, CP 55,940 **2** remained the most potent analogue, however ring sizes up to cyclooctanol and C4 short chain alkyl groups (up to a butyl chain), with or without functionalized termini (ether, 1° amine, amide, hydroxylamine), were all well tolerated with little affect upon CB_1 affinity (all analogues retained CB_1 affinity of <15 nM)[158].

To the best of our knowledge, the effect of modifying NCCs with bulky substituents has not been published, however it is prudent to comment that due to the NCCs exhibiting structural and SAR similarities to the CC the placement of bulky substituents on an NCC is likely to have similar effects to those shown by the CC (section 1.4.2). The stereochemical requirements for the NCC are the same as for the CC with the natural stereochemistry of Δ^9-THC (6a*R*, 10a*R*) being required in NCCs (3*R*, 4*R*) to give optimum CB_1 binding [80,158]. A further stereochemical requirement that is present within the NCC pharamacophore is the requirement of the NAH to be β to the cyclohexane ring[134]. The likely biological binding conformation of CP 55,940 **2** (and conformationally restricted analogues of it), determined by NMR and computational studies, has been postulated to have the NAH, the SAH and the phenol hydroxyl all on the upper face of the conformer giving the molecule an amphipathic nature (Figure 1-14)[160,161]. Therefore to be on the same face as the other two hydroxyls the NAH must be in the equatorial conformation.

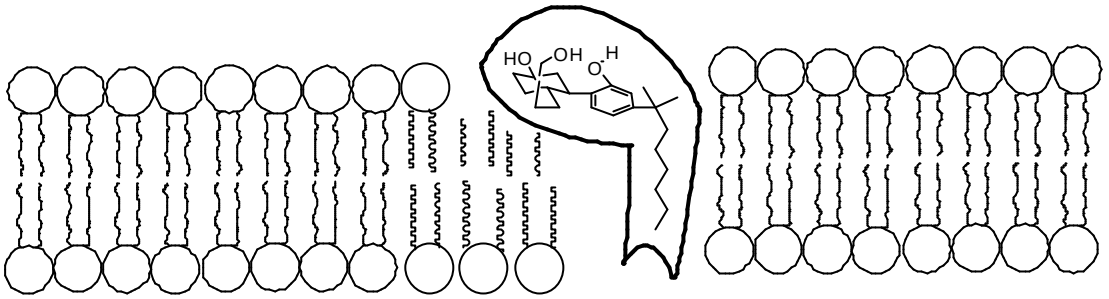

Figure 1-14 A ligand-membrane-receptor hypothesis model for CP 55,940 **2** binding to the cannabinoid receptor adapted from reference 160.

1.4.3.1 CB_2 selective non-classical cannabinoids.

The first report of a CB_2 selective NCC ligand appeared in the literature in 1999 from the Mechoulam group based at Hebrew University[162]. The compound, code-named HU308 (**30**, Figure 1-15), showed agonist properties at the CB_2 receptor with a K_i of 23 nM. HU308 **30** exhibited little affinity to the CB_1 receptor (K_i >10 μM). The compound was first synthesized 9 years previously as part of the group's investigations into the stereochemistry requirements/synthesis of Δ^8-THC derivatives[163]. Thus, their rational for designing this type of compound to be CB_2 selective is not included in the 1999 report other than to say that the dimethoxy groups in HU308 **30** are based on the increase in CB_2 selectivity shown by the methyl ether derivatives of CC such as L759633 (**21** Figure 1-12); a CB_2 selective ligand. Later Huffman *et al.* synthesized a pyridone analogue of CP 47,497[164]. The resulting distereoisomers of the pyridone analogue **31** and **32** (Figure 1-15) were found to have similar high affinities at the CB_2 receptor (**31** 56 & **32** 50 nM) and lower affinities at the CB_1 receptor (**31** 973 & **32** 1054 nM). This result was surprising as it was known that an α-NAH in NCCs does not bind as well as the β conformation and yet both of these compounds (**31** and **32**) bound equally well (section 1.4.3). This result may be explained by these novel compounds adopting a different binding confirmation to that of CP 55,940 **2** and CP 47,947 **29** in the receptor. The CB_2 selectivity of **31** & **32** described may be attributed to them being equivalent of 1-deoxy-Δ^8-THC analogues such as JWH133 (**27**, Figure 1-12) and posess selectivity for similar reasons as described in section 1.4.2.4.

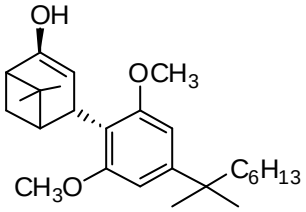

HU308 **30**

(Ki CB_1 >10μM, CB_2 23nM)[a]

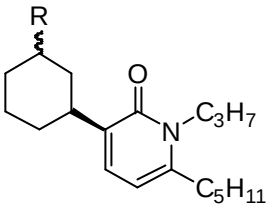

31 R =  (Ki CB_1 973nM, CB_2 56nM)[b]

32 R =  (Ki CB_1 1054, CB_2 50nM)[b]

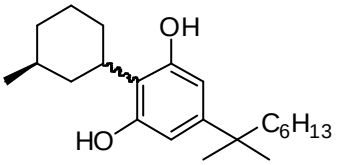

O1826 **33**

(Ki CB_1 40nM, CB_2 1nM)[c]

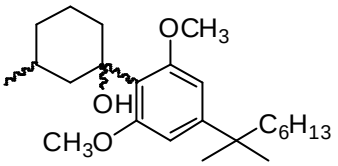

O1966A **34**

(Ki CB_1 5055nM, CB_2 23nM)[c]

Figure 1-15 The structure and *in-vitro* binding affinity of CB_2 selective NCC. a ref. 162, b ref. 164, c ref. 165.

One large study into the SAR of NCC at the CB_2 receptor used phenol and resorcinol benzenoid rings with various carbo/heterocyclic moieties to generate 41 analogues which were subjected to pharmacological testing[165]. The two examples shown in Figure 1-15 are the potent CB_2 selective compound O1966A **34** and its phenol equivalent O1826 **33**. The authors acknowledge, for compound **34**, that there was a mixture of distereoisomers but gave no further details. These two compounds convey the main findings of this study, *i.e.* masking of the phenol groups as methoxy ethers **34** had the biggest effect on CB_2 selectivity. Of the range of carbo/heterocyclic groups assessed, the cyclohexane ring with a methyl group at C3 and a hydroxyl at C1 (compound **34**) gave the optimum compounds with respect to CB_2 affinity and selectivity[132].

Overall the NCCs show a similar SAR to those observed for the CC ligands (section 1.4.2). It is therefore with similar reasoning that we feel that this class of compound is not suitable to modify with bulky fluorescent dyes to generate high affinity CB_2 selective ligands.

1.4.4 Arachidonic acid derivatives

Arachidonic acid derivatives are the natural ligands for the cannabis receptor. Anandamide **4** (Figure 1-16) was isolated and discovered in 1992 and was shown to be the first of the endogenous ligands to the cannabis receptors[54]. Subsequently a further four arachidonic acid based natural ligands, 2-arachidonoylglycerol **35**[166], 2-arachidonylglyceryl ether (Noladin ether, **36**)[167], Virodhamine **37**[168], and *N*-Arachidonoyldopamine **38**[169], have been postulated as endogenous cannabinoid ligands (Figure 1-16). The roles, biosynthesis and deactivation of this family of endocannabinoids is outside the scope of this thesis and readers are directed to an excellent review on these topic[170]. All of the endocannabinoids are ligands at both the CB_1 and CB_2 receptors with a preference of affinity towards the CB_1 receptor[80]. The published literature concerning synthetic analogues of arachidonic acid have all reported compounds which show selectivity towards the CB_1 receptor[171-175]. Combined with the fact that anandamide is photolabile[§] this class of compound is not suitable for labelling with fluorescent dyes to generate CB_2 selective fluorescent ligands.

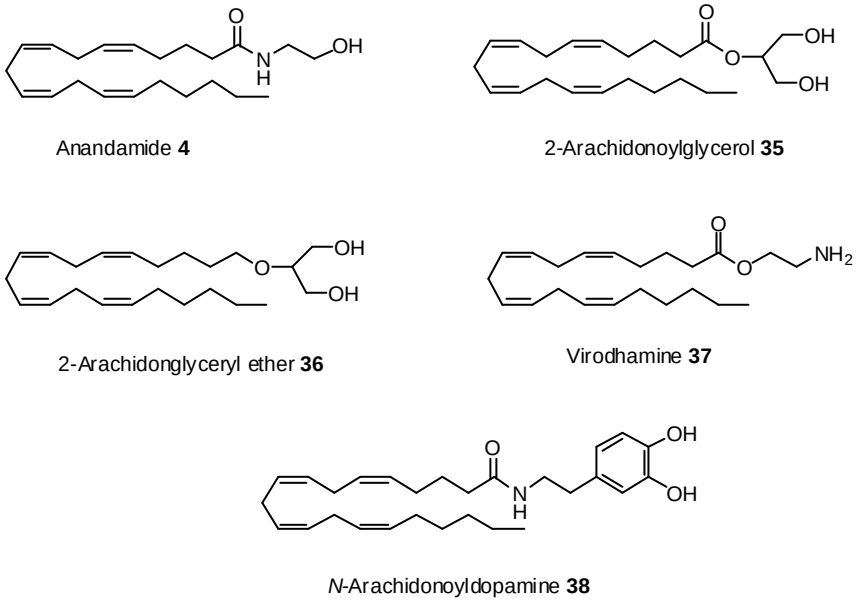

Figure 1-16 Chemical structures of arachidonicAcid cannabinoid ligands.

[§] Although no experiments investigating the photodegradation of Anandamide have been published the commercial suppliers of Anandamide (Tocris) advise in their summary of Product Characteristics "Protect from light". This appears prudent advise when considering that Polyene systems such as Anandamide are well known for their ability to absorb light (i.e. the pigments Retinal & β Carotene)

1.4.5 Pyrazole cannabinoids

The pyrazole class of cannabinoids exhibits the only known antagonist/inverse agonist behavior upon binding to the cannabinoid receptors[80]. The prototypical members of this class are the Sanofi compounds SR141716 **5**[55], a potent CB_1 ligand, and SR144528 **6**[57] a potent CB_2 ligand (Figure 1-17 A & C). SAR studies on the pyrazole pharmacophore, using SR141716 **5** as the lead structure, have been extensive, concentrating on CB_1 receptor binding, and have concluded the following points:

- 3° amides, like compound **43** (Figure 1-17, B), and the replacement of amide functionality by other H-bonding acceptors/donors strongly decrease CB_1 binding affinity compared to 2° amides such as displayed by compound **42**[176,177].
- The optimum group at N1 is 2'',4''-dichlorophenyl. Replacement of this group with cycloalkanes[178], 4'-alkylphenyl moieties[177], or monochlorinated phenyls **39**[176] diminishes CB_1 binding (see Figure 1-17, A).
- The C3 amido group can tolerate replacement of the *N*-piperidine group present in SR141716 with related 5-7 membered rings or cyclohexane without altering binding affinity. Replacement of cyclic groups with linear alkyl chains led to a decrease in affinity in one study[177] but did not alter CB_1 binding in another[179].
- A bulkier substituent than hydrogen (i.e. methyl, bromine or iodine) increases CB_1 affinity in position C4[176,177].
- *Para* (4') substituted alkyl- or halo- phenyl groups all give enhanced CB_1 binding when positioned at C5[176] (Figure 1-17 A & B). However 4'-nitro, 4'-amino and 2'-substituted phenyls at C5 all lead to a decrease in affinity[176]. The potent CB_1 antagonist AM251 **41** was prepared by a simple replacement of the 4'-chlorophenyl group of SR141716 **5** with a 4'-iodophenyl moiety[176]. This useful analogue allows the inclusion of radioactive forms of iodine (I-123) into the synthesis of AM251 **41** which can be used for *in-vivo* imaging.

Unfortunately there are no published SAR studies on the CB_2 selective ligand SR144428 to date. We are therefore left with relatively little information to the nature

of the CB_2 affinity/selectivity exhibited by SR144528 **6** and this will be explored in section 1.4.5.1.

1.4.5.1 CB_2 selective pyrazoles

The current knowledge of the limited SAR for the CB_2 receptor is as follows:

- 3° amides decrease CB_2 affinity (Figure 1-17 B)[176].
- *N*1 substituents consisting of 4''-monosubstituted phenyl **6** and 3''-methylcyclohexyl **40** rings show an increase in CB_2 binding and a decrease in CB_1 binding[176] (Figure 1-17, A & C). This observation is shown in the structure of SR144528 **6** with a 4''-methylbenzyl group replacing the 2'', 4''-dichlorphenyl of SR141716 **5**.
- Hydrogen at position C4 is optimal for CB_2 binding as shown in the structure of SR144528 **6**. However it has recently been shown that a methylene bridge connecting C4 to the neighbouring aromatic residue at C5 significantly increases CB_2 affinity and selectivity[180]. This is likely to be due to increased rigidity within this molecule, rather than steric factors (see below)[180].

The SAR for the CB_2 selective pyrazole cannabinoids has been extremely sparse. There have been no published accounts of any modifications which have incorporated bulky groups or alkyl linker chains. The most interesting set of compounds that incorporated these features, required in fluorescent dye conjugation, were unfortunately not tested with CB_2 receptors[177].

The most important discovery since SR144528 **6**, was published in 2003 by Mussinu *et al.* after we had concluded our own studies[180]. Their group reported the synthesis and pharmacological testing of a number of novel 1,4-dihydroindenol[1,2-*c*]pyrazole based CB_2 selective ligands (Figure 1-17 D). They used a common medicinal chemistry approach of introducing a conformational restriction into analogues of SR141716 in an attempt to permit the ligand to bind with high affinity and selectivity to a desired receptor[181].

A

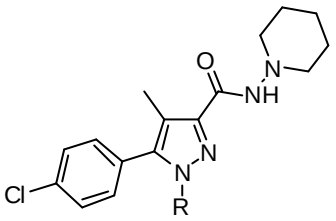

		R	Ki (nM) CB_1	Ki (nM) CB_2
SR141716A	**5**	2",4"-dichlorophenyl	12	1640[a]
	39	4"-chlorophenyl	60	836[a]
	40	3"-methyl-cyclohexyl	494	281[b]

B

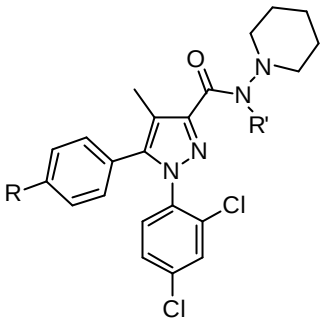

	R	R'	Ki (nM)[a] CB_1	Ki (nM)[a] CB_2
AM251 **41**	I	H	8	2290
42	Br	H	12	1010
43	Br	CH_3	77	1260

C

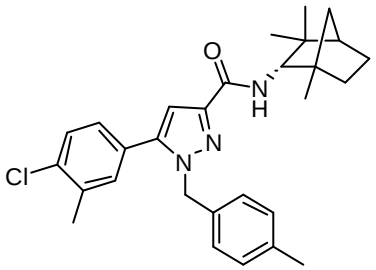

	Ki (nM)[c] CB_1	Ki (nM)[c] CB_2
SR144428 **6**	400	0.6

D

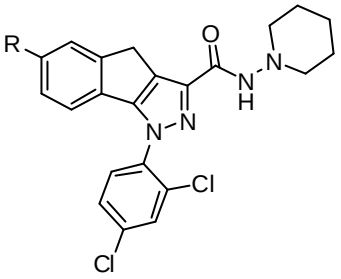

	R	Ki (nM)[d] CB_1	Ki (nM)[d] CB_2
44	Cl	2050	0.34
45	CH_3	363	0.04

Figure 1-17 The structure and *in-vitro* pharmacology of the pyrazole cannabinoids. A) The effect of the N1 substitution. B) The effect of amide substitution and halogen exchange. C) The prototypic CB_2 ligand SR144528. D) The novel 1,4-dihydroindenol[1,2-*c*]pyrazole CB_2 selective cannabinoids. a. ref 176 b. ref 178 c. ref 57 d. ref 180.

Their discoveries were evidence that the rigid 1,4-dihydroindenol derivatives showed extensive selectivity towards the CB_2 receptor even when the substituents at N1, C3 and C5 were previously thought to confer CB_1 selectivity. Thus the rigid analogue of SR141716 **44** has >6000 fold CB_2 selectivity with a sub-nanomolar K_i of 0.34 nM and their 6-methyl analogue **45** is the most potent and selective CB_2 ligand described to date (Figure 1-17 D). Unfortunately molecular modelling studies undertaken with SR144528 **6** showed that the 1,4-dihydroindenol methylene bridge would be located deep within CB_2 receptor binding pocket, pointing down towards the intra-cellular

side[182]. This is an unsuitable locus for manipulation since the fluorescent dye should be located away from the receptor (*i.e.* on the extracellular face) so as to minimise perturbation of ligand-receptor interactions. According to Gouldson's model the site with most potential for modification would be the 4''-benzylic methyl group of SR144528 which lies towards the top of the receptor pocket[182].

However, up until we concluded our studies, the lack of CB_2 receptor SAR for the pyrazoles meant that using the template of SR144528 **6** as a lead compound for conjugation with a fluorescent dye would be difficult in regards to fluorescent dye placement.

1.4.6 Indole based cannabinoids

The indoles were the first class of cannabimimetics that were not structurally related to Δ^9-THC. Researchers at Stirling Winthrop reported a new family of indoles which possessed cannabinoid properties[52]. Constrained analogues of the non-steroidal anti-inflammatory drug Pravadoline **46** (Figure 1-18) were synthesized which exhibited reduced inhibition of the cyclo-oxygenase enzyme but increased affinity to the CB_1 receptor[53]. R-(+)-Win 55212-2 **3** (Figure 1-18) has been the most studied compound arising from this program. It displays high stereospecific affinity for both the CB_1 and CB_2 receptor with a K_i range of 1.89-123 nM and 0.28-39.3 nM respectively[80]. Most studies show that Win 55212-2 **3** exhibits a modest selectivity in favour of the CB_2 receptor[80]. The key structural features necessary for high CB_1 binding have been summarized by the authors in a large SAR study which evaluated 125 non-constrained analogues of Win 55212-2 3 **3**[183]. They concluded;

- A bicyclic (preferably 1-naphthoyl) substituent is required at C3 of the indole.
- A small substituent (or better no substituent) is required at C2 of the indole.
- An aminoethyl (preferably morpholinoethyl) substituent is required at N1 of the indole which lead to the early generic name for this series of compounds to be aminoalkylindole (AAI).

Compound **47** (Figure 1-18) is the resultant compound which has nanomolar displacement values at the CB_1 receptor.

However this model SAR has now been superceded by other developments which have shown that the N1 aminoethyl group can be replaced with simple *n*-alkyl chains[184] such as JWH007 **48** and the indole structure can be simplified to a pyrrole **49**[185] or an indene **50** [186] structure with the compounds retaining cannabinoid properties (Figure 1-18).

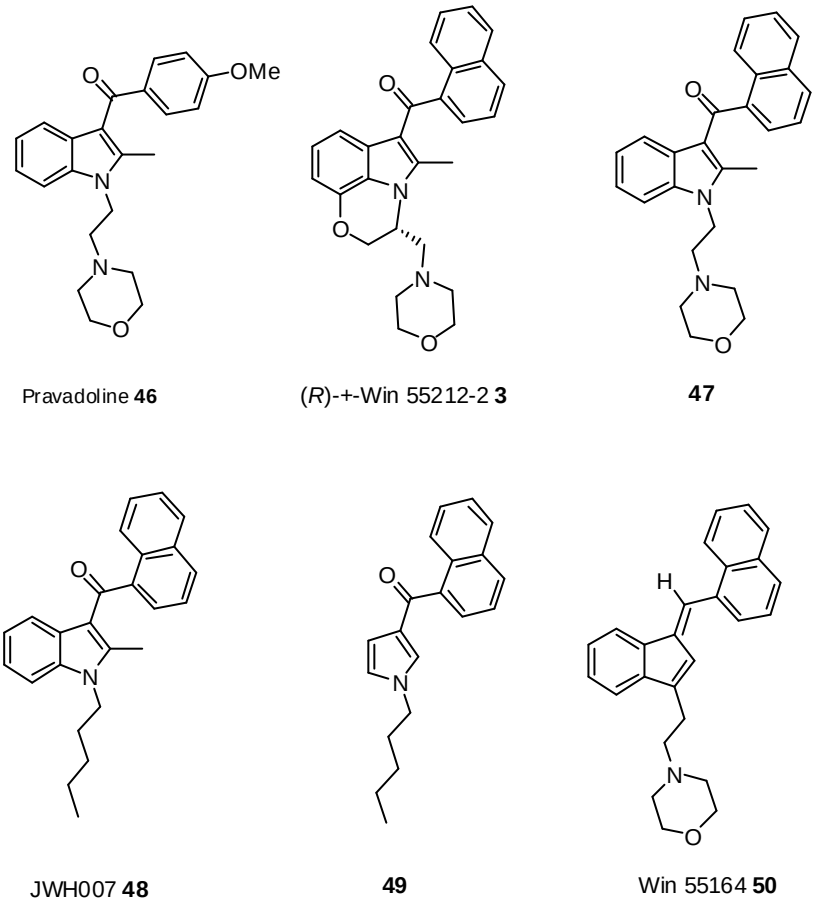

	Ki (nM) CB_1	CB_2
Pravadoline **46**	2511	NR[a]
Win 55212-2 **3**	1.9-123	0.3-39[b]
47	16	NR[a]
JWH007 **48**	9.5	2.9[c]
49	87	NR[d]
Win 55164 **50**	2.7	2.7[e]

Figure 1-18 The structures and *in-vitro* pharmacology of indole based cannabinoids. a ref. 187 b range of values given ref. 80 c ref. 122 d ref. 188 e ref. 189. NR not reported.

1.4.6.1 Modeling studies on indoles

The intimate ligand-receptor interactions of the indole cannabinoids has been studied to a greater depth than for any other class of compound and this makes them an interesting class of cannabinoids to interrogate using molecular modelling to guide the choice of fluorescent dye placement. A short summary of the modelling studies performed to date will be considered.

Early studies simply superimposed the AAI pharmacophore over the structure of Δ^9-THC by aligning the naphthyl ring of the AAI over rings B & C of Δ^9-THC, the carbonyl group of the AAI over the C1 phenol of Δ^9-THC, and the N1 substituent of the AAI was aligned with the C3 side chain of Δ^9-THC, illustrated in Figure 1-19. From the proposed model, indole analogues with simple N1 *n*-alkyl chains instead of aminoalkyl chains and simplified pyrrole analogues were synthesized and screened and showed that binding to the CB_1 receptor was retained[184,188].

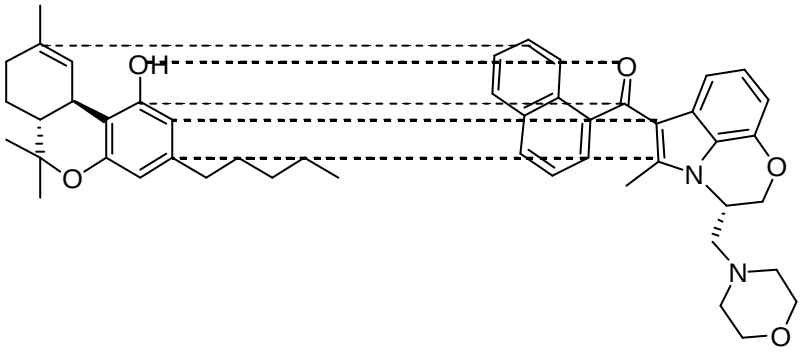

Figure 1-19 The suggested alignment of CCs with indole based cannabinoids proposed by Huffman *et al*[184].

Later receptor mutational[152] and docking[190] studies indicated that there could be divergence within the binding site of Win 55212-2 **3** from that of other classes of cannabinoid ligand, therefore the structural superimposition of AAI with Δ^9-THC giving rise to the cannabimimetic 1-*n*-alkly indoles and the pyrrole series may have been serendipitous.

The binding conformation and the amino acid residues involved in indole-receptor interactions have been reported. The bioactive conformation of the indole cannabinoids was determined in one study by Reggio *et al.* to be in the s-*trans* form. The s-*trans* form results in the aryl system lying close the indole C2 and the carbonyl

oxygen lying near to the indole C4 (Figure 1-20).They demonstrated that the rigid AAI mimic (*E*)-Naphthylideneindene (which is the rigid s-*trans* form of Win 55212-2 **3**) bound with greater affinity to the CB_1 and CB_2 receptors than the (*Z*)-isomer[189] (Figure 1-20).

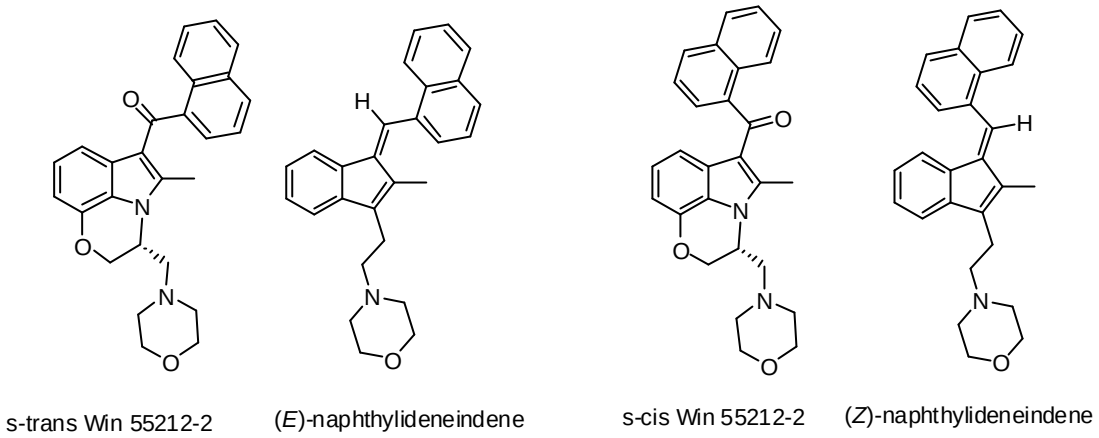

Figure 1-20 Relationship between the s-*trans* and s-*cis* conformers of Win 55212-2 and the respective rigid *E* and *Z* indenes.

Directly contrasting this result was a later publication by Xie *et al.* which used 2D NMR and molecular dynamics experiments to demonstrate that the low energy conformation of Win 55212-2 **3** in solution was in fact the s-*cis* form[191] (Figure 1-20). We will report in chapter 6 our findings concerning the binding conformation of Win 55212-2 **3** obtained from molecular modelling studies.

Many independent studies have demonstrated that the indoles bind to the cannabinoid receptors primarily by aromatic stacking interactions. SAR determinations detailed in 1.4.6 show that 3-naphthoyl indoles *c.f.* 3-benzoyl indoles and indoles *c.f.* pyrroles exhibit increased binding to the cannabinoid receptor mirroring the increase in aromatic character exhibited by these compounds[183,188]. Further SAR studies involving the (*E*)-Naphthylideneindene[186,189] and the completely hydrocarbon based 1-pentyl-indene[192] demonstrate that the major interactions of binding at the cannabinoid receptor are aromatic and Van Der Waals. Molecular modelling has also been used to show the type and location of the interactions taking place between the indole cannabinoids and the receptor. Chin *et al.* was able to determine that TM 3 plays an important role in the selectivity of some of the indole cannabinoids for the CB_2 receptor by generating a hybrid CB_1 receptor that contained TM 3 of the CB_2 receptor. These hybrid receptors were capable of binding the indoles

Win 55,212-2 **3** and JWH015 (**53**, Figure 1-21) with greater affinity than the wild type CB_1 receptor[193]. A single point mutation experiment which altered a non-conserved CB_2 Phenylalanine residue (F197) to the corresponding CB_1 amino acid Valine demonstrated through computer modelling analysis, that F197, as part of an aromatic cluster in TM 3-4-5, was crucial in the selectivity of Win 55212-2 for the CB_2 receptor[194]. Molecular modelling experiments using the global minimum energy conformations of several 3-Indolyl-1-naphthylmethanes and 3-(1-naphthoyl)indole compounds, into an activated CB_1 receptor model, have also shown that these molecular structures bind by aromatic stacking interactions with residues present in TM 3-4-5-6[192].

In summary, molecular modelling and SAR techniques have been used by a number of independent researchers to give a model of the indole cannabinoids binding to the cannabinoid receptor. The models show that 3-substituted indoles bind primarily through aromatic stacking interactions with residues within TM 3-4-5-6. In addition, the CB_2 selectivity of these compounds may be inferred by a phenylalanine residue (F197) only present in the CB_2 receptor which can form an extra aromatic-aromatic interaction with the indole structure.

1.4.6.2 CB_2 selective indoles

The first indole cannabinoid ligand which showed significant CB_2 selectivity was the prototypical compound Win 55212-2 **3**[135]. Although most published data demonstrates that Win 55212-2 **3** is selective towards the CB_2 receptor, the results also show that the compound has high affinity for the CB_1 receptor[80,135]. Further exploitation of the SAR generated two compounds L768242 **51** and JWH015 **53** (Figure 1-21) which demonstrated high affinity and selectivity for the CB_2 receptor. Gallant *et al.* generated several compounds of the L768242 **51** type by switching the substitution pattern of the aroyl and morpholino groups from the established 3-aroyl-1-aminoalkyl to 1-aroyl-3-aminoalkyl[195]. They demonstrated that the *N*1-(2, 3-dichlorobenzoyl) group had as high an affinity to the receptors as *N*1 naphthoyl substitution, suggesting that the dichlorophenyl was isosteric to the naphthyl system. The Huffman group synthesized JWH015 **53** (Figure 1-21) in 1994 based on the alignment of indole with Δ^9-THC shown in Figure 1-19, however it was only shown

to be CB_2 selective in 1996 when it was first tested in membranes containing CB_2 receptors[196]. SAR of this type of *N*-alkylindole has been extensive; however no bulky substituents have been evaluated for effects on the pharmacophore scaffold. The SAR on this type of compound can be summarized as follows:

- The optimum *N*1 substituent for CB_2 selectivity is *n*-propyl. Smaller alkyl groups abolish binding at both receptors, whilst extending the chain length up to *n*-hexyl increases CB_2 affinity but at the expense of selectivity[122]. This can be shown in the compounds **48**, **52**, and **53** (Figure 1-21). Heptyl chains, as in **55**, start to decrease affinity at both receptor types. This trend fits the hypothesis that the nitrogen of the indole is equivalent to the C3 side chain of CC as shown in Figure 1-19, as in the CC a short C3 side chain is optimum for CB_2 selectivity (see - 1.4.2.4).
- Methyl substitution at C2 of the indole leads to compounds with increased affinity at the CB_2 receptor[122]. This is illustrated by the difference between JWH015 **53** and compound **54** which lacks the methyl group and shows a 10 fold loss in CB_2 affinity (Figure 1-21). Larger *n*-alkyl chains and branched alkyls at C2 however attenuate binding at both receptors[135].
- Substitutions on the 3-naphthoyl moiety (4-methoxy- & 7-methyl-1-naphthoyl substituents were evaluated) gave compounds with similar selectivity and affinity to the unsubstituted naphthoyl analogues[122,135].

Other CB_2 selective indoles have recently been published in the literature. Bristol Myers Squibb developed a range of 3-amido substituted indoles based on evidence of CB_2 selectivity shown by the indole cannabinoids and the amide containing Japan Tobacco cinnamides[126]. Their studies produced a number of CB_2 selective ligands shown in Figure 1-21 and generated some interesting SAR for the purposes of designing fluorescent labelled CB_2 ligands[197].

- The C3 amido aromatic amino acid of **56** could be replaced with non-aromatic amide groups retaining CB_2 affinity (although CB_1 affinity was not reported)[197].

- Chiral discrimination was observed in compound **56** as its enantiomer showed minimal CB_2 binding[197].
- Inclusion of a C7 methoxy group in **56** increased CB_2 affinity from 250 nM to 8 nM[197].
- The C3 amido functionality was further developed to contain the bulky (*S*)-fenchyl group (as used in SR144528 **6,** Figure 1-17). Compound **57** demonstrated that the molecular space within the receptor at C3 was able to accommodate large bulky substituents[197] (Figure 1-21).
- Derivatives of **57** where the substitution at N1 was varied indicated that simple *n*-pentyl chain gave the highest CB_2 affinity (5 nM), CB_1 binding was not reported as the compound showed little activity in an *in-vivo* inflammatory model[197].
- C2 derivatives of **57** showed that the methyl or hydrogen substituent was optimal for CB_2, with larger alkyl groups reducing CB_2 affinity[197].

An interesting CB_2 selective indole AM1241 **58** (Figure 1-21), with *in vivo* activity, has recently been reported in a patent[198] and in subsequent pharmacological papers[72,73,113,120]. The compound has shown promising results in various pain models when used *in vivo* (see - 1.3.4.4.1). The compound has a bulky 2-iodo-5-nitrobenzoyl substituent at C3 and utilizes a *N*-methylpiperidinyl group at N1. In order to retain CB_2 binding the stereochemistry of the N1 substituent must retain the *R* configuration which is also a requisite in Win 55212-2 **3**[198].

Overall the indole cannabinoids represent an excellent class of compounds for our purposes of conjugation to fluorescent dyes. Indole based cannabimimetics have nanomolar affinity and appear to show a natural selectivity towards the CB_2 receptor. They are chemically simple and stable, and appear to tolerate bulky substituents in the C3 position. We planned to exploit the established knowledge regarding ligand-receptor interactions to build an *in-silico* model which can be interrogated to provide guidance in the synthesis of novel CB_2 selective fluorescent ligands and will report our results in chapter 6.

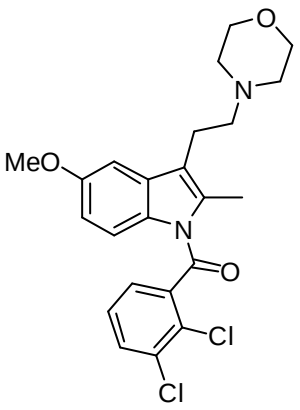

L768242 **51**

(Ki CB_1 1917nM, CB_2 12nM)[a]

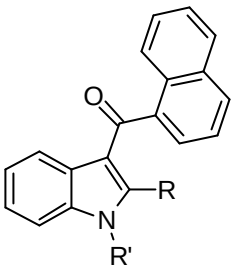

	R'	R	Ki (nM)[b] CB_1	CB_2
52	CH_3	CH_3	>10000	5050
JWH015 **53**	C_3H_7	CH_3	383	14
54	C_3H_7	H	1050	170
JWH007 **48**	C_5H_{11}	CH_3	10	3
55	C_7H_{15}	CH_3	311	141

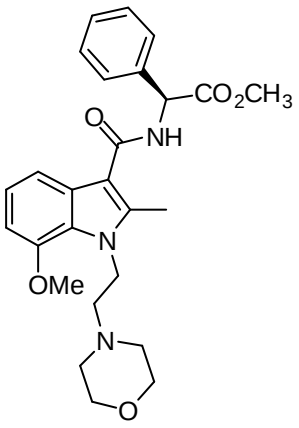

56

(Ki CB_1 4000nM, CB_2 8nM)[c]

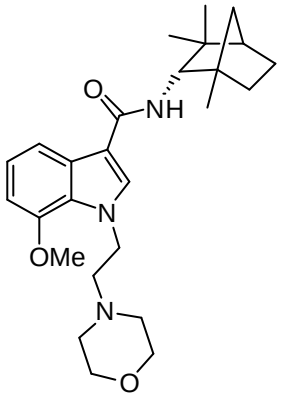

57

(Ki CB_1 380nM, CB_2 12nM)[c]

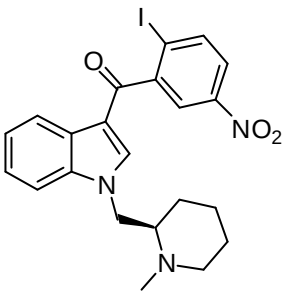

AM1241 **58**

(Ki CB_1 680nM, CB_2 2nM)[d]

Figure 1-21 The CB_2 selective indoles. a ref. 195, b ref. 122, c ref. 197, d ref. 113.

1.4.7 Japan Tobacco ligands

This set of compounds consisting of benzamides, cinnamides and heterocylic structures (Figure 1-22) are set aside from the other categories of cannabinoid ligand due to their chemical structure not fitting any of the other cannabimimetic classes detailed in section 1.4. First reported in 1997, 391 compounds, mainly consisting of substituted aromatic amides were cited. Pharmacological data demonstrating high CB_2 selectivity and affinity was reported for 32 of these compounds[126]. The patent gives

limited pharmacology data but includes K_i binding values from rat cerebellum and spleen membranes. Detailed pharmacology on compound JTE907 (**66**, Figure 1-22), which is similar in structure to compounds from their original patent, was reported elsewhere in which JTE907 **66** was shown to have inverse agonist properties at the CB_2 receptor. In addition, it displayed a variable K_i value in human, mouse and rat CB_2 receptors of 36, 1.6, and 0.4 nM respectively[125]. Independent testing of the binding affinity of one other member of the Japan Tobacco compounds was reported by the Bristol Myers Squibb company in 2002. Compound **61** (R=OH) exhibited a 100 fold increase in K_i value in their human CB_2 receptor assay compared to the K_i obtained from the rat CB_2 receptor reported in the original patent (Figure 1-22)[197]. These patterns of receptor species differences in the Japan Tobacco compounds were not evident when we embarked on our investigations however we will be reporting on these differences in chapters 4 and 5.

The Japan Tobacco compounds possessed excellent diversity in the chemical structures and groups tolerated whilst retaining high CB_2 selectivity and affinity. The compounds still remain today the most selective and high affinity ligands to the CB_2 receptor reported. The key SAR to these compounds can be summarized as follows:

- Amide type functionality attached either directly to a benzenoid ring (as in **62**-**65**, Figure 1-22) or positioned through a 2 carbon linker which allows conjugation between the amide and benzenoid ring (as in cinnimides **59**-**61**, & **66**, Figure 1-22) is observed in each of the compounds.
- An *n*-pentyl chain which is *meta* to the amide connection to the benzene ring is observed in all of the active compounds. The *n*-pentyl chain is connected to the benzene ring through a heteroatom (O, N and S).
- The position *para* to the amide connection to the benzene ring can accommodate long chain alkyls attached to the ring through a heteroatom.
- An *N* -ethylaromatic moiety is a preferred substituent on the amide group. The aromatic group observed was mainly tyramine based although in compounds **60**, **61** (R=H), **65**, and **66** show that the phenol group is not essential for binding.

The Japan Tobacco compounds represent a lead set of compounds for derivatisation with fluorescent dyes. Their large CB_2 affinity and selectivity should allow modifications with fluorescent dyes resulting in fluorescent CB_2 ligands. The SAR they display shows tolerance to long alkyl chains on the benzamide ring as demonstrated by compound **62** and **65,** and they can tolerate a wide range of structural diversity on the *N*-amide substituent as demonstrated in compounds **61**, **64**, **65**, and **66**. It is for this reason that the Japan Tobacco compounds represent the class of compounds that we feel most likely to tolerate modifications to allow conjugation to fluorescent dyes and we will report on our investigations in chapters 2, 4 and 5.

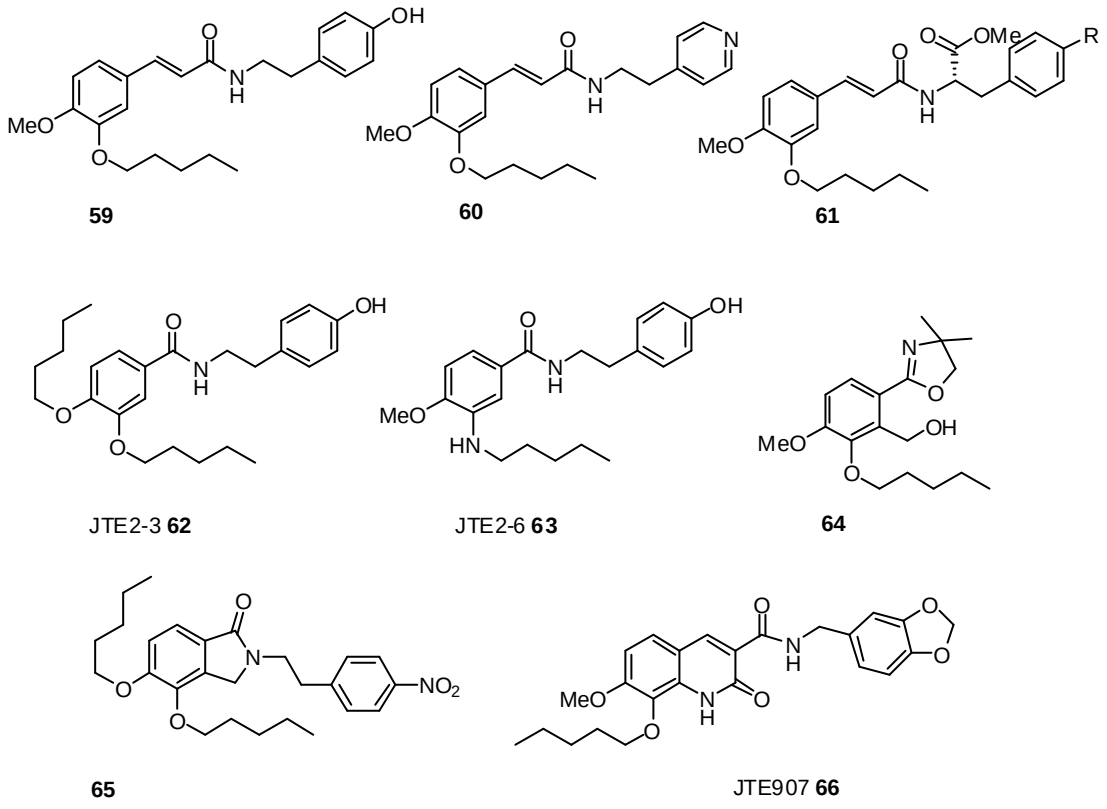

	Ki (nM) CB_1	CB_2
59	400	1.8[a]
60	3700	44[a]
61 (R = OH)	480	1.4[a] (rat receptors)
	5700	120[b] (human receptors)
61 (R = H)	>1000	86[b] (human receptors)
JTE2-3 **62**	>3300	0.4[a]
JTE2-6 **63**	500	1.1[a]
64	650	11[a]
65	2600	1.8[a]
JTE907 **66**	2370	36[c] (human receptors)
	1060	1.6[c] (mouse receptors)
	1050	0.4[c] (rat receptors)

Figure 1-22 The structure and *in-vitro* pharmacology of the Japan Tobacco ligands. a. ref 126, b ref. 197, c ref. 125.

1.5 Research aims

We aim to design and synthesize novel CB_2 ligands which are conjugated to fluorescent dyes making them suitable for use in confocal microscopy and SMD applications. By using both classical SAR and molecular modeling approaches we will interrogate cannabinoid lead structures in-order that we can locate the fluorescent dye upon the pharmacophore whilst retaining cannabinoid activity. From our extensive literature search conducted on the cannabinoid ligands we will be using the Japan Tobacco ligands and the indole cannabinoids as lead structures for conjugation to fluorescent dyes. We will report the design, synthesis and pharmacology of these ligands in subsequent chapters. As the nature of our work is directed towards the greater understanding of the CB_2 receptor we will also be reporting serendipitous results, relating to ligand-receptor binding at the CB_2 receptor, obtained through our molecular modelling and pharmacology findings. These specifically relate to an unusual species selectivity encountered with a Japan Tobacco compound and a hypothesis to how it occurs.

2 Fluorescent CB_2 ligand based on a modification to the benzamide ring of a Japan Tobacco Compound.

2.1 Background to designing a GPCR fluorescent ligand.

A review of the literature quickly determined that only one fluorescent cannabinoid ligand, SK-4-45-1 **67**, had previously been reported[20]. The ligand was a fluorescently labelled derivative of anandamide and displayed no detectable binding to the CB_1 receptor (Figure 2-1)[20]. SK-4-45-1 **67** was however recognised by the anandamide transporter system and was subsequently used to track the re-uptake of anandamide into intracellular compartments.

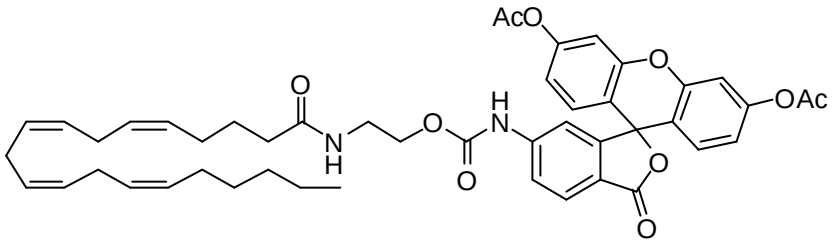

SKM 4-45-1 **67**

Figure 2-1 The structure of SKM 4-45-1 **67**. A substrate for the anandamide transmembrane carrier

Due to the inability of SKM 4-45-1 **67** to bind to the cannabinoid receptor, and the reported photo-instability and CB_1 selectivity of anandamide derivatives previously discussed in section 1.4.4 it became obvious that a novel approach to designing a fluorescent CB_2 ligand was required.

Several fluorescent ligands which bind to GPCRs have previously been reported, alongside their pharmacological data and use in various fluorescent assays. A short discussion of adenosine and serotonin fluorescent ligands will be given to introduce the reader to the concepts and decisions taken during the work described.

2.1.1 Fluorescent adenosine agonist ligands

The adenosine receptors are a class of three (A_1, A_2, A_3) GPCR receptors that have important roles in physiology and the pathology of disease[199]. They are therefore important receptors to understand and as a result selective adenosine fluorescent

ligands have been designed for use in fluorescent applications. Original work by Macchia *et al.* was able to show that attachment of a Dansyl fluorescent dye, via an alkyl linker, to N^6 of the adenosine agonist NECA **68** (Figure 2-2) proceeds with retention of A_1 receptor binding[200]. The rational in attaching the fluorescent dye in this way came from previous SAR which demonstrated that alkyl linkers, terminating in a bulky substituent at N^6 led to compounds with high affinity and selectivity at the A_1 receptor[199,201]. Macchia *et al.* assessed the effect of different alkyl chain lengths (from C3 to C12) used to tether the Dansyl molecule to the NECA ligand (**69a-f**, Figure 2-2**)**. They found that the C6 alkyl chain **69c** was optimum for A_1 binding affinity with a K_i of 27 nM determined using radioligand binding. Chain lengths of C3 **69a** and C4 **69b** gave compounds with a K_i of < 100 nM, but increasing the alkyl chain length above C6 led to incremental decreases in binding affinity; with the C12 linker compound **69f** having a binding affinity of 3400 nM. The group were able to use **69c** to visualize the A_1 receptor in rat cerebellar cortex using fluorescence microscopy. As an extension to their work they acknowledged in a subsequent publication that the Dansyl-NECA ligands could be improved by altering the fluorophore to one with a longer λ_{abs}[202]. The short λ_{abs} (340 nm) necessary to excite the Dansyl dye is known to cause problems in biological experiments due to cells and tissues autofluorescing at this wavelength[203]. Their solution was to substitute the Dansyl dye with the longer λ_{abs} dye 7-Nitrobenzofurazan (NBD, λ_{abs} 465 nm) to give compounds **70a-e** (Figure 2-2). By changing the dye the reported pharmacological profile of the compounds surprisingly changed from being A_1 selective using Dansyl to A_3 selective using NBD (see table in Figure 2-2). This result was not commented upon by the authors, but it does suggest that the choice of fluorescent dye can significantly affect the pharmacology of the conjugated ligand. An alternative explanation was that the binding assay used to determine the K_i of the NBD ligands **70a-e** utilised a radiolabelled *antagonist* instead of a radiolabelled *agonist*, which was used for the Dansyl compounds **69a-f**. Antagonists are known to switch A_1 receptors to their low affinity binding state[204] resulting in the lower K_i observed. The NBD series also demonstrated that increasing alkyl linker length resulted in compounds with increased binding affinity towards the A_3 receptor. This is opposite to the Dansyl series and may be due to differing modes of binding mechanism displayed by the two

differing fluorophores. The NBD ligand **70d** was used to visualise the A_3 receptor in CHO cells using confocal microscopy.

Our research group was interested in generating fluorescent adenosine agonists that were more suitable for use with SMD applications. Using the N^6 alkyl NECA compounds **69** & **70** discussed above as a lead molecule the boron containing fluorophore BODIPY® 630/650 was chosen as a substitute dye for Dansyl or NBD. The BODIPY® 630/650 dye was chosen as it has an λ_{abs} of 633nm producing much lower levels of cellular autofluorescence[203]. It also displays high molecular brightness, is subject to low photobleaching rates and has a low percentage of triplet states; important factors in SMD (section 1.1.2.2.1)[205]. Commercially available BODIPY® 630/650 is only available with a C6 alkyl chain already incorporated onto the dye[206], therefore a short alkyl linker of 4 carbon units was incorporated at the N^6 position and conjugated to the BODIPY® 630/650 dye to produce **71**[207]. This ligand was shown in a reporter gene efficacy assay, quantified through Luciferase expression, to have equivalent potency to the high affinity A_1 agonist N^6-cyclopentyl adenosine (CPA)[207]. Initial displacement binding studies on this ligand at the A_1 receptor has shown it to have a biphasic binding curve with a detectable low affinity binding K_i of 22 μM. This is 100 fold less potent than NECA, but due to the antagonist radioligand binding assay used it is likely to be reporting on the binding to A_1 receptors in the low affinity binding state - in a similar way to the results from the NBD series of drugs. The BODIPY-NECA compound **71** has been successfully used in SMD and single cell applications[207].

We have successfully applied the same methodology used for **71** to fluorescently label the endogenous ligand adenosine[25]. Thus adenosine was modified with a N^6 aminobutyl tether and conjugated to BODIPY® 630/650 to give **72** (Figure 2-2). This ligand shows similar efficacy to the agonist NECA **68** using a cAMP sensitive secreted placental alkaline phosphatase (SPAP) reporter gene assay[25]. Agonist activity of adenosine was retained and the results from radioligand competition binding studies are awaited. The BODIPY-adenosine ligand **72** has been used in confocal microscopy and FCS experiments to report on the location and function of the A_1 receptor[25].

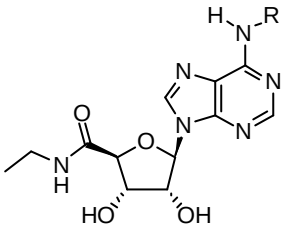

NECA **68** R = H

69 R = 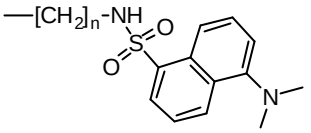

a: n=3; **b**: n=4; **c**: n=6; **d**: n=8; **e**: n=10; **f**: n=12

***In-vitro* Radioligand binding data**

compound	n	Ki (A_1, nM)	Ki (A2, nM)	Ki (A_3, nM)
68	N/A	200[a]	15[a]	8.2[a]
69a	3	42[a]	4300[a]	1800[a]
69b	4	70[a]	9500[a]	2000[a]
69c	6	27[a]	4300[a]	3600[a]
69d	8	111[a]	>10000[a]	252[a]
69e	10	234[a]	>10000[a]	1100[a]
69f	12	3400[a]	>10000[a]	2500[a]
70a	2	>10000[b]	6750[b]	56[b]
70b	4	>10000[b]	>10000[b]	381[b]
70c	6	>10000[b]	6083[b]	24[b]
70d	8	3476[b]	5096[b]	7.4[b]
70e	10	6350[b]	6100[b]	28[b]
71	4	22000[c]	N/D	N/D

70 R = 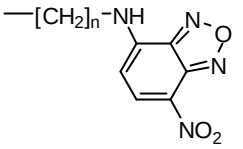

a: n=2; **b**: n=4; **c**: n=6; **d**: n=8; **e**: n=10;

71 R = 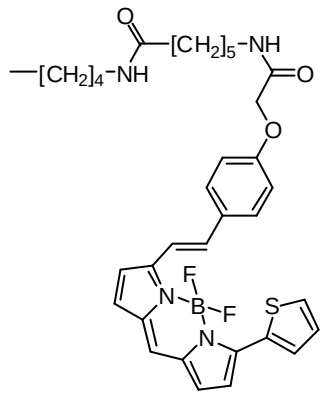

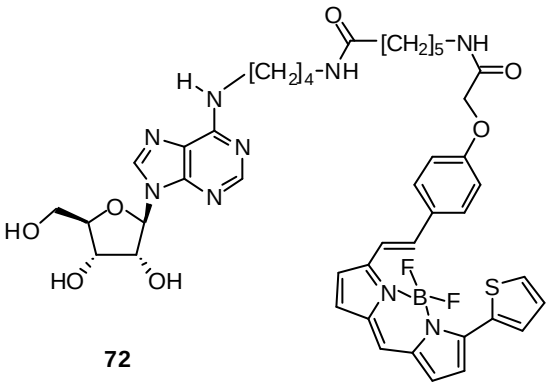

72

Figure 2-2 The structure and K_i values of fluorescent adenosine agonists. a ref. 200, b ref. 202, c ref. 208

2.1.1.1 Synthetic strategy used for fluorescent adenosine agonists

Compounds **69**-**71** were synthesised by an amine substitution of a common 6-chloropurine **73** intermediate. The differences in the synthesis of the Dansyl, NBD and BODIPY® ligands relate to when the fluorescent dye was introduced into the molecule as shown in Scheme 2-1.

In the synthesis of the Dansyl ligands the Dansyl dye was pre-conjugated with the alkyl linker and the amine group of the alkyl linker was reacted with the 6-chloropurine **73** to give the acetonide intermediate. The acetonide was hydrolysed using aqueous acid to yield the final ligands **69a-f** (Scheme 2-1, A). The disadvantage of this technique is that in-order to displace the 6-chloropurine **73** the fluorophore is exposed to the forcing conditions of refluxing in EtOH. Also this method relied upon deprotecting the acetonide using acid hydrolysis in the presence of the fluorophore. This method is inappropriate for labelling with labile fluorophores.

The methodology used to synthesise the NBD ligands **70a-e** overcame the synthetic flaw of exposing the dye to forcing chemical conditions by using mono-Boc protected diaminoalkyl linkers. The linker was installed without the fluorophore, and de-protection of the Boc group exposed the1° amine which was conjugated to the NBD fluorophore(**74**, Scheme 2-1, B). The acetonide protection was kept in place during the conjugation as NBD-Cl can react with hydroxyl functional groups. Acetonide de-protection, was carried out in the presence of the NBD fluorophore, however this procedure would affect acid sensitive fluorophores if they had been used.

The synthesis of the BODIPY® ligand **71** (Figure 2-2) utilised methodology that produced intermediate **75**, which was suitable for conjugation with any amine reactive fluorescent dye and avoided the need for further chemical manipulation (i.e. de-protection) once the fluorophore was installed. By using the commercially available BODIPY® 630/650 activated as the succinimidyl ester (OSu) we were able to label selectively at the 1° amine without affecting the free hydroxyl groups present on the molecule[209,210]. Compound **71** was purified by preparative TLC. Similar methodology was also employed successfully in the synthesis of the fluorescent adenosine ligand **72** (Figure 2-2)[25].

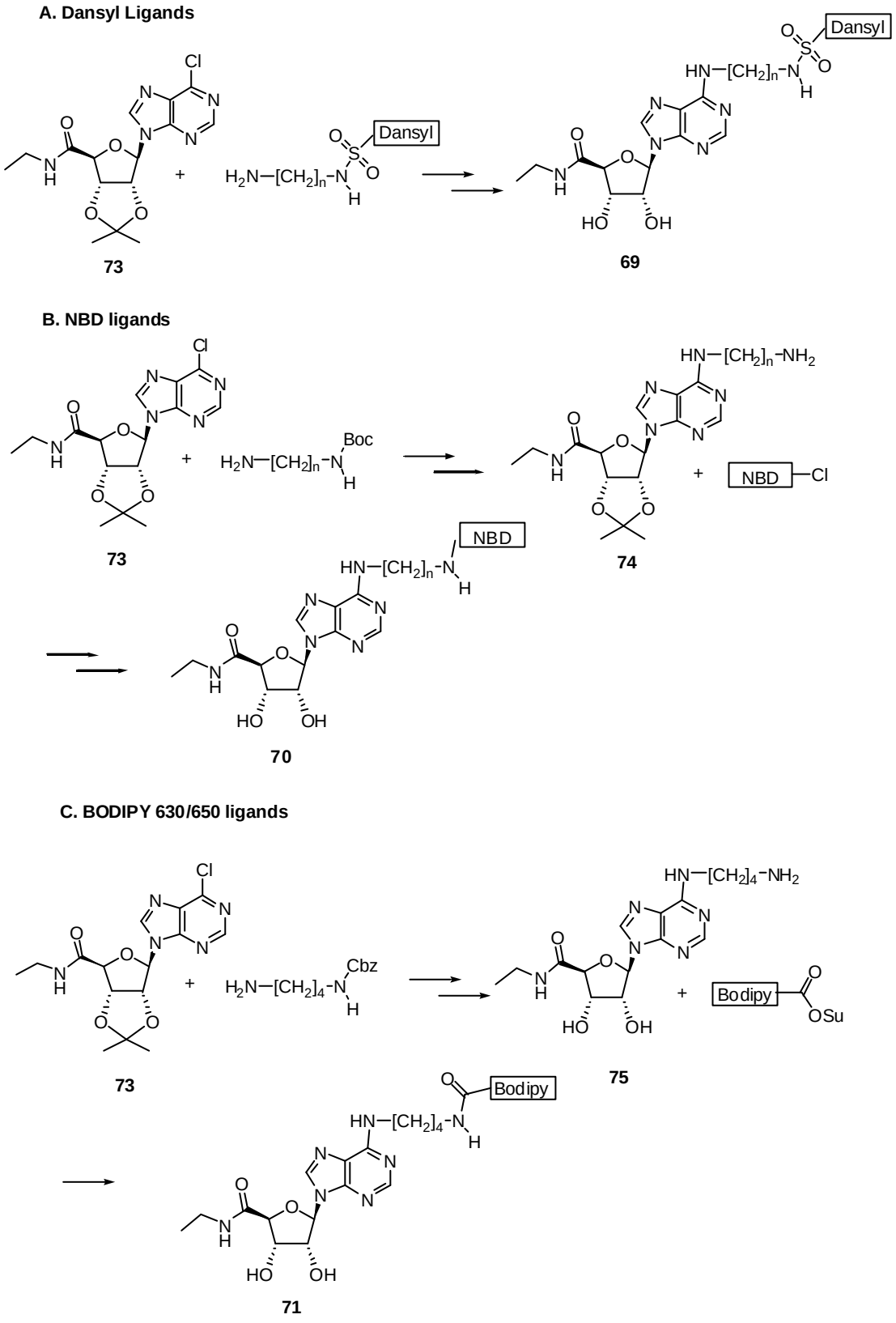

Scheme 2-1 The different synthetic methodology used to install the fluorescent dye onto the NECA based fluorescent adenosine agonists.

2.1.2 Fluorescent Serotonin ligands

Various fluorescent agonists and antagonists have been prepared against 3 of the 14 known Serotonin (5HT) GPCRs. The methodology used in both the design and the synthesis of these 5HT ligands is very similar to that used in the synthesis of the fluorescent adenosine agonists (section 2.1.1) *i.e.* a 1° amine terminating alkyl chain is installed at a position upon a 5HT ligand known to tolerate molecular extension and conjugated to an appropriate fluorescent dye in the final synthetic step.

Wohland *et al.* was able to label an experimental Glaxo Wellcome $5HT_{3a}$ antagonist GR-119566X **76** (Figure 2-3) which already possessed an aminopropyl chain installed in the drug molecule[33]. They simply reacted GR-119566X **76** with different fluorophores and following purification, tested the ligands for affinity at the $5HT_3$ receptors. GR-119566X **76** was labelled with 4 different dyes, fluorescein (λ_{abs} 494 nm, λ_{Em} 518 nm) **77a**, NBD (λ_{abs} 465 nm, λ_{Em} 535 nm), Rhodamine 6G (λ_{abs} 556 nm, λ_{Em} 578 nm) **77b** and Cy5 (λ_{abs} 649 nm, λ_{Em} 670 nm) **77c**, which spanned a range of absorption and emission wavelengths (Figure 2-3)[33]. They reported that ligands **77a** & **b** both exhibited sub-nanomolar Kd values whilst the Cy5 containing ligand **77c** had an increased Kd of 18 nM, which they attributed to the increased steric hindrance of the dye.[33]. The authors went on to use these fluorescent ligands in Fluorescence Correlation Spectroscopy experiments and were therefore able to comment upon the suitability of the 4 fluorescent dyes evaluated in this SMD application[33,34]. They concluded that the Cy5 and the Rhodamine dyes were the most suitable for SMD applications due to the high count rate, high photostability, and high signal to noise ratio of the dyes. Finally the group concluded with a statement that should be considered when designing fluorescent ligands suitable for SMD work "…a suitable ligand for FCS has to weigh between the higher accuracy of a high count fluorophore and the presumed disturbance of the ligand-receptor interaction by this label"[33].

A separate group utilised SAR data from a series of benzopyran based $5HT_{1A}$ ligands[211] to design fluorescent $5HT_{1A}$ agonists[212]. They employed an aminobutyl linker, previously shown to tolerate bulky aromatic substituents, in order to fluorescently label the ligand (**78**, Figure 2-3).

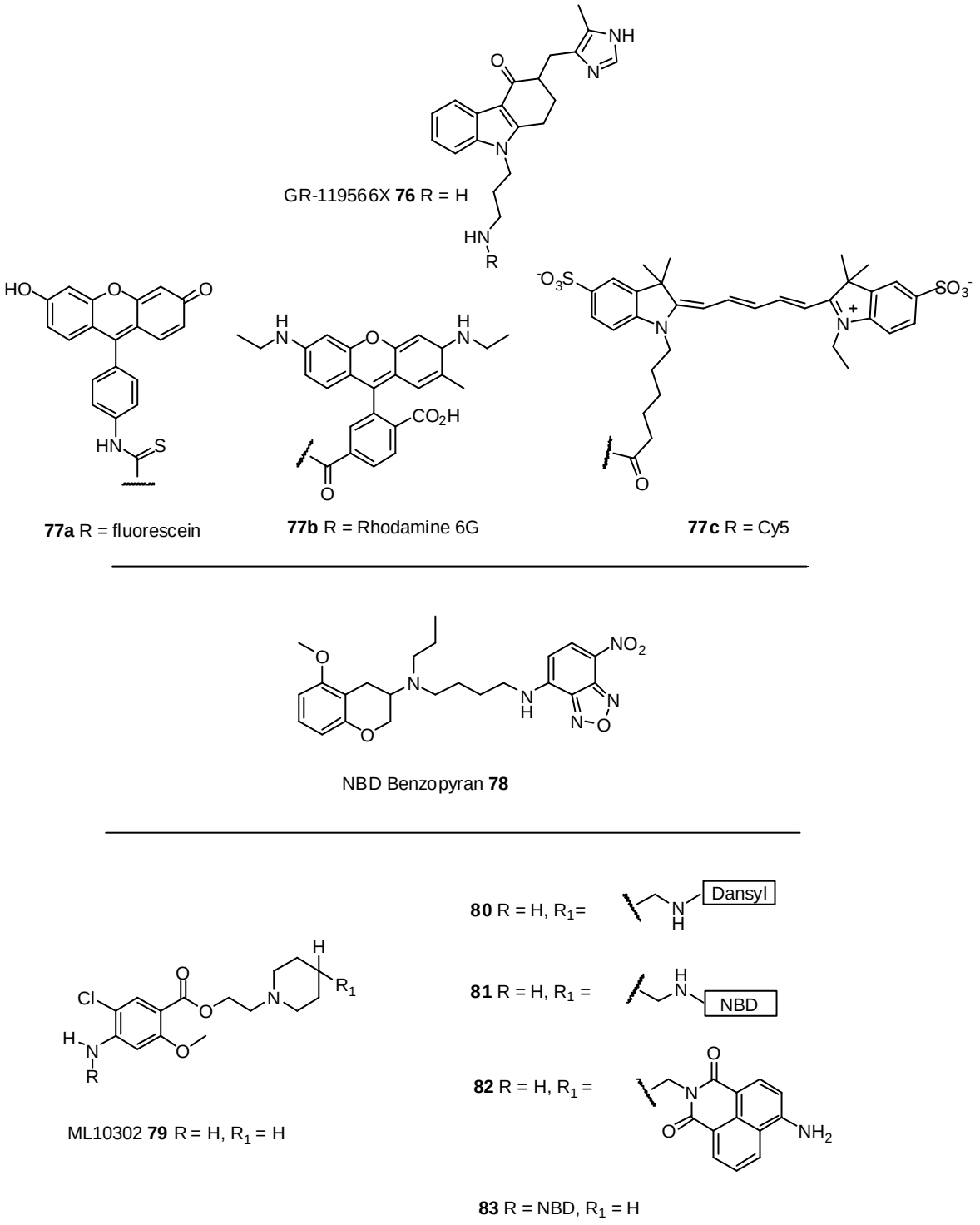

Figure 2-3 The structures of fluorescent 5HT agonist and antagonists.

They chose to label the ligand with both commercially available NBD dye and a novel "in-house" coumarin based dye which exhibited higher λ_{Em} (550 nm) wavelengths. The NBD labelled ligand **78** actually had an increased affinity and selectivity towards the 5-HT_{1A} receptor when compared to the non-fluorescent ligands from the original SAR study. Ligand **78** was successfully used in a FIDA based experiment[40].

The final set of fluorescent serotonin ligands to be considered were designed using the $5HT_4$ antagonist ML10302 (**79**, K_i = 1 nM, Figure 2-3) as a template[213]. By utilising a computational based model of ML10302 **79** docked into the $5HT_4$ receptor they were able to predict areas upon the pharmacophore that would tolerate attachment of a fluorescent dye. Their hypothesis was that the piperidine of ML10302 **79** was in the vicinity of the top of the receptor binding pocket and that alkyl tethers conjugated to this ring would place the fluorescent dye in a position favourable for binding. By analogy this placed the aromatic ring of ML10302 **79** at the bottom of the $5HT_4$ receptor binding pocket where it was not expected to tolerate a bulky fluorescent dye.

Compounds **80**-**83** are some examples from their study which helps to clarify their hypothesis (Figure 2-3). A short C1 linker installed at position 4 on the piperidine moiety and coupled to Dansyl, NBD and a naphthalimide derivative gave compounds **80**, **81**, and **82** which bound to $5HT_4$ receptors with 7, 7.5, and 64 nM affinities respectively. Compound **82** was used to highlight $5HT_4$ receptors on C6 glial cells and report on subcellular localisation[213]. As a negative control to their computational model hypothesis they labelled the aniline nitrogen of ML10302 with NBD and Dansyl dyes as in compound **83.** These compounds exhibited no affinity towards the $5HT_4$ receptors proving that the dye needed to be positioned away from the binding pocket in-order to retain receptor affinity and supporting their original hypothesis.

2.1.1 Summary of the design and synthesis requirements of fluorescent ligands

The series of serotonin and adenosine fluorescent ligands have shown that it is possible to fluorescently label a selection of selective high affinity receptor ligands with a large fluorescent dye, and still retain the high selectivity and receptor affinity exhibited by the non-fluorescent ligand. The key requirements to successfully generating a fluorescent ligand can be summarised as follow;

- The use of an alkyl linker to separate the fluorophore from the pharmacophore.
- The positioning of the alkyl linker must be on an area of the pharmacophore known to tolerate molecular extension using previously elucidated SAR.
- The use of a 1° amine as an attachment point for the fluorescent dye.
- Careful selection of suitable fluorophore is required to control both the pharmacology and the fluorescent application of the ligand.

These parameters have not only been used successfully to generate fluorescent adenosine and Serotonin ligands but when applied to small ligands to other receptor types have generated useful fluorescent ligands for the Histamine H_1[214] and H_2[215], the Muscarinic M_1[216], the Opioid Mu[217], and the β[23] and α_1[21] adrenergic receptor types. We wish to apply these same principles into the design and synthesis of a fluorescent cannabinoid CB_2 ligand.

2.2 Designing a fluorescent cannabinoid CB_2 ligand

From the principles applied in section 2.1 we designed the ligand using the following criteria.

- Selection of a suitable CB_2 selective ligand.
- Selection of an appropriate site within the chosen CB_2 ligand to be modified for fluorescent dye conjugation.
- Choice of length and terminating chemical group employed upon the alkyl linker.
- The fluorescent dye to be conjugated to the CB_2 ligand.
- The synthetic strategy to be utilised in building the fluorescent CB_2 ligand.

Each of these will be considered separately and the rational of our choices are discussed.

2.2.1 Selection of a suitable CB_2 ligand

A thorough review of the available cannabinoid ligands was completed in section 1.4. We concluded that no single CB_2 selective ligand possessed every parameter which was required for successful conjugation with a fluorescent dye *i.e.*

- A high affinity towards the CB_2 receptor (i.e. $K_i \leq 20$ nM).
- A high CB_2/CB_1 selectivity (≥ 20).
- Chemical stability to hydrolysis, light and enzymatic degradation.
- SAR data providing evidence that the ligand can tolerate molecular extension and bulky substituents.
- Has a structure that allows its synthesis outside the Misuse of Drugs act.

We therefore selected a CB_2 ligand which demonstrated as many of the required parameters as possible. As discussed in section 1.4.6 the series of Japan Tobacco compounds were chosen as our primary lead compounds. From this selection of ligands the compound JTE2-6 **63** (Figure 2-4) demonstrated a high CB_2 selectivity (> 455 fold) and affinity (K_i = 1.1 nM) whilst incorporating different chemical functionalities allowing a selective chemical synthesis. Therefore JTE2-6 **63** was selected as a lead molecule to be conjugated to a fluorescent dye.

2.2.2 Selection of a suitable site upon JTE2-6 for conjugation

The successful fluorescent ligands, encountered in section 2.1, each incorporated an alkyl linker that acted as both a spacer and tether to the fluorescent dye. Therefore we planned to incorporate a similar linker onto JTE2-6 **63**. The alkyl linker needed to be carefully position upon JTE2-6's pharmacophore in-order that the compound's CB_2 receptor affinity was retained. The pharmacophore of JTE2-6 was interrogated by considering which parts of the structure were communal within all of the active Japan Tobacco ligands (see Figure 2-4).

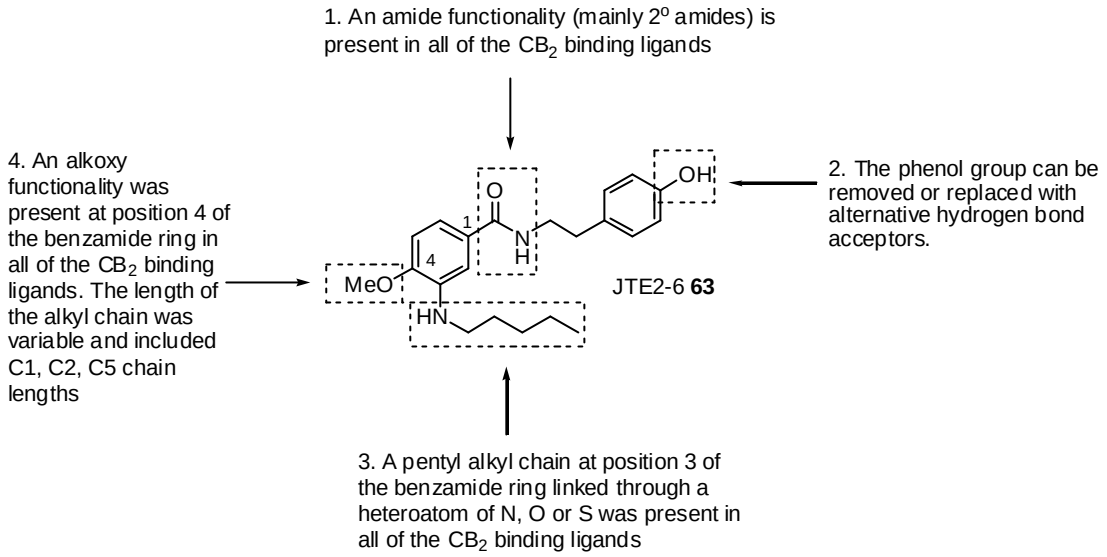

Figure 2-4 A breakdown of the SAR data available for the key functional groups of JTE2-6 **63**.

Considering the structure of JTE2-6 **63** from Figure 2-4 it was clear that the functionality which demonstrated an ability to tolerate molecular extension with alkyl chains was position 4 upon the benzamide ring. Structures similar to JTE2-3 **63** have been shown to tolerate extension with pentyl chains and still retain excellent affinity and selectivity towards the CB_2 receptor (*i.e.* compounds **62** & **65**, figure 1-22)[126]. Other groups present on JTE2-6 **63** such as the phenol, amide and aniline functionality that could also be used to conjugate the fluorescent dye were not considered for derivatisation due to the lack of previous evidence demonstrating extension upon these positions.

2.2.3 Determining a suitable linker

Two strategies were considered regarding the length of the linker. The first strategy involved a SAR approach, synthesising a number of ligands with differing alkyl lengths, and testing the pharmacology of all of these ligands conjugated to a single fluorophore to determine an optimum length. This approach was adopted by Macchia *et al.* in their synthesis of the NECA based adenosine ligands **69** and **70**[200,202]. The second approach involved using one alkyl chain length and conjugating this ligand to different fluorescent dyes and testing the pharmacology of these compounds. This approach has been more extensively used in other receptor systems such as serotonin[33,212] and histamine[214,215] ligands. The advantage of the latter technique is

that it has been shown that the fluorescent dye may alter the pharmacology and the application of the fluorescent ligands and is therefore more important to evaluate than the length of the alkyl linker alone. Also the Japan Tobacco compounds have shown previous evidence that molecule extension is tolerated at position 4, however there is no evidence that a bulky substituent will be tolerated at the terminal end of the alkyl chain. Thus, it was felt that a short length alkyl chain linker coupled to different fluorescent dyes would determine quickly if this type of derivatisation would be tolerated by the CB_2 receptor. Optimisation of the linker length would be considered at a later date.

From section 2.1 it was observed that each of the fluorescent ligands discussed incorporated a 1° amine group which was conjugated with the fluorescent dye. This is advantageous as the high reactivity of 1° amines and the number of commercially available amine reactive dyes will allow for a simpler synthesis. We therefore planned to incorporate a short alkyl linker (between C4 – C8) terminating in a 1° amine functionality at position 4 of JTE2-6 **63** (Figure 2-4).

2.2.4 Selection of a fluorophore

The choice of fluorophore which is to be used for the CB_2 ligand is of critical importance, if the fluorescent ligand is to retain potent pharmacology and find use in fluorescence confocal microscopy and SMD applications. Previous work discussed in chapter 2.1 evaluated many different types of fluorophore in similar ligands to those we wish to produce. In general, smaller molecular weight dyes were preferred such as Dansyl **84** and NBD **85**, presumably chosen for their small steric impact upon the ligand causing less ligand-receptor perturbations (Figure 2-5). The small fluorophores Dansyl **84** and NBD **85** were successfully utilised in a number of GPCR ligands having activity at the adenosine[200,202], serotonin[33,212,213], and histamine[214,215] receptors. These dyes have advantages of being small, and cheap to purchase, however their spectral properties are not ideal for biological applications. The absorption and fluorescence emission spectra and quantum yields of the Dansyl **84** and NBD **85** dyes are markedly dependant on solvent, in particular both dyes suffer from very low (<0.01) quantum yields in water[218]. The short excitation wavelengths of Dansyl (λ_{abs} = 340-350 nm)[218] and NBD (λ_{abs} = 470 nm)[218] are also problematic for biological

applications due to the high energy radiation necessary for excitation, damaging cells and promoting autofluorescence. These factors make them less suitable for SMD applications although both probes have been used successfully in confocal microscopy applications[200,202].

Two red-absorbing dyes have been evaluated in fluorescent receptor ligands. The BODIPY® and Cyanine (Cy) dyes (**86** & **87**, Figure 2-5) have both found use in fluorescent ligands for SMD applications[25,33]. The BODIPY® dyes have been used extensively in our own adenosine ligands[24,25,207] as well as in other receptor ligands such as the muscarinic M1[216], the opioid μ[217] and β adrenergic[23] receptors. The reasons cited for using this unusual boron containing fluorophore include high quantum yield (approaching unity), photostability, low pH dependence and low percentage of triplet states[25,217]. A disadvantage of the BODIPY® dyes commonly cited is a very small Stoakes shift which can cause problems with internal conversion quenching (section 1.1.1) between two dye molecules in close proximity of each other[218]. However this is only a problem observed when there is the potential to multi-label a molecule with more than one fluorophore (i.e labelling large proteins) and is not a problem in the work we are conducting. The Cyanine dyes also have an excellent λ_{abs} for SMD applications with little autofluorescence observed[218]. However due to their structure containing *trans* double bonds, *trans-cis* photo induced isomerization is a problematic factor in FCS experiments[205] They also have a considerably smaller quantum yield (~ 0.3) than the BODIPY® fluorophores[33].

The BODIPY® dyes are available from Molecular Probes and have a number of spectral properties[219]. Depending on its structure, a wide range of emission wavelengths can be obtained ranging from 510 to 665 nm. In our previous work with the adenosine receptor ligands BODIPY® 630/650 **86** (the dyes are named BODIPY® $\lambda_{abs}/\lambda_{em}$) was chosen, as its spectrum was optimal for the excitation source (633 nm He-Ne laser) and matched a common optical filter (LP650) of the in-house FCS and confocal microscopy equipment. The long excitation wavelength also resulted in less cellular autofluorescence and damage[25,205].

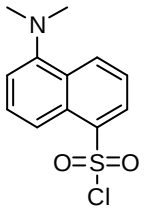

Dansyl Chloride **84**
λ_{abs} = 340-350 nm, λ_{em} = 510-560 nm[1]

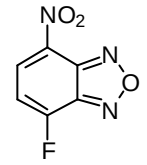

4-fluoro-7-nitrobenzofurazan **85**
(or 4-fluoro-7-Nitro-2,1,3- Benzoxadiazole (NBD-F)
λ_{abs} = 470 nm, λ_{em} = 540 nm[1]

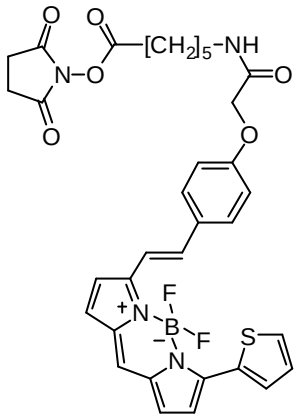

Bodipy® 630/650-X OSu **86**
Molecular Probes
λ_{abs} = 629 nm, λ_{em} = 646 nm[2]

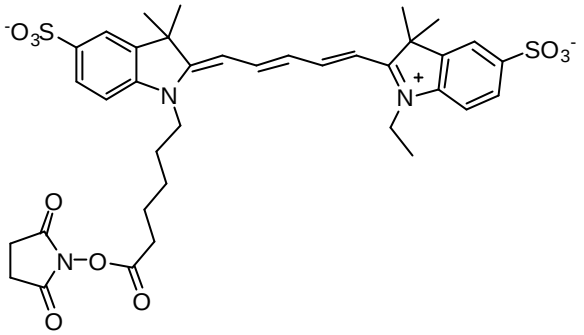

Cy5-OSu **87**
Amersham Biosciences
λ_{abs} = 647 nm, λ_{em} = 663 nm[2]

Figure 2-5 The structures of the amine reactive fluorescent dyes that were evaluated for use in the CB_2 fluorescent ligands. Supply information is given when the dye is sold exclusively by one company. Spectral data is given for amine conjugates of the dye as NBD-F and Dansyl chloride are non-fluorescent. 1. ref.218, 2. ref. 205.

For this work we have opted to conjugate our CB_2 ligand with the small and cheaper Dansyl dye **84**, and utilise the BODIPY® 630/650 **86** dye to produce CB_2 ligands for confocal microscopy and SMD applications.

2.2.5 Synthetic strategy

A synthetic strategy, enabling the factors discussed in sections 2.2.1 to 2.2.4 to be incorporated into the target molecule, needed to be established. The target molecule was designated fluorophore-JTE2-6 **i** and was subjected to a retrosynthesis analysis shown in Scheme 2-2.

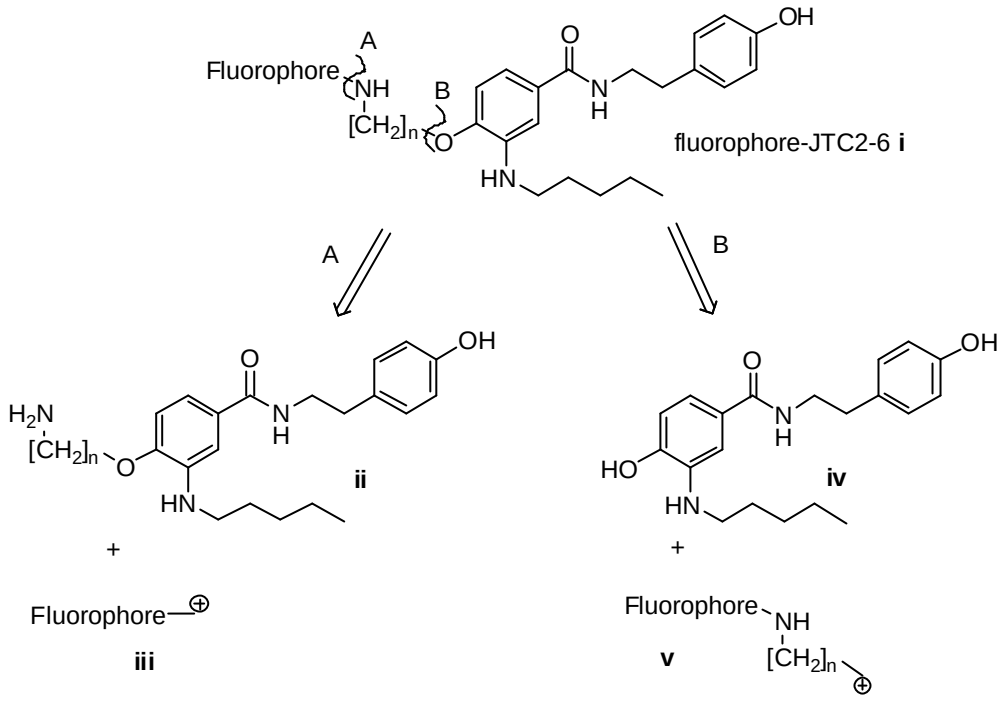

Scheme 2-2 The retrosynthesis of the target molecule fluorophore-JTE2-6.

From Scheme 2-2 two disconnections, A and B, were possible. The fluorophore is required to be conjugated to the ligand in the last step, as this protects it from any chemical and light degradation inflicted by being introduced too early in the synthesis, whilst allowing a 'generic' molecule to be synthesised which can be conjugated to a choice of fluorophores. Disconnection A confers more advantages to the synthesis than B due to factors discussed in section 2.1.1.1. Disconnection A allows the commercially available fluorophores Dansyl-Cl **84** and BODIPY 630/650 X OSu **86** (represented by synthon **iii**) to be installed under mild conditions during the final step. Disconnection B is less efficient and requires the fluorophore to be pre-conjugated with the linker (represented by synthon **v**) which would expose the fluorophore to the chemical conditions required for conjugation via an ether linkage.

Compound **ii** can be subjected to further retrosynthesis as shown in Scheme 2-3. Disconnection E is not a valid pathway as it leads to chemoselectivity problems with three nucleophilic groups present in compound **x** (2 x phenol, 1 x amine). Disconnection C and D are both lead to accessible compounds; **vi**, **vii** (tyramine) and **viii**. The 1° amine group will be protected with a suitable protecting group in order that the chemical steps remain selective. Compounds **vi** and **viii** from disconnections C and D will be further analysed in Scheme 2-4.

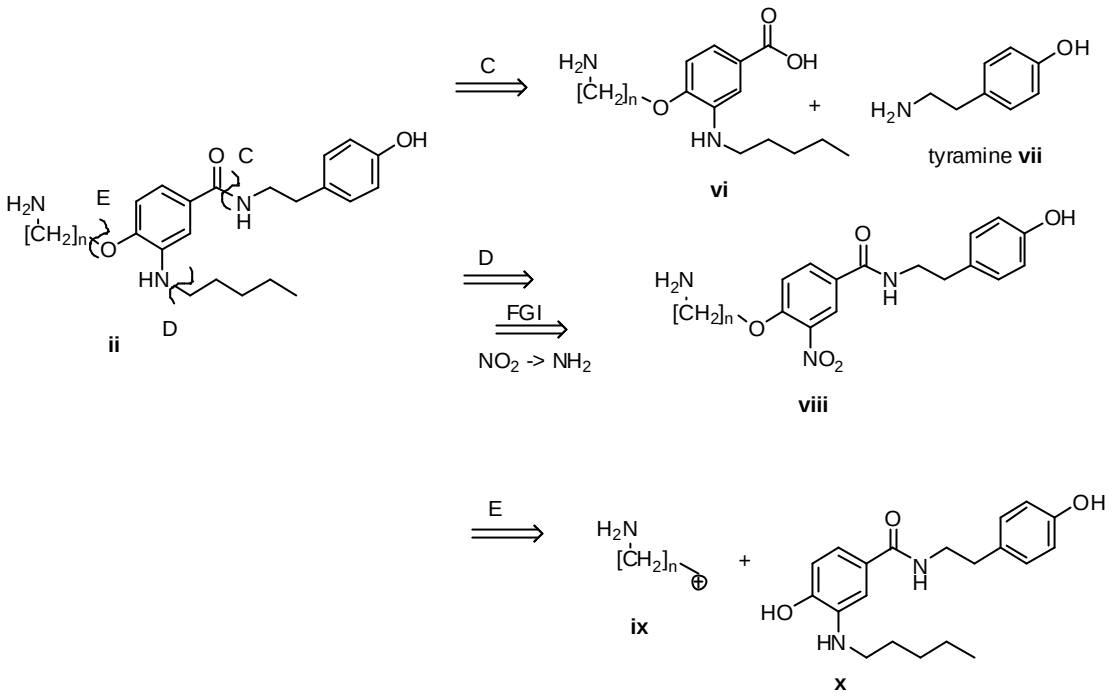

Scheme 2-3 Possible retrosynthetic routes from compound **ii**. FGI = functional group interconversion

Two routes were planned for synthetic evaluation from compounds **vi** and **viii** converging with a common intermediate **xi**.

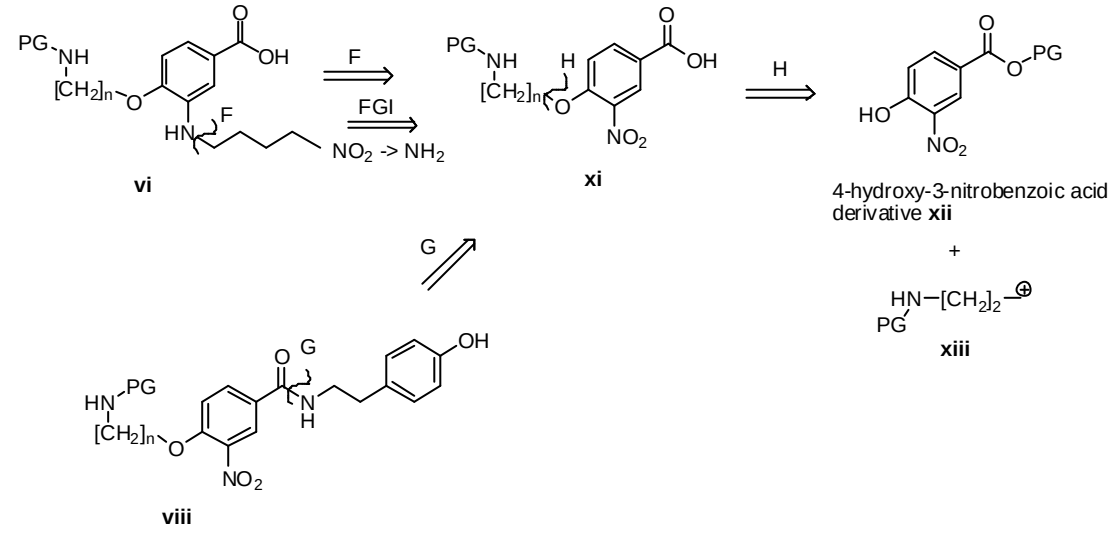

Scheme 2-4 Retrosynthetic analysis on compounds **vi** and **viii**. PG = protecting group. FGI = functional group interconversion

The common intermediate **xi** can be broken down to commercially available 4-hydroxy-3-nitrobenzoic acid **xii** and a protected aminoalkyl synthon **xiii**. Evaluation of compounds that would give access to the synthon **xiii** showed that the aminoalkyl alcohols were commercially available. Protection with the acid labile *tert*-Butoxycarbonyl (Boc) protecting group followed by *in situ* activation of the alcohol employing Mitsunobu conditions would be used to generate synthon **xiii**. Considering which aminoalkyl alcohols were commercially available we found that they were restricted to 3-aminopropan-1-ol, 4-aminobutan-1-ol, 5-aminopentan-1-ol, and 6-aminohexan-1-ol. 6-Aminohexan-1-ol **88** was chosen for this synthesis as it fulfilled all of the requirements discussed in section 2.2.3.

2.3 Chemistry results

N-Benzyloxycarbonyl-6-aminohexan-1-ol **89** was synthesised in high yield according to a published procedure using Boc_2O in aqueous dioxane[220] (Scheme 2-5). The alcohol **89** was activated *in situ* using standard Mitsunobu conditions[221] of PPh_3, diethylazodicarboxylate (DEAD) and coupled to the commercially available methyl 4-hydroxy-3-nitrobenzoate to afford ester **90**. Saponification using LiOH revealed the benzoic acid **91**.

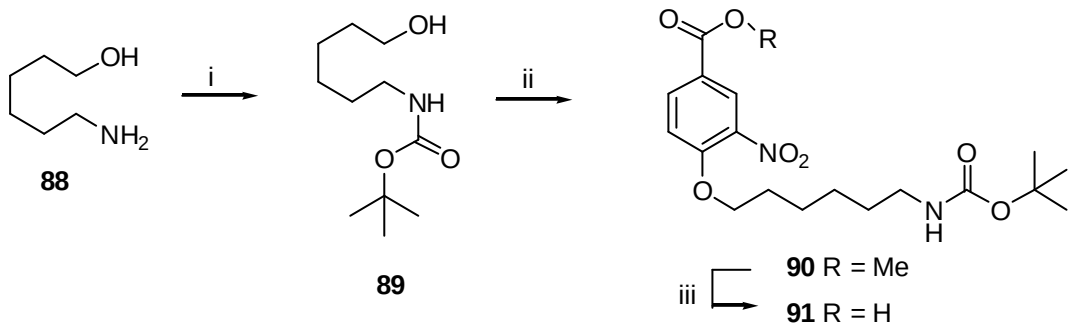

Scheme 2-5 Reagents, conditions and yields: (i) Boc_2O, dioxane, $NaHCO_3$, water, rt, 2h, (99%); (ii) methyl 4-hydroxy-3-nitrobenzoate, DEAD, PPh_3, THF, rt, 5h, (66%); (iii) LiOH, MeCN, H_2O, 50 °C, 30min, (100%).

The carbamate N-H proton of compound **91** displayed an unusual NMR spectrum involving a splitting of its peak between the usual upfield position of 4.64ppm (70% split) and a downfield position of 6.30ppm (30% split) in $CDCl_3$ (Figure 2-6). The proton could be brought into 100% of its normal field alignment (4.64ppm) by the

addition of D_2O (result not shown). The splitting was observed on different concentrations and batches of the acid **91**. This effect was also observed in aminobenzoic acid derivatives **92** and **93** (Scheme 2-6) but was not observed with the precursor methyl ester **90** (results not shown).

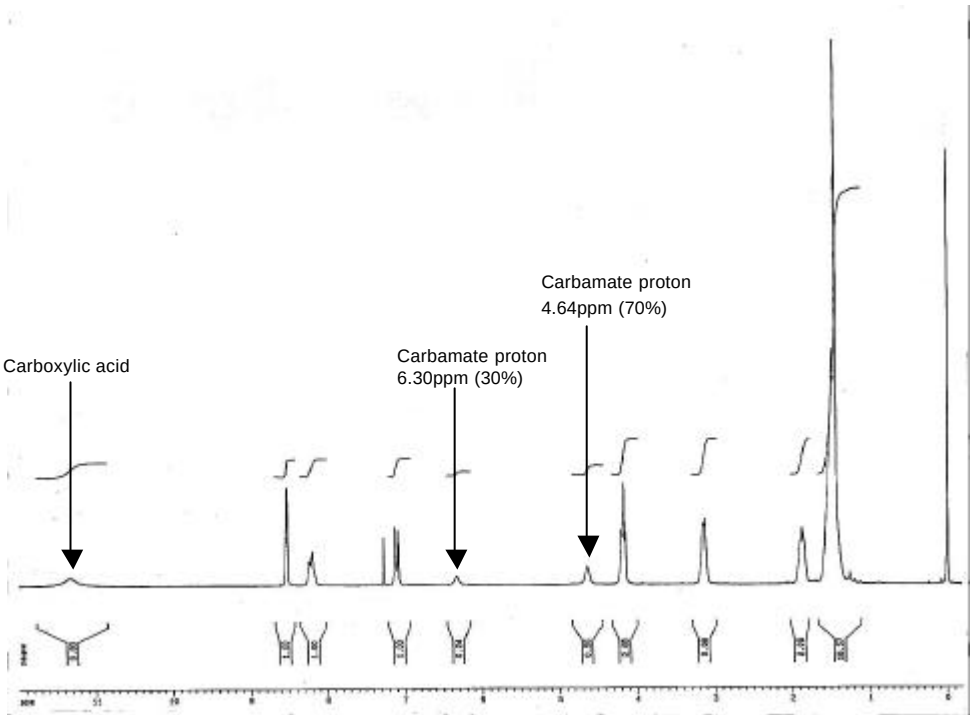

Figure 2-6 ^{1}H NMR showing the unusual splitting of the carbamate proton of 91. The proton could be brought into 100% alignment at 4.64ppm by the addition of D_2O.

The benzoic acid derivative **91** was used in two different competing routes towards the target molecule as discussed in the retrosynthetic analysis in section 2.2.5 (route F and G, Scheme 2-4). Following route F the nitro group was reduced using hydrogen and Pd catalysis to afford the aniline **92** in good yield (Scheme 2-6). Reductive alkylation to the substituted aniline **93** with pentanal and $NaCNBH_3$ proceeded in low yield (24%). Peptide coupling of **93** with tyramine was attempted using a number of coupling reagents including CDI, DCC, and oxalyl chloride/DMF (Vilsmeier reagent), however all attempts to form the peptide bond resulted in complex mixtures and corresponding low yielding reactions.

The alternative route shown by G (Scheme 2-4) involved coupling the nitro-acid **91** directly with tyramine. Thus activation of the acid **91** with CDI followed by tyramine coupling afforded **94** in excellent yield (79%).

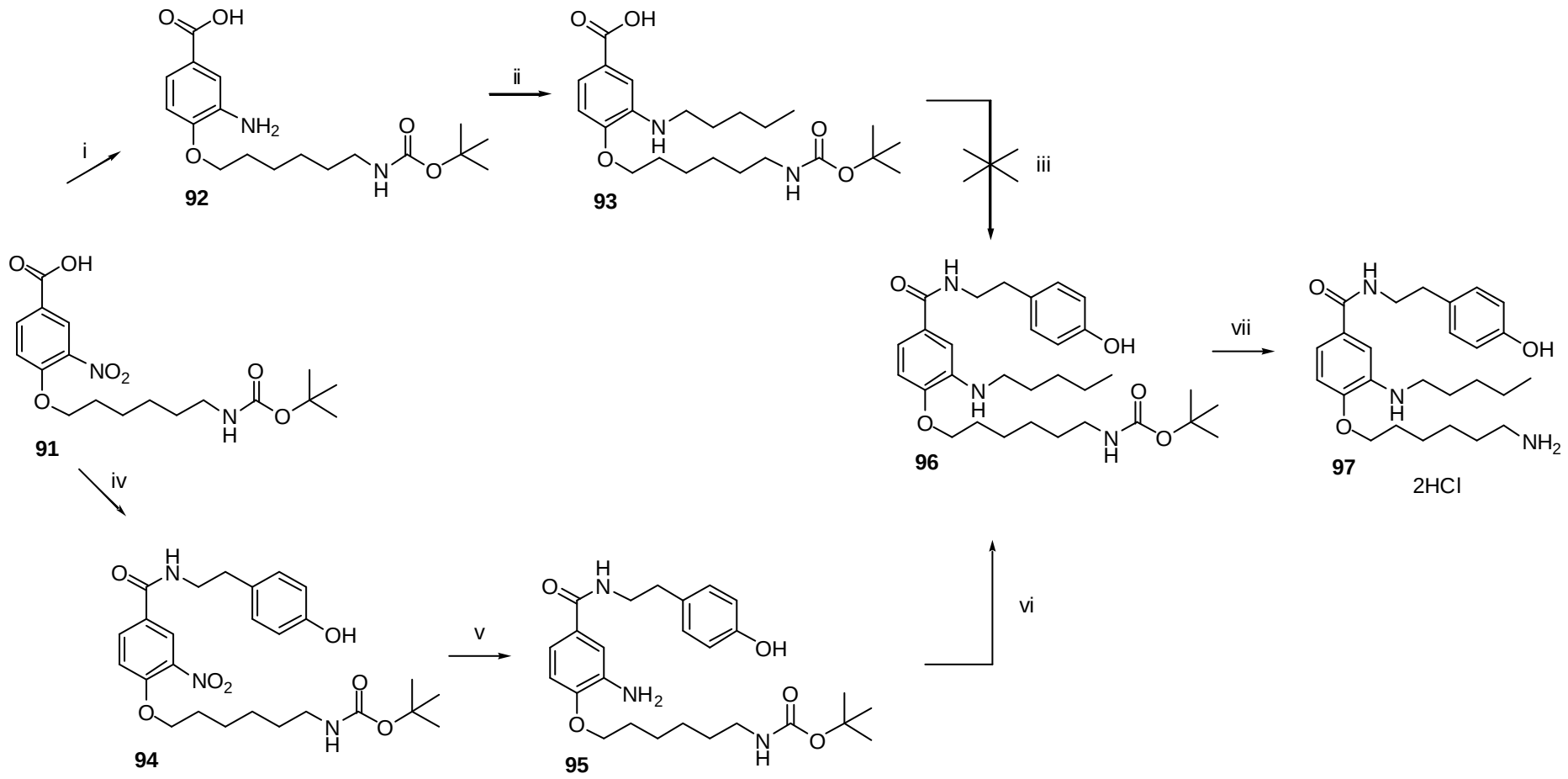

Scheme 2-6 Reagents, conditions and yields: (i) H_2, Pd/C, EtOH, rt, 12h, (76%); (ii) pentanal, $NaCNBH_3$, MeOH, 4h, rt, (24%); (iii) CDI, MeCN, tyramine, rt, 24h, (no reaction) or oxalyl chloride, DMF, pyridine, DCM, tyramine, rt, 24h, (no reaction) or DCC, DCM, tyramine, rt, 24h, (no reaction); (iv) CDI, MeCN, tyramine, rt, 12h, (79%); (v) H_2, Pd/C, EtOH, rt, (69%); (vi) pentanal, $NaCNBH_3$, MeOH, rt, 4h, (71%); (vii) AcCl, MeOH, rt, 18h, (65%).

An alternative coupling using the Vilsmeier reagent formed *in situ* (oxalyl chloride/DMF) to form the acid chloride followed by tyramine coupling was assessed. This reaction resulted in a low yield (14%) involving a difficult work-up to isolate the product.

Nitro group reduction of **94** gave aniline **95** which exhibited the expected loss of the Nitro IR stretch (1559 & 1391 cm^{-1}) and an upfield shift of the benzamide ring protons. Accompanying the change, from the electron withdrawing effects of the nitro group to the electron rich aniline, was an alteration of the compounds physical properties, such that they exhibited fluorescence under long wave UV light. Compound **96** was shown to exhibit a λ_{abs} 313 nm and a λ_{em} 386 nm.

Alkylation of aniline **95** was evaluated using 1-iodopentane[222] and $NaHCO_3$, or reductive alkylation[223] using pentanal and $NaCNBH_3$. Alkylation using the alkyl halide gave a lower yield (25%) and a more difficult reaction mixture to purify than the reductive alkylation reaction (71%) which was used in all subsequent reactions. Acidolysis of the Boc protecting group of **96** using methanolic HCl relinquished the target congener **97** as its corresponding crystalline dihydrochloride salt.

2.3.1 Conjugation with amine reactive dyes

The congener **97** was coupled with the amine reactive dyes Dansyl chloride **84** and BODIPY® 630/650-X OSu **86** (B, Scheme 2-7). In-order to react with both dyes, the free base of congener **97** was generated *in situ* from the hydrochloride salt. The coupling reactions were therefore conducted in a 50:50 MeCN/aqueous sodium bicarbonate buffer (pH 8.3) designed to liberate the free base and promote organic solubility without generating the phenoxide ion (< 2 % in solution[**]) which could cause problems with chemoselectivity.

The coupling reaction with Dansyl chloride **84** gave two major fluorescent products. Isolation of these, using preparative TLC, and subsequent mass spectrometry showed that the mono and bis Dansylated products had been formed with molecular weights of 675 and 908 respectively. The desired mono Dansyl product Dansyl-JTE2-6 **99** was obtained in 19% yield and characterised by ^1H NMR using reverse phase HPLC analysis to assess purity.

[**] Calculated using the Henderson-Hasselbalch equation using a pKa of 10.0 for phenol.

Chemoselective acylation of the 1° amine of **97** with BODIPY® 630/650-X OSu ester **86** afforded the target molecule BODIPY-JTE2-6 **100** in 63% yield, following purification using preparative TLC, verified by mass spectrometry, ^{1}H NMR and reverse phase HPLC.

The chemoselectivity of the 1° amine of **97** towards succinimidyl esters was tested in a model reaction. A pseudo fluorophore succinimido 1-naphthaleneacetate **98** was prepared using DCC coupling of 1-naphthylacetic acid and *N*-hydroxysuccinimide (A, Scheme 2-7). The use of the pseudo fluorophore avoided the expense and complex NMR spectra associated with BODIPY® 630/650-X OSu **86**. Full chemical analysis (MS, elemental, ^{1}H & ^{13}C NMR, ^{1}H-^{1}H & ^{13}C-^{1}H COSY NMR) of the acylated compound **101** isolated from this reaction confirmed that only the desired 1° amine of **97** reacts with succinimidyl esters.

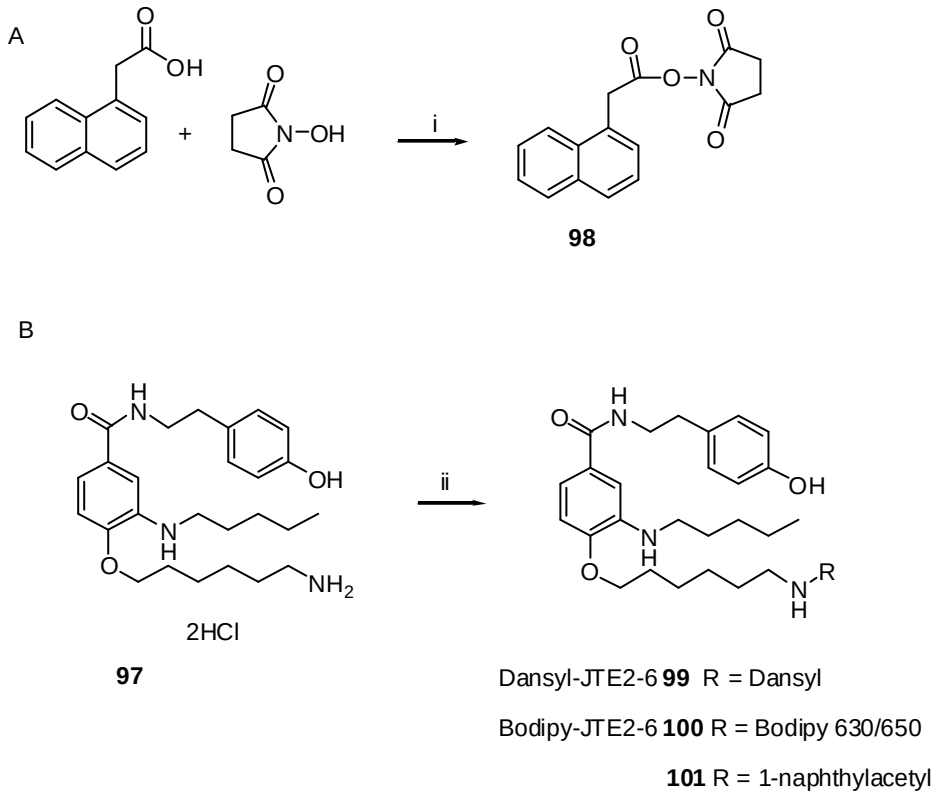

Scheme 2-7 A. The synthesis of succinimido-1-naphthaleneacetate. B. Conjugation reaction of **97** with amine reactive fluorophores and pseudo fluorophores. Reagents, conditions and yields: (i) DCC, DCM, rt, 12h, (47%); (ii) Dansyl-Cl **84** or BODIPY 630/650-X OSu **86** or **98**, $NaHCO_{3\ (aq)}$ pH 8.3: MeCN 1:1, rt, 1-12h, (19-63%).

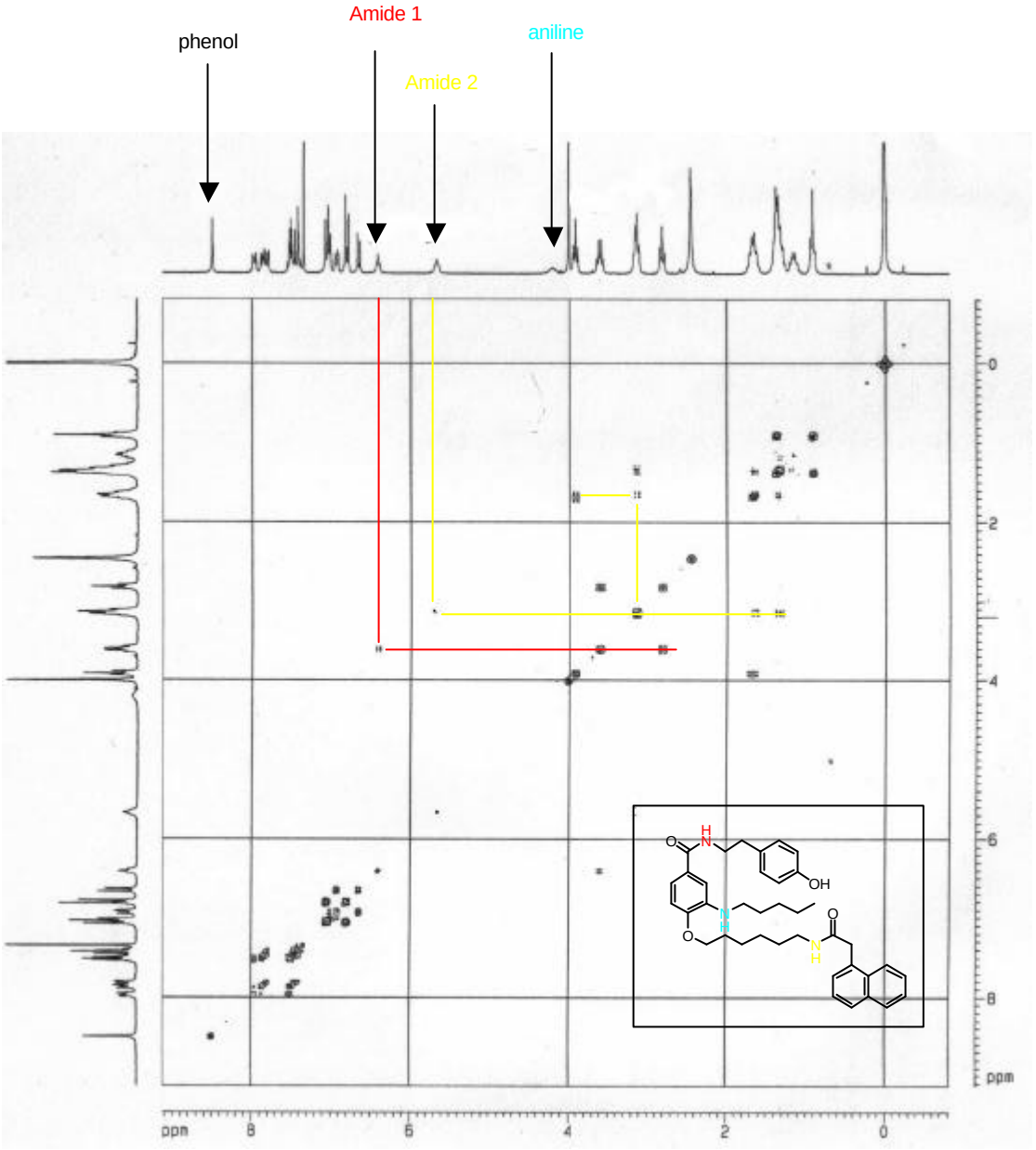

Figure 2-7 ^{1}H-^{1}H COSY NMR spectrum of **101** ran in $CDCl_3$ and D^6-DMSO. The spectrum shows the coupling of the 4 exchangeable protons present within the molecule to neighbouring protons. The phenol and aniline protons show no coupling patterns whilst amide 1 (6.3 ppm) shows a coupling pattern to the phenyl ethyl moity (shown by the red line). Amide 2 (5.7 ppm) shows a coupling pattern to the oxygen containing hexyl chain (shown by the yellow line).

The following data provided evidence that the 1° amine of **97** was reacting with one molecule of succinimido 1-naphthaleneacetate under the coupling conditions employed.

- Elemental analysis and ES-MS confirmed that only one naphthylacetyl group was conjugated in the final product.

- ^{1}H-^{1}H COSY coupled with D_2O shakes were able to identify each of the exchangeable protons present in **101** (Figure 2-7, D_2O shake data not shown) and an interpretation of the data is as followed:

    - 1 phenol proton (singlet, 8.3 ppm) coupled to no other protons.
    - 1 amide proton (triplet, 6.3 ppm) coupled to the phenylethyl moiety.
    - 1 amide proton (triplet, 5.7 ppm) coupled to the oxygen linked hexyl chain (five couplings can be observed in the COSY due to two methylene protons within the chain occurring at the same chemical shift).
    - 1 aniline proton (broad singlet, 4.3 ppm) coupled to no other protons.

2.4 Pharmacology results

The pharmacology of Dansyl-JTE2-6 **99** and BODIPY-JTE2-6 **100** was assessed by competitive radioligand displacement of the non-selective cannabinoid [^{3}H] CP55, 940 from cellular membranes containing human CB_2 receptors and was performed as previously described by Leggett *et al.*[224]. Both Dansyl-JTE2-6 **99** and BODIPY-JTE2-6 **100** failed to displace any of the [^{3}H] CP 55,940 from cell membranes prepared from CHO cells expressing the human CB_2 receptor up to a concentration of 10^{-4} mol/L (100 μM) (Figure 2-8). The low affinity of BODIPY-JTE2-6 **100** was also confirmed using cell membranes prepared from HEK cells expressing the human CB_2 receptor by an independent group at the University of Connecticut, Storrs, USA (Figure 2-8). In all experiments it was clear that the IC_{50}, and therefore K_i, values were > 10 μM for both Dansyl-JTE2-6 **99** and BODIPY-JTE2-6 **100**.

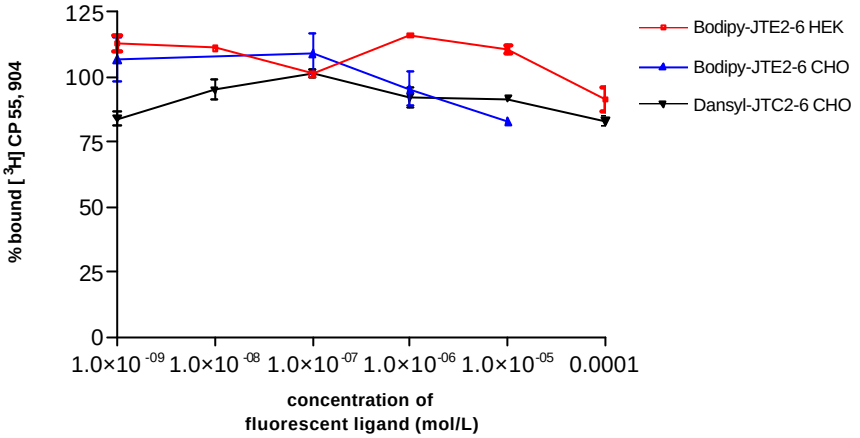

Figure 2-8 Radioligand displacement of [^{3}H] CP 55,940 from cell membranes (CHO & HEK) containing human CB2 receptors using Dansyl-JTE2-6 **99** and BODIPY-JTE2-6 **100**.

2.5 Use of Dansyl-JTE2-6 and BODIPY-JTE2-6 in fluorescence confocal microscopy.

The two fluorescent ligands Dansyl-JTE2-6 **99** and BODIPY-JTE2-6 **100** were used in confocal experiments to demonstrate whether the ligands had the potential to highlight CB_2 receptor membrane binding. Known concentrations of fluorescent ligand were incubated with CHO cells expressing human CB_2 receptors and images were recorded at various time courses throughout the experiment. To assess whether the fluorescence observed was due to specific CB_2 binding, CHO cells were pre-incubated with a blocking concentration of a non-fluorescent cannabinoid ligand (1 µM HU210 **14**) and the fluorescent ligand **99** or **100** was subsequently introduced. Images collected from this experiment were compared to those conducted without the HU210 **14** present, to determine if any fluorescence observed was due to CB_2 receptor binding. Various concentrations of **99** and **100** ranging from 10 – 400 nM were used in these experiments. When concentrations of 200 nM or below were used, the fluorescence observed was weak even when laser power and pin-hole aperture was increased. Increasing the concentration of the fluorescent ligand to 400 nM showed intra-cellular fluorescence after 5 minutes; however, this fluorescence could not be blocked or reduced by pre-incubation with HU210 for either Dansyl-JTE2-6 **99** or BODIPY-JTE2-6 **100** (Figure 2-9). Background fluorescence from the CB_2 transfected CHO cells was negligible for both of the excitation wavelengths used (i.e.363 nm (Dansyl) and 633 nm (BODIPY®) - Result not shown).

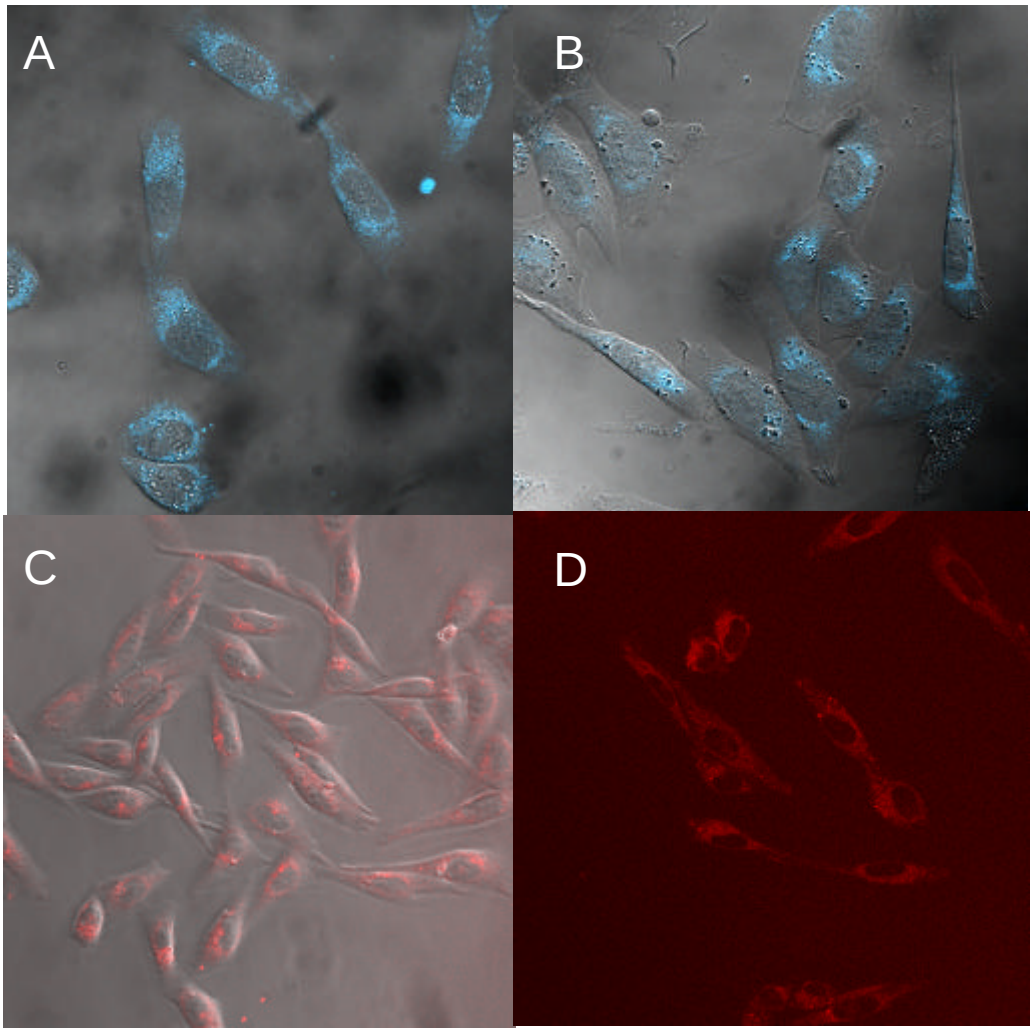

Figure 2-9 Representative confocal slice images of human CB_2 transfected CHO cells incubated with Dansyl-JTE2-6 **99** (A & B) and BODIPY-JTE2-6 **100** (C & D). Images taken at 10 mins after the fluorescent ligand was introduced using a Zeiss axiovert 100 with LSM510 confocal. Images A & C are for un-treated cells whilst images B & D are of cells that have been pre-incubated with 1μM HU210. Fluorescent ligand concentration in each experiment was 400 nM. Fluorescence was obtained for images A & B by using laser excitation at 363 nm through a Plan-apochromat 63x/1.4NA oil immersion objective and a LP560 emission filter. Pinhole diameter was 166μm. Fluorescence was obtained for images C & D by using laser excitation at 633 nm through a Plan-apochromat 63x/1.3 oil immersion objective and a LP650 emission filter. Pinhole diameter was 79μm.

2.6 Discussion

An efficient eight-step synthesis starting from commercially available materials and utilising established synthetic techniques was used to generate two target fluorescent ligands Dansyl-JTE2-6 **99** and BODIPY-JTE2-6 **100**.

During the compounds' synthesis a number of interesting discussion points were established and are examined below.

The ^{1}H NMR analysis of the benzoic acid derivatives **91**, **92** and **93** (Scheme 2-5 & 2-6) showed an unusual splitting pattern within the spectrum for the carbamate N-H proton that deserves further comment (Figure 2-6). Our initial thoughts were that the erroneous peak observed at 6.30ppm (0.3 protons) was due to contamination. However this peak was consistently observed in the spectrum from a number of different analytically pure samples of **91**. A D_2O shake upon this sample, to identify exchangeable protons, simultaneously eliminated the erroneous peak at 6.30ppm and increased the area of the peak at 4.64ppm to 1 proton. The peak at 4.64ppm, which is the normal shift for a carbamate proton, slowly decayed as the N-H bond was replaced with the unobservable N-D bond. This result is indicative that the carbamate N-H proton in anhydrous solution is involved in hydrogen bonding which is destroyed upon the addition of D_2O. The downfield 6.30ppm shift is likely to represent the carbamate N-H proton whilst engaged in hydrogen bonding, most likely to the carbonyl oxygen of the acid functionality as depicted in Figure 2-10.

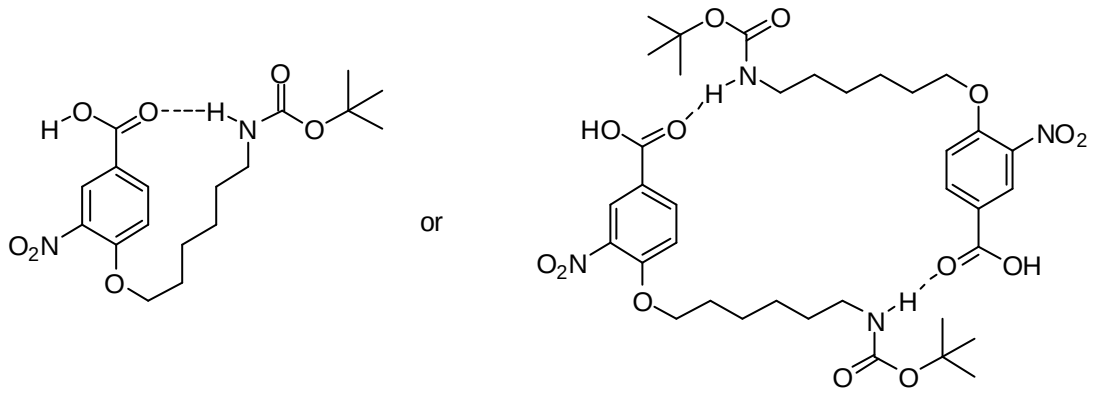

Figure 2-10 Postulated intra and inter molecular H-bonding of the carbamate N-H proton in the benzoic acid derivative **91**.

The precursor methyl ester **90** did not exhibit this carbamate splitting pattern presumably due to the ester functionality not being able to align correctly to evoke hydrogen bonding.

Condensation with tyramine was assessed using both the nitro-acid **91** and the aniline-acid **93**. The latter was associated with complex mixtures and low yields, whilst the nitro-acid **91** coupled to tyramine using CDI in high yield. The difference between these two reactions lay in the disparity between the electron withdrawing

nitro group and the nucleophilic aniline. The aniline was potentially able to react with CDI[225], the *O*-Acylisourea formed with DCC, and the acid chloride formed with the Vilsmeier reagent and hence reduced yields and complex mixtures were observed. The nitro group therefore functioned as a masked amino group, and permitted reactions involving the external nucleophile, tyramine, to proceed unhindered giving intermediate **94**.

The change accompanying the reduction of the nitro group, to compounds possessing fluorescent characteristics was investigated to establish if we could use them directly as a fluorescent ligand without the need to label them with a peripheral dye. The fluorescent properties of compound **96** was determined and found to be unsuitable for use in confocal microscopy or FCS (λ_{abs} 313 nm, λ_{em} 386 nm). The low wavelength λ_{abs} would cause problems with cellular autofluorescence, and the small stoakes shift (73 nm) would make detecting the fluorescence over the background difficult (see section 2.2.4).

The selectivity of succinimidyl esters to acylate 1° amines over other nucleophilic sites was tested in a model reaction between the congener **97** and succinimido 1-naphthaleneacetate **98**. Although the literature would suggest that this reaction is selective to the amine, detailed mechanistic reasoning for amine reactivity was sparse, with stronger basicity, lower steric bulk and the hard basic nature of the 1° amine being shown to increase reactivity with OSu esters[210]. One report however demonstrated that OSu esters, under appropriate conditions can react with serine, threonine and tyrosine hydroxyls in peptide structures[226]. Since **97** displayed three potential nucleophilic sites that could potentially react with BODIPY® 630/650-X OSu **86**, and that the ^{1}H NMR spectra of the BODIPY® 630/650 conjugate **100** was complicated with unresolved protons, the use of the model reaction was necessary and justified to provide conclusive evidence of selectivity. The detailed chemical analysis of the 1-naphthyl-conjugate **101** confirmed that only the desired 1° amine of **97** reacted stoichiometrically with succinimido 1-naphthaleneacetate **98**. The model reaction when combined with reported amine selectivity of OSu esters, a high yield (63%), correct Molecular ion mass, and correct ^{1}H NMR spectrum led us to conclude that selective acylation of the 1° amine of **97** by BODIPY® 630/650-X OSu **86** was achieved.

The affinity of Dansyl-JTE2-6 **99** and BODIPY-JTE2-6 **100** at the human CB_2 receptor was demonstrated to be extremely low. Concentrations of 10^{-4} mol/L of the fluorescent ligands were unable to displace any detectable amount of [^{3}H] CP55, 940 from membrane homogenates containing CB_2 receptors. Any attempt to test concentrations of the fluorescent ligands above 10^{-4} mol/L resulted in precipitation of the drug from the assay solution. BODIPY-JTE2-6 **100** was also screened for affinity towards CB_2 receptors in transfected HEK cell lines by an independent group in the USA to confirm the low binding affinity. These results indicate that large molecular weight dyes located on the terminal end of the 4-alkyl chain abolishes binding to the CB_2 receptor, in the Japan Tobacco series of ligands. Further work to elucidate a position on the Japan Tobacco that will tolerate conjugation to fluorescent dyes was therefore required and will be discussed in chapter 3.

Although the CB_2 binding results indicated that the fluorescent ligands did not bind to the CB_2 receptor with any appreciable affinity, it was necessary to confirm this result using a fluorescent based assay. The BODIPY-NECA adenosine agonist **71** showed very low affinity towards the A_1 receptor (K_i = 22000 nM) in radioligand binding experiments but has been used successfully in both confocal microscopy and FCS experiments (section 2.1.1)[25]. Therefore, we tested the two fluorescent cannabinoid ligands **99** & **100** to determine if they could show selective binding to CHO cells expressing the human CB_2 receptor. Intra-cellular fluorescence was observed for both ligands after 5 minutes at concentrations of 400 nM. This fluorescence was not reduced/abolished when the cells were pre-incubated with the high affinity cannabinoid agonist HU210 **14**, demonstrating that the fluorescence observed was non-specific. The fluorescence observed is most likely due to leeching of the highly lipophilic molecules into the cell through the phospholipid membrane. These results indicate that the two ligands **99** & **100** had no appreciable affinity towards the human CB_2 receptor and were unsuitable as fluorescent CB_2 receptor ligands. The following chapter will discuss our continued efforts to use our initial findings of fluorescently labelling JTE2-6 **63**, to develop modified strategies leading towards a fluorescent CB_2 ligand.

2.7 Conclusions

- We successfully synthesised a derivative of the CB_2 selective ligand JTE2-6 **63**, incorporating an alkyl linker which was labelled with the dansyl and BODIPY® fluorescent dyes.
- A model reaction, using a pseudofluorophore, demonstrated that succinimidyl esters react preferentially with 1° amines when other nucleophilic sites are present.
- The two fluorescently labelled derivatives of JTE2-6 **63** were found to have lost extensive binding affinity at the CB_2 receptor, establishing that bulky substituents at the 4-benzamide position of JTE2-6 **63** was not tolerated within the CB_2 receptor binding pocket.
- The two fluorescent labelled ligands Dansyl-JTE2-6 **99** and BODIPY-JTE2-6 **100** were unable to detect membrane receptor binding in CHO cells expressing the CB_2 receptor, using fluorescent confocal microscopy detection.

3 Molecular modelling of the CB_2 receptor and docking of JTE2-6

Our initial work outlined in chapter 2, concerned modifications to the benzamide ring of JTE2-6 **63**. This approach led to compounds with little affinity to the human CB_2 receptor. This work was carried out rationally with the knowledge that the Japan Tobacco compounds could tolerate molecular extension from the benzamide ring (section 2.2). Prior to our work it was not clear whether a bulky substituent (such as a fluorescent dye) could be incorporated at the terminal end of the alkyl linkers and still retain binding affinity to the CB_2 receptor. Our results with Dansyl-JTE2-6 **99** and BODIPY-JTE2-6 **100**, led us to believe that the benzamide ring of the Japan Tobacco compounds may be positioned deep within the receptor binding pocket when bound within the CB_2 receptor, resulting in large steric/electrostatic clashes with the fluorophore. To test this hypothesis, we embarked on a methodology inspired by Berque-Bestel *et al.* who had designed fluorescent serotonin $5HT_4$ ligands based on ML10302 **79**. This process successfully employed computer modelling of the ligand-receptor complex to guide the positioning of the fluorescent dye (section 2.1.2)[213].

3.1 Computational modelling a of G-protein coupled receptor

G-protein coupled receptors (GPCRs) are seven transmembrane (TM) proteins responsible for the transduction of signals from extra cellular ligands into intra cellular secondary messengers (section 1.3.1). The characteristic structure and intimate relationship with the cellular membrane, makes determination of their 3D structure extremely difficult using standard approaches such as X-ray crystallography and NMR. Although over 12000 structures are deposited in the Protein Data Bank (PDB) by the year 2000 only one of them belonged to the GPCR family[84]. Computational methods have therefore been employed by scientists who wish to study the 3D structure of GPCRs.

3.1.1 Crystal structure template

Many of the early techniques used to model GPCRs were based upon the structure of Bacteriorhodopsin, a 7TM protein which is not associated with a G-protein, since this was the only X-ray crystallography data of a 7TM protein that was available[227]! Recently a high-resolution (2.8 Å) structure of a genuine G-protein associated protein, Bovine Rhodopsin, has been published[81,228]. Comparison of the 3D structures of Bacterio- and Bovine Rhodopsin clearly showed that their 3D structures are significantly different[84]. Some authors have stated that using Bacteriorhodopsin, as a 3D template for modelling GPCRs, leads to models which are too poor to be used for 'rational drug design'[227].

The high-resolution X-ray data of Bovine Rhodopsin used to construct models of GPCRs has recently replaced Bacteriorhodopsin as the template of choice when modelling GPCRs. This template, based on an actual G-protein coupled receptor, is easier to justify as a model and has received positive support in the field of GPCR modelling[82,83,229], however some authors do remain sceptical to the accuracy of the GPCR model generated[84,227]. Use of homology modelling to the 2.8Å model of Bovine Rhodopsin has been demonstrated to yield excellent results in the study of a number of GPCR systems including the dopamine D_2 & D_3 receptors, muscarinic M_1 receptor, and vasopressin V1a receptor[82,83,229].

3.1.2 Sequence alignment

The generic procedure for producing a homology protein model based on comparative modelling has been described by Andrew Leach[230]. The specific methods (or "…recipe [*sic*]…") for homology modelling of GPCRs, using the Bovine Rhodopsin template, have been described by Oliveira *et al.*[231], and is depicted in Figure 3-1. In brief the primary amino acid sequence of the receptor to be modelled is extracted from a sequence data base *i.e.* Swiss-Prot[††]. The primary amino acid sequence can then be aligned against the sequences of other GPCR family members, including Bovine Rhodopsin. The objective of a sequence alignment is to position the amino acid sequences so that the matched stretches of amino acids correspond to common

[††] http://ca.expasy.org/sprot/

structural or functional features (such as the TM α-helices of GPCRs). Gaps in the aligned sequence correspond to regions where polypeptide loops are deleted or inserted. Various alignment algorithms may be used to 'score' the arbitrary alignments and the objective is to ascertain the alignment with the best score. Scoring can be derived from a number of different factors. The simplest type of score is the percentage sequence identity, which gives a score equal to the number of identical matches between the two alignments. This method can be extended by giving positive scores to amino acid residues that are topologically equivalent *i.e.* similar shape, electronic, hydrogen-bonding and hydrophobic properties. The more useful and complicated sequence alignment algorithms are outside the scope of this work but readers are directed to an excellent review of the mathematics behind the techniques[230]. In brief these powerful algorithms use a dynamic programming technique based around matrix problem solving methods. The system uses *gap penalties*, which introduces a negative scoring into the alignment when the sequence has gaps introduced into it to enhance the sequence identity. To cut down computer processing time and to allow for multiple sequence alignments, heuristic search methods such as, FASTA, BLAST and CLUSTAL W are commonly used by molecular modelling laboratories[230,232]. These programmes generally work by rapidly identifying regions of potential interest using fast look-up methods and then expand regions locally to identify the alignment. Alignment of GPCR proteins is made slightly easier, over other protein classes, in that they posses a highly conserved residue in each of the seven TM α-helices[182]. Thus highly conserved residues are matched up first and then the alignment algorithm is allowed to run. Once a satisfactory alignment has been found for the structurally conserved sequences (*i.e* the TM α-helices), the 3D model of Bovine Rhodopsin can be mutated to the amino acids present in the GPCR to be modelled. The intra- and extracellular loops can be added by searching protein databases for the X-ray coordinates of similar peptide sequences to the loop sequence present in the GPCR sequence. Once the model has been constructed it is refined by using molecular mechanics and molecular dynamics to give an energy minimised representation of the GPCR.

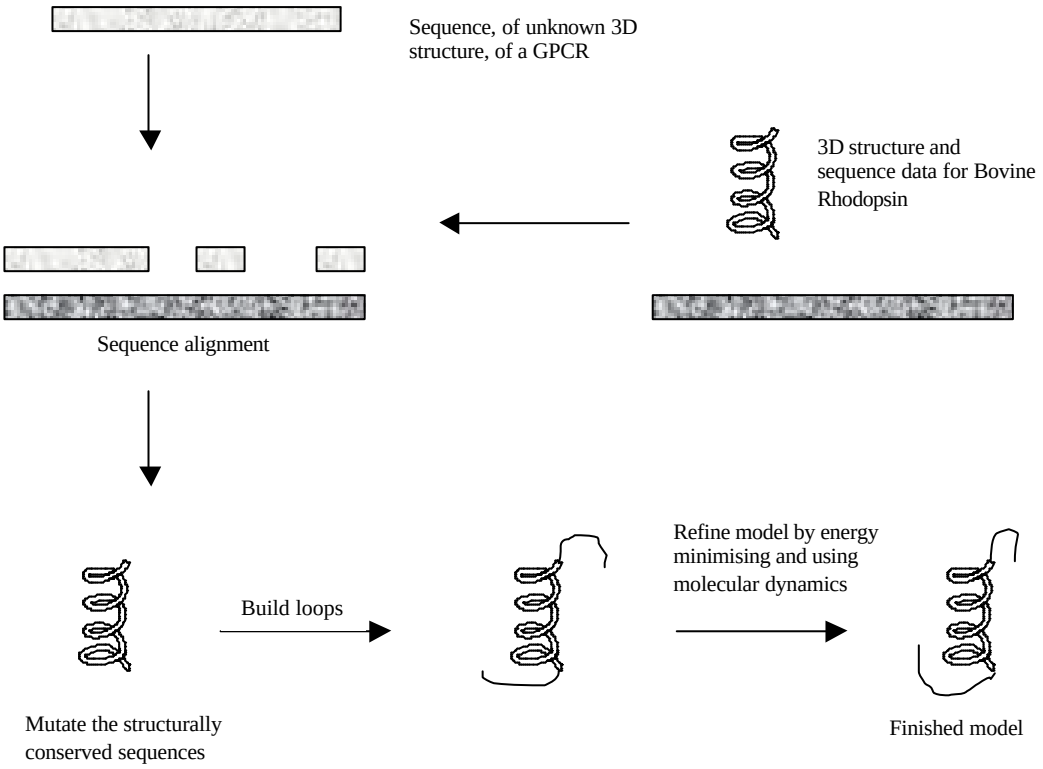

Figure 3-1 Cartoon schematic of generating a 3D GPCR model from the X-ray crystallography data from Bovine Rhodopsin.

3.1.3 Energy minimisation and molecular dynamics

Energy minimisation techniques use complicated mathematical models to lower the potential energy surfaces of macromolecules. Adjusting the internal or Cartesian co-ordinates of the atoms in the structure reduces the electronic and steric interactions occurring within the molecule leading to a lower energy structure. Minimisation methods are capable of finding one of the many energy minimums for a structure; however the minima located may not be the overall global energy minimum (Figure 3-2). This is because minimisation algorithms move the energy in a 'downhill' direction and thus are not capable of surmounting energy barriers to achieve the global energy minimum.

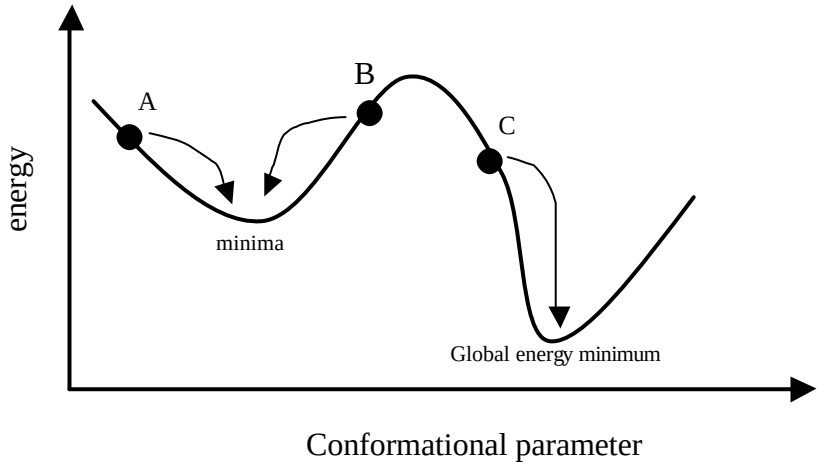

Figure 3-2 A schematic one-dimensional energy surface. The diagram shows that energy minimisation techniques can only move in a 'downhill' direction to the nearest energy minimum. Thus A and B will both find the same energy minimum but it would only be the starting structure C that could find the global energy minimum for this structure.

The actual mathematics used for energy minimisation are outside the scope of this work, however for further information readers are directed to Leach's excellent description of the techniques involved[233]. The main techniques used in energy minimisation are:

- Steepest decent – A nonconvergent first-order minimisation. This method uses a displacement opposite to the potential energy gradient which is added to the coordinates at each step. The step size is increased if a lower energy results; otherwise it is decreased.
- Conjugate gradient – A convergent first-order minimisation. This method makes use of the minimisation history, as well as the current gradient to determine the next step.
- Newton-Raphson method – A second-order derivative method. A very powerful method which uses large amounts of computer memory and is therefore a slow computing process. Due to the memory restrictions this technique is currently limited to systems with about 200 atoms or less[234].
- **A**dopted-**B**asis set **N**ewton-**R**aphson (ABNR) - A convergent method which combines the reduced computing power of first-order techniques with the

increased chance of finding the lowest potential energy state from using the more powerful second order methods.

The choice of which energy minimisation method to use is a balance of a number of factors, including computer processing time, the robustness of the method employed and how far the starting structure is away from the energy minimum. For instance steepest descent is extremely useful in producing initial structures that have had most of their high-energy interactions reduced, in contrast convergent methods are much better once the initial strain has been removed[233]. The more powerful second-order methods such as Newton-Raphson are not suitable for use in GPCR modelling. However, the ABNR technique can be used (due to its refinements in its computer processing ability) and is the method of choice for most large systems[234]. Following energy minimisation the GPCR model is ready to use, having had the high-energy steric and columbic interactions removed.

The model can now be subjected to computer simulation methods. The minimised structure represents an individual minimum energy configuration of a system. In the case of macromolecules, such as GPCRs, there are an enormous number of minima which are closely separated to the one found through minimisation techniques. To study how the receptor behaves as it moves through these phases of energy minima, it is necessary to model successive configurations of the system generated by applying Newton's laws of motion to the system: a technique known as Molecular Dynamics (MD)[235]. Newton's laws can be stated as follows:

1. A body continues to move in a straight line at constant velocity unless a force acts upon it.
2. Force equals the rate of change of momentum.
3. To every action there is an equal and opposite reaction.

Thus the whole macromolecule may be simplistically reduced to balls, representing atoms, and springs, representing bonds. If kinetic energy, in the form of heat (300-900K is normal), is introduced into the system then the set of balls and springs are set in motion. The velocities and atomic coordinates, during MD, must be calculated at definitive time points and this is a critical factor in a successful MD. Too small a time frame and the trajectory will only cover a limited proportion of the phase space; too

large and instabilities may arise due to unrealistic collisions between the atoms. The suggested time step for flexible molecules with flexible bonds such as a GPCR is 1.0 x 10^{-15} seconds (1 fs)[235]. Therefore MD simulations comprising even short time frames, limited to a few hundred ps, require large amounts of computing power and need several days of processor time to complete. During an MD simulation the intermediate structures generated can be analysed both in terms of energy functions or observed as a 3D movie simulation to study key interactions. Any of the structures generated from an MD simulation can be subjected to energy minimisation techniques discussed above to give the best possible representation of what the 3D structure of the GPCR may look like.

3.1.4 Ligand docking

Once the initial GPCR receptor has been constructed, a ligand can be docked into the receptor. The docking of a ligand in a GPCR has been recommended to be done using the binding pocket that encases 11-*cis*-retinal; the covalently bound natural ligand of Bovine Rhodopsin[84]. The retinal molecule, bound in Bovine Rhodopsin, is located within the TM regions; specifically interacting with TM 3, 5 and 6[81,83]. It has been shown, mainly through site-directed mutagenesis studies, that for other GPCR systems the small-molecule binding site is also located within the TM regions[84]. Thus, TM 3, 5, 6 and 7 are known to interact with agonist ligands in the β_2-adrenergic receptor, TM 3 has been demonstrated to interact with ligands in the $5HT_{1A}$ receptor, and TM 3, 5 and 7 are involved in the antagonist binding of losartan in the angiotensin II receptor[84]. It is clear from this picture that there is not a common binding pocket for the GPCRs. However, by using the natural retinal binding pocket within Bovine Rhodopsin and using the available site-directed mutagenesis and other 'common knowledge' for a particular ligand-GPCR interaction, it is possible to build a useful and predictive model[84]. It is noteworthy to state that once a ligand has been docked into a GPCR, energy minimisation and molecular dynamics can be used to generate energy minima structures as discussed in section 3.1.3.

3.2 Previous modelling of the CB_2 receptor

The CB_2 receptor, a member of the GPCR superfamily, has been cloned and characterised in human, rat and mouse species[4,104-106] (section 1.3.4). To date, like all other GPCRs, there is no X-ray crystallography or conclusive NMR data available to help elucidate the 3D structure of the CB_2 receptors. Knowledge of the 3D structure would help researchers understand the intimate ligand-receptor interactions occurring within the receptor. Specifically it would allow us to determine the best position to locate a fluorescent dye on the Japan Tobacco pharmacophore.

To allow us to accurately represent the 3D structure of the CB_2 receptor we considered work previously undertaken by other researchers, who have examined the molecular pharmacology of the CB_2 receptor using mutagenesis and molecular modelling techniques.

3.2.1 Mutational analysis

Studies using single-point mutations and chimeric receptors have been used to locate important binding interactions necessary for selective CB_2 binding. A summary of this work is shown in Table 3-1.

In the absence of a 3D-crystal structure, accurate modelling of the integral membrane proteins depends heavily on mutational analysis. This technique can afford information on the key amino acids and regions of amino acids that are important to receptor function. Mutations have concentrated on the suspected binding pockets located within the extra cellular loops (EL) and the transmembrane (TM) regions. Shire *et al.*, commented that the experimental protocol for mutational analysis of the cannabinoid receptors is more difficult than with other GPCRs[236]. His reasons were based on the low amino acid identity between CB_1 and CB_2 receptors, particularly in TM 1, TM 4 and TM 5 (section 1.3.4), and that the cannabinoid subfamily are characterised by structural features not found in the majority of GPCRs. Thus, the lack of EL 1/TM 3 cysteines, the absence of a highly conserved proline residue in TM 5, and the unusual 2 cysteine residues found in EL 2 of CB_1 and CB_2 make extrapolation of previous mutations to GPCRs extremely difficult.

Mutational work has shown there may be different binding pockets for the different sub-classes of cannabinoid ligands[154,182,194]. The aminoalkylindoles (e.g. Win 55212-2 **3**), classical cannabinoids (e.g. CP 55, 940 **2**) and the biarylpyrazole (e.g. SR

144528 **6**) have been shown by mutational analysis to form distinct binding interactions with different amino acids within the CB_2 receptor.

CB_2 residue mutated	Mutation	Effect on Ligand Binding	Amino Acid position	Reference
Lys 109	Ala	CP55,940 (=), Win 55212-2 (=)	TM 3	154
Lys 109	Arg	CP55,940 (=), Win 55212-2 (=)	TM 3	154
Ser 112	Gly	CP55,940 (-), Win 55212-2 (=)	TM 3	154
Phe 197	Val	CP55,940 (=), Win 55212-2 (-)	TM 5	194
Tyr 190[a]	Phe	CP55,940 (=), Win55212-2 (=)	TM 5	237
Tyr 190[a]	Ile	Abolished binding	TM 5	237
Trp 172	Phe	CP55,940 (=), Win55212-2 (=)	TM 4	238
Trp 172	Ala	Abolished binding	TM 4	238
Asp 130	Ala	HU-210 (-), Win 55212-2 (-)	TM 3	239,240
Ser 161	Ala	CP55,940 (=), Win 55212-2 (=), SR144528 (-)	TM 4	182
Ser 165	Ala	CP55,940 (=), Win 55212-2 (=), SR144528 (-)	TM 4	182
Cys 174	Ser	Abolished binding	TM 4	182
Cys 179	Ser	Abolished binding	EL 2	182
Cys 175	Ser	CP55,940 (=), Win 55212-2 (-), SR144528 (-)	EL 2	182

Table 3-1 A summary of the mutational work published on the CB_2 receptor, including the amino acid residue mutated, the position within the receptor and the reference. (=) binding is not significantly different from wild type. (-) binding is significantly reduced from wild type. TM transmembrane. EL extra cellular loop. (a) **In their publication McAllister *et al*[237].refer to this residue as Tyr 191. This was a typographical error confirmed in a personal communication from the authors**.

The binding of Win 55212-2 **3**, a CB_2 selective indole cannabinoid (section 1.4.6), to the CB_2 receptor has been shown to involve important aromatic stacking interactions; rather than ionic- or H-bonding interactions[194]. Experimental evidence for this has involved mutation of the unique Phe 197 found in CB_2 to a valine resulting in a 14 fold decrease in Win 55212-2 **3** binding[194]. Other single point mutations of aromatic residues (Trp 172 & Tyr 190) to non-aromatic amino acids have also been show to significantly reduce the binding of Win 55212-2 **3**[237,238]. However, when conservative mutation of these residues to the aromatic amino acid Phe was conducted, binding of Win 55212-2 **3** was unaltered[237,238]. Further evidence of aromatic stacking interactions involving Win 55212-2 **3**, including SAR data, are discussed in section 1.4.6.1. Furthermore, mutations of H-bonding or ionic bonding residues such as Ser 112[154], Ser 161[182], Ser 165[182], and Lys 109[154] within the CB_2 receptor failed to alter the binding of Win 55212-2 **3**. A chimeric receptor generated by replacing the TM 3

region of a CB_1 receptor with TM 3 of the CB_2 receptor, increased the binding of Win 55212-2 **3**[193]. This result demonstrated that subtype selectivity of Win 55212-2 **3** for the CB_2 receptor may be a result of amino acid residues present in TM 3. Further work by this group pointed to residue Ser 112 in the CB_2 receptor (analogous to Gly 195 in CB_1) as key to the subtype specificity of Win 55212-2 **3**. This was demonstrated by mutating Gly 195 in CB_1 to Ser[193]. The four-fold increase in binding of Win 55212-2 **3**, to this mutant, was attributed to CB_2's Ser 112 being involved in crucial interactions with Win 55212-2 **3**. However, later work, mutating Ser 112 to Gly in the CB_2 receptor failed to support this argument[154]. Chimeric work by Shire *et al.* has demonstrated that only TM 4-EL 2-TM 5 (Phe 197 is found in TM 5) of the CB_2 receptor is necessary for Win 55212-2 **3** selectivity[236].

Studies to show the effect of certain amino acids in the CB_2 receptor on the binding of the non-classical cannabinoid CP 55,940 **2** have been unclear. It was initially thought that hydrogen bonding interactions would play an important role in binding due to the number of hydroxyl groups present on CP 55,940 **2** (figure 1-13). However mutation of Lys 109 (analogous to Lys 192 in the CB_1 receptor) to Ala and Arg, had no effect on the binding of CP 55,940 **2** to the CB_2 receptor[154]. This is in direct contrast to the mutation of Lys 192 in the CB_1 receptor which was shown to be critical for binding of these ligands[152]. These two results would indicate that H-bond interactions, occurring between Lys and hydroxyls in the cannabinoids, are important in the CB_1 receptor but not required in the CB_2 receptor. A separate study showed that a H-bonding interaction between CP 55,940 **2** and the CB_2 receptor was contributing to the ligand-receptor binding[154]. They mutated Ser 112 present in TM 3 of the CB_2 receptor to Gly and reported that this change significantly reduced the binding of CP 55,940. It was concluded that hydrogen bond interactions between the NAH (Figure 1-13) and Ser 112 in TM 3 was important for CB_2 binding of CP 55,940 **2**.

SAR work with classical and non-classical cannibinoids has probed the importance of the phenol group and the NAH function of CP-55,940 **2** and similar molecules. These studies have clearly shown that the hydroxyl groups present in the molecules are not required for CB_2 binding (sections 1.4.2.4 & 1.4.3.1) and it is likely therefore that hydrogen bonding interactions are not involved in the binding of these cannabinoids in the CB_2 receptor.

Mutational analysis probing the binding interactions of SR 144528 **6** has been conducted. Initial work by Shire *et al.* concentrated on replacing regions of the CB_1 receptor, that has essentially no affinity with SR144528 **6**, with the analogues regions from the CB_2 receptor and monitoring the binding of SR144528 **6** to the chimeric receptor[236]. They demonstrated that TM 4-EL 2-TM 5 of the CB_2 receptor was responsible for the CB_2 selectivity of SR144528 **6**. Further work by the same group, using single point mutations, indicated both Ser 161 and Ser 165 on TM 4 contributed to H-bonding interactions with SR144528 **6**[182]. Mutation of a non-conserved Cys 175 residue in CB_2's EL 2 abolished binding of SR144528 **6**, but did not adversely affect CP 55, 940 **2** or Win 55212-2 **3**[182]. This sulphur-containing residue was postulated to form either direct sulphur-π interactions, or an undetermined disulphide bridge, which are considered important to ligand recognition. Other work has shown that independent mutation of Cys 174 and Cys 179 results in receptors that do locate to the membrane, but fail to bind any of the cannabinoid ligands tested[236]. A structurally vital disulphide bridge has been proposed between them[182]. The highly conserved DRY motif (Asp 130, Arg 131, and Tyr 132 in the TM 3 of the CB_2 receptor) found in the majority of GPCRs has been evaluated for its role in ligand binding. In a CB_2 mutational study it was found that Asp 130 mutations markedly reduced all classical and indole cannabinoid binding[239].

In summary, these data indicates that there are different binding interactions occurring with the different classes of chemical ligands. Specific amino acid changes may affect the binding of just one ligand, such as Ser 112 or Phe 197, or may abolish binding for all of the cannabinoid classes tested, such as Tyr 190 or Trp 172 (Table 3-1). This may be indicative of whether the amino acid involved is associated with key ligand-receptor interactions or is involved in the overall structure of the TM helix and therefore the shape of the binding pocket. The most consistent data discussed regards the binding of Win 55212-2 **3**, for which an aromatic-aromatic ligand-receptor binding nature has clearly been established. This has specifically involved the residue Phe 197, present in the CB_2 receptor, and is thought to confer an extra aromatic interaction that results in CB_2 selectivity of Win 55212-2 **3**.

3.2.2 Molecular modelling studies

The first computational model of a cannabinoid receptor, conducted in 1995, was for the CB_1 receptor[153,190]. Their methodology aligned the TM regions of the CB_1 receptor with the sequences of 58 other GPCRs, using the highly conserved amino acids present in each of the TM helices. TM 5 of the CB_1 (and the CB_2 receptor) which does not contain the highly conserved proline used for alignment, needed to be identified using structural alignment based on its hydrophobicity profile. The helices were modelled using the ChemProtein module (Chem-X suite) and aligned to the TM helix bundle present in the X-ray structure of Bacteriorhodopsin. This original model of the CB_1 receptor, was then adapted by researchers interested in the CB_2 receptor by mutating the CB_1 residues into corresponding sequence-aligned CB_2 residues[153,154,194]. Thus, early modelling of the CB_2 receptor was based entirely on a CB_1 receptor model; which was originally based on the non G-protein associated Bacteriorhodopsin. A later CB_2 model employed similar methodology used above, but mutated a model of the β_2-adrenoreceptor to the CB_2 receptor based on sequence alignment data of the human CB_2 receptor aligned to sequences of the β-adrenoreceptor family[182]. The original model of the β_2-adrenoreceptor was built using the crystal structure of Bacteriorhodopsin as a template[241]. Therefore two different methods used to construct the CB_2 receptor were both based on the crystal structure data of Bacteriorhodopsin, which, as discussed in section 3.1, has limitations and has been superseded by Bovine Rhodopsin [227]. After we had concluded our own studies, Xie *et al.* published a further model of the CB_2 receptor[242]. They were the first to publish a CB_2 receptor model based on the 2.8Å crystal structure data from Bovine Rhodopsin aligning Bovine Rhodopsin with five cannabinoid receptors (including the human CB_2 receptor) and four other GPCRs.

3.2.2.1 Results from previous CB_2 models

Each of the previous models conformed to the classical shape of a GPCR receptor, consisting of seven alpha helical TM regions arranged in a 'barrel' formation, which were linked by extra and intra-cellular loops. To provide information on the intimate interactions occurring within the CB_2 receptor binding pocket, three of the CB_2 models were used in ligand-receptor binding simulations with different cannabinoid

ligands[154,182,194]. The data from these studies, suggested that the binding site within the CB_2 receptor was located within the TM bundles - although the exact combination of TM helices involved was ligand dependent. The results from these three studies are summarised as follows;

Song *et al*. evaluated the binding of Win 55212-2 **3**[194]. They proposed aromatic stacking interactions, occurring between amino acids present within TM 3, 4 and 5 and Win 55212-2 **3**, to be the primary ligand-receptor interactions. They reported that selectivity shown by Win 55212-2 **3** for CB_2 receptors is due to an extra aromatic interaction that can be formed between Win 55212-2 **3** and Phe 197 on the CB_2 receptor. Phe 197 is not present in the CB_1 receptor and cannot form this extra interaction. Other amino acids shown to form ligand interactions are detailed in Table 3-2.

CP 55,940 **2** was docked in a model generated by Tao *et al*[154]. They demonstrated that its binding had elements of hydrophobic and hydrogen-bonding interactions with the receptor. The most important of these interactions was established to be a H-bond between Ser 112 and the NAH of CP 55,940 **2**. Other ligand-receptor interactions associated with amino acids present within TM 3, 6 and 7 were highlighted in their study but were not discussed.

SR 144528 **6** was docked in a CB_2 model generated by the Gouldson group[182]. From their work, they proposed that the interactions of SR 144526 **6** with the CB_2 receptor were a mixture of aromatic, hydrophobic and hydrogen bonding. The H-bonds were formed between the pyrazole nitrogen and the carbonyl group of SR 144528 **6** (figure 1) and the hydroxyl hydrogens of Ser 161 and Ser 165 located in TM 4. Other contacts made with SR 144528 **6** are listed in Table 3-2. The TM helices involved in SR144528 **6** binding are 3, 4 and 5. Importantly, this model has several features in common with the one proposed by Song *et al.* for Win 55212-2 **3** binding[194], especially the importance of aromatic stacking and the involvement of common aromatic amino acids namely Phe 197 and Trp 194. The similarity in the two models is important, as the two groups produced independent work, and used different sequence alignment protocols. In addition both groups had distinct mutagenesis data which was used as an initial anchor point for ligand docking.

Ligand used to explore binding pocket	Key amino acid residues shown to be involved in binding	Type of ligand-receptor interaction involved	TM location of the amino acid residue
Win 55212-2 **3**[1]	Phe 106	Aromatic	3
	Phe 117	Aromatic	3
	Trp 194	Aromatic	5
	Phe 197	Aromatic	5
SR 144528 **6**[2]	Leu 125	Hydrophobic	3
	Leu 126	Hydrophobic	3
	Ser 161	H-bond	4
	Ser 165	H-bond	4
	Trp 172	Aromatic	5
	Trp 194	Aromatic	5
	Phe 197	Aromatic	5
CP 55, 940 **2**[3]	Ser 112	H-bond	3
	Thr 116	H-bond	3
Solvent-accessible methods[4]	Phe 117	Aromatic	3
	Tyr 190	Aromatic	5
	Phe 197	Aromatic	5
	Trp 258	Aromatic	6

Table 3-2 Key amino acid residues implicated in forming important ligand-binding from computational modelling studies. 1 ref 194. 2 ref 182. 3 ref 154. 4 ref 242.

The CB_2 receptor constructed using the template of Bovine Rhodopsin, published after we had concluded our work, did not use a ligand docking experiment to investigate the ligand binding pocket[242]. Instead they used solvent-accessible surface approaches to determine the amino acids that could form interactions in a ligand binding pocket. The amino acid residues highlighted in their discussion are shown in Table 3-2. Their studies showed that the binding site was amphipathic with a hydrophilic centre located close to the extracellular loop 2 (shown in blue) and a hydrophobic cleft buried deeper in the receptor (shown in yellow) which is 'framed' with the aromatic residues Phe 117 (TM 3), Phe 197 (TM 5) and Trp 258 (TM 6) (Figure 3-10). Overall the helices postulated to be involved with the binding pocket were TM 3, 5, 6, and 7.

In conclusion the various modelling studies conducted to date have shown that the ligand binding pocket is located within the TM helices of the CB_2 receptor. The exact TM helices and amino acid residues involved in ligand binding is dependent upon the cannabinoid that was used in the study. TM 3, 4, 5, 6 and 7 have each been shown to be involved in ligand binding. The most consistent interaction demonstrated to be important is aromatic-aromatic in nature, with three of the four models specifically highlighting Phe 197 as an amino acid crucial to ligand binding. Interestingly, the analogous residue to Phe 197 in other GPCRs have also been reported to be an important binding residue in the β-adrenoreceptor and serotonin receptors[194]. The binding models proposing TM 4 as a binding helix are unusual in GPCR modelling. However previous studies implicating TM 4 in binding have been reported for the neuropeptide type receptors *i.e.* substance P, neurotensin type 1 and neuropeptide Y type 1[182]. The data provided from these studies were used to guide our experimental modelling work.

3.3 Experimental results - molecular modelling of the CB_2 receptor

3.3.1 Sequence alignment

The human CB_2 receptor was initially sequence aligned against human CB_1 and the Bovine Rhodopsin (BR) sequences obtained from Swissprot (Swissprot reference numbers: P34972 (CB_2), P21554 (CB_1), and P02699 (BR)) using the sequence alignment program ClustalW (Version 1.81)[232]. Manual alignment of the CB_2 sequence with Bovine Rhodopsin was conducted to locate the homology aligned regions. Three different alignments were generated by varying the alignment of TM 5 of the CB_2 receptor with the corresponding Bovine Rhodopsin sequence. TM 5 of the CB_2 receptor does not contain the usual conserved proline within its sequence and has been a difficult issue to resolve for each of the groups conducting modelling of the cannabinoid receptors (see section 3.2.2). The three different alignments we used are shown in Figure 3-3.

Alignment 1

```
hCB2 --MEECWVTEIANGSKDGLDSNPMKD--YMILSGPQKTAVAVLCTLLGLLSALENVAVLY 56
BR   MNGTEGPNFYVPFSNKTGVVRSPFEAPQYYLAEPWQFSMLAAYMFLLIMLGFPINFLTLY 60

hCB2 LILSSHQLRRKPSYLFIGSLAGADFLASVVFACSFVNFHVFHGVDSKAV--FLLKIGSVTMT 116
BR   VTVQHKKL-RTPLNYILLNLAVADLFMVFGGFTTTLY-TSLHGYFVFGPTGCNLEGFFATLG 120

hCB2 FTASVGSLLLTAIDRYLCLRYPPSYKALLTRGRALVTLGIMWVLSALVSYLPLMGWT-CC 176
BR   GEIALWSLVVLAIERYVVVCKPMSNFRFGEN-HAIMGVAFTWVMALACAAPPLVGWSRYI 179

hCB2 PRP--CSELFPLIPNDYLLSWLLFIAFLFSGIIYTYGHVLWKAHQHVASLSGHQDR-QVP 232
BR   PEGMQCSCGIDYYTPHEETNNESFVIYMFVVHFIIPLIVIFFCYGQLVFTVKEAAAQQQE 239

hCB2 GMARMRLDVRLAKTLGLVLAVLLICWFPVLALMAHSLATTLSDQVKKAFAFCSMLCLINS 292
BR   SATTQKAEKEVTRMVIIMVIAFLICWLPYAGVAFYIFTHQGSDFGPIFMTIPAFFAKTSA 299

hCB2 MVNPVIYALRSGEIRSSAHHCLAHWKKCVRGLGSEAKEEAPRSSVTETEADGKITPWPDS 352
BR   VYNPVIYIMMNKQFRNCMVTTLCCGKNPLGD--DEASTTVSKTETSQVAPA-------- 348

hCB2 RDLDLSDC 360
BR   -------- 
```

Alignment 2

```
hCB2 --MEECWVTEIANGSKDGLDSNPMKD--YMILSGPQKTAVAVLCTLLGLLSALENVAVLY 56
BR   MNGTEGPNFYVPFSNKTGVVRSPFEAPQYYLAEPWQFSMLAAYMFLLIMLGFPINFLTLY 60

hCB2 LILSSHQLRRKPSYLFIGSLAGADFLASVVFACSFVNFHVFHGVDSKAV--FLLKIGSVTMT 116
BR   VTVQHKKL-RTPLNYILLNLAVADLFMVFGGFTTTLY-TSLHGYFVFGPTGCNLEGFFATLG 120

hCB2 FTASVGSLLLTAIDRYLCLRYPPSYKALLTRGRALVTLGIMWVLSALVSYLPLMGWT-CC 176
BR   GEIALWSLVVLAIERYVVVCKPMSNFRFGEN-HAIMGVAFTWVMALACAAPPLVGWSRYI 179

hCB2 PRP—---CSELFPLIPNDYLLSWLLFIAFLFSGIIYTYGHVLWKAHQHVASLSGHQDRQVP 232
BR   PEGMQCSCGIDYYTPHEETNNESFVIYMFVVHFIIPLIVIFFCYGQLVFTVKEAAAQQ-QE 239

hCB2 GMARMRLDVRLAKTLGLVLAVLLICWFPVLALMAHSLATTLSDQVKKAFAFCSMLCLINS 292
BR   SATTQKAEKEVTRMVIIMVIAFLICWLPYAGVAFYIFTHQGSDFGPIFMTIPAFFAKTSA 299

hCB2 MVNPVIYALRSGEIRSSAHHCLAHWKKCVRGLGSEAKEEAPRSSVTETEADGKITPWPDS 352
BR   VYNPVIYIMMNKQFRNCMVTTLCCGKNPLGD--DEASTTVSKTETSQVAPA-------- 348

hCB2 RDLDLSDC 360
BR   -------- 
```

Alignment 3

```
hCB2 --MEECWVTEIANGSKDGLDSNPMKD--YMILSGPQKTAVAVLCTLLGLLSALENVAVLY 56
BR   MNGTEGPNFYVPFSNKTGVVRSPFEAPQYYLAEPWQFSMLAAYMFLLIMLGFPINFLTLY 60

hCB2 LILSSHQLRRKPSYLFIGSLAGADFLASVVFACSFVNFHVFHGVDSKAV--FLLKIGSVTMT 116
BR   VTVQHKKL-RTPLNYILLNLAVADLFMVFGGFTTTLY-TSLHGYFVFGPTGCNLEGFFATLG 120

hCB2 FTASVGSLLLTAIDRYLCLRYPPSYKALLTRGRALVTLGIMWVLSALVSYLPLMGWT-CC 176
BR   GEIALWSLVVLAIERYVVVCKPMSNFRFGEN-HAIMGVAFTWVMALACAAPPLVGWSRYI 179

hCB2 PRP----CSELFPLIP------NDYLLSWLLFIAFLFSGIIYTYGHVLWKAHQHVASLSGHQDRQVP 232
BR   PEGMQCSCGIDYYTPHEETNNESFVIYMFVVHFIIPLIVIFFCYGQLVFTVKEAAA-----QQQE-- 239

hCB2 GMARMRLDVRLAKTLGLVLAVLLICWFPVLALMAHSLATTLSDQVKKAFAFCSMLCLINS 292
BR   SATTQKAEKEVTRMVIIMVIAFLICWLPYAGVAFYIFTHQGSDFGPIFMTIPAFFAKTSA 299

hCB2 MVNPVIYALRSGEIRSSAHHCLAHWKKCVRGLGSEAKEEAPRSSVTETEADGKITPWPDS 352
BR   VYNPVIYIMMNKQFRNCMVTTLCCGKNPLGD--DEASTTVSKTETSQVAPA-------- 348

hCB2 RDLDLSDC 360
BR   -------- 
```

Figure 3-3 The three sequence alignments used to generate the different CB_2 receptor models, which vary in the alignment of TM 5. The TM helices are highlighted in the following colours: 1 (yellow); 2 (green); 3 (turquoise); 4 (magenta); 5 (red); 6 (grey); 7 (blue). hCB_2 – human CB_2 sequence. BR – Bovine Rhodopsin sequence. Amino acids represented by standard single letter codes.

3.3.2 Homology modelling to Bovine Rhodopsin

The 3D crystal structure of Bovine Rhodopsin (BR) was extracted from the Protein Data Bank and imported into Sybyl® (Tripos). The BR model was modified by removing the B chain and the glycosylations associated with the molecule. Using *Mutate Monomers* each of the BR helices were mutated to the aligned sequences shown in Figure 3-3 to generate the three different alignment models. The remaining loop sections of the CB_2 model were completed by searching the PDB database using the *Build Loops* function for matching amino acid sequence to the CB_2 loop sequences. The highest scored loops were inserted into the model and manual selection of the best fitting loops was employed. The final models were checked for amino acid chirality, proline ring integrity and were finally screened against the original CB_2 sequence for monomer sequence. The three models were then subjected to energy minimisation within Sybyl® using 100 Steepest Descent iterations followed by 500 Conjugate Gradient steps using the standard Sybyl® setup for each minimisation. The three models, produced by the homology modelling described, are shown in Figure 3-4. The amino acid structures displayed in ball and stick style are the key amino acids previously shown to be important in ligand-receptor binding (see Table 3-1 and Table 3-2). The Ramachandran plots for all three receptors were generated using the programme PROCHECK[243] and are shown in Figure 3-4. For further details on Ramachandran plots, readers are directed to the original paper by Ramachandran *et al*.[244]. The shaded areas of the plots (red, yellow, pink) correspond to the contoured distribution of the ϕ and ψ torsion angles between amide bonds, averaged from the X-ray crystallography data accumulated for 118 protein structures. It is clear from these plots that all three structures have amino acid backbones conformations that are typically found in many other protein structures. Alignment 3, possessed the most favourable conformational space according to the Ramachandran analysis with 74.1% of the residues lying in the most favoured region (22.1% in allowed regions; 2.2% in generously allowed regions; 1.6% in disallowed regions).

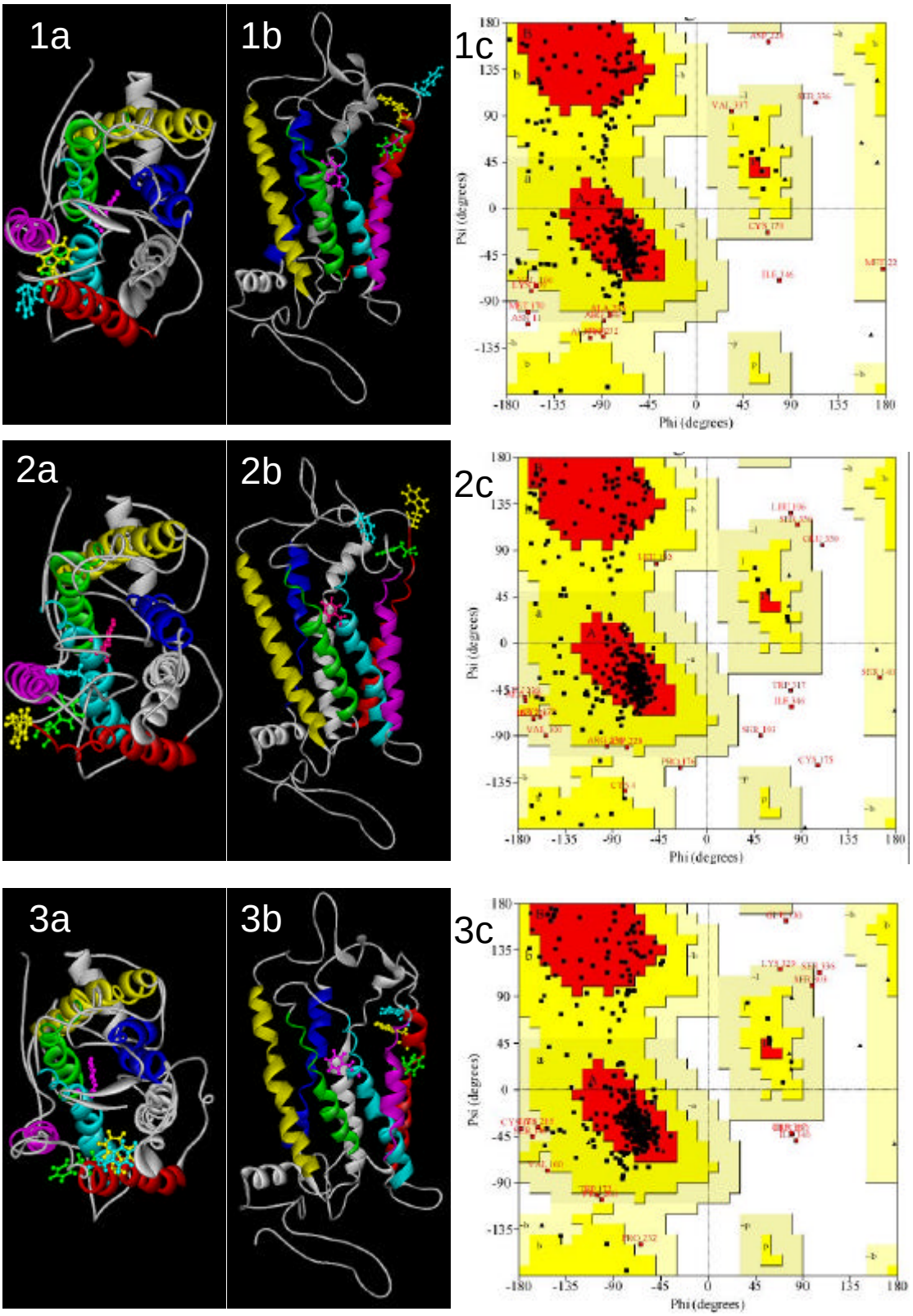

Figure 3-4 Representations of the three human CB_2 models built by homology modelling to Bovine Rhodopsin. 1a Alignment 1 view from top. 1b Alignment 1 view from side. 1c Ramachandran plot of Alignment 1. 2a Alignment 2 view from top. 2b Alignment 2 view from side. 2c Ramachandran plot of Alignment 2. 3a Alignment 3 view from top. 3b Alignment 3 view from side. 3c Ramachandran plot of Alignment 3. Amino acids shown are Phe 117 (Magenta), Tyr 190 (Cyan), Trp 194 (yellow), Phe 197 (green). Helix colour: 1, 2, 3, 4, 5, 6, and 7. Ramachandran plot - darker colours represent favourable regions of amide bond torsions with black dots representing amino acids from the CB_2 receptor model.

Alignment 3 also had the key amino acids, implicated in ligand binding, located within the TM regions when compared to the other two models. It was therefore decided to discard Alignments 1 and 2 and continue only with Alignment 3. The model from Alignment 3 was energy minimised using the ABNR minimisation algorithm using CHARMM software[234], using the protocol: minimise hydrogens only (100 steps); minimise side chains only (2000 steps); minimise complete structure (25000 steps) until the root-mean-square-derivative (RMSD) reached 0.005 KJmol^{-1}. No C or N end-caps were used and a dielectric constant of 4.0 was utilised to mimic the phospholipids membrane. This model will now be referred to as Alignment 3.

3.3.3 Docking JTE2-6 into the CB_2 receptor

JTE2-6 **63** was constructed using Spartan PCPro (Wavefunction Inc.). Geometry optimisation was undertaken using quantum mechanical methods, namely *ab initio* Hartree-Fock calculations at the 3-21G* level. In addition, partial atom charges were calculated using the electrostatic surface potential (ESP) method. JTE2-6 **63** was interactively docked into Alignment 3 using Phe 197 as an anchor point for an aromatic-aromatic interaction with the ligand. JTE2-6 **63** was docked into the binding pocket in both a phenol-up and phenol-down position as shown in Figure 3-5.

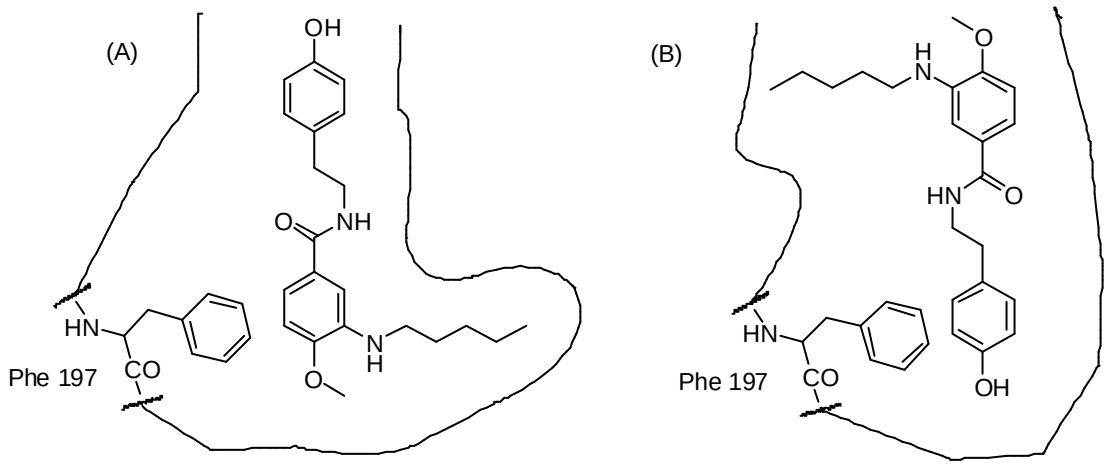

Figure 3-5 JTE2-6 **63** was docked into the CB_2 receptor in the (A) phenol-up and (B) phenol-down position using Phe 197 as a guiding anchor point.

The ligand-receptor complexes were further optimised using energy minimisation and molecular dynamics. In our studies, we applied the CHARMM force field with an 8 Å

cut-off for non-bonded interactions to optimize the ligand-receptor model. In order to mimic the hydrophobic transmembrane environment we set the dielectric constant to a value of 4.0. The molecular dynamics protocol consists of: i) initial minimisation of 2500 iterations of ABNR conjugate gradients minimisation until the RMSD becomes less than 0.005 KJmol^{-1}; ii) MD simulations were performed by placing a harmonic constraint on the 7 backbone α-helices, heating the structure to 300K over 1ps, and running at constant temperature (300K) for 100 ps with a 1fs time step; iii) quenching the structure to 0K over 1 ps, removing all constraints and final minimisation using ABNR conjugate gradients (6000 iterations) until the RMSD became less than 0.005 KJmol^{-1}.

The energy of the two complexes was monitored throughout the molecular dynamics experiment at 0.5 ps time intervals. The plot of the total energy of the complex *versus* time is shown in Figure 3-6.

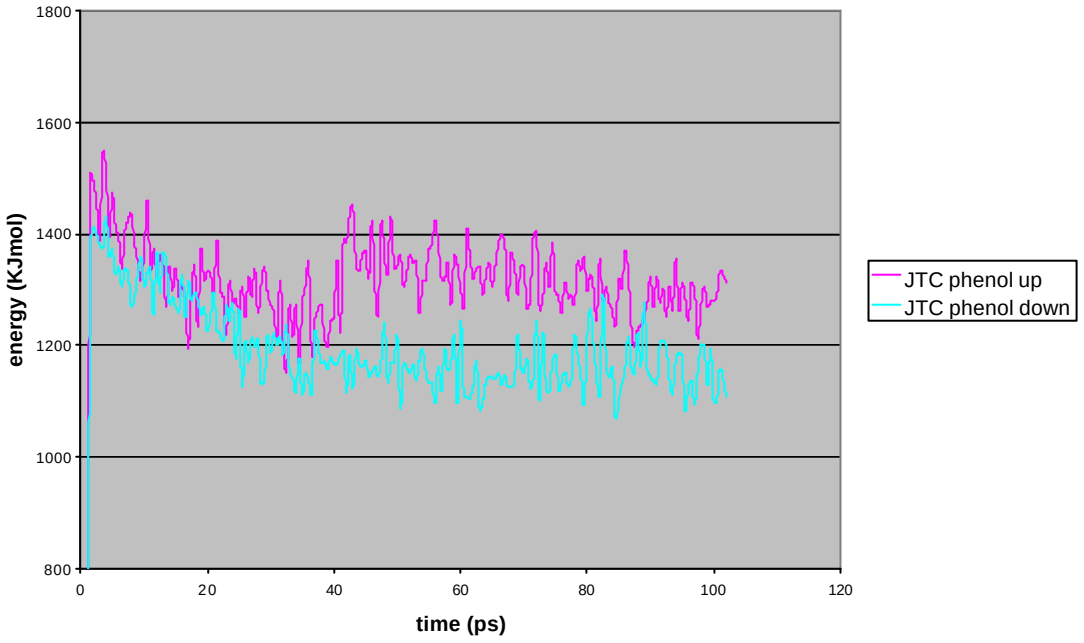

Figure 3-6 Energy profile of JTE2-6**63**-CB_2 receptor complex over a 0.1 ns molecular dynamic simulation performed at 300K using the CHARMM force field.

It is clear from the above graph that the energy of both systems increased rapidly during the first ps as the systems were heated from 0K to 300K. Once 'energised' both systems energy decrease over the first 40 ps. In the phenol-down complex this lower energy is continued during the rest of the simulation but in the phenol-up

complex the energy is transiently raised at around 40 ps before falling again over the remaining period of the simulation.

The final energy minimised ligand-receptor complexes are shown in Figure 3-7.

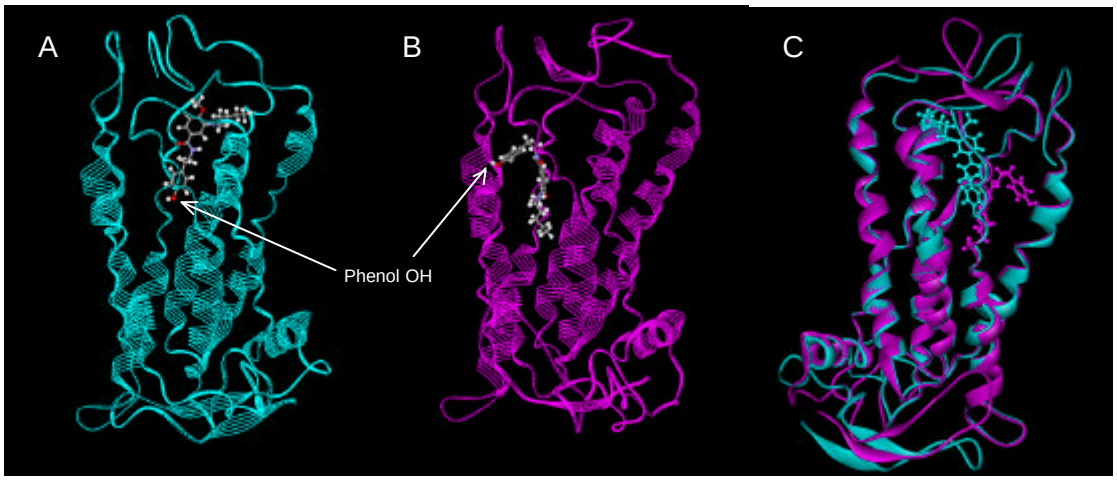

Figure 3-7 Representations of JTE2-6 **63** docked into the human CB_2 receptor (Alignment 3). (A) Phenol-down model. (B) Phenol-up model. Both these images show the ligand JTE2-6 **63** in its final binding position/conformation. Model is being viewed with TM 6 front and centre. (C) Overlay of phenol-up (magenta) and phenol-down (cyan) bound into the CB_2 receptor showing the relative positions of the ligand in both models. Model is being viewed with TM 2 front and centre. TM 4 has been removed for clarity.

From Figure 3-7 it can be seen that the human CB_2 receptor can accommodate JTE2-6 **63** docked in either position. However, the conformation of the ligand and the absolute binding position of the ligand changes between both models (Figure 3-7, C). The key amino acids involved in ligand-receptor interactions was explored using the programme Ligplot for each model[245]. The results from this analysis are shown in Figure 3-8. It can be clearly seen that the amino acids involved in the binding of JTE2-6 **63** differ between the two docked models. In the phenol-up model the amino acids residues involved are residues that have been demonstrated to be involved in the binding of other cannabinoid ligands (see Table 3-1 and Table 3-2); notably Phe 117, Trp 194, and Phe 197. The residues interacting in the phenol-down model have not been implicated in cannabinoid binding in previous studies and include an interaction with an amino acid located in TM helix 2 (His 95) which has previously not been shown to be involved in cannabinoid binding.

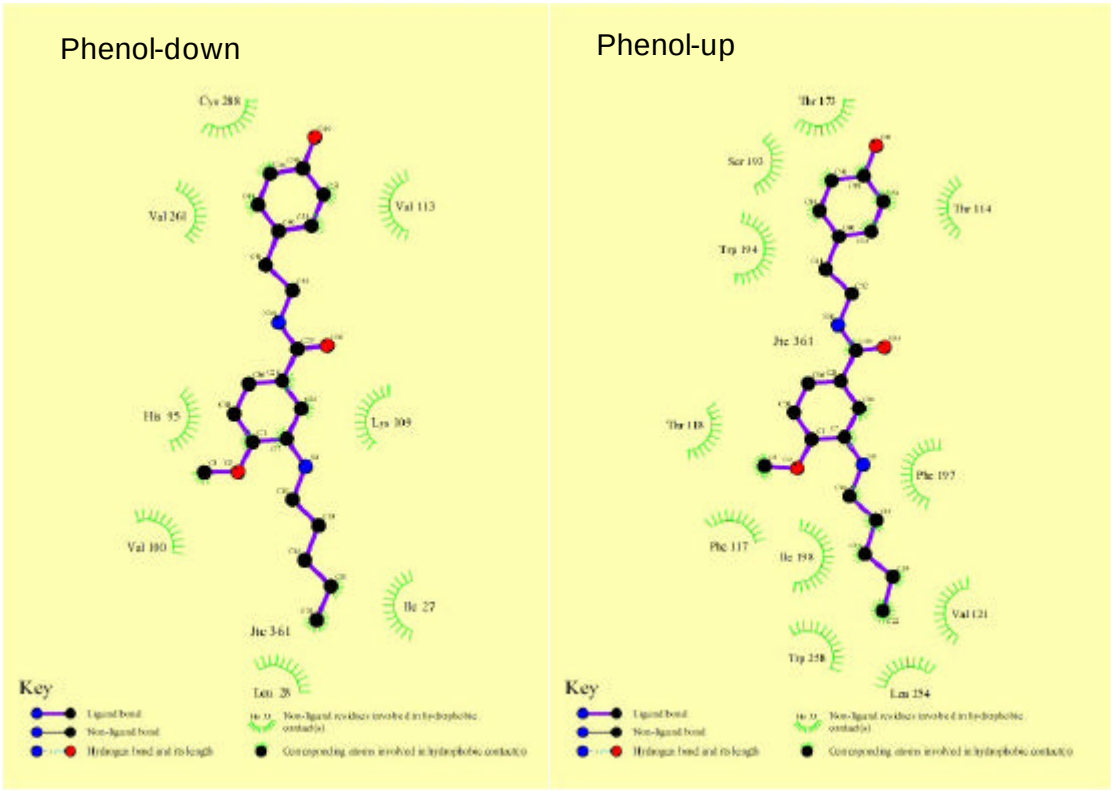

Figure 3-8 Ligplot analysis of the amino acid binding interactions occurring with JTE2-6 **63** docked in the phenol-up and phenol-down position.

3.4 Discussion

The human CB_2 receptor was constructed using homology modelling to a high resolution X-ray crystal structure of Bovine Rhodopsin in-order to determine the probable binding position of the CB_2 selective ligand JTE2-6 **63**. Three different sequence alignment models were constructed varying in the alignment of TM 5 with the Bovine Rhodopsin sequence. Helix 5 in the CB_2 receptor has previously been highlighted as a difficult helix to align due to it lacking a conserved proline residue within the helix. The three different models constructed were compared using conformational space analysis (Ramachandran plots) and visual inspection of four key amino acids (Phe 117, Tyr 190, Trp 194, Phe 197) which have all been implicated in previous mutational analysis and molecular modelling experiments to be associated with TM ligand binding. Alignment 3 was chosen as the best representation of the human CB_2 model for a number of reasons. The Ramachandran plot showed that 98.4% of the amino acids were in a conformation that had been observed from real X-ray crystal structures of 118 other proteins. This was higher than the either alignment

1 or 2 and represented a 'high quality model'[243]. Examination of the residues Phe 117, Tyr 190, Trp 194, Phe 197; demonstrated that only in Alignment 3 were all of these residues present within the proposed binding pocket located in the TM bundle. In Alignment 1 & 2 Trp 190, Trp 194 and Phe 197 were all located either at the top of the TM helices or on the extra cellular loops. As previous studies had shown that Phe 117, Tyr 190, Trp 194, Phe 197 were involved with ligand binding within the TM bundle, Alignment 1 and 2 were rejected and further studies were performed on Alignment 3.

After we had completed our studies, the first CB_2 receptor model based on Bovine Rhodopsin was published[242]. We took the opportunity to compare the work we conducted to their seminal study. The sequence alignment data was compared for the seven TM helices of each model with Bovine Rodopsin; the results are shown below.

```
Xie et al.   PQKTAVAVLCTLLGLLSALENVAVLYLIL           Helix 1
Our study    ---TAVAVLCTLLGLLSALENVAVLYLIL
BR           WQFSMLAAYMFLLIMLGFPNFLTLYVTVQ

Xie et al.   PSYLFIGSLAGADFLASVVFACSFVNFHVF           Helix 2
Our study    ---LFIGSLAGADFLASVVFACSFVN----
BR           PLNYILLNLAVADLFMVFGGFTTTLYTSLH

Xie et al.   KAVFLLKIGSVTMTFTASVGSLLLTAIDRYLCLR       Helix 3
Our study    ----LLKIGSVTMTFTASVGSLLLTAI-------
BR           PTGCNLEGFFATLGGEIALWSLVVLAIERYVVVC

Xie et al.   RALVTLGIMWVLSALVSYLPLMGW                 Helix 4
Our study    -ALVTLGIMWVLSALVSYLPLM--
BR           HAIMGVAFTWVMALACAAPPLVGW

Xie et al.   IPNDYLLSWLLFIAFLFSGIIYTYGHVLW           Helix 5
Our study    ---DYLLSWLLFIAFLFSGIIYTYG----
BR           NESFVIYMFVVHFIIPLIVIFFQYGQLVF

Xie et al.   RLDVRLAKTLGLVLAVLLICWFPVLALMAHSLA       Helix 6
Our study    ---------LGLVLAVLLICWFPVLALMAH---
BR           KAEKEVTEMVIIMVIAFLIQWLPYAGVAFYIFT

Xie et al.   KAFAFCSMLCLINSMVNPVIYAL                 Helix 7
Our study    -AFAFCSMLCLINSMVNPVIYAL
BR           IFMTIPAFFAKTSAVYNPVIYIM
```

Figure 3-9 Comparison of the TM alignments of Xie *et al*.[242], our study and the Bovine Rhodopsin (BR) sequence.

The alignments made in both independent studies matched exactly in the way the CB_2 sequence was aligned to the Bovine Rhodopsin template. The difference in 'helix length' was due to the two different methods used to determine what residues constituted the helix. Xie *et al.* used a hydrophobicity profile to determine the helices

from the sequence alignment[242], in contrast our TM regions were based on those published for the Bovine Rhodopsin sequence in Swissprot. The amino acids proposed to constitute the binding pocket, using solvent accessibility methods, in their model were compared to the same amino acids in our model, viewed from a similar perspective (Figure 3-10).

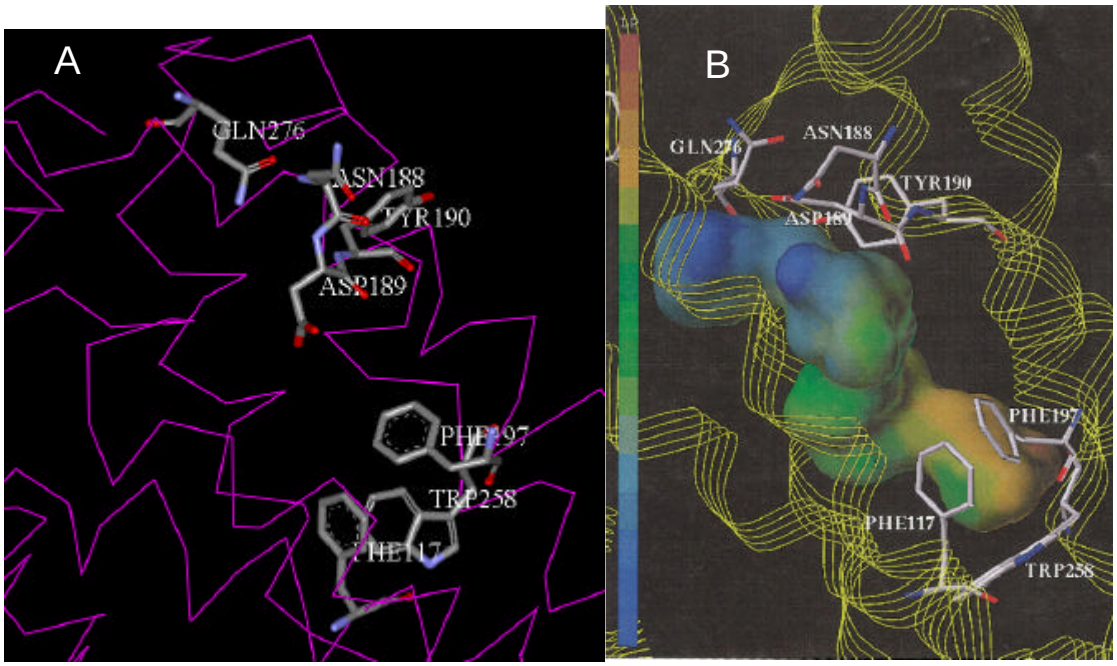

Figure 3-10 Representations of the conformation and relative position of the amino acid residues reported to constitute the binding pocket of the human CB_2 receptor[242]. (A) shows the amino acid alignment from our study of the human CB_2 receptor (Alignment 3) binding the ligand JTE2-6 **63**. The backbone amino acids are shown in simple line form and JTE2-6 **63** is not shown for clarity. (B) is reproduced from Xie *et al.* and shows the binding pocket amino acids as determined by solvent–accessible analysis [242].

The model shown in Figure 3-10 (A) is Alignment 3 of the CB_2 receptor binding the ligand JTE2-6 **63** in the phenol-up position. We chose this model, as the ligand-receptor interactions present, would induce the amino acids to adopt a conformation which best represented their binding conformation. Comparing the two models it can be seen that the amino acids shown each occupy the same area of space within both receptors. It is extremely interesting to note that the three aromatic amino acids that form the hydrophobic cleft at the bottom of the binding pocket are roughly in the same conformation in both independent models.

In conclusion, the model we constructed compares favourably to the published model by Xie *et al*. both in terms of their sequence alignments and the position of key

amino acids postulated to form the binding pocket. This comparison, combined with our assessment of three different aligned sequences, gave us confidence that our model of the human CB_2 receptor was built to the highest standard of GPCR modelling practice.

Ligand docking experiments conducted using the human CB_2 receptor and the Japan Tobacco ligand JTE2-6 **63** have shown that the ligand can bind within the receptor in at least two different orientations – phenol-up and phenol-down. In both experiments, JTE2-6 **63** was interactively docked using Phe 197 as an initial anchor point and the ligand was docked into the receptor in identical energy minimised structural conformation. Thus both models had a similar starting point except that they were docked with a 180 degrees rotational difference. After 100 ps of MD simulation, the final binding conformations of the two ligands within the models vary considerably (Figure 3-7, C). The ligand within the phenol-up model has remained generally within its initial docked position, whilst the phenol-down conformation has moved away from helix 5 into the centre of the receptor. The conformation of JTE2-6 **63** in the phenol-down model has remained very similar to its initial energy minimised conformer. However in the phenol-up system, the phenol ring of JTE2-6 **63** has twisted to form strong aromatic-aromatic interactions with Trp 194 (edge-edge) and Phe 197 (face-face) in the phenol-up system (Figure 3-11). This is not unexpected as both the ligand and the receptor are known to influence each others final conformations in the bound state (Koshland's Theory of Induced Fit[181]).

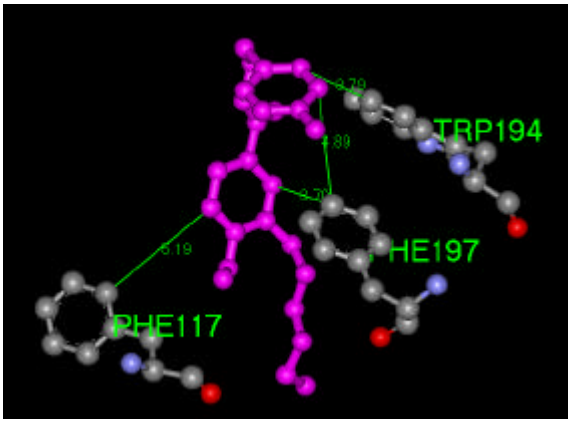

Figure 3-11 JTE2-6 **63** bound in the phenol-up position (shown in magenta) showing the interactions with the aromatic amino acids Trp 194, Phe 197 and Phe 117.

Phe 197 also forms aromatic interactions (edge-edge) with the benzamide ring as does Phe 117 (see Figure 3-11). Examining the energy profile, of the phenol-up complex throughout its 100 ps MD simulation, revealed that the complex was stable (Figure 3-6). The rise in energy at 40 ps was transient and the complex appeared to be approaching steady-state at 100 ps. Although its total energy was higher than the phenol-down complex this does not imply a less favourable model. The energy function is an arbitrary value and can only be used to study events occurring within systems and not across systems. The energy profile for the phenol-down model achieved a steady-state at around 40 ps and there were no notable fluctuations in the profile, also demonstrating that this complex was stable. The amino acids shown to be involved in interactions with JTE2-6 **63**, in the phenol-down position, have previously *not* been implicated in cannabinoid binding. Notably residue analysis showed that TM helix 2 was involved, which is extremely unusual in GPCR ligand binding[84]. The amino acids that were involved in binding JTE2-6 **63**, in the phenol-up position, are residues that *have* been described to be important in cannabinoid binding from many other studies (see Table 3-1 & Table 3-2). We are therefore satisfied that we have demonstrated, using computational methods, that JTE2-6 **63** is likely to be bound within the CB_2 receptor in a phenol-up position. Although theoretically possible to exist, the phenol-down model is not supported by previous experimental evidence. Our experimental data had previously demonstrated that modifying the benzamide ring, located at the bottom of the binding pocket in the phenol-up model, with fluorophores lead to compounds with little affinity to the CB_2 receptor (see chapter 2). We therefore conclude that JTE2-6 **63** is likely to bind in the phenol-up orientation. This is the first time binding of this unusual CB_2 selective cannabinoid has been reported and the utilisation of these results to design a fluorescent CB_2 ligand based on the Japan Tobacco compounds are discussed in the following chapter.

3.5 Conclusions

- We generated a 3D computational model of the human CB_2 receptor based on homology modelling to the high resolution X-ray crystal structure of Bovine Rhodopsin.

- Analysis of the model showed excellent correlation between our postulated binding pocket and previous experimental data, from molecular modelling and single point mutation, including an identical aromatic region within the binding pocket which contained the residue Phe 197.
- The receptor model was used to identify that the likely binding orientation of the CB_2 receptor ligand JTE2-6 **63** was in a phenol-up position, whereby its phenol ring is close to the extra cellular surface of the receptor.
- Computational binding data obtained for JTE2-6 **63** will allow us to develop novel fluorescently labelled derivatives based on this type of compound.

4 Fluorescent CB_2 ligand based on a modification to the phenol ring of a Japan Tobacco Compound

Our studies, outlined in Chapter 3, concerning the binding of the Japan Tobacco compound JTE2-6 **63** (Figure 4-2), to the CB_2 receptor, demonstrated that it was likely to bind in a phenol-up orientation. The work reported below combined this modelling data with our previous work described in Chapter 2 to design an alternative fluorescent CB_2 ligand based on the Japan Tobacco compounds.

4.1 Interrogation of the 'phenol-up' JTE2-6-CB_2 model

The 'phenol-up' model constructed in Chapter 2 was examined to guide our decision on where to locate the fluorescent dye upon the Japan Tobacco compounds. The phenol ring was clearly shown to lie at the top (extra cellular-face) of the receptor. Further interrogation of the structure clearly showed that the phenol ring was in an ideal position within the molecule to elaborate a linker for fluorophore attachment. This is illustrated Figure 4-1.

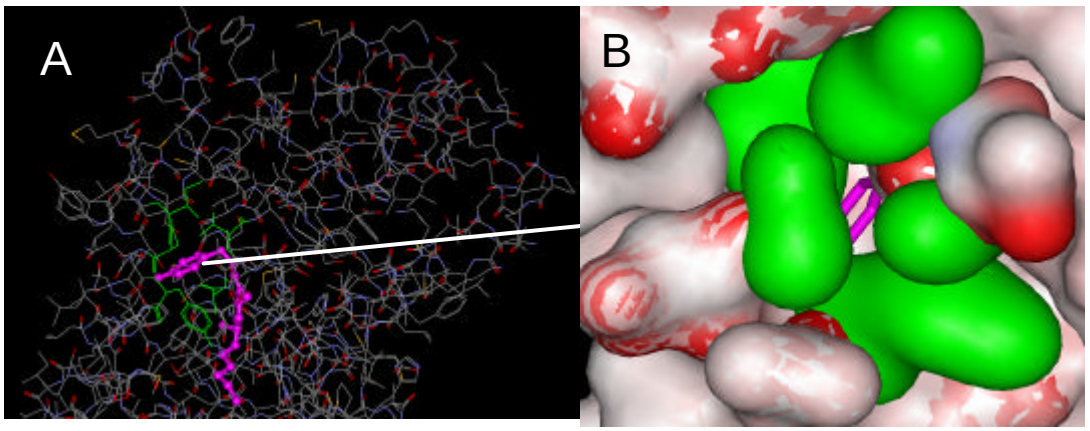

Figure 4-1 JTE2-6 **63** docked into the human CB_2 receptor (Alignment 3). (A) Shows the position of JTE2-6 **63** (magenta) within the receptor. The amino acids shown in green (Ile 186, Pro 187, Tyr 190, Ala 270, and Thr 272) form the entrance to the binding pocket. Inter atomic distances between the hydroxyl-carbon on the phenol ring (C-OH) to the α-carbon of these amino acids range from 3.40 to 6.61 Å. The model is viewed with TM helices 5 and 6 to the front. (B) Electrostatic potential surface representation of the human CB_2 receptor. Red surfaces +ve, blue surfaces –ve, green surfaces are amino acids Ile 186, Pro 187, Tyr 190, Ala 270, and Thr 272 forming the entrance to the binding bocket. The phenol ring of JTE2-6 **63** (magenta) can clearly be observed.

It was envisaged that a carbon linker attached to the JTE2-6's phenol ring (position 2 or 6, or 3 or 5 – see Figure 4-2), would readily exit the binding site thereby allowing attachment of fluorophores without compromising binding of the ligand.

The distances between the amino acids forming the entrance to the binding pocket (shown in green in Figure 4-1) and the ligand was calculated to be between 3.40 and 6.61Å. This equates to between 3 and 7 atomic distances in the linker chain, using a C-C and C-N bond length of 1.54 Å and 1.47 Å respectively as a guide[246], to ensure that the entrance of the binding pocket is avoided by the dye.

In light of this data, we embarked upon the design and synthesis of a Japan Tobacco compound, based on JTE2-6 **63**, functionalised with a linker covalently attached to a carbon atom of the phenol ring. Different fluorophores could then be installed in a chemoselective manner using methodologies discussed in Chapter 2 to generate compounds for evaluation as fluorescent CB_2 selective ligands.

4.2 Designing a fluorescent CB_2 ligand based on molecular modelling of JTE2-6 docked into the CB_2 receptor

The concepts for the design and synthesis of a fluorescent CB_2 selective ligand have been thoroughly covered in Chapter 2. In brief the key requirements of a lead CB_2 ligand conjugated to a fluorescent dye are:

- A high affinity to the CB_2 receptor.
- A high selectivity to the CB_2 receptor versus the CB_1 receptor.
- Modification of the CB_2 ligand with a linker, functionalised at the terminus, to allow for chemoselective ligation to the fluorescent dye.
- A suitable fluorescent dye must be chosen balancing the requirements of fluorescence spectral properties and the steric size of the dye.

In our initial study the compound JTE2-6 **63** was chosen as a lead CB_2 ligand, since it possessed a chemical structure that allowed a selective chemical synthesis of the benzamide ring system to install a functionalised linker at position 4 on this ring. For this study we chose to incorporate the functionalised linker onto the phenol ring of the ligand and hence chemical selectivity within the benzamide portion of the ligand was

not required. It was with this reasoning that we re-examined the range of Japan Tobacco ligands available, using a similar selection criteria as stated in section 2.2.1, but without the requirement of orthogonal chemical groups on the benzamide portion of the ring. The compound JTE2-3 **62** was selected as a lead structure due to its chemical similarity to JTE2-6 **63** (Figure 4-2). This we assumed would mirror similar binding conformations in the receptor and we could therefore translate the modelling data for JTE2-6 **63** and use this for our new lead molecule. However, JTE2-3's **62** enhanced CB_2 affinity (K_i 0.4 nM) and selectivity (>8250:1) over **63** should increase the chance of its fluorescent conjugate remaining a potent CB_2 ligand, whilst its simple benzamide motif will aid in its chemical synthesis.

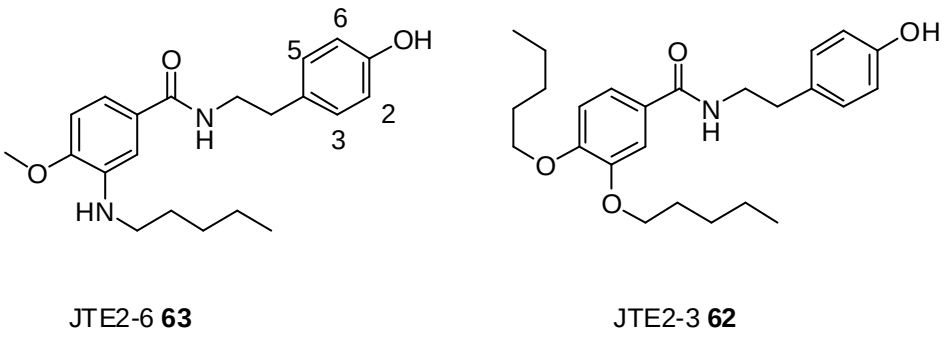

JTE2-6 **63** JTE2-3 **62**

Figure 4-2 Comparison of the Japan Tobacco Ligands JTE2-6 **63** and JTE2-3 **62**. Numbers indicate the position on the phenol ring.

We designed a derivative of JTE2-3 **62** to incorporate an amine functionalised linker at position 2 of its phenol ring. As the entrance to the receptor binding site was between 3.40 and 6.61 Å away from the phenol ring, we chose an aminoethyl linker, incorporating 3 atomic distances, which should position the dye approximately 4.5 Å away from the ligand. This would allow the Dansyl fluorophore, directly coupled to the linker, to be favourably positioned to interact with the aromatic residue Tyr 190 (6.29 Å) (forming the entrance to the binding site) or extend well outside the binding pocket using the pre-installed 10 atom linker of BODIPY 630/650 X. These two fluorescent dyes were used for identical reasons as discussed in Chapter 2.

4.2.1 Synthetic Strategy

A similar strategy to that employed in the synthesis of BODIPY-JTE2-6 **100** and Dansyl-JTE2-6 **99** was instigated for the synthesis of fluorophore-JTE2-3 **I** (Scheme 4-1). In brief the key aim of the synthesis was to install the fluorophore in the last synthetic step, using chemoselective ligation to the linker-terminating 1° amine (retrosynthetic step A, Scheme 4-1). This avoids exposing labile and expensive fluorescent dyes (*i.e.* BODIPY® 630/650) to both unnecessary photo- and chemical degradation during chemical synthesis and purification.

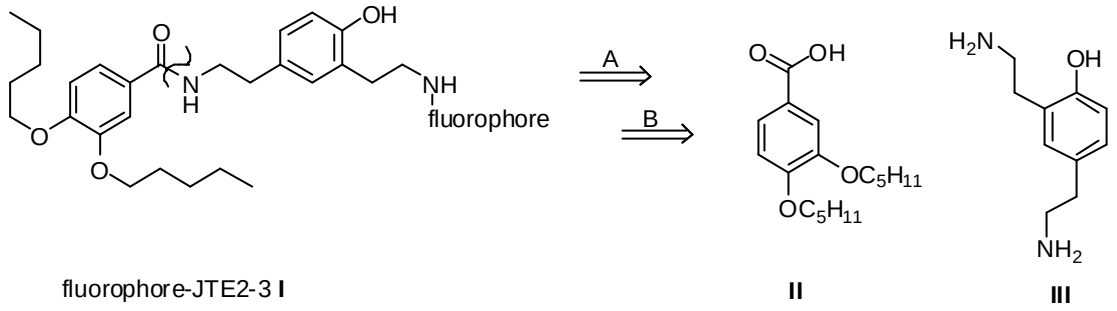

fluorophore-JTE2-3 **I** **II** **III**

Scheme 4-1 Retrosynthetic strategy from the target molecule fluorophore-JTE2-3 **I**

The disconnection made at the amide bond in fluorophore-JTE2-3 **I** (step B, Scheme 4-1), resulted in two synthons; **II**, a Protocatechuic acid (3, 4-dihydroxybenzoic acid) derivative, and **III**, a functionalised tyramine. Reagent **II** was easily accessible from commercial Protocatechuic acid but a literature search established that synthon **III** was a novel compound. A synthetic route, starting from tyramine, was investigated for **III**, which would incorporate orthogonal protection for the two aminoethyl moieties to aid selective coupling to both **II** and the fluorophore dye. The retrosynthetic strategy shown in Scheme 4-2 begins by breaking the carbon-heteroatom bond of the additional aminoethyl functionality on tyramine (Scheme 4-2 step C). The choices of the nitrogen nucleophile **V** which could be used to create the required 1° amine are numerous; and include ammonia; the azide anion; and the phthalimide anion as examples. Reagents **VI** and **VII** (Scheme 4-2) are equivalent reagents to synthon **IV** with both containing an electrophillic carbon. The leaving group (LG) of synthon **VII** may be a halogen atom, however if one considers it instead to be an activated alcohol (*i.e.* mesylate), then both the aldehyde **VI** and

alcohol precursor to **VII** can be easily accessed by a functional group interconversion (FGI) from the allylic compound **VIII** using ozonolysis. Compound **VIII** was simplified, by breaking the aromatic-allyl bond, shown in step D, to give the target starting material (tyramine **IX**) and synthon **X**.

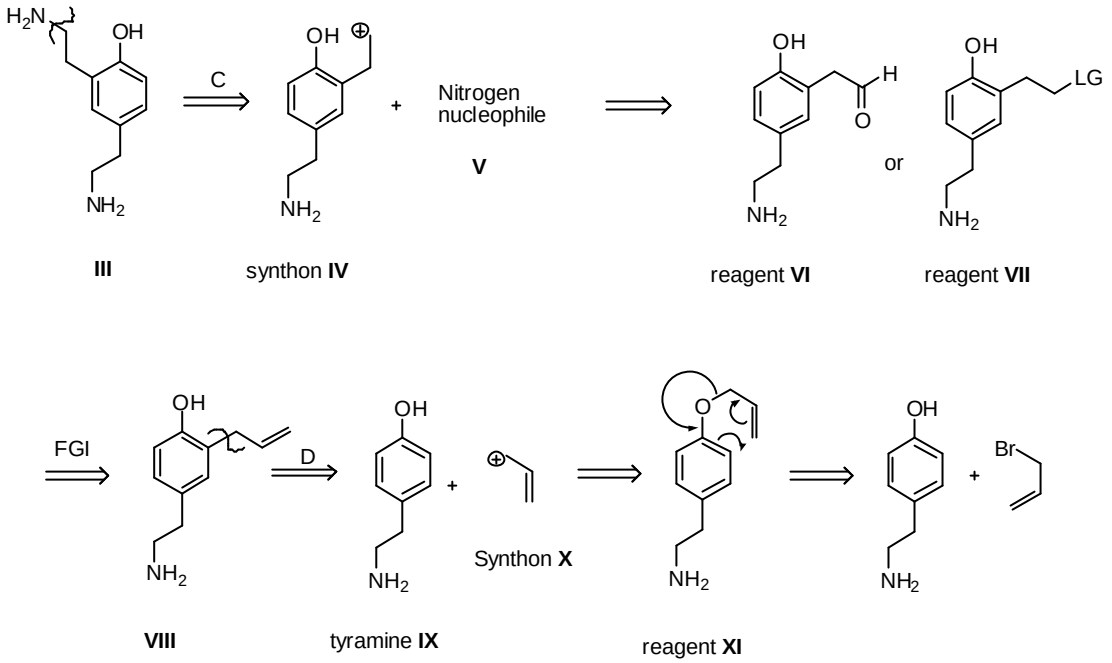

Scheme 4-2 Retrosynthetic analysis for the molecule **III**. LG = Leaving group. FGI = functional group interconversion.

Obviously synthon **X** could represent the allyl halide, and using Friedel-Crafts alkylation the allyl group could be installed. However chemoselectivity and poly-substitutions were envisaged to be problematic. To avoid these side reactions reagent **XI** was proposed to undergo a [3, 3]-sigmatropic Claisen rearrangement leading to mono-substituted 2-allyl product. Reagent **XI** was easily constructed from tyramine and allyl bromide. It should be noted that throughout this synthesis, protecting group chemistry would need to be adeptly utilised in-order for the synthesis to proceed smoothly and to finish with both of the 1° amines orthogonally protected. It is known that the Benzyloxycarbonyl (Cbz) protecting group is both thermo and Lewis acid stable[247]; conditions which are commonly used to evoke the Claisen rearrangement, and we planned to utilise this group to protect the amine group of tyramine. With this protection present throughout the reactions, we could protect the second amine group

orthogonally with the *tert*-Butoxycarbonyl (Boc) group, which was successfully used in the synthesis of BODIPY- and Dansyl-JTE2-6 **100** & **99**.
The synthesis of un-modified JTE2-3 **62** was also undertaken, enabling us to assess the effect of the fluorescent dye conjugation upon the binding affinity. This ligand is not commercially available and a synthesis from **II** (Scheme 4-2) and tyramine offered an attractive route to the compound.

4.3 Chemistry results

The Protocatechuic acid derivative **105** was synthesised in high yield from commercially available Protocatechuic acid **102** as shown in Scheme 4-3.

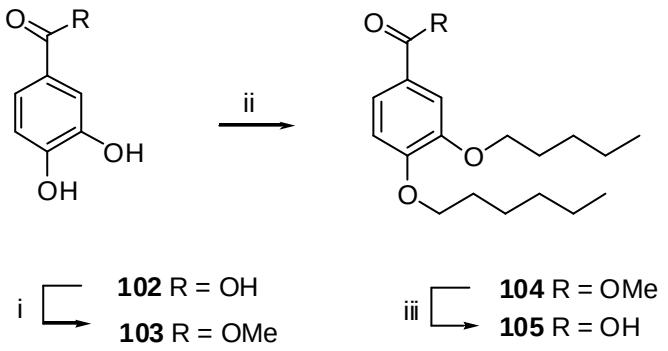

Scheme 4-3 Synthesis of the Protocatechuic acid derivative. Reagents, conditions and yields: (i) MeOH, H^+, reflux, 2h, (92%); (ii) 1-bromopentane, K_2CO_3, DMF, 90 °C, 1h, (72%); (iii) LiOH, MeCN, H_2O, reflux, 1h, 90%

The 2-aminoethyl tyramine derivative **117** was synthesised in ten steps from commercially available tyramine (Scheme 4-4). Following protection of tyramine's amino group to its corresponding benzyl urethane **107**, phenolic allylation afforded ether **108**. The Claisen sigmatropic rearrangement was assessed using thermal and Lewis acid catalysed methods. Lewis acid catalysis using $AlCl_3$[248] yielded a chlorinated product (shown by the distinctive mass spectrum, with a 3:1 ratio of the ^{35}Cl and ^{37}Cl isotopes in the product[249]) in overall low yield. Thermal rearrangement was tested by heating the allyl ether in refluxing diphenyl ether solvent (b.p. 258 °C) and by heating to 280 °C neat in a sealed tube. Both methods yielded the desired rearranged product **109** in yields of 56 and 47% respectively. Due to the increased yield and the easier experimental protocol, the Claisen rearrangement was carried out

in diphenyl ether during subsequent reactions. Benzyl ether protection of the phenol **110** was used to prevent reaction with functional groups, to be installed in subsequent steps, via 5-membered intramolecular reactions. The olefin was oxidised by two different routes to the corresponding aldehyde **111** and alcohol **112**. Oxidation to the 1, 2-diol, using catalytic OsO_4 and *N*-methylmorpholine oxide, as a stoichiometric oxidant, followed by $NaIO_4$ mediated oxidative cleavage, yielded the aldehyde **111** in high yield. Use of the safer polymer bound OsO_4[250] was also assessed but produced poor conversion to the diol. Ozonolysis, using a $NaBH_4$ reductive work-up yielded the alcohol **112**. Interesting ozonolysis under milder reductive conditions (using dimethylsulfide (DMS)) failed to yield the aldehyde **111**!

Various reductive amination methods were tested to assess whether the aldehyde **111** could be directly modified to the amine in one-pot. However all attempts using ammonia and ammonium salts failed to give any of the desired amine **115**. The amine **115** was successfully accessed by sequential activation of the alcohol **112** (to the Mesylate **113**), substitution by azide and reduction of the resulting azide **114** using Ph_3P and water. Orthogonal Boc protection of this amine to give **116** and concomitant hydrogenolysis of the benzyl and Cbz groups yielded the *ortho* substituted tyramine **117** required for coupling. Coupling with the *bis*-(pentoxy)protocatechuic acid derivative **105** using CDI proceeded to give **118**. Formation of the HCl salt of the 2-aminoethyl derivative of JTE2-3 **119** was afforded by acidolysis of the Boc protecting group of **118** using methanolic HCl. Unlabelled JTE2-3 **62** was synthesised by coupling **105** with tyramine **106** using CDI in high yield (75%) (Scheme 4-5).

Ligation of **118** with Dansyl-Cl **84** and BODIPY® 630/650 X OSu **86** (Figure 2.5) was accomplished using methodology used in the successful synthesis of Dansyl- and BODIPY-JTE2-6 (**99** & **100**) (Chapter 2; Scheme 4-5). The free amine of **118** was liberated and reacted rapidly with the amine reactive fluorescent dyes. The fluorescent products from these reactions were confirmed by mass spectrometry, ^1H NMR and reverse phase HPLC to be the desired structures; Dansyl-JTE2-3 **120**, and BODIPY-JTE2-3 **121**.

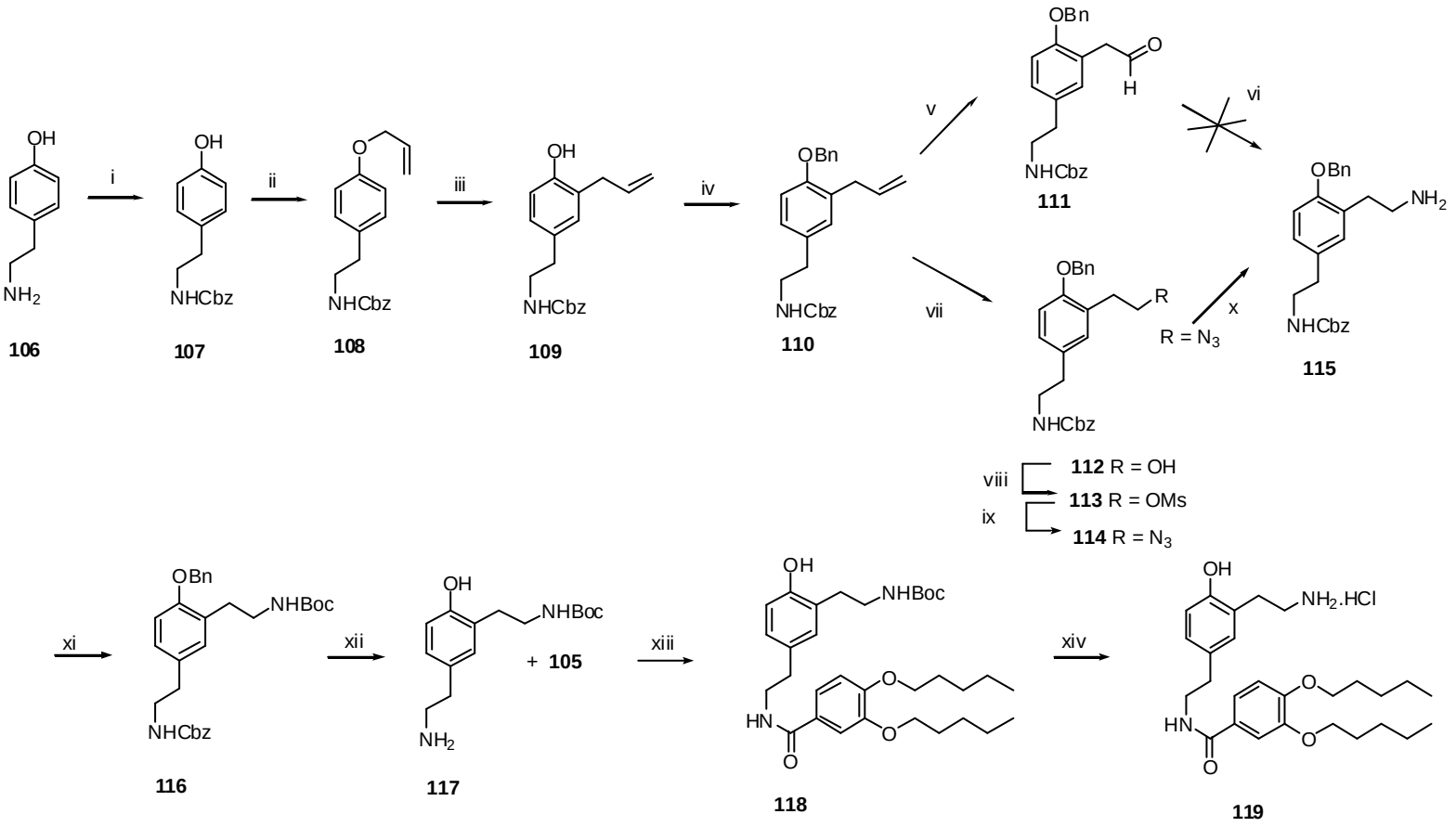

Scheme 4-4 Synthesis of 2-aminoethyl derivative of JTE2-3. Reagents, conditions and yields: (i) Benzyl chloroformate, DIPEA, DMF, MeCN, rt, 24h, (57%); (ii) allyl bromide, K_2CO_3, MEK, reflux, 18h, (96%); (iii) Ph_2O, reflux, 1h, (56%); (iv) BnBr, K_2CO_3, MEK, reflux, 12h, (80%); (v) OsO_4, NMO, acetone, H_2O, rt. then $NaIO_4$, H_2O, THF, rt, (79%); (vi) NH_3 or NH_4^+, $NaCNBH_3$, MeOH, AcOH, H_2O, rt, (no reaction); (vii) O_3, DCM, MeOH, -78 °C, then $NaBH_4$, rt, 12h; (viii) MsCl, Et_3N, DCM, 0 °C; (ix) NaN_3, DMF, 60 °C, 5h; (x) Ph_3P, THF, rt 24h then H_2O, rt, 48h; (xi) Boc_2O, H_2O, dioxane, 0 °C, 1h, (overall for vii-xi 34%); (xii) Pd/C, EtOH, EtOAc, H_2 (1atm), rt, 2h (54%); (xiii) CDI, MeCN, rt, (20%); (xiv) MeOH, AcCl, rt, 4h, (43%).

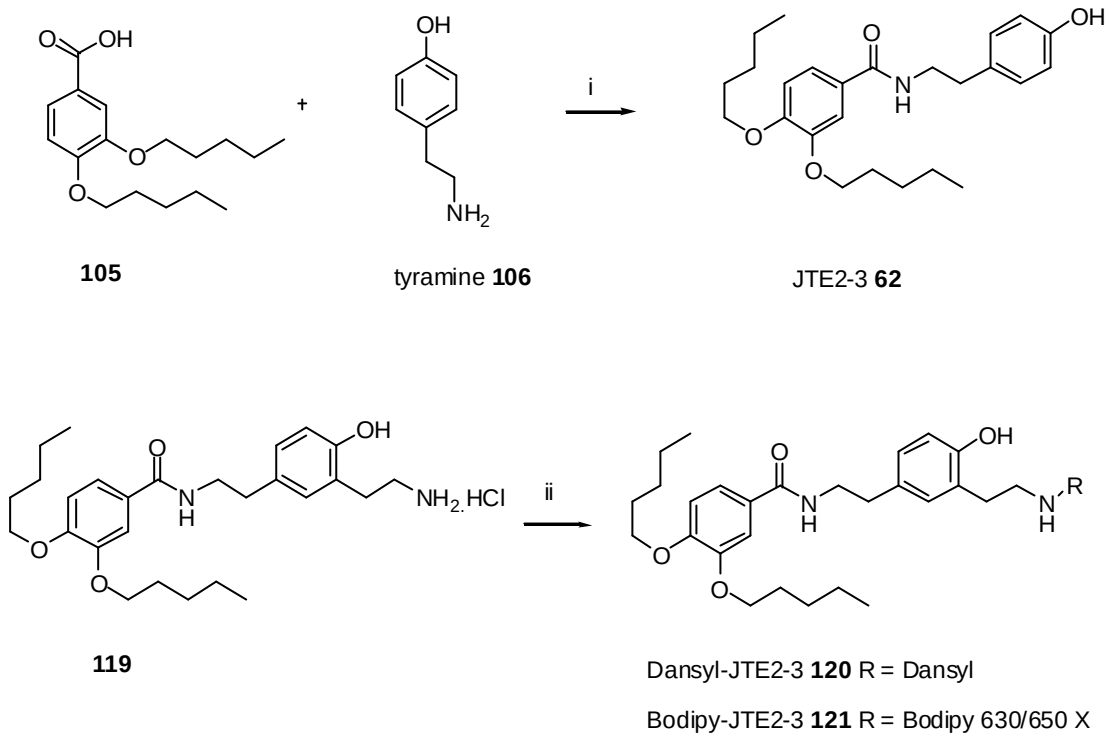

Scheme 4-5 Synthesis of unlabelled and fluorescently labelled JTE2-3. Reagents, conditions and yields: (i) CDI, MeCN, rt, 4h, (75%); (ii) Dansyl-Cl **84** or BODIPY® 630/650-X OSu **86**, $NaHCO_{3\ (aq)}$ pH 8.3: MeCN 1:1, rt, 1-12h, (70-80%).

4.4 Pharmacology of JTE2-3 and BODIPY-JTE2-3

The pharmacology, of JTE2-3 **62** and BODIPY-JTE2-3 **121**, was assessed by competitive radioligand displacement of the non-selective cannabinoid [^{3}H] CP55, 940 from cellular membranes containing human CB_2 receptors and was performed as previously described in section 2.4. BODIPY-JTE2-3 **121** failed to displace any of the [^{3}H] CP 55,940 from cell membranes prepared from CHO cells expressing the human CB_2 receptor up to concentrations of 10^{-5} mol/L (10 μM) (Figure 4-3 A). Surprisingly the unlabelled JTE2-3 **62** exhibited a much lower affinity than expected, with concentrations of 10^{-5} mol/L (10 μM) displacing only 40% of the bound [^{3}H] CP 55,940 in the CHO cell membrane assay. The absence of any displacement by BODIPY-JTE2-3 **121** (no displacement observed at 32 μM) and the lower than expected affinity of JTE2-3 **62** were corroborated using cell membranes prepared from HEK cells expressing the human CB_2 receptor by an independent group in the USA (Figure 4-3 B). They determined a K_i value of 3.11 μM for JTE2-3 **63** in a HEK cellular membrane assay. The results from both the CHO and HEK assays indicated a

K_i for BODIPY-JTE2-3 **121** of >>32 µM. Binding affinity of Dansyl-JTE2-3 **120** was not determined due to the poor solubility of the compound and that the other ligands tested exhibited such poor binding.

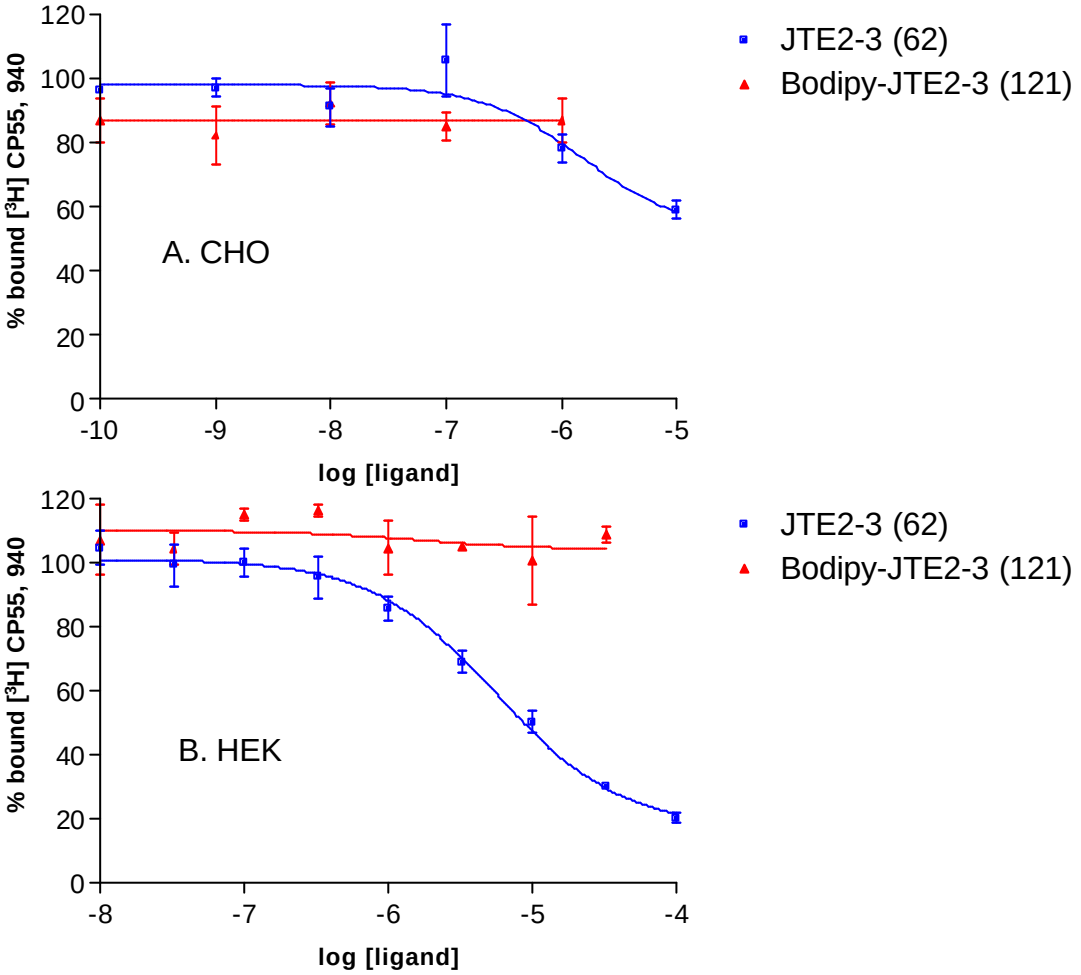

Figure 4-3 Radioligand displacement curves for the compounds JTE2-3 **62** and BODIPY-JTE2-3 **121**. The curves show the percentage of [^{3}H] CP55, 940 displaced from cellular membranes containing the human CB_2 receptor. (A) Demonstrates the displacement from cellular membranes made up of CHO cells expressing the CB_2 receptor (n=3). (B) Demonstrates the displacement from cellular membranes made up of HEK cells expressing the CB_2 receptor (n=4).

4.5 Use of BODIPY-JTE2-3 in Fluorescent Confocal Microscopy

The fluorescent ligand BODIPY-JTE2-3 **121** was used in confocal experiments to demonstrate whether the ligand had the potential to highlight CB_2 receptor membrane binding. Detailed experimental conditions are included in section 2.5 but in brief known concentrations of fluorescent ligand were incubated with CHO cells

expressing human CB_2 receptors and images were recorded at various time courses throughout the experiment. To assess whether the fluorescence observed was due to specific CB_2 binding, fresh CHO cells were pre-incubated with a blocking concentration of a non-fluorescent cannabinoid ligand (*i.e.* 1 μM HU210 **14**) and the fluorescent ligand was subsequently introduced. Images collected from this experiment were compared to those conducted without the HU210 **14** present, to determine if any fluorescence observed was due to CB_2 receptor binding. Various concentrations of **121**, ranging from 10 – 400 nM, were used in experiments. The fluorescence observed was weak even when laser power and pin-hole aperture was increased. Even at concentrations of 400 nM fluorescence from the CHO cells was negligible (results not shown). Background fluorescence from the CB_2 transfected CHO cells was negligible at the excitation wavelengths used (633 nm) (Result not shown).

4.6 Discussion

Synthesis to access JTE2-3 **62** and its 2-aminoethyl derivatives **119**, **120**, and **121** was successfully carried out. The positioning of the 2-aminoethyl linker was guided by molecular modelling results which demonstrated that attachment of a linker at this position should not interfere with the binding of the ligand in the receptor binding pocket.

In order to complete the synthesis of the 2-aminoethyl derivatives of JTE2-3 **62** it was necessary to synthesise a novel *ortho* substituted tyramine derivative **109**. By careful selection of the thermo stable Cbz protecting group[247], we were able to access **109** via a thermally induced [3,3]-sigmatropic Claisen rearrangement. Oxidation of the olefin using two different oxidants (OsO_4 with a $NaIO_4$ cleavage, and O_3) gave the aldehyde **111** and alcohol **112** respectively. Repeated attempts to generate the aldehyde **111** using ozonolysis and DMS failed to give the desired product. A literature report detailing this reaction on a similar allylic benzene system did not suggest that there were any problems during this step, however only brief experimental conditions were reported[248]. It was obvious that the ozonide of **110** could be formed, demonstrated by the successful reduction of this complex using $NaBH_4$. Therefore, we concluded that the problems observed in our synthesis were

due to the DMS reduction step. All attempts to rectify this by altering the conditions of the DMS reduction did not resolve the problem and we had to use the alternative OsO_4 oxidation to generate the aldehyde **111**. Unfortunately reductive amination of this aldehyde **111** failed to give the amine required. We assessed the use of NH_3 and NH_4Cl, as a source of ammonium ion, and combinations of these together to form the imine *in-situ* and reducing it to the amine using $NaCNBH_3$. However we could not detect the 1° amine in any of the attempted reactions. A Beilstein search revealed that other reported experiments using ammonia and aldehydes to give 1° amines often exhibited lower yields (the highest reported was 40%[251]) than the corresponding reaction used to yield 2° and 3° amines. This is presumably due to the fact that once the 1° amine has been formed it is immediately available to react with the aldehyde present and form 2° amines. To produce the amine **115** we therefore had to use a more convoluted route, involving activation of the alcohol to the mesylate and forming the corresponding azide **114**. This was reduced under mild conditions using PPh_3 and water to the corresponding amine **115**. Boc protection of the amine resulted in a compound that was quantified analytically and we calculated an overall yield from the olefin as a respectable 32% for 5 steps; which represents an average yield of 80% for each step. The subsequent chemical reactions leading to the two fluorescent conjugates Dansyl-JTE2-3 **120** and BODIPY-JTE2-3 **121** utilised chemistry fully discussed in section 2.6. The unlabelled ligand JTE2-3 **62** was synthesised to allow us to test the effect of conjugation to the fluorescent dye using a radioligand binding competition assay discussed below.

The affinity of JTE2-3 **62** and BODIPY-JTE2-3 **121** to the human CB_2 receptor was assessed using radioligand competition displacement assays against the non-specific cannabinoid [^{3}H] CP55, 940. The membrane homogenates used were made up from both CHO and HEK cells stably transfected with the human CB_2 ligand. Concentrations of up to 32 μM of BODIPY-JTE2-3 **121** failed to displace any of the [^{3}H] CP55, 940 from the receptors. The K_i value of 3.11 μM obtained for the unlabelled JTE2-3 **62** was much higher than that reported in the literature (0.4 nM)[126]. This represented a difference in affinity to that quoted in the literature of a factor of 7500. JTE2-3 **62** displayed less affinity to the human CB_2 than was expected. Adulterating JTE2-3 **62** with the fluorescent dyes Dansyl and BODIPY effectively abolished any of the human CB_2 receptor binding ability JTE2-3 **62** possessed. This

was confirmed in a fluorescent confocal microscopy experiment, because no membrane binding was observed at concentrations of 400 nM.

The significantly lower affinity of JTE2-3 **62** observed in our displacement experiments, when compared to the literature K_i value, was unexpected and was a matter of concern. Initially we checked that the binding assay was generating meaningful data by performing a saturation radioligand binding experiment (using [^{3}H] CP55, 940) on the CB_2 HEK membranes which yielded a K_d of 5.1 nM (results not shown), which was well within the reported range of 0.29-7.37 nM for this ligand[51]. The analytical data for the compound JTE2-3 **62** was checked against that published in the original patent. ^{1}H NMR and m.p. were identical for our synthesised compound and the literature values (section 8.1). ^{13}C and ES-MS, which were not reported in the patent, were consistent with the structure of JTE2-3 **62**. Finally a fresh stock solution of JTE2-3 **62** was made up to check for errors in ligand concentration. We obtained the same results with the new stock solution and this result forms part of the n = 4 analysis shown in B of Figure 4-3. We had ruled out all experimental error in the calculation of the K_i of JTE2-3 **62** (3.11 μM) and yet could not explain the 7500 fold difference to that reported in the patent (0.4 nM)[126]. Differences between the two experimental protocols used to calculate the K_i of JTE2-3 **62** were checked. The radioactively labelled ligand used and the species of CB_2 receptor tested against differed between the two protocols. [^{3}H] Win 55212-2 and rat CB_2 receptors (derived from rat spleenocytes) were used in the Japan Tobacco publication[126], where we had used [^{3}H] CP55, 940 and the human CB_2 receptor expressed in HEK and CHO cells. [^{3}H] Win 55212-2 is not commercially available so we were unable to assess the effect of using a different radioligand. However we were able to test the affinity of JTE2-3 **62** against the rat CB_2 receptor and discovered that the difference in the different K_i values obtained was due to the species of CB_2 receptor used. A full discussion of this work is reported in Chapter 5.

4.7 Conclusions

- We successfully synthesised a derivative of the CB_2 selective ligand JTE2-3 **62**, incorporating an alkyl linker which we labelled with Dansyl and BODIPY® fluorescent dyes.

- Computational modelling demonstrated that the optimum position for attachment of an alkyl linker was on the phenol ring, as the phenol ring was located near to the top of the receptor binding pocket.
- Development of novel chemistry was established, enabling the synthesis of orthogonally protected 2-aminoethyl tyramine, required for the synthesis of the fluorescent conjugate.
- Binding data for the BODIPY® labelled compound **121**, demonstrated a loss of affinity for the CB_2 receptor (K_i > 32 μM).
- Confocal microscopy experiments showed that BODIPY labelled compound **121** did not bind to human CB_2 receptors expressed in live CHO cells.
- Binding data obtained for the unlabelled lead compound JTE2-3 **62**, demonstrated it had, surprisingly, 7500 times less affinity to the CB_2 receptor compared to the K_i value reported in the original patent. Thorough analysis of this anomaly suggested that the difference between the two results was due to the different species (rat and human) of receptor used in the binding assay.

5 Species selective nature of JTE2-3

From our investigations in chapter 4, we discovered that the selective CB_2 receptor ligand JTE2-3 **62** displayed a 7500 fold decrease in binding affinity to the human CB_2 (hCB_2) receptor compared to the rat CB_2 (rCB_2) receptor, which was originally reported (K_i hCB_2 = 3.11 μM, rCB_2 = 0.4 nM)[126]. This substantial species dependant behaviour of the ligand was, to the best of our knowledge, the largest that has been reported for any cannabinoid and the details of our work to understand this unusual phenomenon are discussed below.

5.1 The rat and human CB_2 receptor

As discussed previously in section 1.3.4 both the human and rat species of CB_2 receptor have been characterised and cloned. The human receptor, first cloned by Munro *et al.*, consists of 360 amino acids[4], whilst two independent pieces of research have deduced that the rCB_2 receptor contains either 360[105] or 410[106] amino acids depending on which polymerase chain reaction (PCR) primer was employed. It is extremely difficult to clarify which of the two clones actually represents the rCB_2 receptor amino acid sequence, as no independent studies examining the different sequences have been published following the second cloning study. Since being published in July 2002, this most recent study by Brown *et al.*, generating the 410 amino acid containing receptor[106], has only been cited 5 times. By comparison, the original study by Griffin *et al.*, who generated a 360 amino acid receptor[105], has been cited by 13 other researchers since July 2002[‡‡]. This would suggest that to date the sequence generated by Griffin *et al.* has been adopted as the rCB_2 receptor of choice with more of the cannabis research community. From the two primary studies, both groups were able to show that their receptors were able to bind the cannabinoid Win 55212-2 **3**, and both studies demonstrated that this agonist binding gave a measurable change in a downstream signalling pathway of the GPCR (*i.e.* decrease in cAMP[105], and an increase in MAP kinase[106]). The difference between the sequence lengths is related to the carboxyl terminus end (intracellular) of the receptor explaining why the Win 55212-2 **3** binding capability of these two different receptors is unaltered[106].

[‡‡] Web of Knowledge (http://wok.mimas.ac.uk) citation search conducted on 17/06/04

The sequence homology of the rCB_2 receptor with the hCB_2 receptor depends upon which rat clone is being compared. The 360 amino acid rCB_2 clone, is as expected, a closer match to the 360 amino acid hCB_2 receptor generating a sequence homology of 81%[105]. The 410 amino acid clone has a much lower sequence homology to the hCB_2 receptor with only 57% identity retained[106]. With this level of divergence in homology between the two species it is, perhaps, not surprising to discover that cannabinoids may have different affinities and efficacies at the rat and human CB_2 receptors. This observation was highlighted by the authors of the two original rCB_2 cloning publications, who both commented in their respective discussions that species differences between rat and human could be expected to emerge in future studies[105,106]. Unfortunately, it appears that other researchers in the cannabinoid field have failed to recognise this potential pitfall in their studies. This can be demonstrated in the relatively few citations that the two rCB_2 cloning papers have received (35 in total[§§]) and that studies conducted on the rCB_2 receptor are rarely backed up with a corresponding hCB_2 receptor assay[***]. Fortunately, for human drug research, the advances made in genetic engineering has allowed most new cannabinoid ligands to be screened against the hCB_2 receptor stably transfected into CHO or HEK cell lines.

There are a few examples from the literature where cannabinoids have been compared using the same assay conditions, against both the rCB_2 and the hCB_2 receptor. In the following section we will discuss these examples in terms of their relevance to this work.

5.2 Differences between CB_2 ligand binding at the rat and human receptor

There are only three studies directly comparing the affinity of cannabinoid ligands to both the rCB_2 and the hCB_2 receptor. They are limited to testing eight different cannabinoids[57,105,125]. Direct comparison of binding affinity is important, as it overcomes the experimental error associated with different techniques employed by different laboratories performing the binding assay. Comparison of the binding affinity of ligands, performed in different independent studies have been reviewed[51,80] but due to the variability of these results it is difficult to draw meaningful comparisons from the work.

[§§] Web of Knowledge (http://wok.mimas.ac.uk) citation search conducted on 17/06/04
[***] Author's personal observation.

A summary of both the direct and indirect comparative work is shown in Table 5-1. Griffin *et al.* analysed their affinity data for statistical significance between the rCB_2 and hCB_2 receptor[105]. Using this study it was straightforward to determine which of the ligands tested showed significant species differences. Their analysis of seven different cannabinoids demonstrated that only three, JWH051 (classical cannabinoid), Win 55212-2 **3**, and anandamide **4** had significant differences between the rat and human CB_2 receptors[105]. The differences observed for the three cannabinoid ligands were a 9, 8, and 32 fold decreased affinity to the rCB_2 receptor respectively[105]. The observation that SR144528 **6** exhibited little species selectivity was corroborated in a study by Rinaldi-Carmona *et al.* which reported that the rCB_2 and hCB_2 affinities were similar[57], however work by Iwamura *et al.* was able to show an 8 fold decreased affinity to the hCB_2 receptor (Table 5-1)[125]. Iwamura *et al.* also demonstrated that Win 55212-2 **3** had a 5 fold decreased affinity towards the rCB_2 receptor[125], which is in agreement with the results generated by Griffin *et al.*[105].

The results for Win 55212-2 **3** and Δ^9-THC **1**, shown in Table 5-1, highlights how difficult interpreting results obtained from different laboratories can be. Using Win 55212-2 **3** as an example, it can clearly be seen that although two studies both examined the same ligand on the rat and human CB_2 receptors, they have both produced different K_i values for the two receptor species (rCB_2 K_i = 10.4 or 1.30 nM and hCB_2 K_i = 1.19 or 0.29 nM). It was for this reason that where possible we tried to compare direct experimental comparisons of K_i values to assess for species' differences.

The two most significant results relating to our work are for the compounds JTE1-22 **61** and JTE907 **66** (Table 5-1). These Japan Tobacco compounds were shown to exhibit large species differences in affinity, between the rat and human CB_2 receptor. The direct comparison conducted by Iwamura *et al.* of the compound JTE907 **66** demonstrated that the compound had a 95 fold less favourable binding affinity to the hCB_2 receptor than to the rCB_2 (K_i 35.9 and 0.38 nM respectively)[125]. This interesting result was attributed to the low sequence homology between the rat and human receptors and to the novel structure of JTE907 **66**[125]. The one indirect comparison included in Table 5-1, is of another Japan Tobacco compound, JTE1-22 **61**, which is of interest to us. The results, are extracted from the original Japan Tobacco patent[126] and from a later publication by the Bristol Myers Squibb (BMS)

company who were interested in employing the novel structures as a template for their own CB_2 receptor ligands[197]. The original patent reported affinity of JTE1-22 **61** in rat splenocyte membranes whilst workers at BMS screened the compound in the hCB_2 receptor expressed in CHO cells. It is observed, from Table 5-1, that the binding of **61** at the rat and human receptors differs by a factor of 86. The low K_i observed in the rCB_2 receptor (1.4 nM) is altered to a moderate K_i value in the hCB_2 receptor (120 nM). Although the BMS workers who tested the compound in human CB_2 receptors did not comment on the species difference, this second example of a Japan Tobacco compound exhibiting a large difference in affinity towards the CB_2 receptor is noteworthy. Both of the ligand comparisons available for the Japan Tobacco ligands, show large differences (86 and 95 fold) in affinity between the rat and human CB_2 receptor, with a higher binding observed at the rCB_2 receptor.

We will be demonstrating, in the remainder of this chapter, our own evidence that another of Japan Tobacco's amide containing cannabinoid also displays a species selective binding, with greater affinity observed for the rCB_2 receptor. We will also extend the use of molecular modelling discussed in chapter 3 to explore the intimate nature of ligand-receptor binding to rationalize these findings.

Compound	Study type	rCB_2 K_i (nM)	hCB_2 K_i (nM)	hCB_2/rCB_2 ratio	Statistical analysis	Reference (s)
SR144528 **6**	Direct	0.30	0.32	1	NS	105
	Direct	0.24	1.99	8	ND	125
	Direct	0.30	0.60	2	NS	57
Win 55212-2 **3**	Direct	10.4	1.19	0.1	$P < 0.05$	105
	Direct	1.30	0.29	0.2	ND	125
Δ^9-THC **1**	Direct	28.3	44.9	1.6	NS	105
	Direct	6.80	3.13	0.5	ND	125
JWH015 **53**	Direct	269	98.4	0.4	NS	105
JWH051	Direct	3.16	0.33	0.1	$P < 0.05$	105
JTE907 **66**	Direct	0.38	35.9	95	ND	125
JTE1-22 **61**	Indirect	1.4[a]	120[b]	86	ND	a = 197 b = 126

Table 5-1 Comparisons of the binding affinity (K_i (nM)) of a selection of cannabinoids towards the rCB_2 and hCB_2 receptor. ND not determined. NS not significant.

5.3 Pharmacology results

In-order to be able to directly compare human *versus* rat affinities of JTE2-3 **62** it was necessary for us to calculate its K_i value at the rCB_2 receptor using a radioligand displacement assays. From the result obtained we could directly compare the rat K_i value to the human K_i obtained in chapter 4. The K_i value is calculated using the Cheng and Prussoff equation which uses the K_d value of the radioactive ligand ([^{3}H] CP55, 940) being displaced. Therefore a standard curve was first produced in order to determine the K_d value of [^{3}H] CP55, 940 in a rat splenocyte assay. A method by DeBlasi *et al* was followed whereby [^{3}H] CP55, 940 is displaced by cold CP55, 940; which avoids the use of problematic saturation binding experiments[252]. Full details of the preparation of the rat splenocyte membranes and the binding experiment are given in the experimental section (section 8.2)

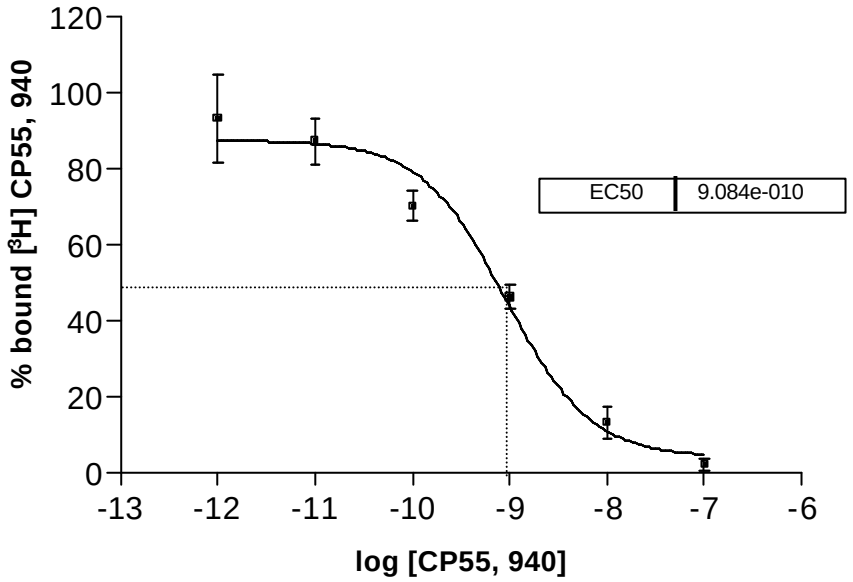

Figure 5-1 Graph used to calculate the Kd of [^{3}H] CP 55, 940, showing the displacement of [^{3}H] CP 55, 940 from membranes derived from rat splenocytes by cold CP 55, 940 (n=3).

The displacement graph shown in Figure 5-1 was used to calculate the EC_{50} of 0.91 nM. Using the calculation from DeBlasi *et al.*[252], shown below, we calculated the K_d of [^{3}H] CP 55, 940 to be 0.59 nM.

DeBlasi *et al.* calculation[252]: $K_d = EC_{50} - L$

$K_d = 0.91 - 0.32$

$K_d = 0.59$ nM

where:

L = concentration of radioligand (nM)

EC_{50} = concentration of CP 55, 940 that displaces half the specific binding of [^{3}H] CP 55, 940 (nM)

K_d = equilibrium dissociation constant for [^{3}H] CP 55, 940 (nM)

Using the calculated K_d value of 0.59 nM for [^{3}H] CP 55, 940 we were able to use the Cheng and Prussoff calculations, within GraphPad® Prism3, to determine the K_i of JTE2-3 **62** using a competitive radioligand displacement of the non-selective cannabinoid [^{3}H] CP 55, 940 from rat splenocyte membranes. The displacement of [^{3}H] CP 55, 940 by JTE2-3 **62** from the rCB_2 receptor is shown in Figure 5-2. From this curve the K_i value for JTE2-3 **62** was calculated to be 5.02 nM (95% confidence intervals 0.85 – 29 nM). This value is 600 fold less than the K_i of 3.11 μM calculated for the hCB_2 receptor in chapter 4.

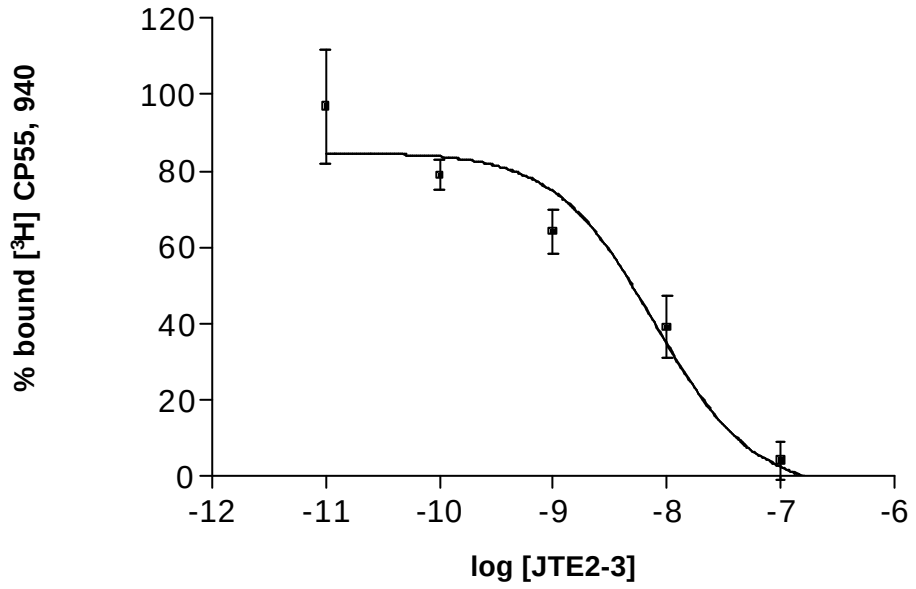

Figure 5-2 Displacement curve of [^{3}H] CP 55, 940 by JTE2-3 62 from membranes derived from rat splenocytes (n=3).

Due to the species selective nature of JTE2-3 **62** (and at least two other Japan Tobacco Compounds), it became prudent for us to retest the two BODIPY® Japan Tobacco fluorescent derivatives synthesised in chapters 2 and 4, against the rCB_2 receptor. Thus Bodipy-JTE2-6 **100** and Bodipy-JTE2-3 **121** were used in competitive displacement assays against [^{3}H] CP 55, 940 using membranes from rat splenocytes. The binding curves from these assays are shown in Figure 5-3

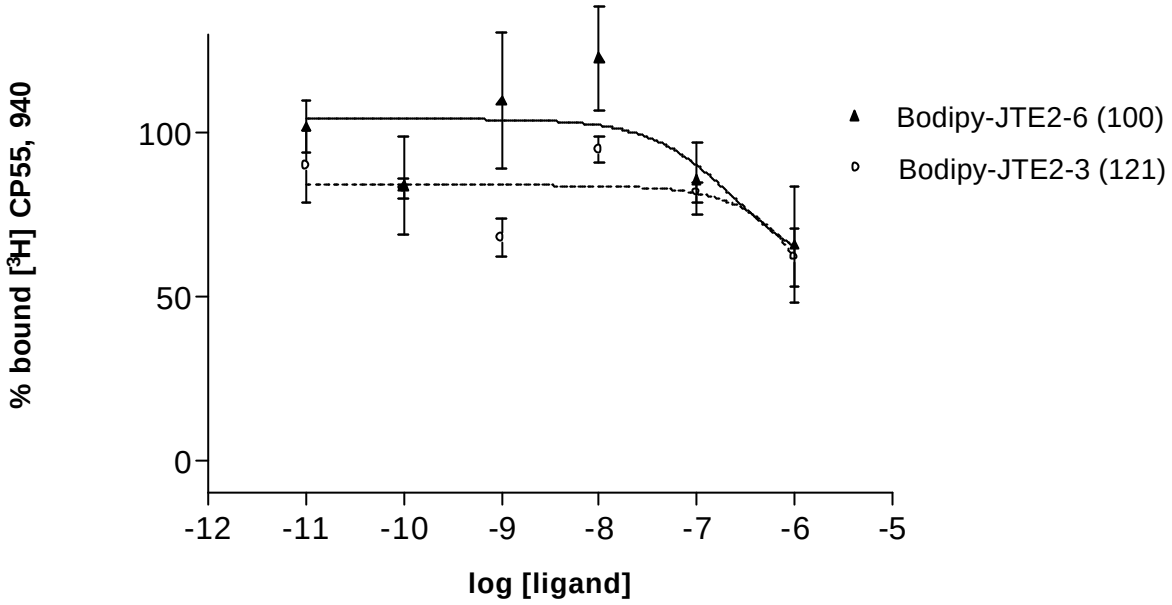

Figure 5-3 Displacement curve of [^{3}H] CP 55, 940 by Bodipy-JTE2-6 **100** (solid) and Bodipy-JTE2-3 **121** (dashed) from membranes derived from rat splenocytes (n=4).

Although the K_i for both Bodipy-JTE2-6 **100** and Bodipy-JTE2-3 **121** could not be calculated from this assay due to maximal [^{3}H] CP 55, 940 displacement not being achieved, it could be shown that at concentrations of 1 μM, 44% and 48% of the bound [^{3}H] CP 55, 940 could be displaced by Bodipy-JTE2-6 **100** and Bodipy-JTE2-3 **121** respectively. This should be compared to no detectable displacement with these compounds at concentrations ≥ 32 μM at the hCB_2 receptor.

5.4 Molecular modelling results

We explored the nature of the species selectivity using the molecular model of the CB_2 receptor discussed in chapter 3. In order to investigate the possible differences between the binding of JTE2-3 **62** in the rat and human CB_2 receptor we first

constructed the rCB_2 model by homology modelling to the hCB_2 previously generated. This was achieved by changing the non-conserved sequences in the hCB_2 receptor to the corresponding rCB_2 receptor residue, using similar experimental protocol detailed in section 3.3. The rCB_2 sequence was sequence aligned against the hCB_2 and mouse CB_2 (mCB_2) sequences (Swissprot reference number Q9QZN9 (rCB_2), P47936 (mCB_2), P34972 (hCB_2) using the alignment program ClustalW (Version 1.81)[232]. The alignment generated is shown in Figure 5-4

```
rCB2    MEGCRELELTNGSNGGLEFNPMKEYMILSDAQQIAVAVLCTLMGLLSALENVAVLYLILS 60
mCB2    MEGCRETEVTNGSNGGLEFNPMKEYMILSSGQQIAVAVLCTLMGLLSALENMAVLYIILS 60
hCB2    MEECWVTEIANGSKDGLDSNPMKDYMILSGPQKTAVAVLCTLLGLLSALENVAVLYLILS 60

rCB2    SQRLRRKPSYLFIGSLAGADFLASVIFACNFVIFHVFHGVDSRNIFLLKIGSVTMTFTAS 120
mCB2    SRRLRRKPSYLFISSLAGADFLASVIFACNFVIFHVFHGVDSNAIFLLKIGSVTMTFTAS 120
hCB2    SHQLRRKPSYLFIGSLAGADFLASVVFACSFVNFHVFHGVDSKAVFLLKIGSVTMTFTAS 120

rCB2    VGSLLLTAVDRYLCLCYPPTYKALVTRGRALVALGVMWVLSALISYLPLMGWTCCPSPCS 180
mCB2    VGSLLLTAVDRYLCLCYPPTYKALVTRGRALVALCVMWVLSALISYLPLMGWTCCPSPCS 180
hCB2    VGSLLLTAIDRYLCLRYPPSYKALLTRGRALVTLGIMWVLSALVSYLPLMGWTCCPRPCS 180

rCB2    ELFPLIPNDYLLGWLLFIAILFSGIIYTYGYVLWKAHQHVASLTEHLDRQVPGIARMRLD 240
mCB2    ELFPLIPNDYLLGWLLFIAILFSGIIYTYGYVLWKAHRHVATLAEHQDRQVPGIARMRLD 240
hCB2    ELFPLIPNDYLLSWLLFIAFLFSGIIYTYGHVLWKAHQHVASLSGHQDRQVPGMARMRLD 240

rCB2    VRLAKTLGLVMAVLLICWFPALALMGHSLVTTLSDKVKEAFAFCSMLCLVNSMVNPIIYA 300
mCB2    VRLAKTLGLVLAVLLICWFPALALMGHSLVTTLSDQVKEAFAFCSMLCLVNSMVNPIIYA 300
hCB2    VRLAKTLGLVLAVLLICWFPVLALMAHSLATTLSDQVKKAFAFCSMLCLINSMVNPVIYA 300

rCB2    LRSGEIRSAAQHCLTGWKKYLQGLGSEGKEEAPKSSVTETEAEVKTTTGPGSRTPGCSNC 360
mCB2    LRSGEIRSAAQHCLIGWKKYLQGLGPEGKEEGPRSSVTETEADVKTT------------- 347
hCB2    LRSGEIRSSAHHCLAHWKKCVRGLGSEAKEEAPRSSVTETEADGKITPWPDSRDLDLSDC 360
```

Figure 5-4 The sequence alignment of the rat, mouse and human CB_2 receptors. Highlighted amino acids are non-conserved between the rat and human CB_2 sequence.

From the sequence alignment shown in Figure 5-4, we mutated the non-conserved amino acids highlighted, from the residue contained in the hCB_2 receptor, to the corresponding residue present in the rat sequence. The rCB_2 receptor sequence was subjected to energy minimisation within Sybyl® using 100 Steepest Descent iterations followed by 500 Conjugate Gradient steps using the standard Sybyl® setup.

JTE2-3 **62** was constructed using Spartan PCPro (Wavefunction Inc). Geometry optimisation was undertaken using quantum mechanical methods, namely *ab initio* Hartree-Fock calculations at the 3-21G* level. In addition, partial atom charges were calculated using the ESP method. JTE2-3 **62** was interactively docked into both the rat and human CB_2 receptor models using Phe 197 as an anchor point for an aromatic-aromatic interaction with the ligand **62** in a similar manor to that depicted in figure 3.5.

The two ligand-receptor complexes were further optimised using energy minimisation and molecular dynamics. In our studies, we applied the CHARMM force field with an 8 Å cut-off for non-bonded interactions to optimize the ligand-receptor model as previously stated in section 3.3.3. It is clear from Figure 5-5 (A and B) that JTE2-3 **62** in both the human and the rat receptor occupy very similar positions within the receptor. The overlay of the bound ligand demonstrates that the phenol ring in the hCB_2 receptor has rotated into a more planar position relative to the rCB_2, which as a consequence, has shifted the amide carbonyl group into a different alignment from that observed in the rCB_2 receptor Figure 5-5 (C). The key amino acids involved in ligand-receptor interactions were located using the programme LigPlot for each model[245]. The results from this analysis are shown in Figure 5-6. It is evident that JTE2-3 **62** bound into the rCB_2 receptor is associated with four extra amino acid interactions than when bound in the hCB_2 receptor. The most striking difference in the interactions observed between the two species is that JTE2-3 **62** is capable of forming a hydrogen bond (H-bond), involving its carbonyl oxygen and the residue Thr 173 in the rCB_2 receptor but not in the hCB_2 receptor. Other contacts made with the ligand, in both receptor species, are hydrophobic and aromatic interactions. It is interesting to note that Phe 117, Phe 197 and Trp 194, important residues in CB_2 receptor binding, are shown to form interactions with the ligand in the rCB_2 model.

Investigations into why the ligand adopts a different conformation, in the rCB_2 and hCB_2 receptor, initially concentrated on its contacts made with Thr 173. This residue, present in both receptor sequences, was highlighted and shown to adopt very similar conformations in both receptors (Figure 5-7, A). Investigation of the non-conserved amino acids, highlighted in Figure 5-4, was unable to detect any significant differences in the binding pocket shape which could alter the bound conformations of JTE2-3 **62** and therefore evoke the hydrogen bond observed in the rCB_2 receptor (results not shown). 3D visualisation of both models, in which the ligand binding amino acids (identified by LigPlot; Figure 5-6) were highlighted, was able to identify a difference in the conformation of Glu 8, located in the extra cellular loop (EL) 1, between the rat and human species. Glu 8, which makes a contact with JTE2-3 **62** in the hCB_2 receptor, can be seen to adopt a position in the hCB_2 receptor that is altered from the corresponding residue in the rCB_2 receptor (Figure 5-7, B & C). A distance of 1.42 Å and 4.79 Å was measured between the carboxylic acid group of Glu 8 found within the hCB_2 receptor, and the phenol oxygen of JTE2-3 **62** in its final bound

conformation within the rat and human receptors respectively. Therefore the carboxylic acid group of Glu 8, is involved in a clash with the phenol ring of JTE2-3 **62** in the hCB_2, but not in the rCB_2 receptor.

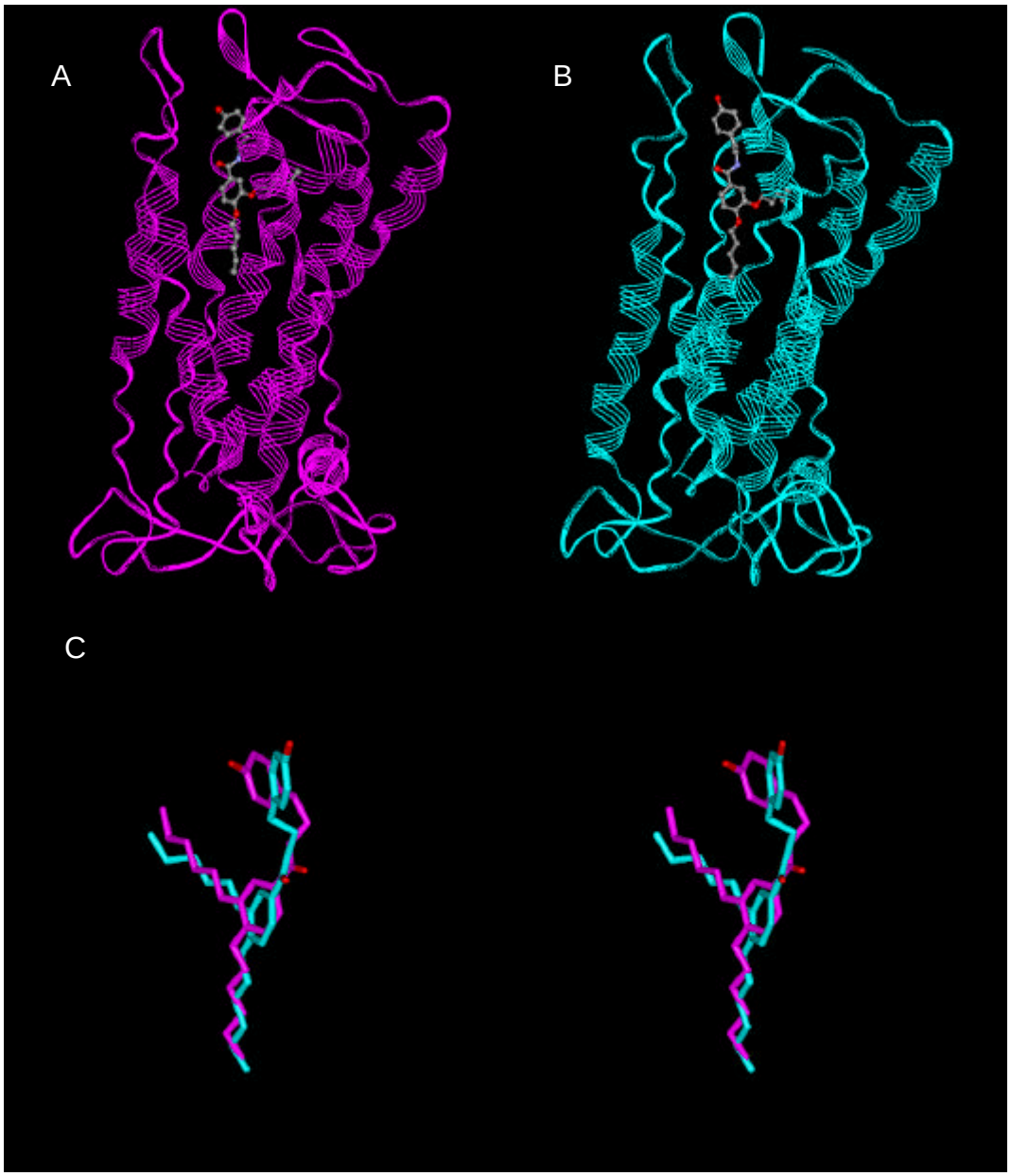

Figure 5-5 Representations of JTE2-2 **62** docked into the hCB_2 and rCB_2 receptor. (A) Shows the relative position of JTE2-3 **62** in its final binding position/conformation in the hCB_2 receptor. Model is being viewed with TM 5 & 6 front and centre. (B) Shows the ligand JTE2-3 **62** in its final binding position/conformation in the rCB_2 receptor. Model is being viewed with TM 5 & 6 front and centre. (C) Stereoview of the overlay of JTE2-3 **62** in the bound conformation from the hCB_2 (magenta) and rCB_2 (cyan) receptor. The oxygen atoms shown in red are the phenol (top) and the amide carbonyl (lower).

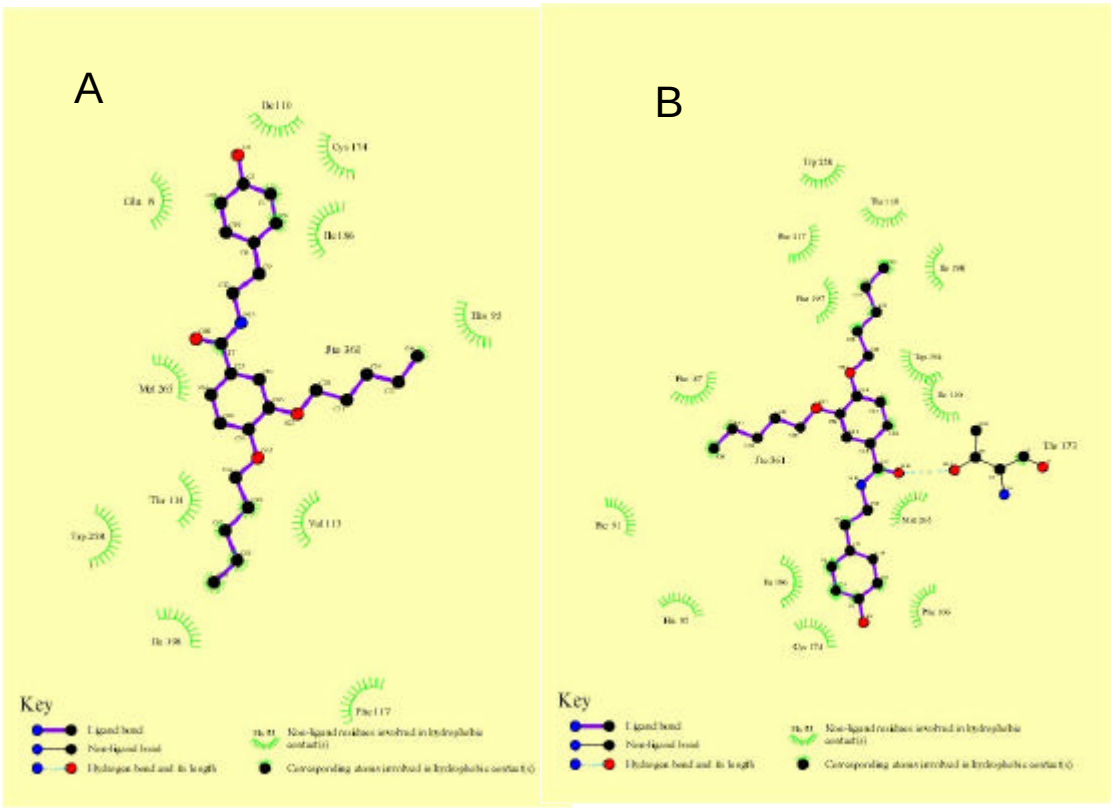

Figure 5-6 Ligplot analysis of the amino acid binding interactions occurring with JTE2-3 **62** docked in the hCB_2 (A) and rCB_2 (B) receptor.

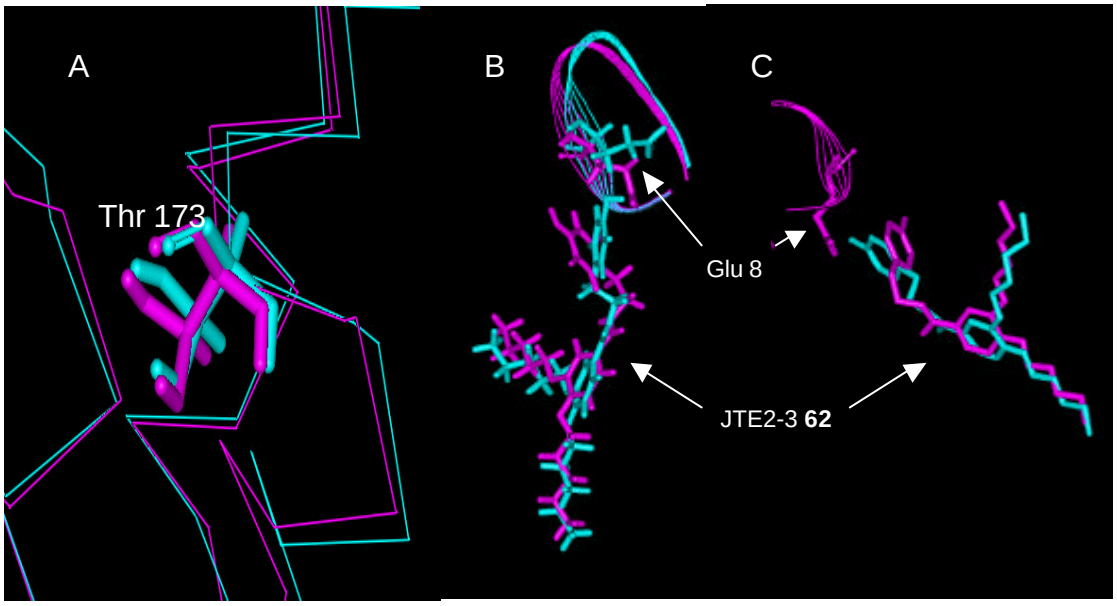

Figure 5-7 Investigation into the binding conformation of JTE2-3 **62** in the hCB_2 (magenta) and rCB_2 (cyan) receptor. (A) Shows the similar conformation of Thr 173 in the hCB_2 and rCB_2 receptor. (B) An overlay image of the ligand bound in both receptors showing the interactions with EL 1 (Met 1 – Gly 12); specifically with residue Glu 8. (C) An alternative view of the bound ligand interacting with Glu 8. EL 1 of the rCB_2 is not shown for clarity.

5.5 Discussion

It has been previously shown, in chapter 4, that the ligand JTE2-3 **62** binds to the hCB_2 receptor with 7500 fold less affinity than the rCB_2 receptor. In order to qualify these data we have determined the K_i value of JTE2-3 **62** in the rCB_2 receptor in our own laboratories. The assay, using membranes derived from rat splenocytes, was validated by determining the K_d value of a known cannabinoid ligand [^{3}H] CP 55, 940. The calculated K_d value of 0.59 nM was within the reported range of 0.29-7.37 nM for this ligand[51] and we were therefore confident in using the assay to calculate K_i values of unknown compounds. Using this assay we determined the K_i value of JTE2-3 **62** at the rCB_2 receptor to be 5.02 nM (95% confidence intervals 0.85 – 29 nM). Although this value is 12 fold higher than the one reported in the original patent (0.4 nM)[126], it still supports the original hypothesis that a large increase in affinity is observed when the ligand is binding to the rCB_2 receptor compared to the hCB_2 receptor. Discussion in section 5.2 highlighted work on other cannabinoids, namely JWH051, Win 55212-2 **3**, and anandamide **4**, that have statistically shown a species preference. Other cannabinoids, particularly the Japan Tobacco compounds JTE1-22 **61** and JTE907 **66** also exhibit a strong selectivity towards the rCB_2 receptor. The 600 fold difference in affinity between the rat and human species demonstrated in chapters 4 and 5 is to the best of our knowledge, the largest species selectivity demonstrated by any cannabinoid to date. The authors of the original rCB_2 cloning papers, both concurred that due to the low sequence homology between rat and human CB_2 sequences, they would anticipate large differences between a ligand's affinity or potency at the rCB_2 and hCB_2 receptors to be reported in future pharmacological studies; and warned researchers of the potential pitfalls in extrapolating data derived from the rCB_2 receptor into human models[105,106]. In this study we have demonstrated that the cannabinoid ligand JTE2-3 **62** does not bind with equal affinity to the rat and human CB_2 receptor. Extrapolating CB_2 data from rat to human models may also have proved unpredictable for Japan Tobacco Inc. as they have withdrawn their benzamide drug, JTE907 **66**, from phase II human clinical trials for undisclosed reasons[†††].

In using the Japan Tobacco compounds as lead molecules in designing fluorescent CB_2 selective ligands (chapters 2 and 4) we did not recognise the

[†††] Information obtained from the Japan Tobbaco Inc. website (www.jti.co.jp) which shows that compound JTE907 did not progress to phase II trials for an anti-allergy compound in May 2003.

importance of species selectivity, as very little literature existed to consolidate previous work and the species selectivity exhibited were not as large as we encountered. Therefore fluorescent conjuagtion of these ligands with fluorescent dyes, which is normally associated with a reduction in receptor binding, was unlikely to yield high affinity fluorescent ligands for the hCB_2 receptor. In order for the fluorescent probe to fulfil its potential as a tool in molecular pharmacology and drug discovery, discussed in section 1.1, it is highly desirable that the fluorescent ligand should have good affinity towards the hCB_2 receptor.

When we retested the two BODIPY® labelled derivatives, Bodipy-JTE2-6 **100** and Bodipy-JTE2-3 **121**, against the rCB_2 receptor they did demonstrate an albeit moderate affinity, displacing 44% and 48% of the bound [^{3}H] CP 55, 940 respectively, at concentrations of 1 μM. This demonstrated to us that the overall strategy adopted for fluorescently labelling these cannabinoids, appeared to be partially successful. Unfortunately, the CB_2 affinity shown was still too poor for use in fluorescence experiments and it was decided not to pursue them as novel CB_2 selective ligands. Instead we concentrated our efforts in designing a high affinity CB_2 selective fluorescent ligand with affinity for the hCB_2 receptor, and this work is discussed in chapter 6.

Due to the importance and magnitude of the species selectivity exhibited by JTE2-3 **62** we used computational methods to determine the nature of the species difference. Analysis of the ligand-receptor interactions occurring in both the rCB_2 and hCB_2 receptors, demonstrated that a key difference between the two species was the presence of a strong H-bonding interaction occurring within the rat receptor and not within the human receptor. It is well known that binding interactions occurring between a receptor and a ligand are crucial to prevent the ligand drifting in and out of the binding site; with stronger binding interactions leading to ligands with higher affinity to the receptor. The rCB_2-ligand complex crucially has four extra amino acid interactions, including a strong H-bond, when compared to the hCB_2-ligand complex (Figure 5-6). These extra binding interactions, especially the H-bonding, may well account for the higher K_i value observed in the rat receptor. The H-bond occurring within the rCB_2 receptor exists between the amide carbonyl oxygen of JTE2-3 **62** and the residue Thr 173. The location and conformation of Thr 173 in both species of receptor is almost identical and it is therefore the conformation or position of the

ligand within the binding site that has determined whether a H-bond can form (Figure 5-7, A). Figure 5-5 shows that the conformation of JTE2-3 **62** is different in both receptor types; with the phenol ring in the hCB_2 receptor being twisted into a more planar conformation. The result of this twist is that the carbonyl oxygen is shifted out of the plane necessary to form the crucial H-bond with Thr 173 (1.8 Å, 120°[230]). The receptor interactions that result in the phenol ring twisting in the hCB_2 receptor were investigated and we hypothesised that this was due to the conserved Glu 8 residue located in EL 1. From Figure 5-7 (B & C) it is possible to show that Glu 8 within the hCB_2 receptor protrudes further into the binding cavity than is observed in the rCB_2 receptor. Although Glu 8 is conserved between both species it is located in an EL loop which is only 50% homologous between the two species (Figure 5-4). The different conformations of the EL 1, adopted by both species, may result in the Glu 8 positional differences observed. The consequence of Glu 8 extending into the binding cavity is shown in Figure 5-7 C. One can envisage that when JTE2-3 **62** is docked within the hCB_2 receptor, the close proximity of Glu 8 (1.42 Å), induces a steric interaction which forces the phenol ring down into a planar position, thus shifting the amide carbonyl into a non-H-bonding position. The Japan Tobacco compounds are by far the most species selective of any of the cannabinoids reported in the literature. By using the data from our study it is possible to hypothesise that the difference in binding is due to the amide group within the structure forming a H-bond in the rat, but not the human, receptor. If this evidence is proven by further studies then compounds such as the Japan Tobacco benzamide **65** (figure 1-22), containing a conformationally restricted amide, may be less susceptible to the species differences.

It is finally worth stating that the CB_2 model we have used to study the binding of the Japan Tobacco ligands is a high quality GPCR model, which is comparable to a similar peer reviewed model by Xie *et al*.[242]. However, GPCR modelling remains in its infancy and consequently is still limited in a number of areas; namely that water is not present within the molecular dynamics simulation; the template of Bovine Rhodopsin represents the receptor in the 'off (unbound) state'; and the receptor is not coupled to the G-protein during the simulation. These limitations are likely to cause inaccuracies within any model produced, and may explain why modelling of JTE2-3 **62** in the hCB_2 appeared to give positive binding results when in reality the ligand had poor affinity to this receptor. There is currently a large interest in overcoming these

limitations in GPCR modelling and we hope to use future developments in this area to refine our own CB_2 model[82-84,227,229,253].

5.6 Conclusions

- The K_i value of JTE2-3 **62** in the rCB_2 receptor was found to be 5.02 nM which was 600 fold less than the K_i value obtained for the hCB_2 receptor. This difference in species selectivity is the largest reported for any cannabinoid.
- Our use of JTE2-3 **62** as a lead molecule for conjugating with fluorescent dyes was unable to take account of this largely unrecognised species difference. It was therefore not surprising to find that conjugating a fluorescent dye to a ligand with low affinity to the hCB_2 receptor, relinquished fluorescent conjugers with associated poor hCB_2 affinity.
- Retesting the affinity of the fluorescent conjugers BODIPY-JTE2-6 **100** and BODIPY-JTE2-3 **121** in rCB_2 receptors, revealed that they were able to displace approximately 40% of the radiolabelled [^{3}H] CP 55,940 from the receptors, albeit at high concentrations (1 μM). Hence they also mirrored the species selectivity pattern as no displacement was observed when they were tested at this concentration against the hCB_2 receptor.
- Molecular modelling was used to understand the nature of the species selectivity. It was observed that JTE2-3 **62** was able to form extra receptor interactions, including a strong hydrogen bond, in the rCB_2 receptor potentially leading to the lower K_i observed.
- The hydrogen bond interaction was investigated and found to form between the carbonyl of JTE2-3 **62** and Thr 173 in the rCB_2 receptor. The bond could not form in the hCB_2 receptor due to a steric clash between Glu 8 and the phenol ring resulting in the ligand adopting a different binding conformation in which the ligand's carbonyl group was twisted away from Thr 173.
- Due to the species selectivity exhibited by the Japan Tobacco compounds we decided to adopt a new strategy to develop fluorescent CB_2 ligands, with affinity at the hCB_2 receptor.

.

6 Fluorescent CB_2 ligand based on a modification to JWH015

Our previous studies have concentrated on the synthesis of fluorescent cannabinoids based on modifications to Japan Tobacco compounds, which have been demonstrated to posses an unusual species preference towards the rat CB_2 receptor. As previously discussed in chapter 1, our aim for these fluorescent ligands was to give cannabis researchers a unique tool which could be used to further our understanding of the CB_2 receptor system and to allow for the fast pharmacological screening of novel cannabinoid compounds. To fulfil these requirements, the fluorescent CB_2 ligand should have an acceptable affinity towards the human CB_2 (hCB_2) receptor. Our attentions were therefore refocused, upon conjugating a CB_2 selective ligand with proven affinity at the hCB_2 receptor to a fluorescent dye. The work reported below describes our efforts to design a fluorescent CB_2 ligand, using computational *de novo* design on the hCB_2 ligand JWH015 **53**.

6.1 JWH015

JWH015 **53** (Figure 6-1), discussed fully in section 1.4.6, was chosen for the lead molecule in this study for a number of reasons. Previous discussion, in section 2.2.1, outlined the general requirements of a cannabinoid that was required in-order to successfully conjugate to a fluorescent dye. JWH015 **53** possessed all of these requirements - shown below;

- K_i at the hCB_2 receptor of 14 nM[122]
- 27 fold CB_2/CB_1 selectivity[122]
- Chemically stable, no known light or enzymatic stability issues
- Comprehensive SAR conducted for the molecule[122,135]
- Is not included in the substances listed in the Misuse of Drugs Act

In addition, JWH015 **53** had a number of advantages with regards to the specific strategy we planned to use in this work; *de novo* drug design. The molecule is structurally similar to Win 55212-2 **3** (Figure 6-1), a molecule which had been extensively interrogated by molecular modelling and mutational analysis techniques.

We therefore envisaged docking Win 55212-2 **3** into the hCB_2 receptor, generated in chapter 3, using previous published data concerning Win 55212-2 **3** binding. Structural similarities between JWH015 **53** and Win 55212-2 **3**, will be used to superimpose common structural motifs (*i.e.* naphthyl rings) of the two molecules, in-order to generate an accurate model where JWH015 **53** is bound in the hCB_2 receptor (Figure 6-1).

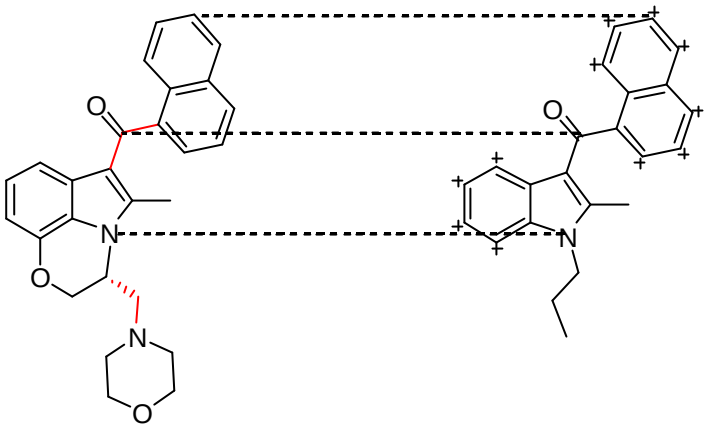

Win 55212-2 **3** JWH015 **53**

Figure 6-1 Structures of Win 55212-2 **3** and JWH015 **53**. Dashed lines indicate common structural motifs used in structural alignment of the molecules in molecular modelling. + indicates a grow point used in LigBuilder. Red line indicates a rotatable bond used in conformational analysis.

Using previous SAR data for JWH015 **53**[122,135] and SAR from similar molecules, described in detail in section 1.4.6, a number of positions upon JWH015 **53** were identified that could potentially tolerate extension and bulky substituents. These positions were selected as 'grow points' on the molecule, in-order that the *de novo* drug design program LigBuilder[254] could interrogate them for their ability to tolerate bulky fluorescent dyes.

6.2 LigBuilder

LigBuilder is a free-ware, multi-purpose programme used for structure-based drug design. The programme utilises a protein structure incorporating a docked ligand to 'virtually screen' a large number of molecules to determine if they are able to fit within the binding pocket of the protein. This use of computational methods saves on synthetic effort in developing new ligands towards specific targets. Obviously there are many other software packages, such as DOCK[255], GRID[256], LUDI[257] *etc.*, which are also capable of performing similar analysis, however we chose Ligbuilder due to its accessibility, favourable heterocyclic building block library and reliable 'SCORE' function (used to predict binding affinity)[258].

LigBuilder breaks down the components of *de novo* drug design into separate stages which allows the process to proceed logically from one step to another. Firstly the binding pocket is analysed to determine the size and the nature of key binding interactions. In order to do this a pre-docked ligand must be present within the receptor, so that the programme can identify which area of the protein to probe. The programme then calculates the size of the binding pocket and identifies the key interactions using probe atoms which include; (1) a positively charged sp^3 hybridised nitrogen, as a hydrogen bond donor; (2) a negatively charged sp^2 oxygen, as a hydrogen bond acceptor; (3) a sp^3 carbon atom, probing for hydrophobic interactions[254]. Following scoring and refinement, a computer model of the binding site is stored for use in the second step. The second step is known as a 'building up' process. It uses two different fragment-based algorithms that can GROW or LINK fragments onto a predefined seed structure within the receptor. The GROW strategy, which we employed, uses a pre-placed seed ligand (JWH015 **53** in our work) sited within the binding pocket. Assigned 'grow points' upon the pharmacophore are used by LigBuilder to add candidate fragments, from its database, to the selected site upon the seed molecule. The LINK algorithm was not be used in this work and readers are directed to the original reference for further details[254]. The GROW algorithm selects a hydrogen on the user identified grow points and links it with a candidate fragment to form a new bond. The newly formed bond is then rotated using 15° increments and the programme calculates the resulting steric energy, between the ligand and binding pocket, for each of the 24 conformers. The lowest energy conformations are used in the next step. The conformation selected can then be mutated in terms of its carbon,

nitrogen and oxygen atoms to other atoms in the same hybridisation state. This mutation function is not a random event and takes account of the binding pocket analysis performed in the previous step. Thus, if the region of mutation lies within an area where H-bond donors are present it would only mutate the atoms to those of a H-bond acceptor nature. Finally the GROW algorithm has been enhanced by the input from synthetic chemists; which prevents the programme from designing unreasonable chemical structures. The scoring method used by LigBuilder has been shown in one study to be more reliable than that used by other drug design programmes[258]. The SCORE algorithm is a two phase process which takes into account both the energy contributions made by ligand binding, and applies 'Lipinski rules'[259] to the algorithm to try to prevent non-drug like molecules from being scored highly. Although Lipinski rules apply to developing bioavailable drugs rather than *in vitro* fluorescent ligands, our ligands still require good solubility and other 'drug like' properties to be used successfully in investigating the CB_2 system. We felt that adding this scoring system to our work would generate enhanced fluorescent ligands. Therefore the SCORE algorithm gave each of the tolerated *de novo* structures a generic score which allowed them to be ranked in order of expected affinity to the receptor. LigBuilder has been demonstrated, using thrombin and dihydrofolate reductase, to generate chemical structures similar to the known ligands for these two enzymes[254]. It is worth noting that LigBuilder treats the protein model as a rigid structure throughout the drug design process. This is a disadvantage in computational *de novo* drug design in GPCRs as TM 6 has been postulated to adopt a new conformation upon agonist binding[260]. This inaccuracy in the technique is unavoidable using current computer technology and GPCR molecular modelling techniques (see chapter 3), and may lead to the generation of antagonist ligands. However, this was not viewed as a significant problem since all we required was a high affinity fluorescent ligand (agonist or antagonist) and specifically, in the CB_2 receptor, studies have demonstrated that the conformational shift of TM 6 is not significant in agonist binding[260].

6.3 Molecular modelling

Win 55212-2 **3** was constructed using Spartan PCPro (Wavefunction Inc) and subjected to a conformational analysis about the four rotatable bonds, highlighted in red in Figure 6-1, using the MMFF molecular mechanics forcefield. The lowest energy conformation, equivalent to the s-*cis* conformation, was chosen (see section 1.4.6.1 and figure 1-20). Geometry optimisation was undertaken using quantum mechanical methods, namely *ab initio* Hartree-Fock calculations at the 3-21G* level. In addition, partial atom charges were calculated using the ESP method. The *ab initio* geometry and charges were used to parameterise the CHARMM force field through generation of an RTF file.

Win 55212-2 **3** was used in the s-*cis* form despite a previous SAR study by Reggio *et al.*, demonstrating that only the rigid (*E*)-naphthylidene indene (equivalent to s-*trans* Win 55212-2 **3**) was the bioactive conformation in the CB_2 receptor[189] (see section 1.4.6.1 for structures and full discussion). This was decided for a number of reasons detailed below:

- The structure of the (*E*)-naphthylidene indene (figure 1-20) deviates from the indole structure of Win 55212-2 **3** considerably. The (*E*)-naphthylidene indene posses neither the H-bond acceptor ring nitrogen nor the carbonyl oxygen of Win 55212-2 **3** and possess extra π electrons resulting from its extra double bond.
- The binding data presented for the (*E*)- and (*Z*)- naphthylidene indenes shows that although the *E* isomer binds preferentially to the CB_2 receptor (K_i = 2.05 nM), the *Z* isomer (representing s-*cis* Win 55212-2 **3**) also demonstrated nanomolar affinity (K_i = 658 nM)[189].
- Another study, published after the work conducted on the naphthylidene indenes, using high resolution NMR and molecular modelling clearly established that the favourable conformation of Win 55212-2 **3** was s-*cis*[191].
- Our own geometry optimisation demonstrated that there was a difference in energy between the lowest energy state s-*cis* and s-*trans* confomers of 2.5 Kcal mol^{-1} and 62% of the lowest energy conformers resided in the s-*cis* form (results not shown).

Our major concern about refining the s-*cis* model, obtained through our own geometry optimisation studies and supported by previous NMR data[191], to the s-*trans* conformation, previously hypothesised by Reggio *et al.* to be the bioactive conformer, was the methodology used in their hypothesis[189]. Although (*E*)-naphthylidene indene was clearly shown to have a higher affinity to the CB_2 receptor, it included in its structure an additional double bond whilst it did not have two H-bond acceptors that are present in Win 55212-2 **3**. Thus; although the indene analogues would suggest that the s-*trans* form of Win 55212-2 **3** was the binding conformation, we felt that the two structures were too diverse to correlate together. Subsequent to their SAR study, Reggio *et al.* published molecular modelling results which showed that only the s-*trans* isomer of Win 55212-2 **3** could bind successfully in the CB_2 receptor[194] and concluded that this was proof of their hypothesis that the s-*trans* conformation being bioactive was correct. We will demonstrate below that in our own work, s-*cis* Win 55212-2 **3** was not only tolerated in the CB_2 receptor, but also displayed very similar binding interactions to those obtained for the s-*trans* confomer.

Win 55212-2 **3** was interactively docked into the CB_2 receptor (Alignment 3 as described in section 3.3.) using Phe 197 (see section 3.3.3 for the importance of Phe 197) as an anchor point for an aromatic-aromatic interaction with the indole ring of Win 55212-2 **3**, as previously described[194]. As Win 55212-2 **3** was able to dock into the binding pocket in both a naphthyl-up and naphthyl-down position (Figure 6-2) and only limited unsubstantiated evidence existed that the 'correct' position was naphthyl-up[194], we decided to model and assess both possible complexes.

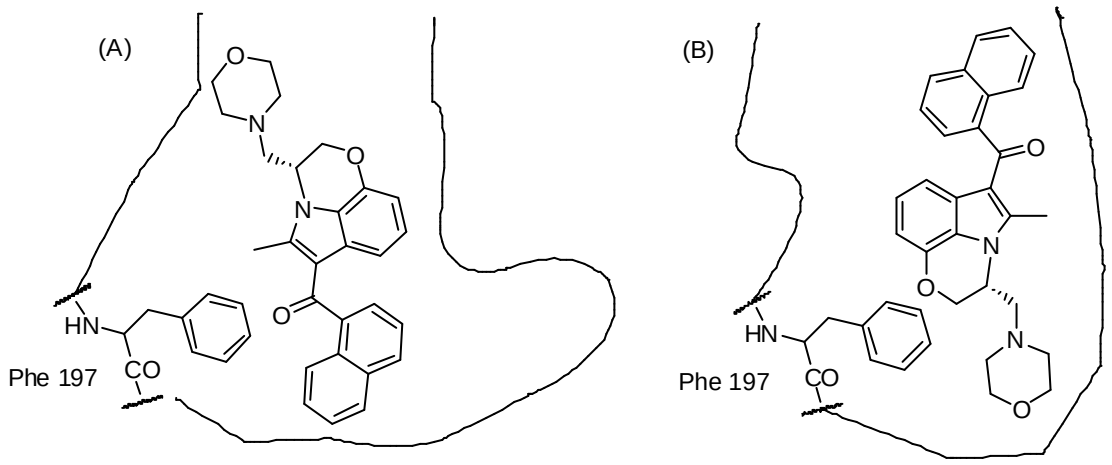

Figure 6-2 Win 55212-2 **3** docked in the s-*cis* conformation to the CB_2 receptor. (A) naphthyl-down and (B) naphthyl-up position using Phe 197 as an anchor point.

Both ligand-receptor complexes were optimised using energy minimisation and molecular dynamics. In our studies, we applied the CHARMM force field with an 8 Å cut-off for non-bonded interactions to optimize the ligand-receptor model. In order to mimic the hydrophobic transmembrane environment we set the dielectric constant to a value of 4.0. The molecular dynamics protocol consisted of: i) initial minimisation of 2500 iterations of ABNR conjugate gradient minimisation until the RMSD became less than 0.005 KJmol^{-1}; ii) MD simulation, placing a harmonic constraint on the 7 backbone α-helices and heating the structure to 300 K over 1 ps, conducted at constant temperature (300 K) for 100 ps with a 1 fs time step; iii) quenching the structure to 0 K over 1 ps and removing all constraints with a final minimisation using ABNR conjugate gradients (6000 iterations) until the RMSD became less than 0.005 KJmol^{-1}.

The energy of the two complexes was monitored throughout the molecular dynamics experiment at 0.5 ps time intervals. The plot of the total energy of the complex vs time is shown in Figure 6-3.

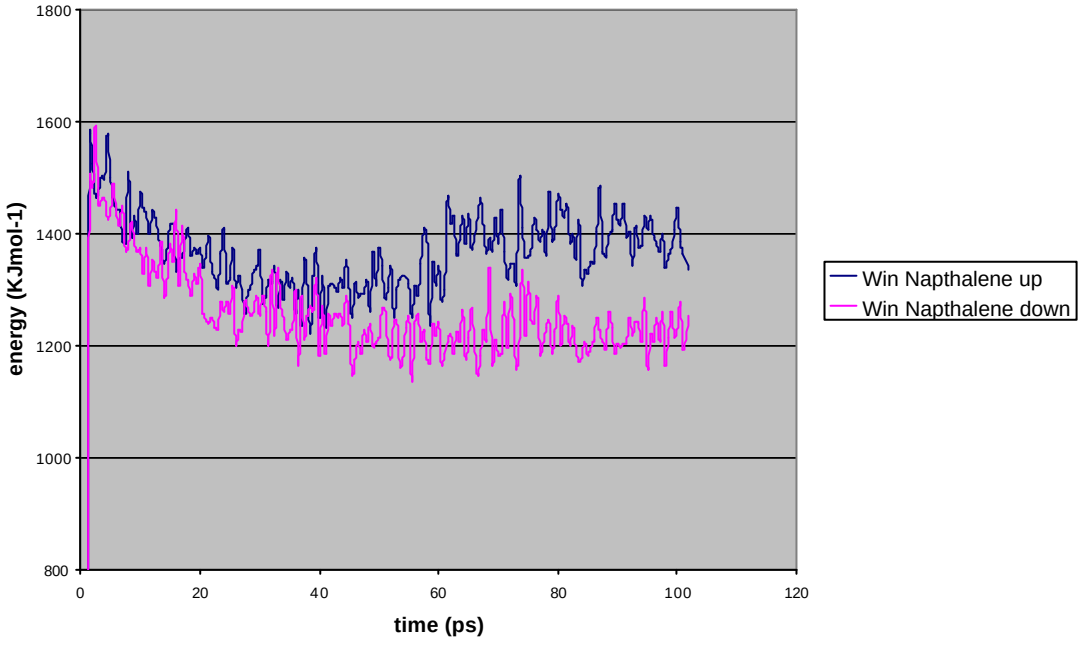

Figure 6-3 Energy profile of Win 55212-2 **3**-CB_2 receptor complex over a 0.1ns molecular dynamic simulation performed at 300 K using the CHARMM force field.

The above graph demonstrates that once 'energised', the energy function of both complexes stabilises over the first 60 ps. In the naphthyl-down complex equilibrium is

maintained but in the naphthyl-up complex the energy increases at 60 ps and remains approximately 200 KJmol^{-1} higher than the corresponding naphthyl down model. The final energy minimised complexes are shown in Figure 6-4.

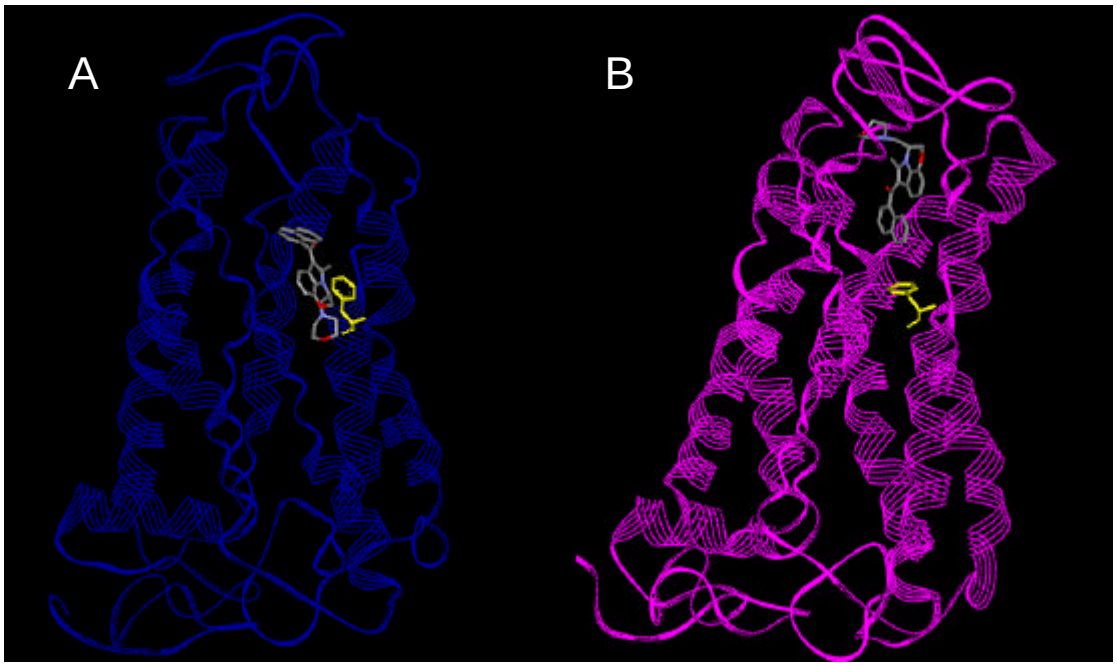

Figure 6-4 Representations of Win 55212-2 **3** docked in the s-*cis* conformer in the hCB_2 receptor. (A) a naphthyl-up and (B) a naphthyl-down position. Residue shown in yellow is Phe 197.

Figure 6-4 clearly illustrates that the final position of Win 55212-2 **3** in the naphthyl-down model has shifted away from Phe 197; used as the initial anchor point to dock the ligand. The naphthyl-up complex retained close interactions between the ligand's indole ring and Phe 197. The ligand in both simulations retained its s-*cis* configuration.

The key amino acids involved in ligand-receptor interactions were explored using the programme Ligplot for each model[245]. The results from this analysis are shown in Figure 6-5. It was demonstrated that as expected, the shift in the position of the ligand, shown in Figure 6-4, resulted in markedly different amino acids residues that formed interactions with Win 55212-2 **3** in the naphthyl-up and naphthyl-down model. The ligand, docked in the naphthyl-up position, was shown to form hydrophobic and aromatic interactions with a number of residues that have been demonstrated, in previous studies, to interact with cannabinoids (see section 3.2); notably Phe 117, Trp 194, and Phe 197 (Figure 6-6). Further examination of the naphthyl-up model demonstrated that Win 55212-2 **3** was located within an aromatic

cluster formed by Phe 117, Trp 194, and Phe 197 (Figure 6-6). Phe 117 and Phe 197 form face-face aromatic interactions with the indoles ring and Trp 194 forms an edge-edge interaction with the naphthyl ring of Win 55212-2 **3** (Figure 6-6). The naphthyl-down complex included a H-bond interaction and three interactions with the EL 1.

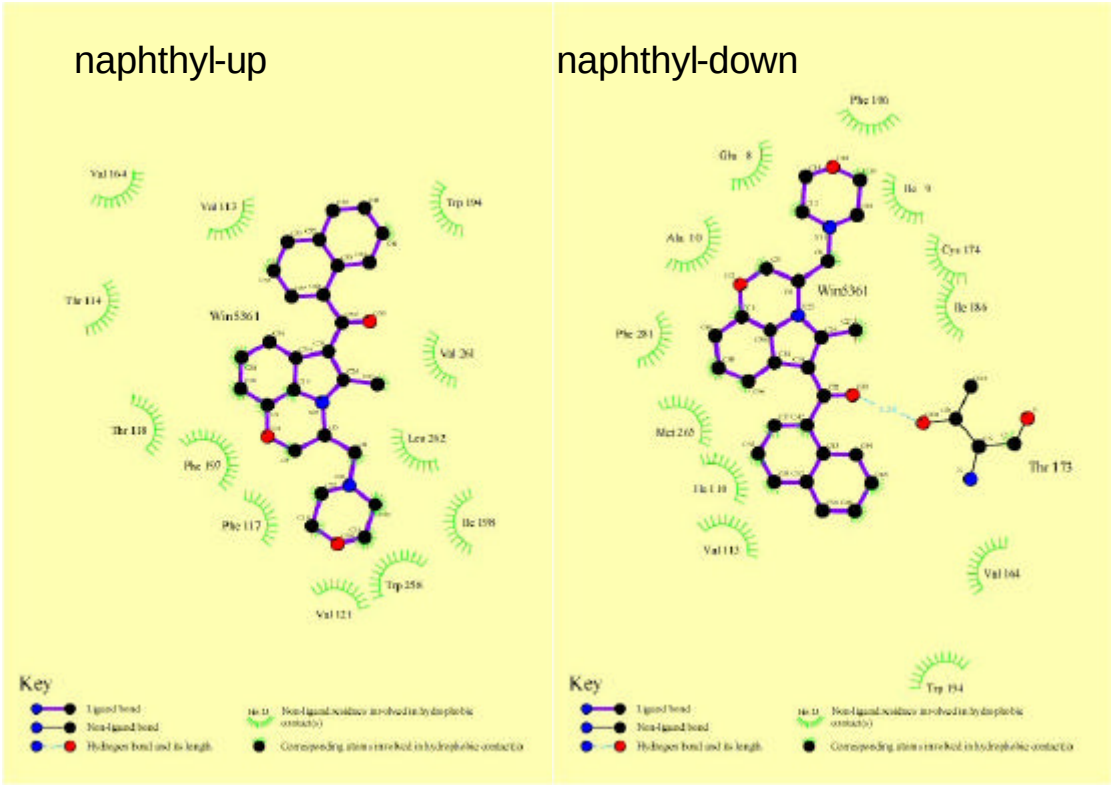

Figure 6-5 LigPlot analysis of the amino acid binding interactions occurring with Win 55212-2 **3** bound in the hCB_2 receptor in the naphthyl-up and naphthyl-down position.

In view of the fact that the naphthyl-up model demonstrated many more similarities to previously published data of Win 55212-2 binding, such as an interaction with Phe 197[194] and predominately aromatic-aromatic and hydrophobic interactions we decided to use this ligand-receptor complex as a template in the *de novo* molecular design.

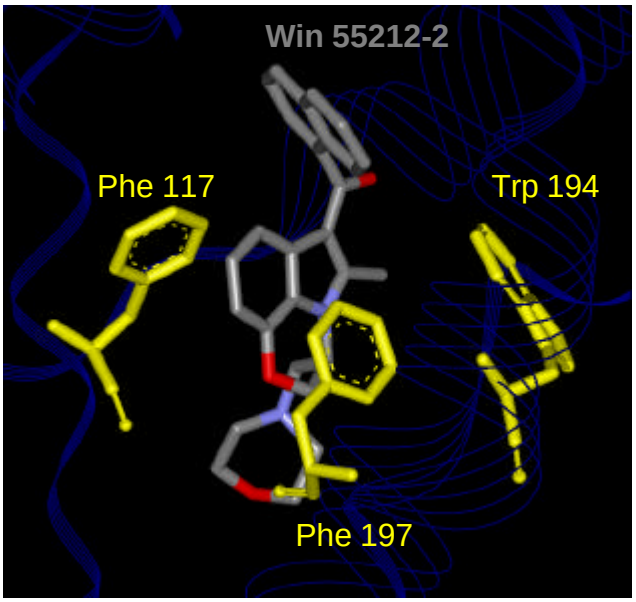

Figure 6-6 Win 55212-2 **3** bound in the s-*cis* conformation into the binding site of the hCB_2 receptor. The aromatic residues, shown in yellow, form an aromatic 'cage' around the ligand.

Structural alignment, by superimposing the naphthyl, carbonyl and indole ring nitrogens of both JWH015 **53** and Win 55212-2 **3** (Figure 6-1), and further energy minimisation using ABNR conjugate gradients (6000 iterations) until the RMSD became less than 0.005 $KJmol^{-1}$, was used to produce a ligand-receptor model where JWH015 **53** was located within the binding pocket. The 'growing points' for JWH015 **53**, shown in Figure 6-1, were added and the molecule was subject to *de novo* design using the programme LigBuilder (section 6.2).

The *de novo* design results were manually screened for molecules that had high scores and chemical structures that resembled known fluorescent molecules. The resounding trend, within the molecules generated, was the diversity and size of substituents that were tolerated at the 3-naphthyl position of JWH015 **53**. Figure 6-7 shows an example of four of the two hundred structures generated. Compounds **122a-d** show a significant diversity in the type of structure that is tolerated at the 3-naphthyl position of JWH015 **53**; with unsaturated alkyl chains **122a**; carbocyclics **122b** &**122d**; and functionalised branched alkyl chains **122c** featuring in the high scoring compounds returned.

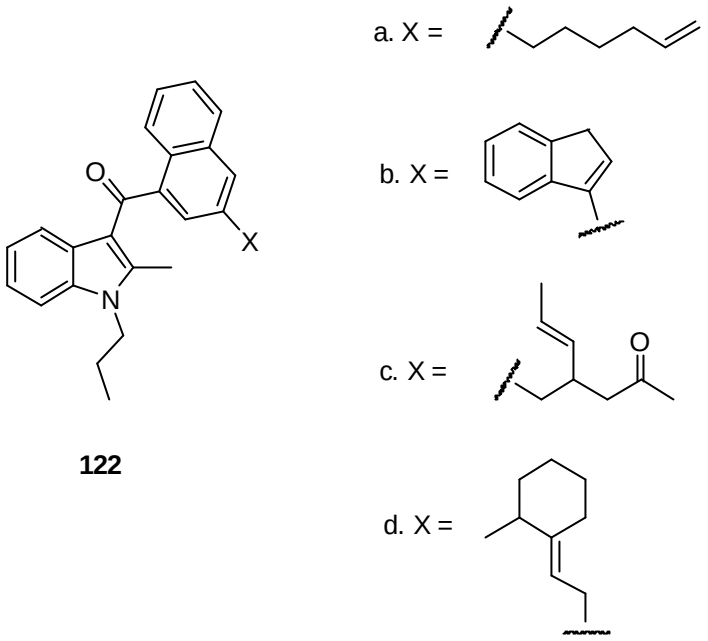

122

Figure 6-7 An example of the 3-substituted naphthyl (Nap) derivatives of JWH015 that were generated by LigBuilder.

Compound **122b** was of specific interest to us as the bulky indene group present within the structure resembled the fluorescent dye NBD **85** (see Figure 2-5). To test whether the indene of **122b** could be replaced with NBD, and still bind to the CB_2 receptor, a NBD equivalent of **122b**, incorporating an amine linkage necessary for chemical synthesis, was modelled. The NBD derivative of **122b** was constructed using Spartan PCPro (Wavefunction Inc). Geometry optimisation was undertaken using quantum mechanical methods, namely *ab initio* Hartree-Fock calculations at the 3-21G* level. In addition, partial atom charges were calculated using the ESP method.

The 2D and 3D structure of this molecule, 3-NBD-JWH015 **123**, is shown in Figure 6-8 (A & B). The molecule was docked into the hCB_2 receptor by superimposing the naphthyl groups of 3-NBD-JWH015 **123** and Win 55212-2 **3**, which had already been docked into the CB_2 receptor as described above, and the resulting complex was further minimised, using ABNR conjugate gradients (25000 iterations) until the functional tolerance was less than 0.00001 $KJmol^{-1}$, to yield a ligand-receptor model where 3-NBD-JWH015 **123** was located within the binding pocket (Figure 6-8, C & D).

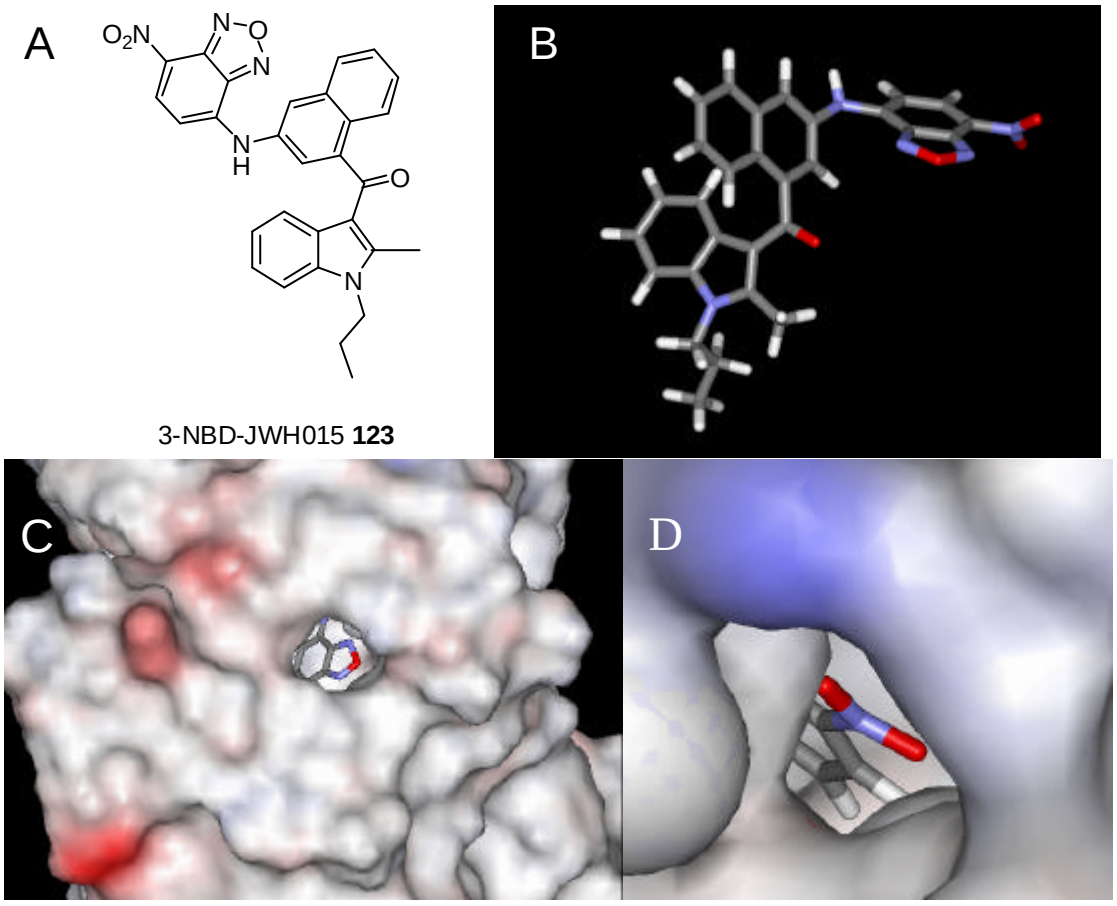

Figure 6-8 The 2D and 3D structure of 3-NBD-JWH015 **123** (A & B). C and D show 3-NBD-JWH015 **123** bound into the solvent accessible surfaces of the hCB_2 receptor. C = view from side looking at the benzofurazan ring of **123**. D = view from the top looking down at the nitro group of **123**.

From the ligand-receptor complex generated it was clear that the hCB_2 receptor could tolerate the proposed ligand 3-NBD-JWH015 **123**. The NBD fluorescent dye was positioned at the top of the receptor binding pocket and was visible when the solvent accessible surfaces were viewed (Figure 6-8, B & C). We therefore concluded that 3-NBD-JWH015 **123** could bind to the hCB_2 receptor and synthesis of this molecule was undertaken.

6.4 Chemistry results

Synthesis of the fluorescent conjuger was accomplished using modifications to a procedure by Bell *et al.*[52] (Scheme 6-1). *N*-Propyl-2-methylindole **125** was accessed by alkylation at N1 of commercially available 2-methylindole **124** using standard methodology. The commercially available 3-nitro-1, 8-naphthalic anhydride **126** was selectively decarboxylated via the mercuric salt of its di-acid to give the desired 3-nitro-1-naphthoic acid[261,262]. The *meta* substitution was confirmed by comparative m.p. with literature values and ^{1}H NMR, which established the presence of two doublets with characteristic meta coupling (J = 2.4 Hz[249]). The acid was converted to its corresponding acid chloride **127** using $SOCl_2$. Lewis acid promoted electrophilic substitution at C3 of 2-methyl-1-*n*-propylindole yielded the 3-nitro derivative of JWH015 **128**. Reduction of the nitro group of **128** to the corresponding amine **129** was achieved using catalytic hydrogenation. The two low yielding reactions leading to the acid chloride **127** (22%) and the 3-aroylindole **128** (19%) are un-optimised and are comparable with previous literature preparations[52,261].

During our synthesis we observed that only non-fluorescent derivatives are formed when NBD is reacted with aromatic amines, due to an internal quenching caused by a photoinduced electron transfer from the aromatic amine to the NBD dye[263,264]. It was therefore necessary to insert a short C2 amide functionalised linker between the aniline nitrogen and the NBD dye, which had previously been shown to prevent the internal quenching mechanism[264]. The short linker was chosen after re-visiting the molecular model of 3-NBD-JWH015 **123** and establishing by visual inspection that the binding pocket encasing the NBD dye was spacious with no amino acid residues within 8 Å of the dye.

Therefore, established carbodiimide chemistry was used to couple Boc protected glycine with the amine of **129**. This was the shortest linker available that produced the required amide bond and contained a functionalised amine group; necessary for conjugation with the dye. Acidolysis of the Boc group of **130** exposed the primary amine **131**, which when coupled with NBD-F **85** (Figure 2-5) afforded the fluorescent conjuger 3-Gly-NBD-JWH015 **132**.

An authentic sample of JWH015 **53** was prepared using an alternative preparation for 3-aroylindoles, also modified from Bell *et al.*[52] (Scheme 6-2). 3-Naphthoyl-2-methylindole **134** was prepared from the magnesium salt of 2-

methylindole, prepared *in situ*, by the action of methylmagnesium bromide on 2-methylindole **124**, and subsequent reaction with 1-naphthoyl chloride **133**. *N*-Alkylation of **133** using 1-bromopropane under standard conditions yielded JWH015 **53** as an oil. Commercial samples of JWH015 **53** have a m.p. supplied with their certificate of analysis[‡‡‡], however we were unable to crystallise the sample to determine a m.p., despite numerous attempts from a number of different solvent systems. The JWH015 **53** synthesised did however exhibit a ^{1}H and ^{13}C NMR, MS, elemental analysis and a TLC R_f which was consistent with the structure of JWH015 **53**.

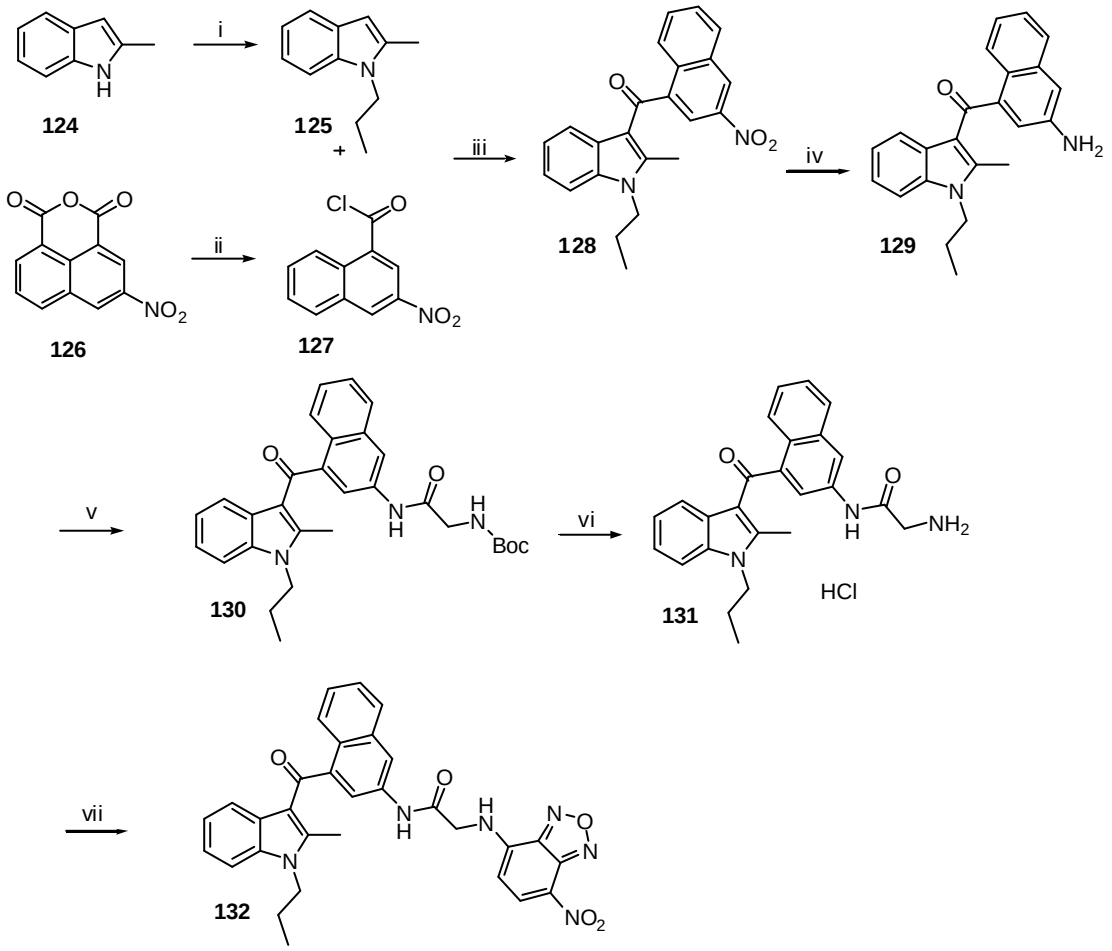

Scheme 6-1 Synthesis of 3-Gly-NBD-JWH015. Reagents, conditions and yields: (i) 1-bromopropane, NaH, DMF, rt, 4h, (97%); (ii) (a) NaOH, water, HgO, AcOH, reflux, 3 days, (b) dil. $HCl_{(aq),}$, reflux, 4h, (c) $SOCl_2$, reflux, 4h, (overall 22%); (iii) $AlCl_{3,}$, DCM, reflux, 30min, (19%); (iv) Pd/C, H_2, EtOH, 1h, (66%); (v) Boc-gly, DCC, DMAP, DCM, rt, 12h, (67%); (vi) MeOH, conc $HCl_{(aq)}$, rt, 12h, (50%); (vii) NBD-F **85**, $NaHCO_{3(aq)}$ pH 8.3: MeCN 1:1, rt, 1h, (46%).

[##] Information obtained from Tocris Cookson website www.tocris.com/searchframeset.htm

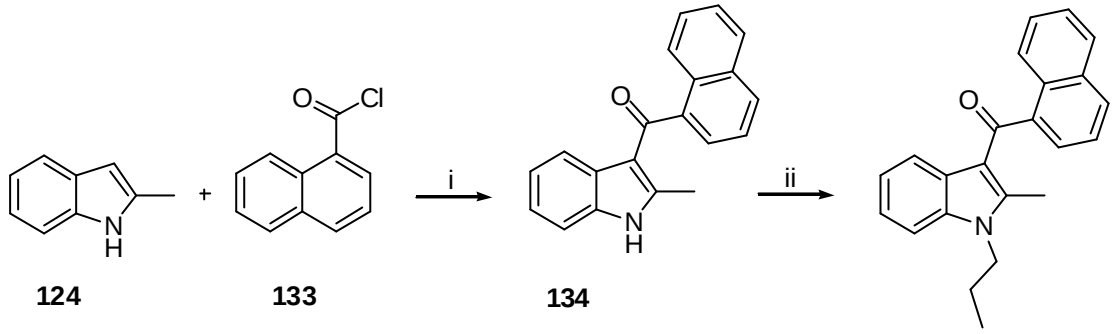

Scheme 6-2 Synthesis of JWH015. Reagents, conditions and yields: (i) MeMgBr, EtOEt, 0 °C-reflux, 2h, (31%); (ii) 1-bromopropane, K_2CO_3, MEK, reflux, (36%).

6.5 Pharmacology results

6.5.1 Radioligand binding

Compounds **53**, **128**, **129**, **131**, and **132** were tested for affinity at the hCB_2 receptor by competitive radioligand displacement of the non-selective cannabinoid [^{3}H] CP 55, 940 from CHO cellular membranes containing hCB_2 receptors and was performed as previously described by Legget e*t al.*[224]. The results of the binding assay are shown in Table 6-1.

Compound identity	K_i hCB_2 receptor (nM)
JWH015 **53**	36 (31-42) (Lit[a] 14 ± 5)
128	143 (56-364)
129	191 (59-622)
131	420 (359-492)
3-Gly-NBD-JWH015 **132**	25% displacement at 10 μM

Table 6-1 Results of a competitive displacement assay at the hCB_2 receptor. Results in parentheses are 95% confidence intervals for three individual experiments ran in triplicate. (a) ref 122.

Each of the compounds, except 3-Gly-NBD-JWH015 **132**, exhibited nanomolar K_i values with respect to the hCB_2 receptor. 3-Gly-NBD-JWH015 **132** did show an affinity towards the CB_2 receptor (25% displacement at 10 μM) however we were unable to calculate a K_i for this compound as any attempt to increase the concentration of the test solution above 10 μM resulted in precipitation in the assay tubes.

6.5.2 Functional assay

Due to the precursor compounds of 3-Gly-NBD-JWH015 **132** exhibiting nanomolar K_i values, we decided to test these compounds in a [^{35}S] GTP-γ-S functional assay to determine to what extent the agonist activity of the original JWH015 **53** lead structure had been retained. For further information on the [^{35}S] GTP-γ-S assay in cannabinoid research, readers are directed towards section 1.3.4.3.2 and a review by Griffin *et al.*[115]. The compounds JTE015 **53**, 3-nitro-JWH105 **128** and 3-amino-JWH015 **129** were assayed for their ability to stimulate [^{35}S] GTP-γ-S binding compared to the potent cannabinoid agonist HU210 **14**, previously described by Leggett e*t al.*[224]. The results are shown in Figure 6-9.

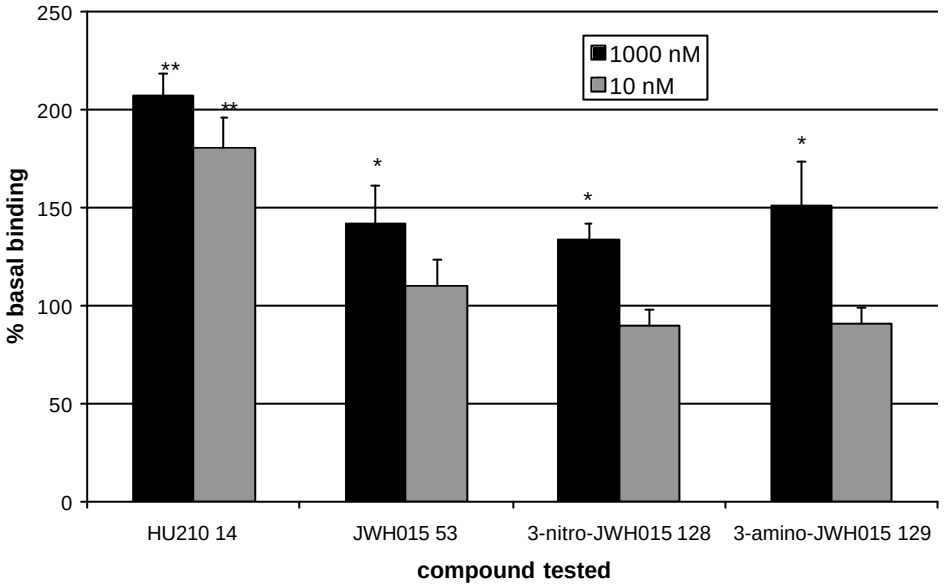

Figure 6-9 Agonist-potentiated [^{35}S] GTP-γ-S binding to CHO cell homogenates containing the hCB_2 receptor (significance levels **P*<0.05, ***P*<0.01 compared to basal binding (100%)). Error bars represent the SEM of three individual experiments ran in triplicate.

From Figure 6-9 it is clear that each of the compounds tested were able to significantly increase [^{35}S] GTP-γ-S binding above basal levels when tested at a concentration of 1000 nM. Only HU210 **14** was able to significantly raise [^{35}S] GTP-γ-S binding above basal level when used at 10 nM concentrations. Comparison of the three indole based compounds tested, **53**, **128**, and **129**, demonstrated that similar levels of receptor stimulation were observed, and Anova analysis was unable to detect

any significant statistical difference between any of the three compounds at concentrations of 1000 nM.

6.6 Confocal microscopy results

The fluorescent ligand 3-Gly-NBD-JWH015 **132** was used in a confocal experiment to demonstrate whether the ligands had the potential to highlight CB_2 receptor membrane binding. A known concentration of 3-Gly-NBD-JWH015 **132** was incubated with live CHO cells expressing human CB_2 receptors and images were recorded at various time courses throughout the experiment. To assess whether the fluorescence observed was due to specific CB_2 binding, CHO cells were also pre-incubated with a blocking concentration of a non-fluorescent cannabinoid ligand (*i.e.* 1 μM HU210 **14**) and the fluorescent ligand was subsequently introduced. Images collected from this experiment were compared to those conducted without the HU210 present, to determine if any fluorescence observed was due to CB_2 receptor binding. At concentrations of 100 nM, **132** exhibited strong intra-cellular fluorescence after 20 minutes; however, this fluorescence could not be blocked or reduced by pre-incubation with HU210 **14** (Figure 6-10**)**. Background fluorescence from the CB_2 transfected CHO cells was negligible for the excitation wavelength used for NBD (488 nm) – result not shown.

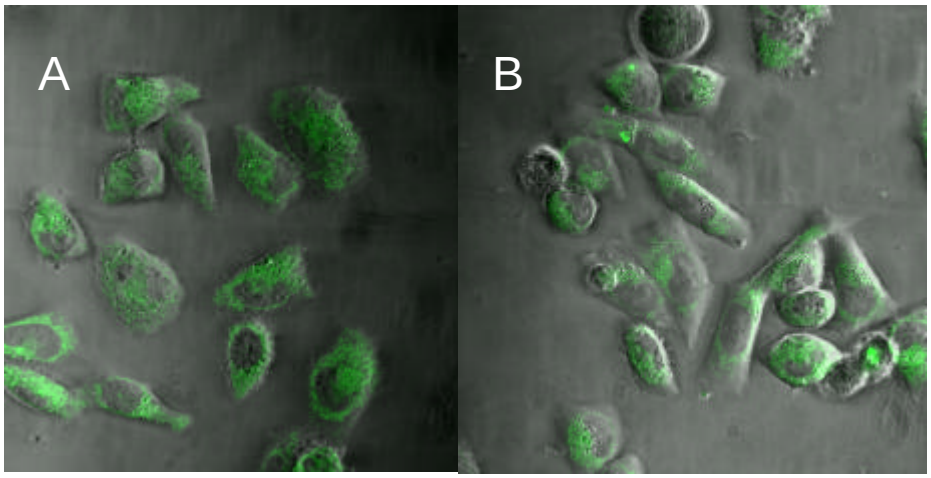

Figure 6-10 Confocal slice, taken at 20 min, of the 3-Gly-NBD-JWH015 **132** (100 nM) binding to live CHO cells expressing the hCB_2 receptor in HEPES buffered saline at 22°C. (A) Overlay of fluorescent channel (LP 505) and phase contrast with no HU210 **14** present; (B) Overlay of fluorescent channel (LP 505) and phase contrast with 1 μM of blocking HU210 **14** present. Argon laser excitation at 488 nm. Slice depth 1.1 nm.

6.7 Discussion

A fluorescent conjugate of the selective hCB_2 ligand JWH015 **53** was synthesised in seven steps following *de novo* drug design using the programme LigBuilder which suggested that the 3-naphthyl position of JWH015 **53** would tolerate bulky substituents, such as fluorescent dyes.

The molecular modelling and subsequent *de novo* design used a model of JWH015 **53** docked into the hCB_2 receptor, which was based on a molecular model generated of a similar indole cannabinoid, Win 55212-2 **3**, bound in the CB_2 receptor. Win 55212-2 **3** was chosen as the precursor model, having previously been studied by molecular pharmacology[194], molecular modelling[194] and SAR experiments[189] providing information to construct our model and subsequently compare it with. As previously discussed in section 6.3, overall evidence supported docking Win 55212-2 **3** in the s-*cis* conformer, despite the (*E*)-naphthylidene indene isomer (postulated to represent the s-*trans* form of Win 55212-2 **3**[189]) possessing greater affinity at the hCB_2 receptor. Our molecular modelling results, which evaluated Win 55212-2 **3** in both the naphthyl-up and naphthyl-down position provided evidence that the s-*cis* form of **3** was tolerated by the hCB_2 receptor when bound in the naphthyl-up position. Evaluation of the naphthyl-up ligand-receptor complex revealed that the crucial aromatic-aromatic interactions at Phe 117, Trp 194 and Phe 197, demonstrated in other experiments to be important[182,189,242], were all present in our model (Figure 6-6). In-fact in our model the ligand's position, relative to the position of these amino acids, was remarkably similar to that of a previous model generated by Song *et al.* in which s-*trans* Win 55212-2 **3** was bound in the hCB_2 receptor[194] (Figure 6-11, A). This is in contrast to their conclusion that the s-*cis* form of Win 55212-2 was not tolerated in the binding pocket, due to a steric clash with a valine residue in TM 3. This clash was examined in our model, by highlighting the Van Der Waals (VDW) radii of each valine residue in TM 3 and checking that there was no overlap with the VDW surface of Win 55212-2 **3** (Figure 6-11, B). It is clear that even the closest valine (Val 164) does not clash with the structure of Win 55212-2 **3** in any way. An explanation of the discrepancy between the two results may be due to their hCB_2 model being homology aligned to the non-G-protein coupled protein BacterioRhodopsin, which as discussed in section 3.1.1, has now been superseded by the use of Bovine Rhodopsin (which was used in our model) to generate a more accurate GPCR model.

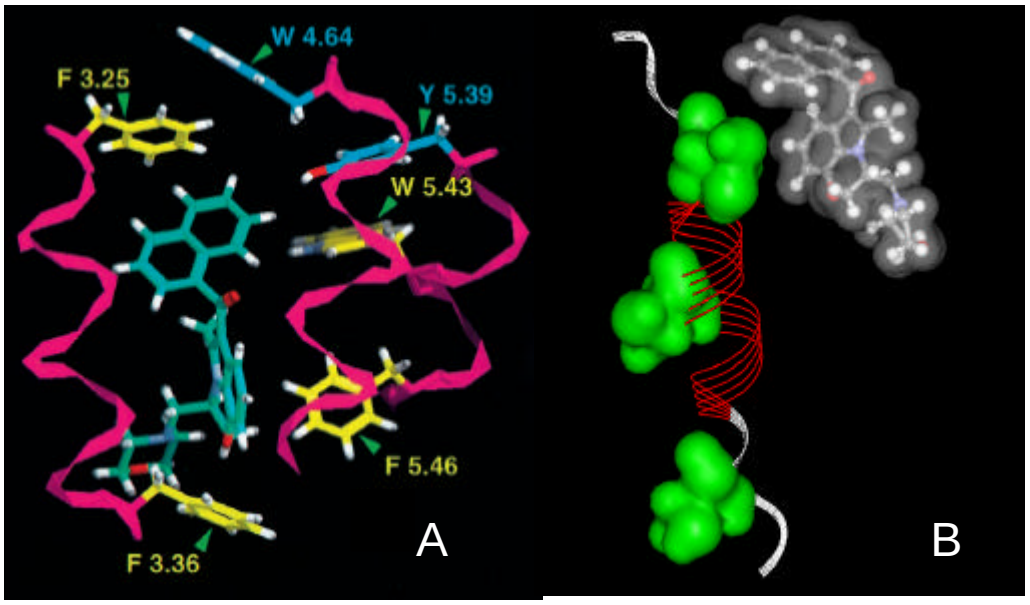

Figure 6-11 (A) The proposed position of Win 55212-2 **3** and binding amino acids (shown in yellow) from the ligand-receptor complex proposed by Song *et al.*[194]. F 3.36 = Phe 117, F 5.46 = Phe 197, W 5.43 = Trp 194. (B) The relationship between the VDW radii for each of the valine monomers (shown in green) present in TM 3 and Win 55212-2 **3** from our model of Win 55212-2 **3** bound to the hCB_2 receptor.

An interesting observation regarding the naphthyl-down complex, was that after molecular dynamic simulation, Win 55212-2 **3** was 'bounced' out of its initial interactively docked binding pocket (Figure 6-2) into a separate binding pocket which was located towards the extra cellular surface of the receptor (Figure 6-4). This resulted in a lower energy complex, shown in Figure 6-3. However, the amino acids binding the ligand have never been demonstrated in any other study to be important in cannabinoid binding. This was very similar to the observations encountered when JTE2-6 **63** was simulated binding in a phenol-down position in the CB_2 receptor discussed in chapter 2.

The model of Win 55212-2 **3** bound both in its s-*cis* conformer and naphthyl-up position was modified to create a model where our lead molecule JWH015 **53** was positioned within the hCB_2 receptor. *De novo* design using LigBuilder was able to determine that bulky substituents were tolerated at the 3-naphthyl position of JWH015 **53**. The molecule 3-NBD-JWH015 **123** (Figure 6-8), incorporating the fluorescent dye NBD at the 3-naphthyl position, was constructed *in silico* and demonstrated, by computational methods, to fit within the binding pocket of the hCB_2 receptor.

During our synthesis towards 3-NBD-JWH015 **123**, we found that only non-fluorescent species are formed when NBD is conjugated to an aromatic amine such as **123**. Literature reports of this behaviour are sparse; however we were able to find two studies in which the mechanism of this fluorescence quenching was investigated[264,265]. One study demonstrated that a photoinduced electron transfer (PET) from the donor (NBD dye) to the acceptor (aromatic amine) was responsible for the quenching observed[265]. The second study was able to determine that a linker, placed between the donor and acceptor prevented PET. The length of the alkyl linker used was inversely proportional to the level of quenching, measured as the quantum yield, observed [264]. Thus; a nonyl chain (C9) was required to totally negate the PET effect. However they also claimed that an amide group within the linker prevented PET occurring, even when the chain length was reduced to an acetyl (C2) spacer [264]. This latter observation became important after we interrogated the 3-NBD-JWH015 **123**-CB_2 receptor model to determine if a linker could be placed in the molecule. The model illustrated that the NBD structure was located in a pocket that could accommodate a short linker of up to three atoms (approximately 4.5 Å in length[246]). We therefore decided to install an amine functionalised acetyl linker to separate the 3-amino-JWH015 **129** and NBD moieties. This was achieved using the amino acid, glycine, as the linker.

The synthesis of the molecule incorporating the glycine linker, 3-Gly-NBD-JWH **132**, was achieved in a seven step convergent synthesis from commercially available 2-methylindole and 3-nitro-1,8,-naphthalic anhydride starting materials. The low yielding reactions leading to 3-amino-JWH015 **128** (19%) and 3-nitro-1-naphthoic acid (22%) were both comparable with previous literature preparations[52,261].

The reaction leading to the 3-nitro-1-naphthoic acid was reviewed due to the fact that there were two carboxylic acid groups which could potentially decarboxylate to give two different products. The mechanism postulated for this reaction (Pesci reaction), by Newman *et al.*, involved the preferential decarboxylation of the acid group in the most electron rich environment (*i.e* position 8 in 3-nitro-1, 8-naphthalic anhydride), due to the increased stability of the transition state as the aromatic-carboxyl bond is broken and the new aromatic-metal bond is formed (Figure 6-12).

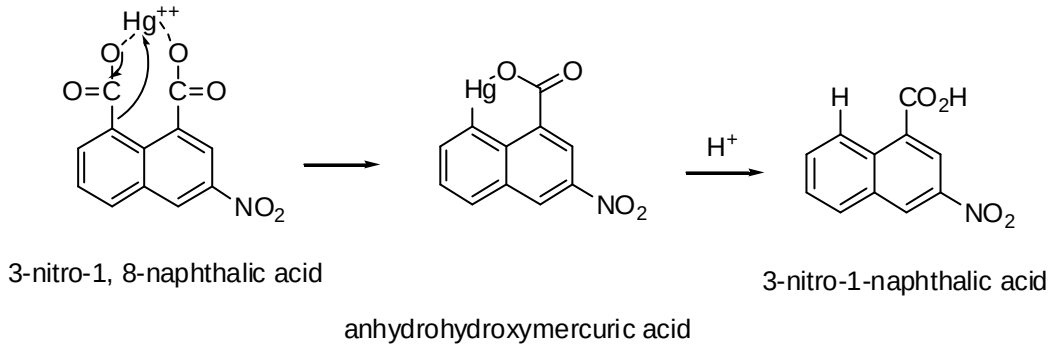

3-nitro-1, 8-naphthalic acid

anhydrohydroxymercuric acid

3-nitro-1-naphthalic acid

Figure 6-12 The Pesci reaction.

The intermediate anhydrohydroxymercuric acid formed was then treated with acid to afford the desired compound. The compound's structure was determined using the usual analytical techniques including comparative m.p. compared to literature reference values; however the most compelling evidence regarding its substitution pattern came from the two *meta* coupled doublets observed in its ^{1}H NMR spectrum, as the spectrum for 6-nitro-1-naphthoic acid would contain only one *meta* coupled doublet in its spectum. Following synthesis we were able to test the compounds' pharmacology.

The fluorescent conjuger 3-Gly-NBD-JWH **132** was found to have low affinity towards the hCB_2 receptor in a competitive radioligand binding assay (25% displacement at 10 μM). This reduction in receptor affinity compared to the original unlabelled JWH015 **53** was attributed to the addition of the bulky fluorophore and linker system causing steric and electronic clashes within the receptor. However it did still retain some affinity to the hCB_2 receptor and we evaluated its use as a fluorescent cannabinoid in a fluorescence confocal microscopy experiment. Unfortunately due to the compound's low receptor affinity, requiring high concentrations of ligand to be used, combined with the high lipophillicity of the ligand we were unable to detect membrane binding. Instead we observed a non-specific accumulation within the cytosol (Figure 6-10).

The modification to the 3-naphthyl position JWH015 **53** was assessed. Having discovered that 3-Gly-NBD-JWH **132** retained some of its affinity to the hCB_2 receptor we decided to test three of the 3-naphthyl precursors, **128**, **129**, and **131** (Scheme 6-1) to determine if the smaller substituents, nitro, amine, and *N*-glycyl, also retained affinity to the receptor. From the affinity data we obtained it was noted that the binding affinity of the nitro **128**, amino **129** and *N*-glycyl **131** decreased,

compared to JWH015 **53**, as the steric bulk of the substituent at the 3-naphthyl position increased. Thus the affinity of the smallest substituent, hydrogen **53** exhibited the highest binding, with nitro **128** and amino **129** groups showing a 3.9 and 5.3 fold loss in affinity, the addition of the larger glycine residue **131** decreased the affinity by a factor of 11.6. The glycine-NBD conjugate **132** with the largest substituent at this position demonstrated the largest reduction in binding affinity (K_i of >10 μM). Receptor efficacy studies, measuring agonist stimulated [^{35}S] GTP-γ-S binding, comparing JWH015 **53** with the two highest affinity compounds, 3-nitro-JWH015 **128** and 3-amino-JWH015 **129**, established that 3-naphthyl substitution, with nitro and amine groups retained agonist activity to similar levels shown by JWH015 **53**. This study, demonstrating the effect of substitution at the 3-naphthyl position of JWH015 **53**, has established that limited modification using small substituents is tolerated in terms of receptor affinity and efficacy. This is a notable result for two reasons. (i) to the best of our knowledge it is the first report of the effect of 3-naphthyl modification of JWH015 **53** and will contribute a useful addition to the overall SAR surrounding the indole cannabinoids. (ii) the 3-naphthyl modification was chosen using data obtained from *de novo* drug design. Although the computational modelling was speculative in the size of group that was tolerated by the hCB_2 receptor, it was still able to detect an extra binding pocket, in close proximity to the 3-naphthyl position, which can be exploited. This strengthened our belief that using molecular modelling to study the hCB_2 GPCR was justified and was carried out to the highest standards current modelling techniques would allow. Following the completion of our study, the structure of a novel CB_2 selective indole, AM1241 **58**, was published[72] (Figure 1-21). AM1241 **58** has a 3-(5-iodo-3-nitrobenzoyl)indole core structure, which adds to the evidence that the 3-aryl position of 3-arylindoles may be an important extra binding pocket within the hCB_2 receptor.

6.8 Conclusions

- A computational model, in which Win 55212-2 **3** was bound in its s-*cis* conformer, in the hCB_2 receptor, was established. Analysis of it bound in a naphthyl-up and naphthyl-down orientation demonstrated that it preferentially bound in the naphthyl-up position.
- Our model of the bound s-*cis* conformer was in direct contrast to previous work which had established that only the s-*trans* conformer of Win 55212-2 **3** was bioactive.
- *De novo* drug design established that the 3-naphthyl position of JWH015 **53** tolerated bulky substituents.
- Synthesis of 3-Gly-NBD-JWH015 **132** was successfully completed.
- The fluorescent conjuger **132** retained limited hCB_2 affinity (25% displacement at 10 μM), however the compound was unable to detect receptor membrane binding in live CHO cells expressing the hCB_2 receptor using confocal microscopy.
- Testing of the two 3-naphthyl precursors, 3-nitro-JWH015 **128** and 3-amino-JWH015 **129**, in affinity and efficacy assays, demonstrated that limited modification to the 3-naphthyl position resulted in compounds with retained activity to the hCB_2 receptor. Thus; screening by computational methods was able to successfully predict an area within the hCB_2 binding pocket that would tolerate molecular extension; however it was not able to predict correctly the size of substituent tolerated.

7 Conclusions and future work

This chapter is not intended to replace the individual conclusion sections within the previous chapters, but complements them by pulling together the main findings from each chapter. It will also set out our plans for future work we intend to perform. Overall, this chapter can be divided into three major areas of work:

- Labelling of CB_2 ligands with fluorescent dyes
- Molecular modelling of the CB_2 receptor
- SAR of the indole cannabinoids.

7.1 Labelling of CB_2 ligands with fluorescent dyes

7.1.1 Conclusions

We synthesised five novel ligands, Dansyl-JTE2-6 **99**, BODIPY-JTE2-6 **100**, Dansyl-JTE2-3 **120**, BODIPY-JTE2-3 **121** and 3-GLY-NBD-JWH015 **132**. Unfortunately, despite careful design, using established SAR complemented with in-house computational modelling none retained sufficient affinity to highlight specific hCB_2 receptor binding in fluorescent experiments. It was probable that the reduction in affinity observed was due to increased steric interactions between the ligand and receptor. This effect was exacerbated in the Japan Tobacco derivatives, due to the preferential rat selectivity associated with these ligands. Although unable to bind to the hCB_2 receptor, retesting of the BODIPY® labelled derivatives **100** and **121** in the rCB_2 receptor showed that limited affinity was retained (displacement of 44 & 48% of bound [^{3}H] CP 55, 940 at 1 μM was observed respectively). This demonstrated that the overall strategy we adopted was partially successful.

The *de novo* design used in the synthesis of 3-Gly-NBD-JWH015 **132** led to a compound which was able to displace 25% of the bound radioligand from the hCB_2 receptor when used at a concentration of 10 μM. This is to the best of our knowledge the first report of any fluorescent cannabinoid with affinity to the human CB_2 receptor and represents our lead compound for future development.

7.1.2 Future work

The demand for fluorescent ligands with affinity to GPCRs has strengthened during the three years we have been conducting this research[266]. The case for cannabis research made in chapter 1 remains unchanged. We therefore feel that the need to develop a fluorescent cannabinoid is greater then ever. We plan to use two different strategies which will lead to the generation of the first fluorescent cannabinoid.

- Development of fluorescent conjugates of JWH015 **53**, using 3-Gly-NBD-JWH015 **132** as a lead structure. We plan to exploit, the identification of the 3-naphthyl position as a site capable of modification with fluorescent dyes. Our initial work utilised a small glycine linker to anchor the NBD fluorophore, in-order to keep the dye within the binding pocket. In future work we plan to extend the length of the linker in an effort to exit the binding pocket and tether the fluorescent dye outside of the receptor. This work is envisaged to proceed using a classical SAR approach, involving the synthesis of the core scaffold 3-amino-JWH015 **129**, which may then be coupled, using established chemistry, to an array of *N*-Boc-aminoalkyl acids. Boc deprotection and conjugation with an amine reactive fluorescent dye will give access to a library of compounds for testing. This approach has led to selective fluorescent ligands at the adenosine receptor[25,200,202,207] and we hope to emulate its success for the hCB_2 receptor.
- We also wish to exploit information regarding the non-selective compound CP 55, 940 **2** that came to light during the writing of this thesis[160,161]. Discovery of a postulated binding conformation of CP 55, 940 **2** (figure 1-14), discussed in section 1.4.3, led us to believe that it possible, with minimum synthetic effort, to selectively label each of its three hydroxyl groups, with fluorescent dyes and test the resulting conjugates. Thus by exploiting the chemical differences between the phenol and alcohol (1° & 2°) groups present it will be possible to selectively mask (by protecting groups) or activate a specific hydroxyl and thus conjugate each of the hydroxyls to commercially available acid or halo functionalised fluorescent dyes, via an ester or ether linkage. An example of this is shown in Scheme 7-1 in which the 1° alcohol is selectively protected as the TBDMS silyl ether. The remaining hydroxyls can be orthogonally protected as the acetate ester. Selective cleavage of the silyl ether using the

fluoride ion exposes the 1° alcohol which can be reacted with a fluorescent dye (e.g. NBD-F). We envisage that if the orientation of the hydroxyl groups postulated in fig 1-14 is correct, then the fluorescent dye will exit the top of the binding pocket, thus avoiding steric clashes within the receptor. Obviously the high affinity exhibited by CP 55, 940 **2** towards both CB_1 and CB_2 receptors, will result in a fluorescent ligand which is non-specific to either receptor.

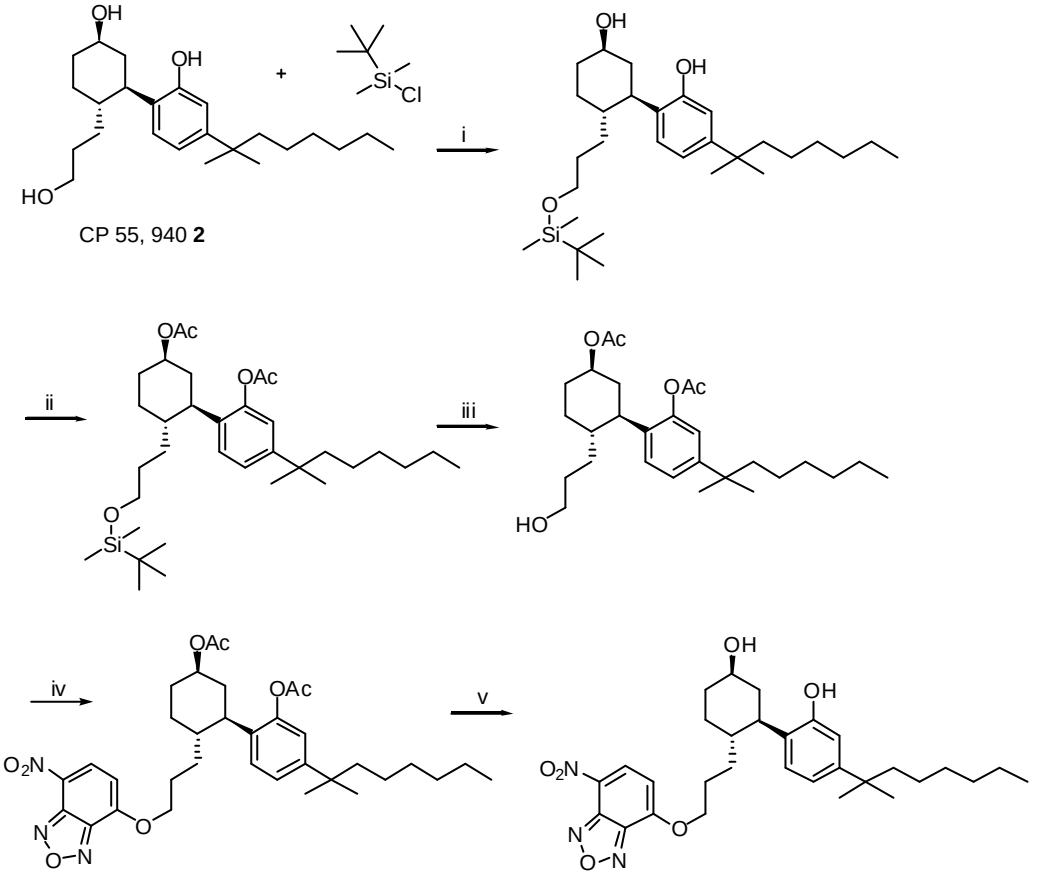

Scheme 7-1 Example of selectively labelling the 1° alcohol of CP 55, 940 **2** using NBD. Proposed reagents: (i) imidazole, DMF. (ii) Ac_2O, acidic clay (iii) TBAF, THF (iv) NBD-F (v) LiOH

7.2 Molecular modelling of the CB_2 receptor

7.2.1 Conclusions

The use of computational modelling of ligand-CB_2 receptor interactions, to aid the design of CB_2 selective ligands, led to useful information about the possible intimate ligand-receptor interactions occurring at the CB_2 receptor. Examination of our model's structure correlated extremely well with previously published CB_2 models and mutational studies in terms of the nature and residues located in the binding pocket and the TM helices involved in ligand binding. The most important residue postulated from previous studies, Phe 197, formed part of an aromatic cleft within our model's pocket and was used to interactively dock subsequent molecules under investigation.

Use of the CB_2 model to investigate ligand binding led to a number of conclusions:

- The ligand JTE2-6 **63** was shown to be capable of docking into the hCB_2 receptor in a phenol-up and phenol-down orientation. Amino acid residue analysis suggested that the likely orientation was phenol-up.
- JTE2-3 **62** exhibited large differences in affinity between the rCB_2 and hCB_2 receptor (K_i = 5.02 nM and 3.11 µM respectively). It was demonstrated using ligand-receptor modelling of both species' receptor that the difference in affinity was due to extra interactions, including a strong H-bond, that could occur within the rCB_2 and not the hCB_2 receptor. It was postulated that Glu 8 in the hCB_2 clashes with JTE-3 **62** causing the ligand to adopt a new binding conformation thus preventing it from forming a H-bond with Thr 173.
- Win 55212-2 **3** was able to bind to the hCB_2 receptor in the s-*cis* form (Figure 1-20) despite previous literature suggesting that only the s-*trans* form was capable of binding[189,194].
- The orientation of bound Win 55212-2 **3** in the hCB_2 binding pocket was determined to be with the naphthalene ring towards the top of the receptor.
- *De novo* drug design upon the CB_2 selective ligand JWH015 **53** successfully predicted a previously unrecognised cleft within the binding pocket. The cleft could be accessed by molecular extension at the 3-

naphthyl position of JWH015 **53**. However, the size of the 3-naphthyl substituent tolerated was overestimated using computational techniques; demonstrated by the decreasing affinity towards the CB_2 receptor as the size of the 3-naphthyl substituent increased.

- *De novo* drug design predicted compounds which retained similar agonist activity to the original seed structure JWH015 **53**. This may be indicative that our model represents the receptor in the activated state. This result is significant as it is generally accepted that GPCR models based on Bovine Rhodopsin represent the receptor in the inactive state.

Our results, obtained using GPCR modelling techniques, are in agreement with a recent publication in which leading GPCR experts concluded that homology models of Bovine Rhodopsin are extremely useful in understanding and exploiting GPCR ligand interactions[266]. However, the limitations of molecular modelling especially regarding the low homology and the inactive state of Bovine Rhodopsin compared to GPCRs under study are recognised in this work and are highlighted by other advocates of this technique[227,253,266].

7.2.2 Future work

We intend to develop the human and rat CB_2 receptor models generated by performing single point mutations on hCB_2 and rCB_2 receptor constructs.

- The hypothesis that Glu 8 in the hCB_2 receptor is responsible for JTE2-3 **62** adopting a less favourable binding orientation will be tested by mutating Glu 8 of the hCB_2 to the smaller amino acid Glycine and testing the affinity of JTE2-3 **62** to this Gly 8 mutant. The expected increase in JTE2-3's **62** affinity to this mutant would support the original hypothesis.
- Thr 173 in the rCB_2 receptor, which is postulated to form an important H-bond with JTE2-3 **62**, will be mutated to the isosteric amino acid Valine. Valine's structure would be unable to form a H-bond with the ligand and we anticipate that a decrease in the ligand's K_i will be observed.

The benefit in conducting mutational analysis on the rat and human CB_2 receptor will provide applied experimental data to a theoretical model. If our hypothesis for the species selectivity of JTE2-3 **62** is proven by *in-vitro* pharmacological analysis it will

provide researchers a unique understanding of the nature of binding of these unusual cannabinoids and provide confidence in the current techniques used for homology modelling of GPCRs.

7.3 SAR of the indole cannabinoids

7.3.1 Conclusions

We found using computational *de novo* modelling that the 3-naphthyl position of JWH-015 **53** tolerated substituents other than hydrogen. It was found that the nitro **128**, amino **129**, and 3-glycyl derivative **131** all retained nanomolar affinity and agonist efficacy to the CB_2 receptor. Introducing the much larger NBD heterocyclic resulted in a compound **132** with significantly reduced affinity at the CB_2 receptor. This work demonstrates that the 3-naphthyl position of JWH-015 can be modified to offer compounds with CB_2 agonist properties. This is the first report of this modification and will contribute a useful addition to the overall SAR of the indole cannabinoids.

7.3.2 Future work

We have recently seen that two licence applications for cannabis medicines, in the form of a sublingual cannabis extract (Sativex®), and the CB_1 antagonist SR141716 **5** (Rimonabant®)[§§§] have been announced. To the best of our knowledge no CB_2 selective ligand has been evaluated for use as a therapeutic agent in man. We intend to exploit our findings concerning the 3-naphthyl position of JWH-015 **53** by synthesising a number of 3-naphthyl analogues for testing in affinity and efficacy assays (*in-vitro*), at the human CB_1 and CB_2 receptors. The 3-naphthyl analogues will be accessed using established chemistry discussed in section 6.4, coupling 3-naphthoic acid derivatives with 2-methyl-1-*n*-propylindole. 3-Naphthoic acid derivatives that are not commercially available may be accessed from 3-nitro-1-naphthoic acid **127** by reduction to 3-amino-1-naphthoic acid, diazotisation and replacement with the nucleophile of choice (e.g. Sandmeyer reaction). This approach will hopefully lead to many novel 3-naphthyl derivatives of the CB_2 selective agonist JWH-015 **53** that may confer advantages as a CB_2 selective ligand in terms of selectivity, potency and solubility.

[§§§] Personal communication - European Society of Cardiology Munich 30th August 2004

8 Experimental

8.1 Chemistry

All m.p. were determined in a glass capillary using a Gallenkamp 3A 3790 melting point apparatus and were corrected using *p*-toluene sulphonamide as a standard (m.p. 137 ^{o}C). FT-infrared spectra were recorded as thin films or KBr discs in the range of 4000-600 cm^{-1} using Avatar 360 Nicolet FT-IR spectrophotometer. ^{1}H NMR were recorded on a Bruker-AMX 250 operating at 250 MHz. Chemical shifts given in δ values are relative to an internal tetramethylsilane standard. The multiplicity of a signal is designated by one of the following abbreviations. s, singlet; d, doublet; t, triplet; q, quartet; br broad; m, multiplet; dd, doublet of doublets etc. All coupling constants, (*J* values) are given in Hertz. ^{13}Carbon NMR were recorded on a Bruker AMX 250 spectrophotometer operating at 62.9 MHz. Electron spray (ES) and atmospheric pressure ionization (AP) mass spectrometry were recorded using a Micromass VG platform, and Fast atomic bombardment (FAB) mass spectrometry were recorded using and a VG Micromass 70E.

Fluorescence data was obtained using a Hitachi F-2500 FL spectrophotometer using a 1 cm quartz cell.

Microanalytical data were obtained on a Perkin-Elmer 240 D elemental analyzer.

Thin layer chromatography (TLC) was performed using Merck silica gel 60 GF_{254} analytical plates. Preparative TLC was performed using Merck silica gel 60 GF_{254} coated glass plates (1mm). Flash chromatography was performed using Merck Kieselgel 60 (0.040-0.063 mm).

HPLC was performed using a Vydac reverse phase C_8 column (150 x 4.6 mm), a flow rate of 1 mL/min and UV detection at 254 nm. Linear gradients were used in all applications. An injection volume of 50 μL, using a 1 mg/mL sample dissolved in HPLC grade MeCN, was used for all samples.

Reagents were all SLR grade or above and purchased through the normal suppliers. Anhydrous grade DMF and EtOEt were used in reactions. The Bodipy fluorophore was obtained via Molecular Probes, Cambridge Bioscience, Cambridge, UK. The 4-fluoro-7-nitrobenzofurazan (NBD-F) fluorophore was obtained via Fluka, Sigma-Aldrich Co. Ltd, The Old Brickyard, Gillingham, Dorset.

pH 8.3 $NaHCO_{3\,(aq)}$ buffer used in fluorophore coupling was made by making a 0.1 M $NaHCO_{3\,(aq)}$ solution (0.84 g $NaHCO_3$ & Q.S. 100 mL water) and titrating to pH 8.3 using 0.1 M $Na_2CO_{3\,(aq)}$ solution (1.06 g Na_2CO_3 & Q.S. 100 mL water).

Preparation of *tert*-butyl 6-hydroxyhexylcarbamate (88)

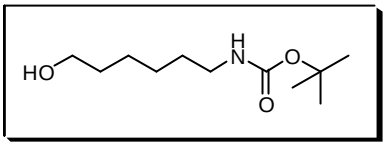

A mixture of 6-amino-1-hexanol (2.0 g, 17 mmol) and di-*tert*-butyl dicarbonate (7.5 g, 34 mmol) was stirred at 0 °C in dioxane (50 mL) and water (10 mL). The reaction was allowed to warm to rt and stirred for 2 h. The reaction was reduced under vacuum to a syrup. The residue was dissolved in ~40 mL of EtOAc, and was washed with sat. $NaHCO_3$ (2 x 20 mL), and brine (20 mL). The organics were dried ($MgSO_4$) and reduced under vacuum to yield ~7 g of yellow oil. Hexane (30 mL) was added to the oil and the solution was cooled and triturated to yield white crystals. The suspension was filtered and the solid was washed with cold hexane to yield the title compound (3.7 g, 99.5%) as a white crystalline material.

m.p. 37-39 °C. Lit [220] 39 °C

^{1}H NMR ($CDCl_3$) δ 4.61 (1H, br s, N-H carbamate**),** 3.62, (2H, q, *J* 6Hz, CH_2-α-O), 3.11 (2H, q, *J* 6Hz, CH_2-carbamate), 2.25 (1H, t, *J* 6Hz, O-H), 1.6-1.2 (17H, m, $C(CH_3)_3$ & CH_2 hexyl).

^{13}C NMR ($CDCl_3$) 156.2 (4°, C=O Boc), 79.1 (4°, C(CH_3) Boc), 62.6 (CH_2, C-α-O), 40.4 (CH_2, C-carbamate), 32.6 (CH_2), 30.1 (CH_2), 28.4 (CH_3 Boc), 26.4 (CH_2), 25.3 (CH_2).

ES-MS MH+ calcd for $C_{11}H_{24}NO_3$ 218.3 found 218.4 (MH+).

FTIR: 3403 (O-H), 3367 (N-H Boc), 2984, 2934, 2856, 1686 (C=O Boc), 1533, 1364, 1288, 1249, 1171, 1061, 998, 869 cm^{-1}

Preparation of *tert*-butyl 6-(4-(methoxycarbonyl)-2-nitrophenoxy)hexylcarbamate (90)

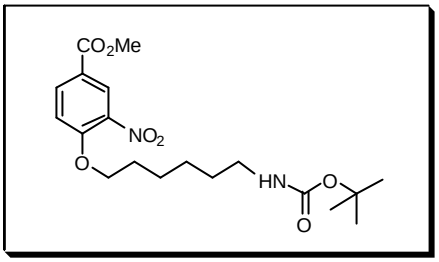

A solution of methyl 4-hydroxy-3-nitrobenzoate (2.0 g, 10 mmol), *tert*-butyl 6-hydroxyhexylcarbamate **89** (2.2 g, 10 mmol) and triphenylphosphine (2.7 g, 10 mmol) was prepared by dissolving the reactants in 60 mL of THF. The mixture was cooled to 0 °C, and a solution of diethyl azodicarboxylate (1.6 mL, 10 mmol) in 10 mL of THF was added. The reaction was allowed to warm to rt and left for 5 h. The solvent was reduced to yield orange oil. The oil was partitioned between $CHCl_3$ (50 mL) and water (50 mL). The organic layer was washed with water (50 mL), before drying ($MgSO_4$) and reduction *in vacuo*. Purification using flash chromatography (50% EtOAc: 50 % hexane) yielded the title compound as an off white solid (2.6 g, 66%).

m.p. 99-101 °C.

^{1}H NMR ($CDCl_3$) δ 8.48 (1H, d, *J* 2Hz, 3-H**),** 8.18 (1H, dd, *J* 9Hz & 2Hz, 5-H), 7.11 (1H, d, *J* 9Hz, 6-H), 4.64 (1H, bs, N-H carbamate), 4.17 (2H, t, *J* 6Hz, CH_2-α-O),

3.93 (3H, s, OMe), 3.12 (2H, q, *J* 6Hz, CH_2-carbamate), 1.90 (2H, m, CH_2 hexyl), 1.6-1.3 (15H, m, $C(CH_3)_3$ & CH_2 hexyl).

^{13}C NMR ($CDCl_3$) 165.0 (4°, C=O ester) 156.0 (4°, C=O Boc), 155.6 (4°, C-4), 139.4 (4°, C-3), 135.2 (C-H, C-6), 127.1 (C-H, C-2), 122.2 (4°, C-1), 113.9 (C-H, C-5), 79.0 (4°, C(CH_3) Boc), 69.9 (CH_2, C-α-O), 52.4 (CH_3, OMe), 40.4 (CH_2, C-carbamate), 30.0 (CH_2), 28.7 (CH_2), 28.4 (CH_3 Boc), 26.3 (CH_2), 25.5 (CH_2).

ES-MS MH+ calcd $C_{19}H_{29}N_2O_7$ 397.5 found 397.4 (MH+)

Anal calcd $C_{19}H_{28}O_7N_2$ C, 57.56, H, 7.13, N, 7.07 % Found C, 57.71, H, 7.12, N, 7.05 %

FTIR: 3290 (N-H Boc), 2972, 2936, 2856, 1719 (C=O ester), 1686 (C=O Boc), 1621, 1533, 1437, 1364, 1275, 1252, 1174, 1024, 993, 874 cm^{-1}

Preparation of 4-(6-*tert*-butoxycarbonylamino-hexyloxy)-3-nitro benzoic acid (91)

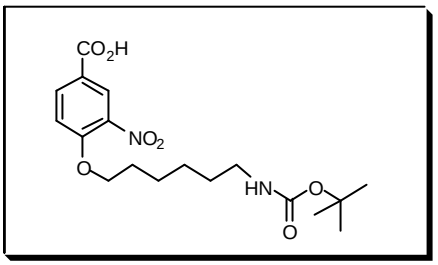

A biphasic solution of *tert*-butyl 6-(4-(methoxycarbonyl)-2-nitrophenoxy)hexyl carbamate **90** (2.0 g, 5 mmol), LiOH monohydrate (1.1 g, 25 mmol), water (20 mL), and MeCN (60 mL) was heated to 50 °C for 30 min. The solvent was removed under vacuum, and the residue was taken up into EtOAc (40 mL) and washed with 2M $KHSO_{4\,(aq)}$ (2 x 40 mL). The combined aqueous layers were re-extracted with EtOAc (40 mL). The organics were combined, brine washed (40 mL), dried ($MgSO_4$), and reduced under vacuum to yield 2.0 g (quantitative) of a pale yellow solid.

m.p. 100-110 °C.

^{1}H NMR ($CDCl_3$) δ 12.0-11.8 (1H, br s, COOH, exchanges D_2O), 8.53 (1H, d, *J* 2Hz, 2-H), 8.22 (1H, br d, *J* 9Hz, 6-H), 7.11 (1H, d, *J* 9Hz, 5-H), 6.3 (0.4H (split), br s, N-H carbamate, exchanges D_2O), 4.64 (0.6H (split), br s, N-H carbamate, increases to 1H D_2O,), 4.18 (2H, t, *J* 6Hz, CH_2-α-O), 3.14 (2H, br d, *J* 6Hz, CH_2-carbamate), 1.90 (2H, m, CH_2 hexyl), 1.6-1.3 (15H, m, $C(CH_3)_3$, & CH_2 hexyl).

^{13}C NMR ($CDCl_3$) 169.0 (4°, C=O acid) 156.5 (4°, C=O Boc), 155.6 (4°, C-4), 139.9 (4°, C-3), 136.1 (C-H, C-6), 128.1 (C-H, C-2,), 122.1 (4°, C-1), 114.3 (C-H, C-5), 79.0 (4°, C(CH$_3$) Boc), 70.3 (CH_2, C-α-O), 40.4 (CH_2, C-carbamate), 30.3 (CH_2), 29.0 (CH_2), 28.8 (CH_3 Boc), 26.7 (CH_2), 25.8 (CH_2).

Anal calcd $C_{18}H_{26}O_7N_2$ C 56.52, H 6.87, N 7.33 % Found C 56.47, H 6.81, N 7.33 %

FTIR: 3322 (COOH), 3390 (N-H Boc) 2988, 2940, 2871, 1704 (C=O acid), 1644 (C=O Boc), 1617, 1534, 1367, 1269, 1164, 842, 684 cm^{-1}.

Preparation of 3-amino-4-(6-*tert*-butoxycarbonylamino-hexyloxy)benzoic acid (92)

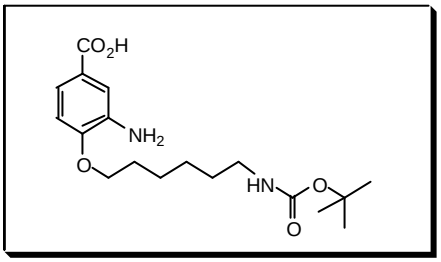

A flask of 4-(6-*tert*-butoxycarbonylamino-hexyloxy)-3-nitrobenzoic acid **91** (0.5 g, 1.3 mmol) and Pd/C (50 mg) in EtOH (& 2 drops of AcOH) was stirred at rt under a H_2 atmosphere (1 atm) for 24 h. The reaction was filtered through a celite pad, concentrated *in vacuo*, and purified by re-crystallisation from EtOAc: Hexane to yield the title compound as an off white solid (350 mg, 76%).

m.p. 104-106 °C

^{1}H NMR ($CDCl_3$) δ 7.52 (1H, dd, *J* 8.4Hz & 2Hz, 6-H), 7.43 (1H, d, *J* 2Hz, 2-H), 6.76 (1H, d, *J* 8.5Hz, 5-H), 6.37 (3H , br s, NH_2 & COOH), 4.64 (1H , br s, N-H carbamate), 4.03 (2H, t, *J* 6Hz, CH_2-α-O), 3.14 (2H, br d, *J* 6Hz, CH_2-carbamate), 1.82 (2H, m, CH_2 hexyl), 1.6-1.3 (15H, m, $C(CH_3)_3$, & CH_2 hexyl).

^{13}C NMR ($CDCl_3$) 172.0 (4°, C=O acid) 156.5 (4°, C=O Boc), 151.6 (4°, C-4), 136.4 (4°, C-6), 122.4 (4°, C-1), 122.1 (C-H, C-6), 116.4 (C-H, C-2), 110.6 (C-H, C-5), 79.0 (4°, C(CH_3) Boc), 68.7 (CH_2, C-α-O), 40.9 (CH_2, C-carbamate), 30.3 (CH_2), 29.5 (CH_2), 28.8 (CH_3 Boc), 26.9 (CH_2), 26.1 (CH_2).

FTIR: 3347 (COOH & NH_2), 2938, 2940, 2871, 1684 (C=O broad), 1617, 1521, 1310, 1227, 996, 760, 645 cm^{-1}.

Preparation of 4-(6-*tert*-butoxycarbonylamino-hexyloxy)-3-pentylaminobenzoic acid (93)

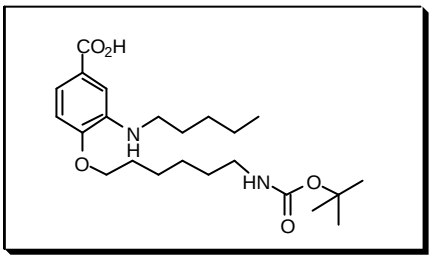

A solution of 3-amino-4-(6-*tert*-butoxycarbonylamino-hexyloxy)benzoic acid **92** (250 mg, 0.68 mmol), valeraldehyde (73 µL, 1.36 mmol), AcOH (79 µL, 1.36 mmol), sodium acetate (93 mg, 0.68 mmol), and sodium cyanoborohydride (43 mg, 0.68 mmol) was stirred in MeOH (10 mL) at rt for 4 h. The solution was evaporated to dryness and the residue was partitioned between water and EtOAc. The aqueous layer was extracted with EtOAc (3 x 40 mL) and the organics were combined, washed with brine (30 mL) and dried ($MgSO_4$). The organics were reduced *in vacuo* and the crude product was purified using flash chromatography (30% EtOAc: 70% Hexane) to give the title compound as an off white solid (68 mg, 24%).

m.p. 96-98 °C

^{1}H NMR ($CDCl_3$) δ 7.47 (1H, dd, *J* 8.4Hz & 2Hz, 6-H), 7.29 (1H, d, *J* 2Hz, 2-H), 6.73 (1H, d, *J* 8.5Hz, 5-H), 6.90 (1H , br s, N-H aniline), 4.61 (1H , br s, N-H carbamate), 4.03 (2H, t, *J* 6Hz, CH_2-α-O), 3.20-3.00 (4H, m, CH_2-carbamate & CH_2-aniline), 1.85 (2H, m, CH_2 hexyl), 1.6-1.3 (19H, m, $C(CH_3)_3$, & CH_2 hexyl), 0.97 ((3H, t, *J* 6.7 Hz, CH_3-pentyl).

^{13}C NMR ($CDCl_3$) 172.6 (4°, C=O acid) 156.5 (4°, C=O Boc), 150.8 (4°), 138.6 (4°), 122.4 (4°), 120.3 (C-H), 110.9 (C-H), 109.6 (C-H), 79.0 (4°, C(CH_3) Boc), 68.7 (CH_2, C-α-O), 44.0 (CH_2, C-carbamate), 30.3 (CH_2), 29.8 (CH_2), 29.5 (CH_2), 28.8 (CH_3 Boc), 26.9 (CH_2), 26.2 (CH_2), 22.9 (CH_2), 14.5 (CH_3).

FTIR: 3390 (COOH & NH_2), 2940, 2871, 1689 (C=O two signals), 1599, 1521, 1310, 1227, 980, 765 cm^{-1}.

Preparation of *tert*-butyl 6-(4-(4-hydroxyphenethylcarbamoyl)-2-nitrophenoxy)hexylcarbamate (94)

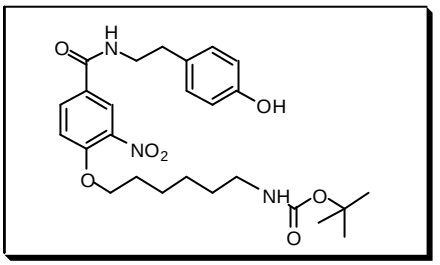

A solution of 4-(6-tert-butoxycarbonylamino-hexyloxy)-3-nitrobenzoic acid **91** (1.01 g, 2.63 mmol) and 1,1-carbonyldiimidazole (0.45 g, 2.77 mmol) was pre-mixed in MeCN (70 mL) for 2 h. Tyramine (0.38 g, 2.77 mmol), was added to the solution. Within 5 minutes the solid had dissolved, and the reaction was left stirring for 18 hours at rt. The reaction was reduced to dryness under vacuum and the residue was dissolved in EtOAc (30 mL), this was washed with water (2 x 15 mL), and 2 M $KHSO_{4\,(aq)}$ (2 x 15 mL). The combined aqueous layers were re-extracted with EtOAc (20 mL). The organics were combined, dried ($MgSO_4$) and reduced to yield 1.34 g of

an off white solid. The product was purified by flash chromatography (5% MeOH: 95% DCM) to yield the title compound as a white solid (1.04g, 79%).

m.p. 140-141 °C.

^{1}H NMR ($CDCl_3$) δ 8.18 (1H, d, *J* 2 Hz, 3-H), 7.90 (1H, dd, *J* 9 Hz & 2 Hz, 5-H), 7.03-7.00 (3H, m, phenol H & 6-H), 6.5-6.3 (2H, m, N-H amide & O-H phenol, exchanges D_2O), 4.70 (1H, br t, N-H carbamate, exchanges D_2O), 4.10 (2H, t, *J* 6 Hz, CH_2-α-O), 3.62 (2H, q, *J* 6.5 Hz, CH_2-amide, q→ t D_2O) 3.10 (2H, q, *J* 6.5 Hz, CH_2-carbamate), 2.81 (2H, t, *J* 7 Hz, CH_2-phenol), 1.80 (2H, m, CH_2-hexyl), 1.5-1.3 (15H, m, $C(CH_3)_3$, & CH_2-hexyl).

^{13}C NMR ($CDCl_3$) 165.5 (4°, C=O amide) 156.2 (4°) 155.4 (4°, C=O Boc), 154.8 (4°, C-OH), 139.2 (4°), 133.2 (C-H), 130.1 (4°), 129.9 (C-H), 126.5 (4°), 124.0 (C-H), 115.8 (C-H) 114.4 (C-H), 79.0 (4°, $\underline{C}(CH_3)_3$ Boc), 70.0 (CH_2, C-α-O), 41.9 (CH_2, C-amide) 40.4 (CH_2, C-carbamate), 34.8 (CH_2 C-phenol) 30.0 (CH_2), 28.8 (CH_2), 28.6 (CH_3, Boc), 26.4 (CH_2), 25.6 (CH_2).

ES-MS MH+ calcd for $C_{26}H_{36}O_7N_3$ 502.6 found 502.4 (MH+), and 524.3 (MNa+).

Anal calcd $C_{26}H_{35}O_7N_3.0.5\ H_2O$ C 61.16, H 7.11, N 8.23 % Found C 61.39, H 6.77, N 8.22 %

FTIR: 3423, 3320, 2937, 1685, 1654, 1637, 1559, 1391, 1321, 1171 cm^{-1}

Preparation of *tert*-butyl 6-(4-(4-hydroxyphenethylcarbamoyl)-2-aminophenoxy)hexylcarbamate (95)

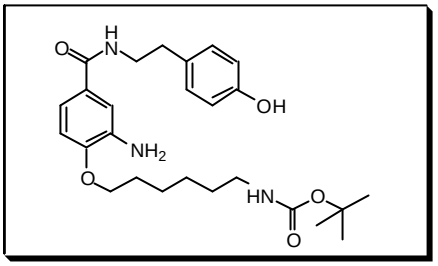

A solution of *tert*-butyl 6-(4-(4-hydroxyphenethylcarbamoyl)-2-nitrophenoxy)hexylcarbamate **94** (876 mg, 1.75 mmol) and Pd/C (175 mg) in EtOH (20 mL) was stirred at rt under a H_2 atmosphere (1 atm) for 6 h. The reaction was filtered through a celite pad, concentrated *in vacuo*, and purified using flash chromatography (70% EtOAc: 30% Hexane). The solid was recrystallised from 70% EtOAc: 30% Hexane to yield the title compound as a white solid (577 mg, 69%).

m.p. 121-122 °C

^{1}H NMR (DMSO-d_6) δ 9.14 (1H, s, O-H, exchanges MeOD), 8.14 (1H, t, *J* 5.5 Hz, N-H amide, exchanges MeOD), 7.12 (1H, d, *J* 2.1 Hz, 3-H), 7.04-6.98 (3H, m, 5-H & phenol H), 6.78 (1H, d, *J* 8.4 Hz, 6-H), 6.71-6.64 (2H, m, phenol H), 4.77 (3H, br s, N-H carbamate & aniline, exchanges MeOD), 3.97 (2H, t, *J* 6.4 Hz, CH_2-α-O), 3.33 (q, *J* 6.5 Hz, CH_2-amide), 2.91 (2H, q, *J* 6.4 Hz, CH_2-aniline, q → t MeOD), 2.67 (2H, t, *J* 6.8 Hz, CH_2-phenol), 1.75-1.62 (2H, m, CH_2 hexyl), 1.5-1.3 (15H, m, $C(CH_3)_3$, & CH_2-hexyl).

^{13}C NMR (MeOD) 170.4 (4°, C=O amide) 158.5 (4°, C=O Boc), 156.9 (4°, C-OH) 150.9 (4°), 137.9 (4°), 131.4 (4°), 130.8 (CH), 128.1 (4°), 118.9 (CH), 116.2 (CH) 114.9 (CH), 111.5 (CH) 79.8 (4°, $\underline{C}(CH_3)_3$ Boc), 69.3 (CH_2, C-α-O), 42.9 (CH_2, C-amide) 41.2 (CH_2, C-carbamate), 35.8 (CH_2, C-phenol) 30.9 (CH_2), 30.2 (CH_2), 28.8 (CH_3 Boc), 27.6 (CH_2), 26.8 (CH_2).

ES-MS MH+ calcd $C_{26}H_{38}N_3O_5$ 472.6 found 472.2 (MH+)

Anal calcd $C_{26}H_{37}O_5N_3.H_2O$ C 63.78, H 8.03, N 8.58 % Found. C 63.85, H 7.80, N 8.28 %

FTIR: 3405, 3300, 2932, 1702, 1677, 1639, 1545, 1228, 1171 cm^{-1}

Preparation of *tert*-butyl 6-(4-(4-hydroxyphenethylcarbamoyl)-2-(pentylamino)phenoxy)hexylcarbamate (96)

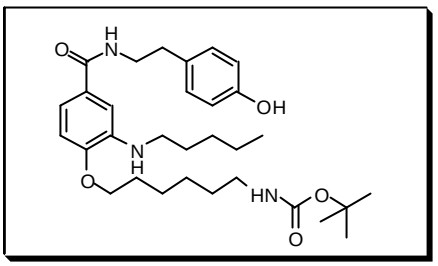

A solution of *tert*-butyl 6-(4-(4-hydroxyphenethylcarbamoyl)-2-aminophenoxy)hexylcarbamate **95** (500 mg, 1.06 mmol), valeraldehyde (113 uL, 1.06 mmol), sodium acetate trihydrate (144 mg, 1.06 mmol), acetic acid (121 uL, 2.12 mmol), and sodium cyanoborohydride (67 mg, 1.06 mmol) was stirred in MeOH (10 mL) at r.t for 18 h. The reaction was reduced *in vacuo*. The residue was dissolved in EtOAc (30 mL), washed with water (3 x 15 mL), and dried $MgSO_4$. After evaporation of solvent the resulting oil was purified using flash chromatography (60% EtOAc: 40% hexane) to yield the title compound as a white solid (411 mg, 71%).

m.p. 159-161 °C

^{1}H NMR ($CDCl_3$) δ 7.07-6.99 (3H, m, phenol Hs & 3-H), 6.89 (1H, dd, *J* 8.2 & 1.9 Hz, 5-H), 6.83 (2H, d, *J* 8.4Hz, phenol H) 6.65 (1H, d, *J* 8.3 Hz, 6-H), 6.31 (1H, br t, *J* 5.5 Hz, N-H amide, exchanges D_2O), 4.65 (1H, br s, N-H carbamate, exchanges D_2O), 3.97 (2H, t, *J* 6 Hz, CH_2-α-O), 3.63 (2H, q, *J* 6.5 Hz, CH_2-amide), 3.12 (4H, m, CH_2-carbamate & CH_2-aniline), 2.82 (2H, t, *J* 6.5 Hz, CH_2-phenol), 1.82-1.77 (2H, m, CH_2-hexyl), 1.56-1.53 (2H, m, CH_2-pentyl), 1.50-1.35 (19H, m), 0.91 (3H, t, *J* 6.7 Hz, CH_3-pentyl)

^{13}C NMR ($CDCl_3$) 168.5(4°, C=O amide) 156.3 (4°, C=O Boc), 155.5 (4°, C-OH) 148.7 (4°), 138.5 (4°), 130.0 (4°), 129.8 (C-H), 127.3 (4°), 115.7 (C-H), 115.0 (C-H) 109.4 (C-H), 108.5 (C-H) 79.4 (4°, C(CH_3), Boc), 68.2 (CH_2, C-α-O), 43.6 (CH_2, C-amide) 41.5 (CH_2, C-carbamate), 40.6 (CH_2, C-aniline) 34.9 (CH_2, C-phenol) 30.1 (CH_2), 29.4 (CH_2), 29.1 (CH_2) 28.8 (CH_3, Boc), 26.5 (CH_2), 25.8 (CH_2), 22.5 (CH_2), 14.1 (CH_3, pentyl).

ES-MS MH+ calcd for $C_{31}H_{48}N_3O_5$ 542.1 found 542.2.

FAB-MS (+ve mode) M+ calcd for $C_{31}H_{47}N_3O_5$ 541.3516 found 541.3528, MH+ calcd for $C_{31}H_{48}N_3O_5$ 542.3594 found 542.3599.

Anal calcd $C_{31}H_{47}O_5N_3$ C 68.73, H 8.74, N 7.76. Found. C 68.46, H 8.85, N 7.81

Fluorescence properties λ_{max} (excitation) 313 nM, λ_{max} (emmision) 386 nM (0.8 mg in 10 mL MeCN)

FTIR: 3338 (broad), 2931, 2852, 1686, 1585, 1514, 1365, 1261, 1170 cm^{-1}.

Preparation of *N*-(4-hydroxyphenethyl)-4-(6-aminohexyloxy)-3-(pentylamino)benzamide dihydrochloride (97)

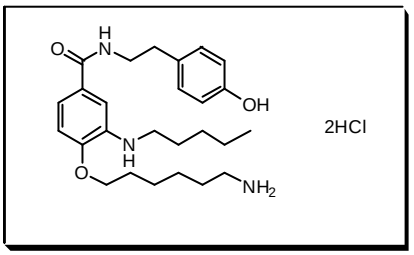

A solution of HCl in MeOH was prepared by the addition of AcCl (400 μL) to MeOH (10 mL). To this solution was added *tert*-butyl 6-(4-(4-hydroxyphenethylcarbamoyl)-2-(pentylamino)phenoxy)hexylcarbamate (145 mg, 0.268 mmol), and the reaction was stirred at rt for 18 h. The residue after evaporation was crystallised from EtOAc: EtOH to yield the title compound as a white solid (89 mg, 65%).

m.p. 150 °C

^{1}H NMR (D_2O) δ 7.53 (1H, dd, *J* 2.2 & 8.7 Hz, 6-H), 7.45 (1H, d, *J* 2.2 Hz, 2-H), 7.01 (1H, d, *J* 8.8 Hz, 5-H), 6.81 (2H, d, *J* 8.8 Hz, phenol H), 6.59 (2H, d, *J* 8.5 Hz, phenol H), 4.00 (2H, t, *J* 6.5 Hz, CH_2-α-O), 3.33 (2H, t, *J* 6.9 Hz, CH_2-amide), 3.12 (2H, m, CH_2-aniline), 2.83 (2H, t, *J* 7.6 Hz, CH_2-amine), 2.57 (2H, t, *J* 6.8 Hz, CH_2-phenol), 1.68 (2H, q, *J* 6.9 Hz, CH_2-β-O), 1.55-1.09 (12H, m), 0.68 (3H, t, *J* 7.0 Hz, CH_3-pentyl)

^{13}C NMR (D_2O) δ 168.7 (C=O amide), 154.5 (4°), 154.3 (4°) 131.4 (4°), 130.6 (C-H), 130.0 (C-H), 126.7 (4°), 124.0 (4°), 122.6 (C-H) 115.7 (C-H), 113.6 (C-H), 69.8 (CH_2, C-α-O), 51.1 (CH_2, C-aniline) 41.6 (CH_2 C-amide) 39.8 (CH_2, C-amine), 34.1 (CH_2, C-phenol), 28.3 (CH_2, C-β-O) 28.1 (CH_2), 27.1 (CH_2), 25.3 (CH_2), 25.1 (CH_2), 21.8 (CH_2), 13.4 (CH_3, pentyl).

AP-MS MH+ calcd for $C_{26}H_{40}N_3O_3$ 442.3 found 442.3 (MH+)

FAB-MS (+ve mode) MH+ calcd for $C_{26}H_{40}N_3O_3$ 442.3070 found 442.3067.

FTIR (nujol) 3342 (NH_3), 3232, 2923, 1622, 1513, 1462, 1376, 1295, 838, 721 cm^{-1}

Labeling of *N*-(4-hydroxyphenethyl)-4-(6-aminohexyloxy)-3-(pentylamino)benzamide with dansyl chloride (99)

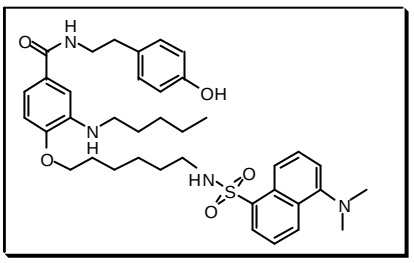

A solution of *N*-(4-hydroxyphenethyl)-4-(6-aminohexyloxy)-3-(pentylamino)benzamide dihydrochloride **97** (15.0 mg, 0.03 mmol) and dansyl chloride **84** (7.9 mg, 0.03 mmol), was stirred at rt in the dark, in MeCN (1 mL) and pH 8.3 $NaHCO_{3\,(aq)}$ buffer (1 mL) for 1 h. The reaction was reduced *in vacuo* and the residue was partitioned between water and $CHCl_3$. The aqueous phase was further extracted with $CHCl_3$ (3 x 20 mL). The organic layers were combined, dried ($MgSO_4$), and reduced. The resulting oil was purified using preparative TLC (50% Acetone: 50% pet ether 40-60) to yield the title compound as a green oil (3.8 mg, 19%).

^{1}H NMR ($CDCl_3$) δ 8.53 (1H, d, *J* 8.4 Hz, 6-H), 8.47-8.22 (2H, m), 7.56-7.48 (3H, m), 7.16 (1H, d, *J* 7.1 Hz), 7.05 (2H, d, *J* 8.5 Hz), 6.98 (1H, d, *J* 2 Hz), 6.89 (1H, dd, *J* 2 & 8.2 Hz), 6.82-6.77 (2H, m), 6.66 (1H, d, *J* 10 Hz), 6.12 (1H, br t, *J* 5.7 Hz, amide), 4.72 (1H, br t, *J* 6 Hz, amide), 3.88 (2H, t, *J* 6.5 Hz, CH_2-α-O), 3.63 (2H, q, *J* 6.6 Hz, CH_2-amide), 3.11 (2H, t, *J* 7.2 Hz, CH_2-aniline), 2.93-2.80 (8H, m, contains s for $N(C\underline{H}_3)_2$), 1.80-1.60 (4H, m), 1.55-1.09 (12H, m), 0.90 (3H, t, *J* 7.0 Hz, CH_3-pentyl)

ES-MS MH+ calcd for $C_{38}H_{51}N_4O_5S$ 675.9 found 675.4 (MH+), 338.4 (- dansyl and C6 linker).

HPLC – gradient 35% → 100% MeCN in water over 30 min. R_t 16.40 min (72% using peak area)

Labeling of *N*-(4-hydroxyphenethyl)-4-(6-aminohexyloxy)-3-(pentylamino)benzamide with BODIPY® 630/650-x, SE (100)

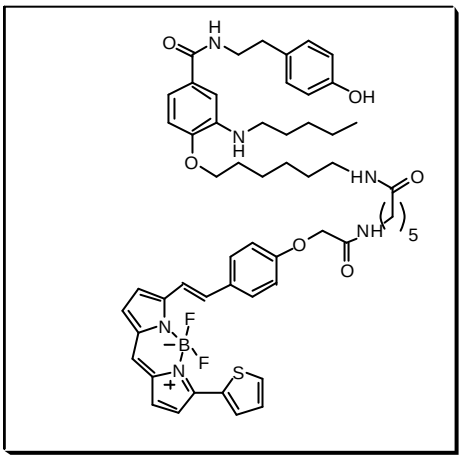

A solution of *N*-(4-hydroxyphenethyl)-4-(6-aminohexyloxy)-3-(pentylamino)benzamide dihydrochloride **97** (2.75 mg, 0.0052 mmol) and Bodipy 630/650-x, SE **86** (3.10 mg, 0.0047 mmol), was stirred at rt in the dark, in MeCN (0.5 mL) and pH 8.3 $NaHCO_{3\,(aq)}$ buffer (0.5 mL) for 1 h. The reaction was reduced *in vacuo* and the residue was partitioned between water and $CHCl_3$. The aqueous phase was further extracted with $CHCl_3$ (3 x 20 mL). The organic layers were combined, dried ($MgSO_4$), and reduced. The resulting oil was purified using preparative TLC (10% MeOH: 90% $CHCl_3$) to yield the title compound as a blue solid (2.90 mg, 63%).

^{1}H NMR ($CDCl_3$) δ 8.19 (1H, d, *J* 3.8 Hz, Bodipy), 7.63-7.52 (2H, m), 7.47 (1H, d, *J* 5 Hz Bodipy), 7.40-7.19 (2H, m), 7.09-6.81 (14H, m), 6.70 (1H, br t, *J* 5.7 Hz, amide), 6.62 (1H, d, *J* 8.2 Hz, JTE), 6.15 (1H, br t, *J* 5.7 Hz, amide), 5.66 (1H, br t, *J* 6 Hz, amide), 4.51 (2H, s, benzylic), 4.19 (1H, br s), 3.94 (2H, t, *J* 6.5 Hz, CH_2-α-O), 3.61 (2H, q, *J* 6.6 Hz, CH_2-amide (β-phenol)), 3.32 (2H, q, *J* 6.7 Hz), 3.18 (2H, q, *J* 6.5 Hz) 3.11 (2H, t, *J* 7.2 Hz, CH_2-analine), 2.09 (2H, t, *J* 6.8 Hz, Bodipy) 1.80-1.20 (23H, m), 0.90 (3H, t, *J* 7.0 Hz, CH_3-pentyl)

ES-MS MH+ calcd for $C_{55}H_{66}BF_2N_6O_6S$ 987.5 found 987.6 (MH+)

HPLC – gradient 35% → 100% MeCN in water over 30 min. R_t 16.52 min (98% using peak area)

Synthesis of succinimido 1-naphthaleneacetate (98)

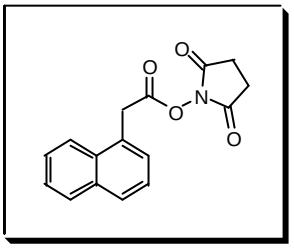

A suspension of 1-naphthylacetic acid (550 mg, 2.88 mmol), *N*-hydroxysuccinimide (330 mg, 2.88 mmol) and DCC (590 mg, 2.88 mmol) was stirred in DCM (25 mL) at rt for 16 h. EtOEt was added to the reaction and the precipitate formed was filtered. The mother liquor was reduced *in vacuo* and the residue dissolved in EtOAc. The organic layer was washed $NaHCO_{3\ (aq)}$ (2 x 20 mL) and brine (20 mL) before drying ($MgSO_4$). The residue after evaporation was purified by flash chromatography (50% EtOAc: 50% hexane) to yield the title compound as a white solid (380 mg, 47%).

m.p. 92-95 °C

^{1}H NMR ($CDCl_3$) δ 7.93 (1H, d, *J* 8.4 Hz, 2-H), 7.85 (2H, m), 7.62-7.41 (4H, m), 4.35 (2H, s, CH_2-naphthalene), 2.72 (2H, s, CH_2-succinimide)

^{13}C NMR ($CDCl_3$) δ 169.1 (C=O, imide), 166.8 (C=O, ester), 133.8 (4°), 131.7 (4°), 128.9 (C-H), 128.8 (C-H), 128.2 (C-H), 127.8 (4°), 126.8 (C-H), 126.1 (C-H), 125.4 (C-H), 123.4 (C-H), 35.4 (CH_2, C-naphthalene), 25.5 (CH_2, C-imide)

ES-MS MH+ & M- In both modes a molecular ion was not detected.

Labeling of *N*-(4-hydroxyphenethyl)-4-(6-aminohexyloxy)-3-(pentylamino)benzamide with succinimido 1-naphthaleneacetate (101)

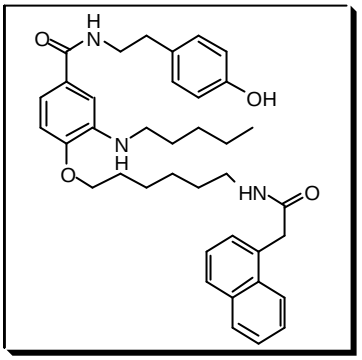

A solution of *N*-(4-hydroxyphenethyl)-4-(6-aminohexyloxy)-3-(pentylamino)benzamide dihydrochloride **97** (27.7 mg, 0.05 mmol) and succinimido 1-naphthaleneacetate **98** (13.9 mg, 0.05 mmol), was stirred at rt, in MeCN (1 mL) and pH 8.3 $NaHCO_{3\,(aq)}$ buffer (1 mL) for 12 h. The reaction was filtered under vacuum to recover the solid. The solid was re-crystallised from MeOH: water to yield the title compound as a white solid (21.8 mg, 73%).

m.p. 149 °C

^{1}H NMR (DMSO-d_6) δ 9.02 (1H, s, O-H), 8.20-8.16 (1H, m, naphthalene), 8.03 (1H, br t, *J* 5.5 Hz, amide), 7.93-7.87 (1H, m, naphthalene), 7.82 (2H, dd, *J* 2 & 7 Hz, naphthalene), 7.56-7.40 (4H, m), 7.19-7.12 (2H, m), 7.05 (2H, d, 8.4 Hz, phenol H), 6.81 (1H, d, *J* 8.2 Hz, naphthalene), 6.73 (2H, d, *J* 8.8 Hz, phenol H), 4.61 (1H, br t, *J* 5.7 Hz, amide), 4.01 (2H, t, *J* 6.5 Hz, CH_2-α-O), 3.94 (2H, s, CH_2-naphthalene), 3.45

(2H, q, *J* 6.1 Hz, CH_2-amide (β phenol), 3.22-3.05 (4H, m), 2.76 (2H, t, *J* 8.0 Hz, CH_2-phenol), 1.75-1.31 (15H, m), 0.90 (3H, t, *J* 7.0 Hz, CH_3-pentyl)

^{13}C NMR (DMSO-d_6) δ 170.8 (C=O amide), 167.9 (C=O amide), 155.8 (4°), 148.3 (4°), 142.5 (4°), 139.0 (4°), 133.9 (4°), 132.1 (4°), 129.7 (C-H), 128.8 (C-H), 128.3 (C-H), 128.2 (C-H), 127.7 (4°), 115.6 (C-H), 114.9 (C-H), 109.2 (C-H), 68.1 (CH_2, C-α-O), 43.5 (CH_2 C-naphthalene) 41.1 (CH_2) 39.3 (CH_2) 34.3 (CH_2), 29.3 (CH_2), 29.1 (CH_2) 28.9 (CH_2), 27.1 (CH_2), 26.3 (CH_2), 25.6 (CH_2), 22.5 (CH_2), 14.1 (CH_3, pentyl).

ES-MS MH+ calcd for $C_{38}H_{48}N_3O_4$ 610.4 found 610.3 (MH+), 472.9 (M-tyramine)

Anal calcd $C_{38}H_{47}O_4N_3$ C 74.85, H 7.77, N 6.89 % Found. C 74.52, H 7.67, N 6.99 %

FTIR: 3423, 3301 (OH), 2928, 2856, 1659 (C=O amide), 1633, 1538, 1512, 1454, 1266, 1241, 1217, 777 cm^{-1}

Preparation of methyl 3, 4-dihydroxybenzoate (103)

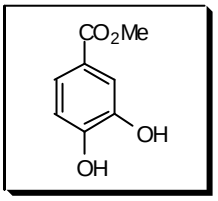

A solution of 3, 4 dihydroxybenzoic acid (2.0 g, 0.013 mol) and conc. H_2SO_4 (5 drops) in MeOH (80 mL) was refluxed for 4 hours and left to stir at room temperature for 48 hours. The solvent was reduced *in-vacuo* and the residue was neutralized by the addition of solid $NaHCO_3$. The neutralized residue was dissolved in EtOAc and washed with sat. $NaHCO_3$ and brine solutions. The organics were dried ($MgSO_4$) and evaporated to yield 2.0 g (92%) of the title compound as a white solid.

m.p. 132-133 °C Lit[267] 133 °C

^{1}H NMR (MeOD) δ 7.46 (1H, d, *J* 2.1Hz, H2), 7.44 (1H, dd, *J* 7.1 & 2.1 Hz, H6), 6.83 (1H, d, *J* 7.1Hz, H5), 3.86 (3H, s, methyl ester).

ES-MS MH+ calcd for $C_8H_9O_4$ 169.1, found *m/z* 169.2 (MH+)

FTIR: 2953, 2871, 1716 (C=O), 1599, 1514, 1436, 1391, 1269, 1132, 1007, 764, 645 cm^{-1}

Preparation of methyl 3,4-bis(pentyloxy)benzoate (104)

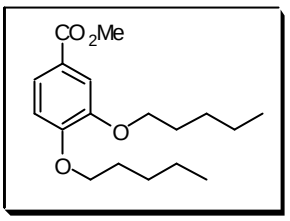

A suspension of methyl 3, 4-dihydroxybenzoate **103** (1.5 g, 8.9 mmol), K_2CO_3 (3.1 g, 22 mmol) and 1-bromopentane (3.9 mL, 31 mmol) were heated at 90 °C in DMF (40 mL) for 1 h. The reaction was filtered and the DMF reduced *in-vacuo*. The residue was dissolved in EtOAc, refiltered and washed with 2M NaOH (3 x 20 mL) and brine (2 x 20 mL). The organics were dried ($MgSO_4$) and evaporated. The title compound was purified from the crude product using flash chromatography (15% EtOAc: 85% hexane) to afford 2.1 g (76%) of colourless oil.

^{1}H NMR ($CDCl_3$) δ 7.63 (1H, dd, *J* 8.5 & 2Hz, 6-H), 7.54 (1H, d, *J* 2 Hz, 2-H), 6.86 (1H, d, *J* 8.5Hz, 5-H), 4.04 (4H, t, *J* 6.6Hz, CH_2-α-O) 3.88 (3H, s, methyl ester), 1.83 (4H, quintet (5), *J* 7Hz, CH_2-β-O), 1.53-1.25 (8H, m), 0.93 (6H, t, *J* 7Hz, CH_3).

^{13}C NMR ($CDCl_3$) δ 167.0 (C=O), 153.2 (4°, C-O aromatic), 148.5 (4°, C-O aromatic), 123.6 (C-H, C-6), 122.4 (4°, C-ester), 114.3 (C-H, C-2), 111.9 (C-H, C-5), 69.3 (CH_2, C-O), 69.0 (CH_2, C-O), 51.9 (CH_3, methyl ester), 28.9 (CH_2), 28.8 (CH_2), 28.2 (CH_2), 22.5 (CH_2), 14.0 (CH_3).

ES-MS MH+ calcd for $C_{18}H_{29}O_4$ 309.1,found *m/z* 309.1 (MH+).

FTIR (thin film): 2953, 2929, 2857, 1686 (C=O ester), 1601,1523, 1434, 1307, 1226, 1135, 761, 643 cm^{-1}

Preparation of 3,4-bis(pentyloxy)benzoic acid (105)

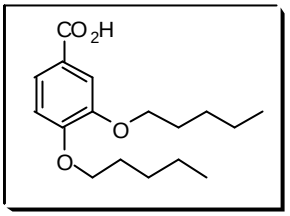

Methyl 3,4-bis(pentyloxy)benzoate **104** (1.82 g, 5.9 mmol) and $LiOH.H_2O$ (2.48 g, 5.9 mmol) were refluxed for 1 h in 50 mL of 60% MeCN: 40% water. Acidification of the reaction (conc. $HCl_{(aq)}$) yielded a white precipitate. The solid was filtered from the reaction and washed with cold water (50 mL) to yield the title compound (1.56 g, 90%).

m.p. 135-137 °C Lit [268]142 °C

^{1}H NMR ($CDCl_3$) δ 7.73 (1H, dd, *J* 8.5 + 2 Hz, 6-H), 7.59 (1H, d, *J* 2 Hz, 2-H), 6.89 (1H, d, *J* 8.5 Hz, 5-H), 4.07 (2H, t, *J* 6.6 Hz, O-CH_2 (*o*), 4.06 (2H, t, *J* 6.6 Hz, O-CH_2 (*p*), 1.85 (4H, m, CH_2 β to ether), 1.43 (8H, m), 0.94 (6H, t, *J* 7 Hz, CH_3).

^{13}C NMR ($CDCl_3$) δ 172.1 (4°, C=O), 154.0 (4°, C-O aromatic), 148.5 (4°, C-O aromatic), 124.5 (C-H), 121.4 (4°, C-1), 114.5 (C-H), 111.8 (C-H), 69.3 (CH_2, C-O), 69.0 (CH_2, C-O), 28.8 (CH_2), 28.7 (CH_2), 28.2 (CH_2), 22.4 (CH_2), 14.0 (CH_3).

ES-MS MH+ calcd for $C_{17}H_{27}O_4$ 295.2, found *m/z* 295.1 (MH+)

FTIR: 3459 (COOH), 3251, 2969, 1688, 1612, 1533, 1443, 1243, 1184, 1099, 984, 764, 623, 591 cm^{-1}

Preparation of *N*-benzyloxycarbonyltyramine (107)

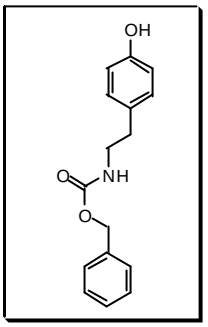

A solution of tyramine (12.0 g 0.0875 mol) and DIPEA (15.2 mL, 0.0875 mol) in 70 mL of 70% MeCN: 30% DMF was cooled to 0 °C. Benzyl chloroformate (10.8 mL, 0.0963 mol) was added dropwise, to the tyramine solution, over 30 min. The reaction was allowed to warm to rt and stirred at this temperature for 24 h. The resulting suspension was filtered. The filtrate was concentrated *in-vacuo* to yield brown oil. The residue was dissolved in EtOAc (100 mL) and washed with 2M $HCl_{(aq)}$ (2 x 50 mL) and brine (1 x 50 mL). The organics were dried ($MgSO_4$), and reduced *in-vacuo* to yield 18 g of white solid. The solid was re-crystallized from water: EtOH to yield the title compound as colourless needle crystals (13 g, 57%).

m.p. 100-102 °C Lit[269] 100 °C

^{1}H NMR ($CDCl_3$) δ 7.42-7.33 (5H, m, Cbz phenyl), 6.99 (2H, d, *J* 8.3 Hz, 2-H & 6-H), 6.75 (2H, d, *J* 8.3 Hz, 3-H + 5-H), 6.37 (1H, s, OH), 5.09 (2H, s, benzylic), 4.87 (1H, br t, N-H carbamate), 3.40 (2H, q, *J* 6.5 Hz, CH_2-N), 2.71 (2H, t, *J* 7 Hz, CH_2-Ph).

^{13}C NMR ($CDCl_3$) δ 157.0 (4°, C-O, C1), 155.1 (4°, C=O), 136.7 (4°, ipso aromatic), 130.2 (4°, C4), 130.2 (CH, x 2 phenol ring), 128.6 (CH, Cbz phenyl), 128.5 (CH, Cbz phenyl), 115.9 (CH, x 2 phenol ring), 67.2 (CH_2, benzylic), 42.9 (CH_2 α Cbz), 35.5 (CH_2 β Cbz).

ES-MS MH+ calcd for $C_{16}H_{18}N_1O_3$ 272.1, found *m/z* 272.0 (MH+) 194.1 (M – phenyl)

FTIR: (KBr) 3331 (O-H, N-H), 1686 (C=O), 1612, 1544, 1514, 1268, 1244, 1139, 824, 746, 695, 528 cm^{-1}.

Synthesis of *O*-allyl-*N*-benzyloxycarbonyltyramine (108)

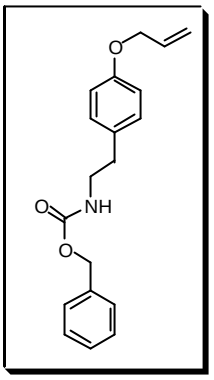

A suspension of *N*-benzyloxycarbonyl tyramine **107** (9.95 g, 0.0367 mol), allyl bromide (4.2 mL, 0.0458 mol), and potassium carbonate (6.33 g, 0.0458 mol) in methyl ethyl ketone (150 mL) was refluxed for 18 h. The resulting fine slurry was filtered and reduced *in-vacuo*. The residue was dissolved in EtOAc (100 mL) and washed with 2M $HCl_{(aq)}$ (2 x 30 mL) and brine (30 mL). The organic layer was dried ($MgSO_4$) and reduced *in-vacuo* to yield the title compound as a white solid (10.9g, 96%).

m.p. 94-95 °C

^{1}H NMR ($CDCl_3$) δ 7.40-7.30 (5H, m, Cbz phenyl), 7.07 (2H, d, *J* 9 Hz, 2-H & 6-H), 6.84 (2H, d, *J* 8. Hz, 3-H & 5-H), 6.05 (1H, ddt, *J* 17.3, 11.9, 5.3 Hz, C-CH=C), 5.45 (1H, ddt, *J* 17.3, 3.0, 1.5 Hz, C=CH *trans*), 5.28 (1H, ddt, *J* 11.7, 3.0, 1.5 Hz, C=CH *cis*), 5.09 (2H, s, benzylic), 4.75 (1H, br t, N-H carbamate), 4.50 (2H, m, O-CH_2-C=C), 3.42 (2H, q, *J* 6.5 Hz, CH_2-Cbz), 2.74 (2H, t, *J* 7 Hz, CH_2-Ph).

^{13}C NMR ($CDCl_3$) δ 157.3 (4°, C-O, C1), 156.3 (4°, C=O), 136.6 (4°, ipso aromatic), 133.4 (CH, CH=), 130.8 (4°, C4), 129.7 (CH, x 2 phenol ring), 128.5 (CH, Cbz phenyl), 128.0 (CH, Cbz phenyl), 117.6 (CH_2, $=CH_2$), 114.9 (CH, x 2 phenol ring), 68.8 (CH_2, O-C-allyl) 66.6 (CH_2, benzylic), 42.9 (CH_2 α Cbz), 35.5 (CH_2 β Cbz).

ES-MS MH+ calcd for $C_{19}H_{22}N_1O_3$ 312.41, found *m/z* 312.1 (MH+), 334.1 (MNa+)

Anal calcd $C_{19}H_{21}N_1O_3.0.25H_2O$ C 72.24, H 6.86, N 4.43 % Found. C 72.39, H 6.58, N 4.40 %

FTIR: (KBr) 3323 (N-H), 3061, 3029, 2944 (CH=CH), 1683 (C=O), 1612, 1542, 1513, 1291, 1244, 1140, 829, 748, 695 cm^{-1}.

Synthesis of 2-allyl-*N*-benzyloxycarbonyltyramine (109)

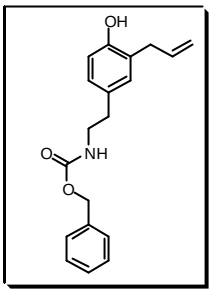

O-Allyl *N*-benzyloxycarbonyltyramine **108** (6.44g, 0.0207 mol) and diphenyl ether (20 mL) was heated at reflux, under a N_2 atmosphere, for 1 h. The diphenylether was removed using high vacuum distillation. Purification by flash chromatography using 30% EtOAc: 70% hexane yielded the title compound as a pale oil, which partially crystallized upon standing at 5 °C (3.63g, 56%).

^{1}H NMR ($CDCl_3$) δ 7.40-7.30 (5H, m, Cbz phenyl), 6.87-6.82 (2H, m, 3-H & 5-H), 6.70 (1H, d, *J* 8. Hz, 6-H), 6.69 (1H, br s, OH, exchanges) 5.96 (1H, ddt, *J* 16.8 & 10.3 & 6.5 Hz, C-CH=C), 5.14-5.04 (4H, m, benzylic & C=CH_2), 4.95 (1H, br t, D_2O exchange, N-H carbamate), 3.42-3.25 (4H, m, Ph-CH_2-C=C & CH_2-N), 2.66 (2H, t, *J* 7 Hz, CH_2-Ph).

^{13}C NMR ($CDCl_3$) δ 156.7 (4°, C=O), 152.9 (4°, C-O, C-1), 139.7 (CH, CH=), 136.3 (4°, ipso aromatic), 130.5 (CH, C-3), 130.2 (4°, C-4), 128.5 (CH, Cbz phenyl), 128.1 (CH, Cbz phenyl), 127.6 (CH, Cbz phenyl), 127.5 (CH Cbz phenyl), 127.0 (CH, C-5), 126.1 (4°, C-2), 116.0 (CH_2, =CH_2), 115.6 (CH, C-6), 66.8 (CH_2, benzylic), 42.5 (CH_2 α Cbz), 35.1 (CH_2 β Cbz) 34.6 (CH_2, Ph-C-allyl).

ES-MS MH+ calcd for $C_{19}H_{22}N_1O_3$ 312.41, found *m/z* 312.1 (MH+), 251.0

Anal calcd $C_{19}H_{21}N_1O_3$ C 73.29, H 6.80, N 4.50 % Found. C 73.09, H 6.71, N 4.52 %

FTIR: (thin film) 3341 (O-H, N-H), 3065, 3032, 2939 (CH=CH), 1693 (C=O), 1610, 1510, 1133, 819, 737, 697 cm^{-1}.

Synthesis of 2-allyl-*O*-benzyl-*N*-benzyloxycarbonyltyramine (110)

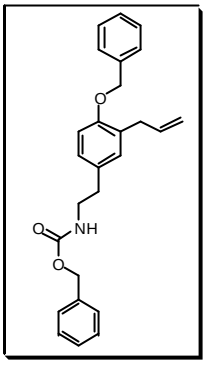

2-Allyl-*N*-benzyloxycarbonyltyramine **109** (1.83g, 5.9 mmol), benzyl bromide (0.97 mL, 7.3 mmol), and K_2CO_3 (1.01g, 7.3 mmol) were refluxed in methyl ethyl ketone (50 mL) for 12 h. The reaction was filtered and reduced *in-vacuo*. The residue was taken up into EtOAc (50 mL) and washed with 2M NaOH (2 x 30 mL) and brine (30 mL). The organics were dried ($MgSO_4$) and reduced to leave a residue, which upon trituration with cold hexane yielded the title compound as a white solid after filtration (1.88g, 80%).

m.p. 66-67 °C

^{1}H NMR ($CDCl_3$) δ 7.44-7.30 (10H, m, Cbz phenyl & Bn phenyl), 6.98-6.92 (2H, m, 3-H & 5-H), 6.83 (1H, d, *J* 6.2 Hz, 6-H), 5.98 (1H, ddt, *J* 18.8 & 10.1 & 6.7 Hz, C-CH=C), 5.14-5.04 (6H, m, benzylic & C=CH_2), 4.76 (1H, br t, N-H carbamate, exchanges D_2O), 3.45-3.37 (4H, m, Ph-CH_2-C=C & CH_2-N), 2.77 (2H, t, *J* 6.9 Hz, CH_2-Ph).

^{13}C NMR ($CDCl_3$) δ 156.3 (4°, C=O), 155.1 (4°, C-O, C-1), 137.4 (CH, CH=), 136.8 (4°, ipso aromatic), 136.6 (4°, ipso aromatic) 130.8 (4°, C-4), 130.3 (CH, C-3), 129.2 (4°, C-2), 128.5 (CH, Cbz phenyl), 128.1 (CH, Cbz phenyl), 127.7 (CH, Cbz phenyl), 127.4 (CH Cbz phenyl), 127.1 (CH, C-5), 115.6 (CH_2, =CH_2), 111.9 (CH, C-6), 70.0

(CH_2, benzylic Bn) 66.6 (CH_2, benzylic Cbz), 42.4 (CH_2 α Cbz), 35.2 (CH_2 β Cbz) 34.5 (CH_2, Ph-C-allyl).

AP-MS MH+ calcd for $C_{26}H_{28}NO_3$ 402.20, found *m/z* 402.3 (MH+) 358.3 (M – allyl)

Anal calcd $C_{26}H_{27}NO_3$ C 77.78, H 6.78, N 3.49 % Found. C 77.87, H 6.74, N 3.44 %

FTIR: (KBr) 3325 (N-H), 3066, 3033, 2950 (CH=CH), 2896, 2861, 1691 (C=O), 1607, 1541, 1257, 1140, 914, 812, 734, 696 cm^{-1}.

Synthesis of 2-(2-oxoethyl)-*O*-benzyl-*N*-benzyloxycarbonyltyramine (111)

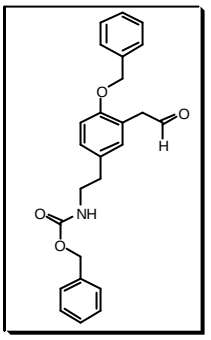

A solution of 2-allyl-*O*-benzyl-*N*-benzyloxycarbonyltyramine **110** (500 mg, 1.25 mmol), *N*-methylmorpholine oxide (292 mg, 2.49 mmol), and 0.1M aqueous solution of osmium tetroxide (1 mL, 0.01 mmol) was stirred at rt in 10 mL of 80% acetone: 20% water for 2 h. The reaction was quenched by adding saturated aqueous sodium sulphite (10 mL). The aqueous reaction was extracted with EtOAc (2 x 30 mL), the combined organics were washed with brine (20 mL) and dried ($MgSO_4$). The organics were reduced *in vacuo* to afford the diol product, which was used without further purification or characterization. The diol was dissolved in 10 mL of 50% water: 50% THF and cooled to 0 °C. Solid $NaIO_4$ (400 mg) was added to the solution and the reaction was allowed to warm to rt. The reaction was diluted with water (30 mL) and the reaction was extracted with ether (2 x 20 mL). The organics were combined, brine washed (20 mL) and dried ($MgSO_4$). Evaporation of the ether yielded the title product as yellow oil (395mg, 79%).

^{1}H NMR ($CDCl_3$) δ 9.70(1H, t, *J* 2Hz, aldehyde), 7.40-7.30 (10H, m, Cbz phenyl & Bn phenyl), 7.06 (1H, d, *J* 8 Hz 5-H), 6.97 (1H, s, 3-H), 6.87 (1H, d, *J* 8 Hz, 6-H),

5.09 (2H, s, benzylic) 5.04 (2H, s, benzylic), 4.94 (1H, br t, N-H carbamate, exchanges D_2O), 3.65 (2H, d, *J* 2Hz, CH_2-CHO), 3.40 (2H, q, *J* 6.6Hz, CH_2-N), 2.70 (2H, t, *J* 6.9 Hz, CH_2-Ph).

^{13}C NMR ($CDCl_3$) δ 199.9 (CH, CHO), 156.3 (4°, C=O), 155.4 (4°, C-O, C-1), 136.8 (4°, ipso aromatic), 136.6 (4°, ipso aromatic), 131.8 (C-H), 131.3 (4°, C-4), 129.0 (CH, Cbz phenyl), 128.6 (CH, Cbz phenyl), 128.5 (CH, Cbz phenyl), 128.1 (CH, Cbz phenyl), 128.0 (CH, Cbz phenyl), 127.1 (CH, Cbz phenyl), 121.7 (4°, C-3), 111.9 (CH, C-6), 70.0 (CH_2, benzylic Bn) 66.6 (CH_2, benzylic Cbz), 45.5 (CH_2, CH_2-CHO), 42.4 (CH_2 α Cbz), 35.2 (CH_2 β Cbz).

AP-MS MH+ calcd for $C_{25}H_{26}NO_4$ 404.5, found *m/z* 404.2 (MH+) 360.1 (M – CH_2CHO)

Synthesis of 2-(2-*tert*-butoxycarbonylaminoethyl)-*O*-benzyl-*N*-benzyloxycarbonyltyramine (116)

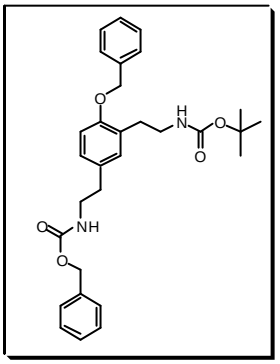

Ozone gas was sparged into a solution of 2-allyl-*O*-benzyl-*N*-benzyloxycarbonyltyramine **110** (1.0 g, 2.5 mmol) in 30 mL of 30% DCM: 70% MeOH, cooled to -78°C, until TLC showed the starting material had been consumed. Sodium borohydride (0.14 g, 3.7 mmol) was added portion wise, over 5 mins, to the ozonide solution and the reaction was allowed to warm to room temperature and stirred for 12 hours. The solvent was reduced *in-vacuo* and the crude oil was purified using flash chromatography (60% EtOAc : 40% hexane) to yield 0.9g of a colourless oil **112**. The oil was used without further characterization or purification in the next step. The oil (850mg) and triethylamine (0.32 mL, 2.3 mol) was cooled to 0 °C in DCM (20 mL). Mesyl chloride (0.18 mL, 2.3 mol) was added and the reaction was stirred at 0°C for 2 h. The reaction was washed with 2M $HCl_{(aq)}$ (2 x 10 mL) and sat. $NaHCO_{3\,(aq)}$ (1 x 10 mL), then dried ($MgSO_4$) and evaporated to yield 0.81 g of solid **113** which was used

in the next reaction without further purification or characterization. The solid **113** (0.76 g, 1.6 mmol) and NaN_3 (0.15 g, 2.4 mmol) was heated to 60 °C in DMF (15 mL) for 5 h. The reaction was quenched with iced water and extracted with chloroform (3 x 30 mL) The organics were dried and reduced to yield 0.48 g of the azide **114** as a solid, which was used in the subsequent reaction without further purification or characterization. The azide **114** and triphenylphosphine (0.32g, 1.2 mol) was dissolved in THF (10 mL), and stirred at room temperature for 24 h. Hydrolysis was afforded by the addition of 0.5 mL of water and a further period of stirring at rt for 48 h. The reaction was reduced *in-vacuo* to yield a yellow oil, which was dissolved in saturated MeOH: $HCl_{(g)}$. The solvent was reduced *in-vacuo* and the oily residue was triturated in ether to yield a 370mg of the amine **115** as a white gummy material. The amine **115** was Boc protected by dissolving the gum in dioxane (15 mL) and 1M NaOH (4 mL). The reaction was cooled to 0 °C and di-*tert*-butyl dicarbonate (201mg, 0.922 mmol) was added and the reaction was stirred for 1 h. The reaction was reduced *in-vacuo* and partitioned between water (20 mL) and EtOAc (20 mL). The aqueous layer was extracted with EtOAc (2 x 20 mL), the organics were combined, dried ($MgSO_4$) and evaporated. The solid was purified by flash chromatography (40% EtOAc: 60% hexane) to yield the title compound as a white solid (350mg, 34% from 2-allyl-*O*-benzyl-*N*-benzyloxycarbonyltyramine **110**).

m.p. 104-105 °C

^{1}H NMR ($CDCl_3$) δ 7.43-7.22 (10H, m, Cbz phenyl & Bn phenyl), 6.97-6.78 (2H, m, 3-H & 5-H), 6.80 (1H, d, *J* 8.7 Hz, 6-H), 5.07-5.01 (5H, m, 2 x benzylic & N-H carbamate), 4.77 (1H, br t, N-H carbamate), 3.42-3.33 (4H, m, 2 x CH_2-N), 2.80 (2H, t, *J* 6.4 Hz, CH_2-Ph) 2.70 (2H, t, *J* 6.8 Hz, CH_2-Ph), 1.39 (9H, s, $C(CH_3)_3$).

^{13}C NMR ($CDCl_3$) δ 156.4 (4°, C=O), 155.9 (4°, C-O, C1), 155.4 (4°, C=O), 137.1 (4°, ipso aromatic), 136.6 (4°, C-4), 131.2 (CH, C-3), 131.0 (4°, C-2), 128.6 (CH, Cbz/Bn phenyl), 128.5 (CH, Cbz/Bn phenyl), 128.1 (CH, Cbz/Bn phenyl), 128.0 (CH, Cbz/Bn phenyl) 127.9 (CH, Cbz/Bn phenyl), 127.6 (CH Cbz/Bn phenyl), 127.2 (CH,

C-5), 111.8 (CH, C-6), 78.9 (4°, $C(CH_3)_3$), 70.0 (CH_2, benzylic Bn), 66.5 (CH_2, benzylic Cbz), 42.3 (CH_2 α Cbz), 40.8 (CH_2 α Boc) 35.1 (CH_2 β Cbz), 30.6 (CH_2 β Boc), 28.4 (CH_3, Boc).

ES-MS MH+ calcd for $C_{30}H_{37}N_2O_5$ 505.26, found *m/z* 527.24 (MNa+), 505.35 (MH+), 405.17 (M – Boc).

Anal calcd $C_{30}H_{36}N_2O_5$. 0.5 H_2O C 70.15, H 7.26, N 5.45. Found. C 70.09, H 7.10, N 5.45

FTIR: (KBr) 3360 (N-H), 3065, 3032, 2979, 2934, 1693 (C=O), 1687 (C=O), 1531, 1453, 1274, 1255, 1223, 1130, 809, 733, 697 cm^{-1}.

Synthesis of *N*-(3-(2-*tert*-butoxycarbonylaminoethyl)-4-hydroxyphenethyl)-3, 4-bis(pentyloxy)benzamide (118)

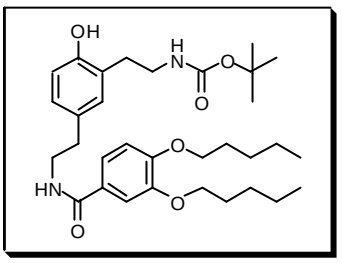

2-(2-*tert*-Butoxycarbonylaminoethyl)-*O*-benzyl-*N*-benzyloxycarbonyltyramine **116** (300 mg, 0.595 mmol) and Pd/C (40 mg) was stirred in 70 % EtOH: 30% EtOAc (15 mL) under a H_2 atmosphere (1 atm), at rt, for 24 h. The reaction was filtered through a Celite pad and concentrated *in-vacuo* to yield 80 mg (52%) of amine **117** as a hydroscopic tacky solid. ^1H NMR showed the characteristic Cbz and Bn signals at δ 7.43-7.22 to be absent. A solution of 3, 4-dipentoxybenzoic acid **105** (80 mg, 0.27 mmol) and 1,1 carbonyldiimidazole (46 mg, 0.29 mmol) was prepared in MeCN (7 mL). The solid **117** from the hydrogenolysis reaction was added, without further purification or characterization, to this activated acid solution and the reaction was stirred at rt for 48 h. The solvent was reduced and the reaction taken up into EtOAc (20 mL), the organic was washed with water (1 x 10 mL), 2M $KHSO_{4\,(aq)}$ (2 x 20 mL), and sat. $NaHCO_{3\,(aq)}$ (2 x 20 mL). The organics were dried ($MgSO_4$), and evaporated

to leave oil that was purified using preparative TLC (45% EtOAc: 55% hexane) to yield the title compound (66 mg, 20% overall yield from 2-(2-*tert*-butoxycarbonylaminoethyl)-*N*-benzyloxycarbonyltyramine) as a colourless oil. A small portion was crystallised from EtOAc: Hexane to yield an analytically pure white solid.

m.p. 141-142 °C

^{1}H NMR ($CDCl_3$) δ 7.39 (1H, d, *J* 1.9 Hz, 2-H), 7.21 (1H, dd, *J* 8.3 & 1.9 Hz 6-H), 6.93-6.80 (2H, m, aromatic), 6.43 (1H, br t, N-H amide), 5.09 (1H, br t, N-H carbamate), 4.00 (2H, t, *J* 6.6 Hz, O-CH_2 (*o*)), 3.99 (2H, t, *J* 6.6 Hz, O-CH_2 (*p*)), 3.60 (2H, q, *J* 6.2 Hz, CH_2-amide), 3.27 (2H, q, *J* 6.2 Hz, CH_2-carbamate), 2.78 (4H, t, *J* 6.4 Hz, 2 x CH_2-Ph), 1.80 (4H, m, CH_2 β to ether), 1.48-1.37 (17H, m, Boc & alkyl chain) 0.93 (6H, m, CH_3).

^{13}C NMR ($CDCl_3$) δ 167.4 (4°, C=O amide) 156.9 (4°, C=O Boc), 153.8 (4°, C-O aromatic), 151.9 (4°, C-O aromatic), 148.9 (4°, C-O aromatic), 130.9 (CH, C-3 tyramine), 130.1 (4°, C-4 tyramine), 128.1 (CH, C-5 tyramine), 126.9 (4°), 125.2 (4°), 119.5 (CH, benzamide), 116.1 (CH, benzamide), 112.7 (CH, benzamide), 112.3 (CH, C-6 tyramine), 79.8 (4°, $C(CH_3)_3$), 69.3 (CH_2, C-O), 69.2 (CH_2, C-O), 41.5 (CH_2 α amide), 41.1 (CH_2-α-carbamate) 34.9 (CH_2 β amide), 31.1 (CH_2-β-carbamate), 28.9 (CH_2), 28.8 (CH_3, Boc), 28.4 (CH_2), 28.2 (CH_2), 22.4 (CH_2), 14.0 (CH_3).

ES-MS MH+ calcd for $C_{32}H_{49}N_2O_6$ 557.4, found *m/z* 579.4 (MNa+), 557.4 (MH+), 457.2 (M – Boc).

Anal calcd $C_{32}H_{48}N_2O_6$ C 69.04, H 8.69, N 5.03. Found. C 68.77, H 8.67, N 5.05

FTIR: (KBr) 3386 (O-H), 3243 (N-H), 2956, 2918, 1688 (C=O), 1633 (C=O), 1509, 1262, 1224, 1134, 1047, 819 cm^{-1}.

Synthesis of *N*-(3-(2-aminoethyl)-4-hydroxyphenethyl)-3,4-bis(pentyloxy)benzamide hydrochloride (119)

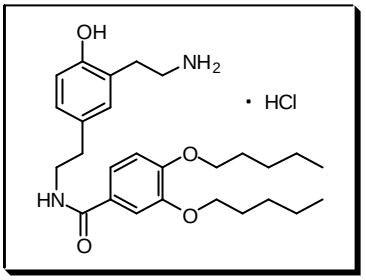

A solution of HCl in MeOH was prepared by the addition of AcCl (400 μL) to MeOH (5 mL). To this solution was added *N*-(3-(2-*tert*-butoxycarbonylaminoethyl)-4-hydroxyphenethyl)-3, 4-bis(pentyloxy)benzamide **118** (50 mg, 0.090 mmol) and the reaction was stirred at rt for 4 h. The solvent was evaporated and the residue was crystallised from EtOAc: EtOH to yield the title compound as a white solid (19 mg, 43%). The compound was not fully soluble in any common NMR solvent *i.e.*$CDCl_3$; DMSO-d_6, D_2O, MeOD, MeCN-d_3.

m.p. 130 °C (dec.)

^{1}H NMR (DMSO-d_6 & MeOD sample not fully soluble) δ 7.29 (2H, br s, aromatic), 6.75 (1H, br s, aromatic), 6.73-6.50 (3H, m, aromatic), 3.60 (4H, br s), 3.30 (2H, br s), 2.95 (2H, br s), 2.76-2.40 (4H, m), 1.40 (4H, br s), 1.05 (8H, m), 0.65 (6H, m).

ES-MS MH+ calcd for $C_{27}H_{41}N_2O_4$ 457.3, found *m/z* 457.3 (MH+)

Anal calcd $C_{27}H_{43}ClN_2O_5$. H_2O C 63.45, H 8.48, N 5.48. Found. C 63.44, H 8.38, N 5.68

Labeling of *N*-(3-(2-aminoethyl)-4-hydroxyphenethyl)-3, 4-bis(pentyloxy)benzamide hydrochloride with BODIPY^{Ò} 630/650-x, SE (121)

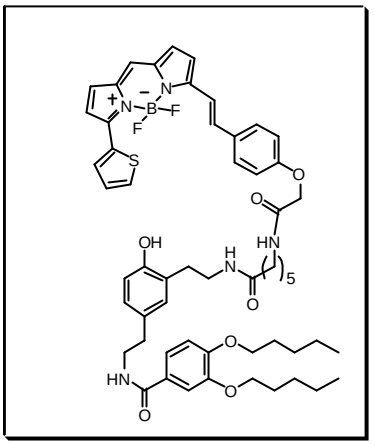

A solution of *N*-(3-(2-aminoethyl)-4-hydroxyphenethyl)-3,4-bis(pentyloxy)benzamide hydrochloride **119** (5.70 mg, 0.011 mmol) and Bodipy 630/650-X, SE **86** (4.12 mg, 0.0062 mmol), was stirred at rt in the dark, in 1.5 mL of 30% MeCN: 70% pH 8.3 $NaHCO_{3\,(aq)}$ buffer for 1 h. The reaction was reduced *in vacuo* and the residue was partitioned between water and $CHCl_3$. The aqueous phase was further extracted with $CHCl_3$ (3 x 20 mL). The organic layers were combined, dried ($MgSO_4$), and reduced. The resulting oil was purified using preparative TLC (10% MeOH: 90% $CHCl_3$) to yield the title compound as a purple solid (3.16 mg, 51%).

^{1}H NMR ($CDCl_3$) δ 8.41 (1H, br s, O-H phenol), 8.20 (1H, d, *J* 1.0 Hz, Bodipy), 7.62-7.55 (2H, m), 7.48 (1H, dd, *J* 1.0 & 5.0 Hz, Bodipy), 7.37 (1H, d, *J* 2.0 Hz, 2-H), 7.33 (1H, br s), 7.21-7.18 (1H, m), 7.16 (1H, dd, *J* 8.3 & 1.9 Hz 6-H), 7.04-6.79 (11H, m), 6.47 (1H, br t, N-H amide), 6.26 (1H, br t, N-H amide), 4.55 (2H, s, benzylic), 4.00 (4H, t, *J* 6.6 Hz, O-CH_2 (*o*) & (*p*)), 3.60 (2H, q, *J* 6.2 Hz, CH_2-amide), 3.40-3.26 (4H, m), 2.78 (4H, t, *J* 6.4 Hz, CH_2-phenol), 2.11 (2H, t, *J* 7.3 Hz, Bodipy) 1.82-1.20 (20H, m) 0.93 (6H, m, CH_3-pentyl).

ES-MS MH+ calcd for $C_{56}H_{67}BF_2N_5O_7S$ 1002.5 found *m/z* 1002.9 (MH+), 1024.5 (MNa+)

HPLC – gradient 35% → 100% MeCN in water over 30 min. R_t 19.62 min (89% using peak area)

Labeling of *N*-(3-(2-aminoethyl)-4-hydroxyphenethyl)-3,4-bis(pentyloxy)benzamide hydrochloride with dansyl chloride (120)

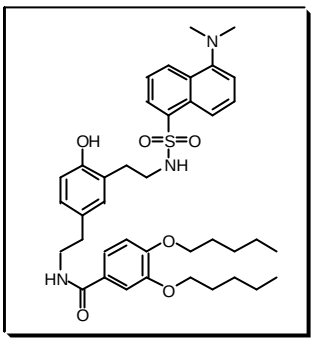

A solution of *N*-(3-(2-aminoethyl)-4-hydroxyphenethyl)-3,4-bis(pentyloxy)benzamide hydrochloride **119** (5.7 mg, 0.011 mmol) and dansyl chloride (3.0 mg, 0.011), was stirred at rt in the dark, in 2 mL of 70% MeCN: 30% pH 8.3 $NaHCO_{3\,(aq)}$ buffer for 12 h. The reaction was reduced *in vacuo* and the residue was partitioned between water and $CHCl_3$. The aqueous phase was further extracted with $CHCl_3$ (3 x 20 mL). The organic layers were combined, dried ($MgSO_4$), and reduced. The resulting oil was purified using preparative TLC (7% MeOH: 93% $CHCl_3$) to yield the title compound as a green oil (2.8 mg, 37%).

^{1}H NMR ($CDCl_3$) δ 8.50 (1H, d, *J* 8.6 Hz, Dansyl), 8.21-8.10 (2H, m, Dansyl), 7.47 (2H, t, *J* 7.3 Hz), 7.35 (1H, d, *J* 1.9 Hz, 2-H), 7.16-7.07 (2H, m), 6.87-6.77 (3H, m), 6.65 (1H, d, *J* 8.1 Hz, 6.12 (1H, br t, N-H amide), 5.87 (1H, br s, O-H), 5.14 (1H, br t, N-H amide), 4.00 (4H, t, *J* 6.6 Hz, O-CH_2 (*o*) & (*p*)), 3.60 (2H, q, *J* 6.2 Hz, CH_2-amide), 3.40-3.26 (4H, m), 2.78 (4H, t, *J* 6.4 Hz, CH_2-phenol), 2.11 (2H, t, *J* 7.3 Hz, Bodipy) 1.82-1.20 (20H, m) 0.93 (6H, m, CH_3-pentyl).

ES-MS MH+ calcd for $C_{39}H_{52}N_3O_6S$ 690.3 found *m/z* 690.2 (MH+)

HPLC – gradient 35% → 100% MeCN in water over 30 min. R_t 18.92 min (95% using peak area)

Synthesis of *N*-(4-hydroxyphenethyl)-3,4-bis(pentyloxy)benzamide (JTE2-3 (62))

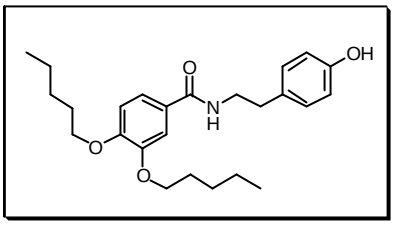

A solution of 3,4-bis(pentyloxy)benzoic acid **105** (300 mg, 1 mmol) and 1,1-carbonyldiimidazole (174mg, 1 mmol) was prepared in MeCN (30 mL). Tyramine (147mg, 1 mmol) was added to the reaction and was stirred at rt for 48 h. The solvent was reduced and the reaction taken up into EtOAc (20 mL), the organic was washed with water (1 x 10 mL), 2M $KHSO_{4\,(aq)}$ (2 x 20 mL), and sat. $NaHCO_{3\,(aq)}$ (2 x 20 mL). The organics were dried ($MgSO_4$), and evaporated to leave oil that was purified by crystallizing from MeCN: water to yield the title compound as white needles (320 mg, 77%).

m.p. 135-136 °C Lit[126] 134-136 °C

^{1}H NMR ($CDCl_3$) δ 7.34 (1H, d, *J* 2.0 Hz, 2-H), 7.14(1H, dd, *J* 2.0 & 8.3 Hz, 5-H), 7.04 (2H, d, *J* 8.5 Hz, phenol aromatic), 6.81 (2H, d, *J* 8.5 Hz, phenol aromatic), 6.80 (1H, d, J 8.3 Hz, 4-H), 6.53 (1H, s, OH), 6.17 (1H, br t, N-H amide), 4.03-3.97 (4H, m, O-CH_2), 3.63 (2H, q, *J* 6.2 Hz, CH_2-amide), 2.82 (2H, t, *J* 6.4 Hz, CH_2-phenol), 1.82-1.74 (4H, m, CH_2-pentyl), 1.50-1.33 (8H, m, CH_2-pentyl) 0.93 (6H, m, CH_3-pentyl).

Lit[126] ^{1}H NMR (DMSO-d_6) δ 9.14 (1H, s), 8.33 (1H, t, *J* 5.4 Hz), 7.42-7.40 (2H, m), 7.04-6.97 (3H, m), 6.68 (2H, d, *J* 8.4 Hz), 4.01-3.96 (4H, m), 3.45-3.32 (2H, m), 2.70 (2H, t, *J* 7.4 Hz), 1.78-1.64 (4H, m), 1.49-1.26 (8H, m) 0.94-0.83 (6H, m).

^{13}C NMR ($CDCl_3$) δ 167.5 (4°, C=O amide) 156.9 (4°), 151.9 (4°), 148.9 (4°), 130.1 (4°), 129.8 (C-H), 126.8 (4°), 119.3 (CH, benzamide), 116.1 (CH, benzamide), 112.6 (CH, benzamide), 112.3 (CH, tyramine), 69.3 (CH_2, C-O), 69.1 (CH_2, C-O), 41.5

(CH_2 α amide), 34.9 (CH_2 β amide), 28.9 (CH_2), 28.8 (CH_3, Boc), 28.2 (CH_2), 22.4 (CH_2), 14.0 (CH_3).

ES-MS MH+ calcd for $C_{25}H_{35}NO_4$ 413.3 found *m/z* 414.2 (MH+)

Synthesis of 3-nitro-1-naphthoic acid (127)

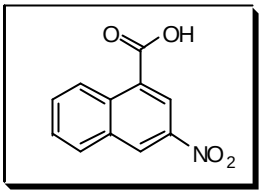

A mixture of 3-nitro-1, 8-naphthalic anhydride (20 g, 0.082 mol), NaOH (11.2 g, 0.281 mol) in water (400 mL) was added to a suspension of HgO_{red} (19.5 g, 0.090mol) in water (50 mL) and acetic acid (40 mL). The mixture which frothed vigorously, was then stirred and heated under reflux for 3 days. The suspension was then hot-filtered and the solid residue was air dried. The solid was then heated under reflux in conc. $HCl_{(aq)}$ (100 mL) and water (200 mL) for 4 h. Hot filtration gave the crude product, which was re-crystallized from hot acetic acid to give 3.85 g (22%) of the title compound as a cream coloured solid.

m.p. 250-252 °C Lit [261] 255-257 °C

^{1}H NMR (DMSO-d_6) δ 13.89 (1H, br s, COOH), 9.22 (1H, d, *J* 2.4 Hz, 4-H), 8.93 (1H, d, *J* 8.6 Hz, 5-H), 8.75 (1H, d, *J* 2.4 Hz, 2-H), 8.43 (1H, d, *J* 8 Hz, 8-H), 7.97-7.89 (2H, m, aromatic).

^{13}C NMR (DMSO-d_6) δ 166.1 (4°, C=O acid), 144.0 (4°), 135.1 (4°), 133.6 (4°), 132.8 (4°), 131.5 (CH), 130.6 (CH), 128.8 (CH), 128.3 (CH), 126.3 (CH), 123.2 (CH).

ES-MS M- calcd for $C_{11}H_7NO_4$ 217.04, found *m/z* 217 (M-).

FTIR: (KBr) 3500 (O-H), 3068, 2641, 1701 (C=O), 1597, 1529, 1453, 1412, 1336, 1287, 1253, 1203, 1102, 915, 796, 760, 687, 500 cm^{-1}.

Synthesis of 2-methyl-1-*n*-propylindole (125)

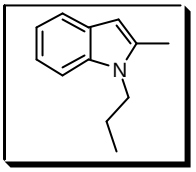

Solid 2-methylindole (1 g, 0.008 mol) was added portion wise to a stirring slurry of NaH (0.2 g, 0.008 mol) in DMF (30 mLs) at 0 °C. To this red solution was added 1-bromopropane (0.8 mL, 0.008 mol) and the reaction was stirred at rt for 4 h. The solvent was removed *in vacuo* and the residue was partitioned between EtOAc (50 mL) and water (50 mL). The organic layer was further washed with water (2 x 50 mL), dried ($MgSO_4$) and reduced to yield the title compound (1.27g, 97%) as a yellow oil.

^{1}H NMR ($CDCl_3$) δ 7.51 (1H, dd *J* 7.3 & 0.9 Hz, aromatic), 7.23 (1H, dd, *J* 7.1 & 1.1 Hz, aromatic), 7.13-7.00 (2H, m, aromatic), 6.21 (1H, s, 3-H), 3.97 (2H, t, *J* 7.2 Hz, N-CH_2), 2.38 (3H, s, CH_3-indole) 1.73 (2H, sextet, *J* 7.4, CH_2-propyl) 0.91 (3H, t, *J* 7.4 Hz, CH_3-propyl).

^{13}C NMR ($CDCl_3$) δ 136.6 (4°), 136.4 (4°), 128.0 (4°), 120.2 (CH), 119.6 (CH), 119.1 (CH), 109.0 (CH), 99.7 (CH), 44.6 (CH_2-*N*-indole), 23.4 (CH_2-propyl), 12.8 (CH_3-indole), 11.5 (CH_3-propyl).

AP-MS MH+ calcd for $C_{12}H_{16}N$ 174.1, found *m/z* 173.9 (MH+).

FTIR: (thin film) 3053, 2964, 2932, 2874, 2641, 1550, 1462, 1399, 1383, 1222, 769, 745cm^{-1}.

Synthesis of 2-methyl-3-(3-nitronaphthoyl)-1-*n*-propylindole (128)

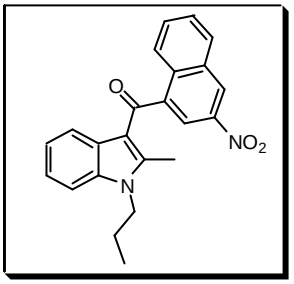

3-Nitronaphthoyl chloride **127** was prepared by refluxing 3-nitro-1-naphthoic acid in thionyl chloride for 4 h. The excess thionyl chloride was reduced *in vacuo*. 2-Methyl-1-*n*-propylindole (0.61 g, 3.5 mmol) and the freshly prepared 3-nitro naphthoyl chloride (1.03 g, 4.4 mmol) were dissolved in DCM (10ml) to give a red solution. Aluminium chloride (0.931g, 7.0 mmol) was gradually added to the reaction at r.t, before the reaction was heated to reflux for 30 minutes. Sodium hydroxide was then added dropwise, until the reaction reached pH 11, and it was filtered free of solids. The organic layer was separated and was washed with 1M sodium hydroxide (2 x 20 mL), brine (1 x 20 mL) and dried ($MgSO_4$). The crude product was purified using flash chromatography (30% EtOAc: 70% hexane) to yield the title compound (0.24 g, 19%) as a yellow foam.

^{1}H NMR ($CDCl_3$) δ 8.92 (1H, d, *J* 2.1 Hz, 4'-H), 8.30 (1H, *J* 2.3 Hz, 2'-H), 8.18-810 (2H, m, aromatic), 7.70-7.55 (2H, m, aromatic), 7.34 (1H, d, *J* 8.2 Hz, aromatic), 7.21-7.10 (1H, m, aromatic), 6.98-6.96 (2H, m, aromatic), 4.13 (2H, t, *J* 8.6 Hz, N-CH_2), 2.57 (3H, s, CH_3-indole) 1.87 (2H, sextet, *J* 7.5, CH_2-propyl) 1.01 (3H, t, *J* 7.4 Hz, CH_3-propyl).

^{13}C NMR ($CDCl_3$) δ 190.5 (4°, C=O), 146.5 (4°), 144.7 (4°), 142.6 (4°), 136.3 (4°), 132.9 (4°), 132.7 (4°), 128.3 (CH), 126.7 (4°), 126.1 (CH), 125.7 (CH), 122.6 (CH), 122.4 (CH), 120.6 (CH), 118.5 (CH), 114.0 (4°), 109.8 (CH), 45.0 (CH_2-*N*-indole), 22.9 (CH_2-propyl), 12.8 (CH_3-indole), 11.5 (CH_3-propyl).

AP-MS M- calcd for $C_{23}H_{20}N_2O_3$ 372.4, found *m/z* 372.1 (M-).

Anal calcd $C_{23}H_{20}N_2O_3$ C 74.18, H 5.41, N 7.52 % Found. C 75.75, H 6.10, N 7.78 %

FTIR: (thin film) 3075, 2965, 2932, 2875, 2641, 1652 (C=O), 1603, 1530 (NO_2), 1504, 1455, 1412, 1333 (NO_2), 1220, 1093, 760 cm^{-1}.

Synthesis of 3-(3-aminonaphthoyl)-2-methyl-1-*n*-propylindole (129)

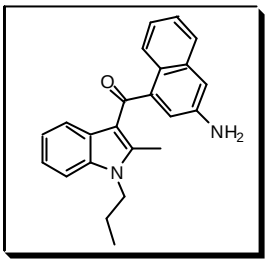

A solution of 2-methyl-3-(3-nitronaphthoyl)-1-*n*-propylindole **128** (240 mg, 0.886 mmol) and Pd/C (32 mg) in 70% EtOH: 30% EtOAc (20 mL) was stirred at rt under a H_2 atmosphere (1 atm) for 1 h. The reaction was filtered through a celite pad, concentrated *in vacuo*, and purified using preparative TLC (50% EtOAc:50% hexane) to yield the title compound as a pale yellow oil (147 mg, 66%). A small portion was crystallized from MeOH/ HCl to give the HCl salt as an analytical sample.

^{1}H NMR ($CDCl_3$) δ 7.84 (1H, d, *J* 8.3 Hz, aromatic), 7.58 (1H, *J* 8.2 Hz, aromatic), 7.25-7.20 (3H, m, aromatic), 7.19-7.08 (2H, m, aromatic), 7.05-6.95 (3H, d, *J* 8.2 Hz, aromatic), 4.03 (2H, t, *J* 7.3 Hz, N-CH_2), 3.91 (2H, br s, NH_2) 2.40 (3H, s, CH_3-indole) 1.76 (2H, sextet, *J* 7.5, CH_2-propyl) 0.94 (3H, t, *J* 7.4 Hz, CH_3-propyl).

^{13}C NMR ($CDCl_3$) δ 193.1 (4°, C=O), 145.7 (4°), 143.5 (4°), 142.0 (4°), 136.1 (4°), 135.4 (4°), 127.0 (4°), 126.6 (CH), 126.1 (4°), 125.4 (CH), 124.9 (CH), 123.3 (CH), 122.2 (CH), 122.1 (CH), 121.3 (CH) 117.5 (CH), 114.7 (4°), 110.3 (CH), 109.4 (CH) 44.8 (CH_2-*N*-indole), 22.9 (CH_2-indole), 12.5 (CH_3-indole), 11.4 (CH_3-propyl).

ES-MS MH+ calcd for $C_{23}H_{23}N_2O$ 343.2, found *m/z* 343.0 (MH+).

Anal calcd $C_{23}H_{23}N_2OCl$ C 72.91, H 6.12, N 7.39 % Found. C 72.72, H 6.16, N 7.13 %

FTIR: (thin film) 3458 (NH_2), 3354 (NH_2), 3223 (NH_2), 3051, 3006, 2965, 2932, 2875, 2641, 1616 (C=O), 1600, 1508, 1416, 1220, 1087, 747 cm^{-1}.

Synthesis of 3-(3-*N*-*tert*-butyloxycarbonylglycylaminonaphthoyl)-2-methyl-1-*n*-propylindole (130)

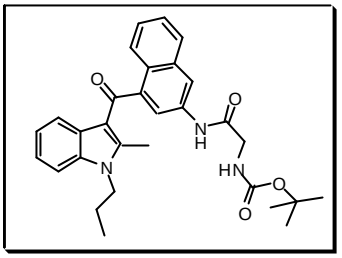

3-(3-Aminonaphthoyl)-2-methyl-1-*n*-propylindole **129** (86mg, 0.205 mmol), N^{α}-Boc-glycine (38mg, 2.15 mmol), DCC (44mg, 2.15 mmol) and catalytic DMAP were dissolved in anhydrous DCM (4 mL). The reaction was stirred at rt for 12 h and then cool filtered and diluted with DCM (30ml). The organic layer was washed with $KHSO_4$ (2×20 mL), $NaHCO_3$ (2×20 mL), and brine (1×20 mL). The reaction was dried ($MgSO_4$) and reduced *in-vacuo* to give a yellow solid. This was purified using preparative TLC (45% ethyl acetate: 55% hexane) to give 67.8mg (67%) of the title compound as a yellow oil.

^{1}H NMR ($CDCl_3$) δ 8.90 (1H, br s, N-H amide), 8.28 (1H, br s, aromatic) 7.89 (1H, d, *J* 8.2 Hz, aromatic), 7.76 (1H, d, *J* 8.1 Hz, aromatic), 7.44-7.25 (5H, m, aromatic), 7.18 (1H, t, *J* 7 Hz, aromatic), 7.02 (1H, t, *J* 7.2 Hz, aromatic), 4.03 (2H, t, *J* 7.3 Hz, N-CH_2), 3.88 (2H, d, *J* 6.9 Hz, CH_2-carbamate), 2.33 (3H, s, CH_3-indole) 1.79 (2H, sextet, *J* 7.5, CH_2-propyl), 1.42 (9H, s, CH_3-Boc), 0.96 (3H, t, *J* 7.4 Hz, CH_3-propyl).

^{13}C NMR ($CDCl_3$) δ 193.1 (4°, C=O), 168.1 (4°, C=O Boc), 156.3 (4°, C=O Boc), 146.4 (4°), 141.2 (4°), 136.2 (4°), 134.5 (4°), 128.2 (4°), 127.3 (4°), 126.6 (CH), 126.8 (4°), 125.9 (CH), 124.9 (CH), 122.5 (CH), 122.4 (CH), 121.3 (CH), 119.2 (CH) 118.6 (CH), 114.6 (4°), 109.6 (CH), 80.2 (4°, Boc), 44.8 (CH_2-*N*-indole), 33.8 (CH_2-gly), 28.3 (CH_3, Boc), 22.8 (CH_2-propyl), 12.6 (CH_3-indole), 11.4 (CH_3-propyl).

AP-MS MH+ calcd for $C_{30}H_{34}N_3O_4$ 500.3, found *m/z* 500.1 (MH+).

FTIR: (thin film) 3307 (br, NH), 3055, 3007, 2973, 2931, 1685 (C=O Boc),1653 (C=O), 1603, 1505, 1418, 1366 1244, 1092, 751 cm^{-1}

Synthesis of 3-(3-glycylaminonaphthoyl)-2-methyl-1-*n*-propylindole hydrochloride (131)

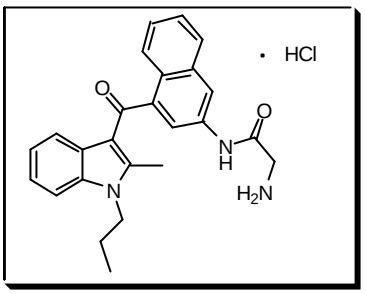

3-(3-*N-tert* butyloxycarbonyl-glycylaminonaphthoyl)-2-*n*-propylindole **130** (58mg, 0.116 mmol) was dissolved in methanol (3 mL) and conc. $HCl_{(aq)}$ (3 mL), and the reaction was stirred at rt for 12 h. The reaction was reduced *in-vacuo* and the product was recrystallised from MeOH: acetonitrile to give 25mg (50%) of the title compound as a pale pink solid.

m.p. 283°C (dec)

^{1}H NMR (MeOD) δ 8.41 (1H, d, *J* 1.8 Hz, aromatic) 7.90 (1H, d, *J* 8.2 Hz, aromatic), 7.83 (1H, d, *J* 8.4 Hz, aromatic), 7.66 (1H, d, *J* 2.1 Hz aromatic), 7.53-7.30 (3H, m, aromatic), 7.20-7.12 (1H, m, aromatic), 7.10-7.05 (1H, m, aromatic), 6.99-6.90 (1H, m, aromatic), 4.21 (2H, t, *J* 7.3 Hz, indole N-CH_2), 3.89 (2H, s, 1°amine-CH_2), 2.45 (3H, s, CH_3-indole) 1.81 (2H, sextet, *J* 7.5, CH_2-propyl), 0.94 (3H, t, *J* 7.4 Hz, CH_3-propyl).

^{13}C NMR (MeOD) δ 195.1 (4°, C=O), 166.3 (4°, C=O amide), 149.0 (4°), 143.4 (4°), 138.4 (4°), 136.8 (4°), 136.2 (4°), 129.6 (CH), 129.1 (4°), 128.7 (CH), 128.6 (4°), 127.6 (CH), 126.4 (CH), 124.1 (CH), 123.7 (CH), 122.2 (CH), 120.2 (CH), 119.6 (CH), 115.8 (4°), 111.7 (CH), 46.1 (CH_2-*N*-indole), 42.7 (CH_2-*N*-amine), 24.8 (CH_2-propyl), 12.6 (CH_3-indole), 11.4 (CH_3-propyl).

AP-MS MH+ calcd for $C_{25}H_{26}N_3O_2$ 400.2, found *m/z* 400.0 (MH+).

Anal calcd $C_{25}H_{26}N_3O_2Cl.0.25\ H_2O$ C 67.79, H 5.69, N 9.49 % Found. C 68.12, H 5.99, N 9.45 %

FTIR: (KBr) 3168 (br, NH HCl salt), 2961, 2585 (amine HCl salt), 1688 (C=O Boc), 1592, 1567, 1499, 1421, 1359 1263, 1091, 750 cm^{-1}

Synthesis of 3-(3-[*N*-(7-nitrobenz-2,1,3-oxadiazol-4-ylglycyl)amino] naphthoyl)-2-methyl-1-*n*-propylindole (132)

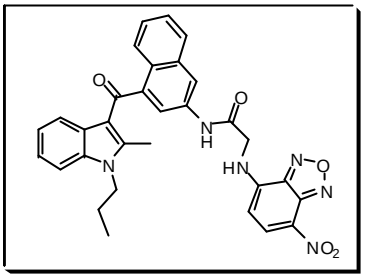

A slolution of 3-(3-glycylaminonaphthoyl)-2-methyl-1-*n*-propylindole HCl **131** (8 mg, 0.023 mmol) and NBD-F (2.85 mg, 0.0156 mmol) in pH 8.3 $NaHCO_{3\ (aq)}$ buffer (0.5 mL) and MeCN (0.5 mL) were stirred at room temperature for 45 min giving an orange precipitate. The solid was filtered and washed with water. The solid was dried (35°C) to yield 4.0mg (46%) of the title product as an orange solid.

m.p. 178 °C (dec.)

^{1}H NMR (DMSO-d_6) δ 10.54 (1H, br s, aromatic), 9.45 (1H, br s, aromatic), 8.55 (1H, d, *J* 8.9 Hz, aromatic) 8.41 (1H, d, *J* not detectable, aromatic) 7.95 (1H, d, *J* 8.2 Hz, aromatic), 7.79 (1H, d, *J* 8.3 Hz, aromatic), 7.66 (1H, d, *J* 2.0 Hz aromatic), 7.60-7.48 (2H, m, aromatic), 7.41-7.32 (1H, m, aromatic), 7.20-7.10 (1H, m, aromatic), 7.01-6.92 (2H, m, aromatic), 6.47 (1H, m, aromatic), 4.45 (2H, br s, amide-CH_2), 4.21 (2H, t, *J* 7.3 Hz, indole N-CH_2), 2.45 (3H, s, CH_3-indole) 1.81 (2H, sextet, *J* 7.2 Hz, CH_2-propyl), 0.91 (3H, t, *J* 7.3 Hz, CH_3-propyl).

ES-MS -ve calcd for $C_{31}H_{26}N_6O_5$ 562.2, found *m/z* 561.1 (M-H)

FAB-MS (-ve mode) M^- calcd for $C_{31}H_{26}N_6O_5$ 562.1965 found 562.1962

HPLC – gradient 35% → 100% MeCN in water over 30 min. R_t 13.64 min (91% using peak area)

Synthesis of 2-methyl-3-(1-naphthoyl)-indole (134)

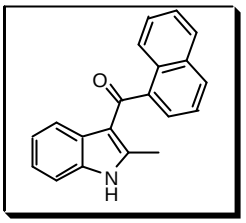

A solution of 2-methylindole (0.50 g, 3.8 mmol) in EtOEt (7 mL) was added dropwise to a stirring solution of 3M methylmagnesium bromide in EtOEt (1.2 mL) at 0 °C. The reaction was allowed to reach rt. 1-naphthoyl chloride was freshly prepared by refluxing 1-naphthoic acid in thionyl chloride for 5 h and removing the excess thionyl chloride *in vacuo*. A solution of 1-naphthoyl chloride (0.62 g, 3.26 mmol) in ether (10 mL) was added to the magnesium indole salt and the reaction was stirred for 45 min at rt and 1.5 h at reflux. The reaction was quenched with the addition of sat. $NH_4Cl_{(aq)}$ and was allowed to stir overnight to afford a fine precipitate. The solids were filtered from the reaction and the solid was refluxed in a solution of MeOH (12 mL), water (3 mL) and NaOH (200 mg) for 2 h. The title compound was filtered from the reaction and dried to yield 287mg (31%) of an off white solid.

m.p. 221 °C Lit[270] 229-230 °C

^{1}H NMR ($CDCl_3$ & DMSO-d_6) δ 11.20 (1H, br s, N-H), 8.10-7.85 (3H, m, naphthalene), 7.53-7.28 (6H, m), 7.18-6.97 (2H, m, indole), 2.19 (3H, s, CH_3).

^{13}C NMR ($CDCl_3$ & DMSO-d_6) δ 193.8 (4°, C=O), 146.6 (4°), 141.1 (4°), 135.6 (4°), 134.0 (4°), 130.5 (4°), 129.9 (CH), 128.6 (CH), 127.9 (4°), 127.1 (4°), 126.6 (CH), 125.8 (CH), 125.5 (CH), 125.2 (CH), 122.6 (CH), 122.1 (CH), 121.3 (CH), 115.0 (4°), 111.4 (CH), 14.9 (CH_3)

AP-MS MH+ calcd for $C_{20}H_{16}NO$ 286.1, found *m/z* 286.2 (MH+).

Anal calcd $C_{20}H_{15}NO$ C 84.19, H 5.30, N 4.91 % Found. C 83.77, H 5.17 , N 4.70 %

FTIR: (KBr) 3170 (N-H), 3105, 3053, 1595 (C=O), 1571, 1436, 1232, 1186, 887, 617 cm^{-1}

Synthesis of 2-methyl 3-(1-naphthoyl)-1-*n*-propylindole (JWH-015 (53))

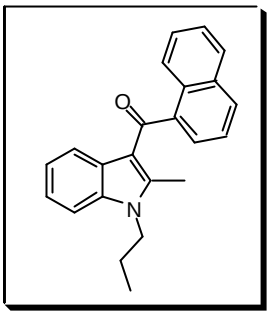

A suspension of 2-methyl-3-(1-naphthoyl) indole **134** (100 mg, 0.351 mmol), 1-bromopropane (75 µL, 0.848 mmol)) and K_2CO_3 (117 mg, 0.846 mmol) was refluxed in methyl ethyl ketone for 12 h. The reaction was filtered and reduced *in vacuo*. The residue was dissolved in MeCN: water and the crystals that formed (38 mg of 2-methyl 3-(1-naphthoyl) indole) were filtered. The mother liquor was reduced to dryness and the residue purified using preparative TLC to yield the title compound (42mg, 36% (59% based on recovered starting material) green oil (R_f 0.2 EtOAc: Pet Ether (1:10)). Attempted crystallization of the oil failed from a number of common solvent systems (i.e. EtOH: water, MeOH: water, MeCN: water, DMF: water, EtOAc: hexane and Acetone: water).

^{1}H NMR ($CDCl_3$) δ 8.10 (1H, d, *J* 8.2 Hz), 7.95 (1H, d, *J* 8 Hz), 7.90 (1H, d, *J* 8.1 Hz), 7.59-7.39 (4H, m), 7.31-7.12 (3H, m), 6.98 (1H, t, *J* 7.2 Hz), 4.07 (2H, t, *J* 7.4 Hz, CH_2-indole), 2.46 (3H, s, CH_3-indole), 1.80 (2H, sextet (6), *J* 7.4 Hz, CH_2-propyl), 0.97 (3H, t, *J* 7.4 Hz, CH_3-propyl).

^{13}C NMR ($CDCl_3$) δ 193.4 (4°, C=O), 145.6 (4°), 140.5 (4°), 136.2 (4°), 134.4 (4°), 129.9 (CH), 128.2 (CH), 127.1 (4°), 126.8 (CH), 125.7 (CH), 125.6 (CH), 125.1 (CH), 122.2 (CH), 121.8 (CH), 114.9 (4°), 109.5 (CH), 44.8 (CH_2-*N*-indole), 22.9 (CH_2-propyl), 12.55 (CH_3-indole) 11.43 (CH_3-propyl).

ES-MS MH+ calcd for $C_{23}H_{22}NO$ 328.2 , found *m/z* 327.9 (MH+).

Anal calcd $C_{23}H_{21}NO.0.5\ H_2O$ C 82.11, H 6.59, N 4.16 % Found. C 82.11, H 6.49, N 4.19 %

8.2 Pharmacology

Rat splenocyte membrane preparation

Adult male Hooded Lister rats were killed by decapitation and spleens were removed, chopped with scissors and rapidly forced through a 70 μM pore size steel mesh with the plunger of a 5 mL syringe into ice-cold phosphate buffered saline (PBS) to produce a single cell suspension. The cells were pelleted by centrifugation, and erythrocytes were lysed with lysis buffer (0.017 M Tris, 0.144 M ammonium chloride, pH 7.2) for 3 mins. The cells were washed twice in PBS and resuspended in Tris buffer (50mM Tris, 100mM NaCl, 10mM $MgCl_2$, pH 7.4). The cell suspension was homogenised with a glass/Teflon homogeniser. The homogenate was centrifuged at 20,000 x g at 4 °C for 10 min and the pellet resuspended in Tris buffer. Homogenisation and centrifugation were repeated twice and the final pellet was resuspended in storage buffer (50mM Tris, 1mM EDTA, pH 7.4) to a protein concentration of 5 mg mL^{-1} for radioligand binding.

hCB_2 CHO cell membrane preparation

CHO K1 cells stably transfected with the hCB_2 receptor were kindly obtained from Dr Darren Smart (GlaxoSmithkline) and were grown in our own laboratories in Dubelcco's modified Eagle's medium (DMEM) containing 5% foetal calf serum, 2 mM L-glutamine, 600 μg/mL Geneticin®, and 300 μg/mL Hygromycin B, in a Sanyo CO_2 incubator (95% O_2: 5% CO_2) at 37 °C. Cells were passaged every 3-4 days, using trypsin to lift the cells, and resuspended in fresh media. Flasks were grown as above to confluence (3 days) and cells were harvested, by removing excess media, and collecting in ice cold PBS using a plastic cell scraper. The cells were washed twice in ice cold PBS. Cell disruption was performed using a Polytron hand held electric

homogeniser in Tris buffer (50mM Tris, 100mM NaCl, 10mM $MgCl_2$, pH 7.4). The homogenate was centrifuged at 20,000 x *g* at 4 °C for 10 min and the pellet resuspended in Tris buffer. Homogenisation and centrifugation were repeated twice and the final pellet was resuspended in storage buffer (50mM Tris, 1mM EDTA, pH 7.4) to a protein concentration of 5 mg mL^{-1} for radioligand binding or 2 mg mL^{-1} for [^{35}S] GTP-γ-S binding and stored at -70 °C.

hCB_2 cell preparation for confocal microscopy

The CHO K1 cells were grown as above except that upon confluence in T175 flasks cells were resuspended in 10 mL of DMEM. 0.5 mL of cell suspension was diluted in a further 10 mL of DMEM and 0.4 mL of this cell suspension was pipetted into 8 well glass bottomed plates. Incubation for 24 h gave plates of approximately 60-70 % confluence which were used in confocal microscopy experiments.

hCB_2 transient transfection and membrane preparation

HEK-293T cells were grown in DMEM with 10% foetal bovine serum and high glucose. Cells were transiently transfected with pcDNA3 encoding CB2 using calcium phosphate precipitation and used for membrane preparation as described previously [271] Briefly, at 24 h post-transfection, cells were harvested, washed twice in PBS and resuspended in PBS with 0.1% v/v protease inhibitor cocktail (Sigma Chemical Co., St Louis, MO, U.S.A.). Cell disruption was performed with nitrogen cavitation at 750 psi for 5 min. Following removal of cell debris and nuclei by differential centrifugation, membranes were resuspended in buffer (25 mM Tris-HCl, pH 7.4, 5 mM MgCl2, 1 mM EDTA) + 7% sucrose. The membrane preparation was diluted to 0.6 mg ml^{-1} total protein concentration and stored at -70 °C.

Radioligand binding in rat splenocyte and hCB_2 CHO membranes

Assay tubes were prepared in triplicate to a final volume of 1ml containing 0.3 nM [^{3}H] CP 55,940 (Perkin-Elmer Life Sciences Inc., U.S.A.) and 250 µg membrane protein and diluted in Tris buffer (50 mM Tris.HCl, 2 mM EDTA, 5 mM $MgCl_2$ also

containing 0.2 mgml_1 bovine serum albumin (BSA), pH7.4). Stock drugs were diluted in the same buffer containing 5 mg ml^{-1} BSA. Tubes were incubated for 90 min at 30 °C. Specific binding was calculated by subtracting nonspecific binding (NSB, determined in the presence of 1 μM HU210 **14**). A Brandel cell harvester (Brandel Inc., Gaitherburg, MD, U.S.A.) was used to separate bound from unbound ligand and the former quantified by liquid scintillation counting. Nonlinear regression analysis was carried out using Graphpad Prism3 (GraphPAD Software, San Diego, CA, U.S.A.). K_i values for the test compounds were determined from IC_{50} values using a K_D of 0.59 nM for [^{3}H] CP 55,940, using the Cheng–Prusoff equation. Results are presented as mean values, with a standard error of the mean (SEM) and 95 % confidence intervals.

Radioligand binding in HEK-293T membrane preparations containing hCB_2 receptors

Radioligand binding assays were performed as previously described [271]. Membrane preparations were incubated with 4 nM [^{3}H] CP, 55,940 with varying concentrations of test compounds. NSB was determined with 1 μM CP 55,940 **2**. All conditions were prepared in triplicate. A Brandel cell harvester (Brandel Inc., Gaitherburg, MD, U.S.A.) was used to separate bound from unbound ligand and the former quantified by liquid scintillation counting. Results were analysed with Prism GraphPAD Software (GraphPAD Software, San Diego, CA, U.S.A.) as previously described[193] using the Cheng–Prusoff equation to determine K_i values with the K_D value of 5.1 nM for CP 55,940 binding to hCB_2 HEK 293T membrane preparations.

[^{35}S]GTP-g-S membrane binding

1 mL of CHO membrane containg the hCB_2 receptor (see membrane preraration above) was preincubated with 100 mM GDP (ICN Biomedicals Inc., U.K.) and 1mM theophylline (Sigma, U.K.) in 15 mL of assay buffer (50mM Tris-HCl, 100mM NaCl,10mM $MgCl_2$ containing 5mg mL^{-1} BSA, pH 7.4) for 20 min at 30 °C. Assay tubes were prepared in triplicate to a final volume of 1 mL and contained 0.5 mL of the preincubated membrane solution, 0.4 nM [^{35}S]GTP-γ-S (Amersham, U.K.) and the appropriate concentrations of drug. The NSB was determined using 100 μM

nonradiolabelled GTP-γ-S **11** and 1 μM HU210 **14** was included as a positive control. Tubes were incubated for 45 min at 30 °C. Free and bound [^{35}S]GTP-γ-S were separated by rapid filtration (using filter mats presoaked in Tris buffer (pH 7.4) containing 5% BSA) and washed with ice-cold Tris buffer (pH 7.4). Data are presented as mean values of % basal binding ± SEM (where basal binding = 100%) for experiments performed in triplicate. Statistical analysis was performed by analysis of variance using Bonferroni *post hoc* tests using GraphPad Prism3.

8.3 Molecular Modeling

All aspects of the molecular modeling methodology relating to the absolute parameters used are fully discussed in the relevant chapters. The software used for the analysis is listed below and operated on a Silicon Graphics interface.

Clustal W – sequence alignment (Version 1.81)
Sybyl – molecular modeling platform (Tripos, St Louis, MO63144)
Spartan PCPro – quantum mechanics software (Wavefunction Inc.)
CHARMM – energy minimization and molecular dynamics[234]
PROCHECK – Protein structure analysis software[243]
Ligplot – Ligand-receptor analysis software[245]
LIGBUILDER – De novo drug design software[254]

8.4 Fluorescence confocal microcopy

Images were taken using a Zeiss axiovert 100 with LSM510 confocal. Fluorescence was obtained by using an appropriate laser excitation wavelength through a Plan-apochromat 63x/1.4NA oil immersion objective and collecting emitted light through an appropriate long pass (LP) emission filter. Pinhole diameter was standardized to 1 area unit.

References

(1) Auer, M.; Moore, K. J.; Myers-Almes, F. J.; Guenther, R.; Pope, A. J.; Stoekli, K. A. Fluorescence Correlation Spectroscopy: Lead Discovery by Miniaturisation HTS. *Drug Discovery Today* **1998**, *3*, 457-465.

(2) McGrath, J. C.; Arribas, S.; Daly, C. J. Fluorescent Ligands for the Study of Receptors. *Trends in Pharmaceutical Sciences* **1996**, *17*, 393-399.

(3) Daly, C. J.; McGrath, J. C. Fluorescent ligands, antibodies, and proteins for the study of receptors. *Pharmacology & Therapeutics* **2003**, *100*, 101-118.

(4) Munro, S.; Thomas, K. L.; Abushaar, M. Molecular Characterization of a Peripheral Receptor for Cannabinoids. *Nature* **1993**, *365*, 61-65.

(5) Howard, A. D. Orphan G-Protein-Coupled receptors and natural ligand discovery. *Trends in Pharmaceutical Sciences* **2001**, *22*, 132-140.

(6) Wise, A.; Gearing, K.; Rees, S. Target Validation of G-protein coupled receptors. *Drug Discovery Today* **2002**, *7*, 235-246.

(7) Deupree, J. D.; Bylund, D. B. Basic Principles for Receptor Binding. *Tocris Reviews* **2002**, *18*.

(8) Hertzberg, R. A.; Pope, A. J. High-throughput screening: new technology for the 21st century. *Current Opinion in Chemical Biology* **2000**, *4*, 445-451.

(9) Wolcke, J.; Ullmann, D. Miniturized HTS technologies - uHTS. *Drug Discovery Today* **2001**, *6*, 637-646.

(10) Harrison, C.; Traynor, J. R. The S-35 GTP gamma S binding assay: approaches and applications in pharmacology. *Life Sciences* **2003**, *74*, 489-508.

(11) Klumpp, M.; Scheel, A.; Lopez-Calle, E.; Busch, M.; Murray, K. J.; Pope, A. J. Ligand Binding to Transmembrane Receptors on Intact Cells or Membrane Vesicles Measured in a Homogenous 1-Microlitre Assay Format. *Journal of Biomolecular Screening* **2001**, *6*, 159-170.

(12) Hill, S. J.; Baker, J. G.; Rees, S. Reporter-gene systems for the study of G-protein-coupled receptors. *Current Opinion in Pharmacology* **2001**, *1*, 526-532.

(13) Moore, K. J.; Turconi, S.; Ashman, S.; Ruediger, M.; Haupts, U.; Emerick, V.; Pope, A. J. Single Molecule Detection Technologies in Miniaturised High Throughput Screening: Fluorescence Correlation Spectroscopy. *Journal of Biomolecular Screening* **1999**, *4*, 335-353.

(14) Brown, S. B. *An Introduction to Spectroscopy for Biochemists*; Academic Press: London, 1980.

(15) Campbell, I. D.; Dwek, R. A. *Biological Spectroscopy*; The Benjamin/Cummings Publishing Co. Inc., 1984.

(16) Herman, B. *Fluorescence Microscopy*; 2nd ed.; BIOS Scientific Publishers: Oxford, UK, 1998.

(17) Song, I.; Hennink, E. J.; Young, I. T.; Tanke, H. J. Photobleaching Kinetics of Fluorescein in Quantitative Fluorescence Microscopy. *Biophysical Journal* **1995**, *68*, 2588-2600.

(18) Song, I.; Varma, J. W.; Verhoeven, J. W.; Tanke, H. J. Influence of the Triplet Excited State on the Photobleaching Kinetics of Fluorescein in Microscopy. *Biophysical Journal* **1996**, *70*, 2959-2968.

(19) Lazo, J. S.; Li, T.; Woo, E.; Settineri, C.; Allan, W. P.; Yalowich, J. C. Chemical Synthesis and Biological Activity of Novel Fluorescent Etoposide Derivative. *Biochemical Pharmacology* **1997**, *53*, 715-722.

(20) Muthian, S.; Nithipatikom, K.; Campbell, W. B.; Hillard, C. J. Synthesis and characterization of a fluorescent substrate for the *N*-arachidonoylethanolamine (anandamide) transmembrane carrier. *Journal of Pharmacology and Experimental Therapeutics* **2000**, *293*, 289-295.
(21) Mackenzie, J. F.; Daly, C. J.; Pediani, J. D.; McCrath, J. C. Quantitative Imaging in Live Human Cells Reveals Intracellular α_1-Adrenoreceptor Ligand-Binding Sites. *Journal of Pharmacology and Experimental Therapeutics* **2000**, *294*, 434-443.
(22) Behrens, U. D.; Wagner, H. J. Localization of Dopamine D_1-Receptors in Vertebrate Retinae. *Neurochemistry International* **1995**, *27*, 497-507.
(23) Heithier, H.; Hallmann, D.; Boege, F.; Reilander, H.; Dees, C.; Jaeggi, K. A.; Arndt-Jovin, D.; Jovin, T. M.; Helmrich, E. J. M. Synthesis and Properties of Fluorescent β-Adrenoreceptor Ligands. *Biochemistry* **1994**, *33*, 9126-9134.
(24) Briddon, S. J.; Middleton, R. J.; Cordeaux, Y.; Flavin, F. M.; Weinstein, J. A.; George, M. W.; Kellam, B.; Hill, S. J. Quantitative Analysis of the Formation and Diffusion of A_1-adenosine Receptor-Antagonist Complexes in Single Living Cells. *Proceedings of the National Acadamy of Sciences* **2004**, *101*, 4673-4678.
(25) Briddon, S. J.; Middleton, R. J.; Yates, A. S.; George, M. W.; Kellam, B.; Hill, S. J. Application of Fluorescence Corelation Spectroscopy to the Measurement of Agonist Binding to a G-protein Coupled Receptor at the Single Cell Level. *Faraday Discuss* **2004**, *126*, 197-207.
(26) Feng, W. X.; Herman, B. *Fluorescent Imaging Spectroscopy and Microscopy*; John Wiley and Sons Inc., 1996.
(27) Medina, M.; Schwille, P. Fluorescence Correlation Spectroscopy for the Detection and Study of Single Molecules in biology. *BioEssays* **2002**, *24*, 758-764.
(28) Eigen, M.; Rigler, R. Sorting Single Molecules: Applications to Diagnostics and Evolutionary Biotechnology. *Proceedings of the National Acadamy of Sciences* **1994**, *91*, 5740-5747.
(29) Elson, E. L.; Magde, D. Fluorescence Correlation Spectroscopy I: Conceptual Basis and Theory. *Biopolymers* **1974**, *13*, 1-27.
(30) Magde, D.; Elson, E. L.; Webb, W. W. Fluorescence Correlation Spectroscopy II: An Experimental Realisation. *Biopolymers* **1974**, *13*.
(31) Enderlein, J. E.; Robbins, D. L.; Ambrose, W. P.; Goodwin, P. M.; Keller, R. A. The Statistics of SMD: An Overview. *BIoimaging* **1997**, *5*, 88-98.
(32) Maiti, S.; Haupts, U.; Webb, W. W. Fluorescence Correlation Spectroscopy: Diagnostics for Sparse Molecules. *Proceedings of the National Acadamy of Sciences* **1997**, *94*, 11753-11757.
(33) Wohland, T.; Friedrich, K.; Hovius, R.; Vogel, H. Study of Ligand-Receptor Interactions by Fluorescence Correlation Spectroscopy with Different Flurophores: Evidence that the Homopentameric 5-Hydroxytryptamine Type 3A Receptor Binds Only One Ligand. *Biochemistry* **1999**, *38*, 8671-8681.
(34) Pick, H.; Preuss, A. K.; Mayer, M.; Wohland, T.; Hovius, R.; Vogel, H. Monitoring Expression and Clustering of the Ionotropic $5HT_3$ Receptor in Plasma Membranes of LIve Biological Cells. *Biochemistry* **2003**, *42*, 877-884.
(35) Schwille, P.; Meyer-Alms, F. J.; Rigler, R. Duel-Colour Fluorescence Cross Correlation Spectroscopy for Multicomponent Diffusional Analysis in Solution. *Biophysical Journal* **1997**, *72*, 1878-1886.

(36) Jung, G.; Wiehler, J.; Gohde, W.; Tittel, J.; Basche, T.; Steipe, B.; Brauchle, C. Confocal Microscopy of Single Molecules of the Green Fluorescent Protein. *Bioimaging* **1998**, *6*, 61-64.
(37) Kettling, U.; Koltermann, A.; Schwille, P.; Eigen, M. Real-Time Enzyme Kinetics Monitered by Dual-Colour Fluorescence Cross Correlation Spectroscopy. *Proceedings of the National Acadamy of Sciences* **1998**, *95*, 1416-1420.
(38) Winkler, T.; Kettling, U.; Koltermann, A.; Eigen, M. Confocal Fluorescence Coincidence Analysis: An approach to Ultra High Throughput Screening. *Proceedings of the National Acadamy of Sciences* **1999**, *96*, 1375-1378.
(39) Pope, A. J.; Haupts, U.; Moore, K. J. Homogenous Fluorescence Readouts for Miniaturised High-Throughput Screening: Theory and Practice. *Drug Discovery Today* **1999**, *4*, 350-362.
(40) Craenenbroeck, E. V.; Vercammen, J.; Mattys, G.; Beirlant, J.; Marot, C.; Hoebeke, J.; Strobbe, R.; Engelborghs, Y. Heuristic Statistical Analysis of Fluorescence Fluctuation Data with Bright Spikes: Application to Ligand Binding to the Human Serotonin Receptor Expressed in *Escherichia coli* Cells. *Biological Chemistry* **2001**, *382*, 355-361.
(41) Gauglitz, G. Optical Detection Methods for Combinatorial Libraries. *Current Opinion in Chemical Biology* **2000**, *4*, 351-355.
(42) Pramanik, A.; Rigler, R. Ligand-Receptor Interactions in the Membrane of Cultured Cells Monitored by Fluorescence Correlation Spectroscopy. *Biological Chemistry* **2001**, *382*, 371-378.
(43) Gaoni, Y.; Mechoulam, R. Isolation, structure and partial synthesis of an active constituent of hashish. *Journal of the American Chemical Society* **1964**, *86*, 1646-1647.
(44) Mathre, M. L. *Cannabis in Medical Practice. A Legal, Historical and Pharmacological Overview of the Therapeutic Use of Marijuana*; McFarland & Company, Inc, 1997.
(45) British Medical Association *Therapeutic uses of cannabis*; Harwood academic publishers, 1997.
(46) Wills, S. *Drugs of Abuse*; The Pharmaceutical Press, 1997.
(47) Advisory Council on the Misuse of Drugs The classification of cannabis under the Misuse of Drugs act 1971; Home Office: London, 2002.
(48) Johnson, M. R.; Melvin, L. S., Jr. Substituted 2-hydroxyphenyl cycloalkanes and their pharmaceutical compositions. In *Eur. Pat. Appl.*; (Pfizer Inc., USA). Ep, 1982; pp 163 pp.
(49) Little, P. J.; Compton, D. R.; Johnson, M. R.; Melvin, L. S.; Martin, B. R. Pharmacology and stereoselectivity of structurally novel cannabinoids in mice. *Journal of Pharmacology and Experimental Therapeutics* **1988**, *247*, 1046-1051.
(50) Matsuda, L. A.; Lolait, S. J.; Brownstein, M. J.; Young, A. C.; Bonner, T. I. Structure of a Cannabinoid Receptor and Functional Expression of the Cloned Cdna. *Nature* **1990**, *346*, 561-564.
(51) Pertwee, R. G. Pharmacology of Cannabinoid CB_1 and CB_2 Receptors. *Pharmacology & Therapeutics* **1997**, *74*, 129-180.
(52) Bell, M. R.; Dambra, T. E.; Kumar, V.; Eissenstat, M. A.; Herrmann, J. L.; Wetzel, J. R.; Rosi, D.; Philion, R. E.; Daum, S. J.; Hlasta, D. J.; Kullnig, R. K.; Ackerman, J. H.; Haubrich, D. R.; Luttinger, D. A.; Baizman, E. R;

Miller, M. S.; Ward, S. J. Antinociceptive (Aminoalkyl)Indoles. *Journal of Medicinal Chemistry* **1991**, *34*, 1099-1110.

(53) Dambra, T. E.; Estep, K. G.; Bell, M. R.; Eissenstat, M. A.; Josef, K. A.; Ward, S. J.; Haycock, D. A.; Baizman, E. R.; Casiano, F. M.; Beglin, N. C.; Chippari, S. M.; Grego, J. D.; Kullnig, R. K.; Daley, G. T. Conformationally Restrained Analogs of Pravadoline - Nanomolar Potent, Enantioselective, (Aminoalkyl)Indole Agonists of the Cannabinoid Receptor. *Journal of Medicinal Chemistry* **1992**, *35*, 124-135.

(54) Devane, W. A.; Hanus, L.; Breuer, A.; Pertwee, R. G.; Stevenson, L. A.; Griffin, G.; Gibson, D.; Mandelbaum, A.; Etinger, A.; Mechoulam, R. Isolation and Structure of a Brain Constituent That Binds to the Cannabinoid Receptor. *Science* **1992**, *258*, 1946-1949.

(55) Rinaldi-Carmona, M.; Barth, F.; Heaulme, M.; Shire, D.; Calandra, B.; Congy, C.; Martinez, S.; Maruani, J.; Neliat, G.; Caput, D.; Ferrara, P.; Soubrie, P.; Breliere, J. C.; Lefur, G. SR141716, a Potent and Selective Antagonist of the Brain Cannabinoid Receptor. *Febs Letters* **1994**, *350*, 240-244.

(56) Rinaldi-Carmona, M.; Barth, F.; Heaulme, M.; Alonso, R.; Shire, D.; Congy, C.; Soubrie, P.; Breliere, J. C.; Lefur, G. Biochemical and Pharmacological Characterization of SR141716, the First Potent and Selective Brain Cannabinoid Receptor Antagonist. *Life Sciences* **1995**, *56*, 1941-1947.

(57) Rinaldi-Carmona, M.; Barth, F.; Millan, J.; Derocq, J. M.; Casellas, P.; Congy, C.; Oustric, D.; Sarran, M.; Bouaboula, M.; Calandra, B.; Portier, M.; Shire, D.; Breliere, J. C.; Le Fur, G. SR 144528, the first potent and selective antagonist of the CB2 cannabinoid receptor. *Journal of Pharmacology and Experimental Therapeutics* **1998**, *284*, 644-650.

(58) Select Committee on Science and Technology Cannabis-The Scientific and Medical Evidence.; House of Lords: London, 1998.

(59) Select Committee on Science and Technology Therapeutic use of cannabis.; House of Lords: London, 2001.

(60) GW Pharmaceuticals Interim Results For The Six Months To 31 March 2003, 2003.

(61) Robson, P. Therapeutic aspects of cannabis and cannabinoids. *British Journal of Psychiatry* **2001**, *178*, 107-115.

(62) Reynolds, J. R. On the therapeutic uses and toxic effects of cannabis indica. *Lancet* **1890**, *i*, 637-638.

(63) McDonald, W. I.; Noseworthy, J. H. *Multiple Sclerosis 2*; Butterworth Heinemann, 2003.

(64) Zajicek, J. Cannabinoids on trial for multiple sclerosis. *Lancet Neurology* **2002**, *1*, 147-147.

(65) Killestein, J.; Hoogervorst, E. L. J.; Reif, M.; Kalkers, N. F.; van Loenen, A. C.; Staats, P. G. M.; Gorter, R. W.; Uitdehaag, B. M. J.; Polman, C. H. Safety, tolerability, and efficacy of orally administered cannabinoids in MS. *Neurology* **2002**, *58*, 1404-1407.

(66) Zajicek, J.; Fox, P.; Sanders, H.; Wright, D.; Vickery, J.; Nunn, A.; A., T. Cannabinoids for treatment of spacticity and other symptons related to multiple sclerosis (CAMS study): multicentre randomised placebo-controlled trial. *Lancet* **2003**, *362*, 1517-1526.

(67) Baker, D.; Pryce, G.; Croxford, J. L.; Brown, P.; Pertwee, R. G.; Huffman, J. W.; Layward, L. Cannabinoids control spasticity and tremor in a multiple sclerosis model. *Nature* **2000**, *404*, 84-87.

(68) Croxford, J. L.; Miller, S. D. Immunoregulation of a viral model of multiple sclerosis using the synthetic cannabinoid R(+)WIN55,212. *Journal of Clinical Investigation* **2003**, *111*, 1231-1240.
(69) Arevalo-Martin, N.; Vela, J. M.; Molina-Holgado, E.; Borrell, J.; Guaza, C. Therapeutic action of cannabinoids in a murine model of multiple sclerosis. *Journal of Neuroscience* **2003**, *23*, 2511-2516.
(70) Lipman, A. G. Pharmacological Approaches to Pain Management: Nontraditional analgesics and Analgesic Adjuncts. *The Management of Pain*; Churchill Livingstone, 1998.
(71) Campbell, F. A.; Tramer, M. R.; Carroll, D.; Reynolds, D. J.; Moore, R. A.; McQuay, H. J. Are cannabinoids an effective and safe treatment option in the management of pain? A qualitative systematic review. *British Medical Journal* **2001**, *323*, 13-16.
(72) Ibrahim, M.; Deng, H.; Zvonok, A.; Cockayne, D.; Kwan, J.; Mata, H.; Vanderah, T.; Lai, J.; Porreca, F.; Makriyannis, A.; Malan, T. Activation of CB2 cannabinoid receptors by AM1241 inhibits experimental neuropathic pain: Pain inhibition by receptors not present in the CNS. *Proceedings of the National Acadamy of Sciences* **2003**, *100*, 10529-10533.
(73) Zhang, J.; Hoffert, C.; Vu, H. K.; Groblewski, T.; Ahmad, S.; O'Donnell, D. Induction of CB2 receptor expression in the rat spinal cord of neuropathic but not inflammatory chronic pain models. *European Journal of Neuroscience* **2003**, *17*, 2750-2754.
(74) Wade, D. T.; Robson, P.; House, H.; Makela, P.; Aram, J. A preliminary controlled study to determine whether whole-plant cannabis extracts can improve intractable neurogenic symptoms. *Clincal Rehabilitation* **2003**, *17*, 21-29.
(75) Plasse, T. F.; Gorter, R. W.; Krasnow, S. H.; Lane, M.; Shepard, K. V.; Wadleigh, R. G. Recent Clinical-Experience with Dronabinol. *Pharmacology Biochemistry and Behavior* **1991**, *40*, 695-700.
(76) Ward, A.; Holmes, B. Nabilone - a Preliminary Review of Its Pharmacological Properties and Therapeutic Use. *Drugs* **1985**, *30*, 127-144.
(77) Abel, E. L. Effects of marihuana on the solution of anagrams, memory and appetite. *Nature* **1971**, *231*, 260-261.
(78) Di Marzo, V.; Goparaju, S. K.; Wang, L.; Liu, J.; Batkai, S.; Jarai, Z.; Fezza, F.; Miura, G. I.; Palmiter, R. D.; Sugiura, T.; Kunos, G. Leptin-regulated endocannabinoids are involved in maintaining food intake. *Nature* **2001**, *410*, 822-825.
(79) Iversen, L. The Science of Marijuana. **2000**.
(80) Howlett, A. C.; Barth, F.; Bonner, T. I.; Cabral, G.; Casellas, P.; Devane, W. A.; Felder, C. C.; Herkenham, M.; Mackie, K.; Martin, B. R.; Mechoulam, R.; Pertwee, R. G. International Union of Pharmacology. XXVII. Classification of cannabinoid receptors. *Pharmacological Reviews* **2002**, *54*, 161-202.
(81) Palczewski, K.; Kumasaka, T.; Hori, T.; Behnke, C. A.; Motoshima, H.; Fox, B. A.; Le Trong, I.; Teller, D. C.; Okada, T.; Stenkamp, R. E.; Yamamoto, M.; Miyano, M. Crystal structure of rhodopsin: A G protein-coupled receptor. *Science* **2000**, *289*, 739-745.
(82) Lu, Z. H.; Saldanha, J. W.; Hulme, E. C. Seven-transmembrane receptors: crystals clarify. *Trends in Pharmacological Sciences* **2002**, *23*, 140-146.

(83) Sakmar, T. P. Structure of rhodopsin and the superfamily of seven-helical receptors: the same and not the same. *Current Opinion in Cell Biology* **2002**, *14*, 189-195.
(84) Becker, O. M.; Shacham, S.; Marantz, Y.; Noiman, S. Modeling the 3D structure of GPCRs: Advances and application to drug discovery. *Current Opinion in Drug Discovery & Development* **2003**, *6*, 353-361.
(85) Patrick, G. L. Receptor Structure and signal tansduction. *An Introduction to Medicinal Chemistry*; 2nd ed.; Oxford University Press, 2001.
(86) Zhang, J.; Barak, L. S.; Anborgh, P. H.; Laporte, S. A.; Caron, M. G.; Ferguson, S. S. G. Cellular trafficking of G protein-coupled receptor/beta-arrestin endocytic complexes. *Journal of Biological Chemistry* **1999**, *274*, 10999-11006.
(87) Cascieri, M. A.; Fong, T. M.; Graziano, M. P.; Tota, M. R.; Candelore, M. R.; Strader, C. D. Signalling through G-protein-coupled receptors. *Signal Transduction*; Chapman and Hall, 1996.
(88) Gilman, A. G. G proteins; Transducers of receptor-generated signals. *Annual Review of Biochemistry* **1987**, *56*, 615-649.
(89) Brown, D. A. G-proteins. *Textbook of Receptor Pharmacology, Second Edition*; 2 ed.; CRC Press, 2003.
(90) Howlett, A. C. Cannabinoid Compounds and Signal Transduction Mechanisms. *Cannabinoid Receptors*; Academic Press, 1995.
(91) Tolkacheva, T. V.; Karpychev, I. V.; Eldarov, M. A.; Skryabin, K. G. The role of G proteins in the specificity of cell response: Structural and functional peculiarities of the alpha subunit. *Molecular Biology* **1996**, *30*, 592-599.
(92) Clapham, D. E.; Neer, E. J. G proteins beta gamma subunits. *Annual Review of Pharmacology and Toxicology* **1997**, *37*, 167-203.
(93) Sternweis, P. C. G-proteins in signal transduction. *Signal Transduction*; Chapman and Hall, 1996.
(94) Gerard, C. M.; Mollereau, C.; Vassart, G.; Parmentier, M. Molecular-Cloning of a Human Cannabinoid Receptor Which Is Also Expressed in Testis. *Biochemical Journal* **1991**, *279*, 129-134.
(95) Chakrabarti, A.; Onaivi, E. S.; Chaudhuri, G. Cloning and Sequencing of a Cdna-Encoding the Mouse Brain-Type Cannabinoid Receptor Protein. *DNA Sequence* **1995**, *5*, 385-388.
(96) Walter, L.; Franklin, A.; Witting, A.; Wade, C.; Xie, Y. H.; Kunos, G.; Mackie, K.; Stella, N. Nonpsychotropic cannabinoid receptors regulate microglial cell migration. *Journal of Neuroscience* **2003**, *23*, 1398-1405.
(97) Di Marzo, V.; Breivogel, C. S.; Tao, Q.; Bridgen, D. T.; Razaden, R. K.; Zimmer, A. M.; Zimmer, A.; Martin, B. Levels, metabolism, and pharmacological activity of anandamide in CB_1 cannabinoid receptor knockout mice: evidence for non-CB_1, non-CB_2 receptor mediated actions of anandamide in mouse brain. *Journal Of Neurochemistry* **2000**, *75*, 2434-2444.
(98) Lichtman, A. H.; Wiley, J. L.; LaVecchia, K. L.; Neviasser, S. T.; Arthur, D. B.; Wilson, D. M.; Martin, B. R. Effects of SR141716 after acute or chronic cannabinoid administration in dogs. *European Journal of Pharmacology* **1998**, *357* 139-148.
(99) Compton, D. R.; Rice, K. C.; de Costa, B. R.; Razaden, R. K.; Melvin, L. S.; Johnson, M. R.; Martin, B. R. Cannabinoid structure activity relasionships: correlation of receptor binding and *in vivo* activities. *Journal of Pharmacology and Experimental Therapeutics* **1993**, *265*, 218-226.

(100) Wiley, J. L.; Lowe, J. A.; Balster, R. L.; Martin, B. R. Antagonism of the discriminative stimulus effects of delta-9-THCin rats and rhesus monkeys. *Journal of Pharmacology and Experimental Therapeutics* **1995**, *275*, 1-6.
(101) Huestis, M. A.; Gorelick, D. A.; Heishman, S. J.; Preston, K. L.; Nelson, R. A.; Moolchan, E. T.; Frank, R. A. Blockade of effects of smoked marijuana by the CB1 selective cannabinoid receptor antagonist SR141716. *Archives of General Psychiatry* **2001**, *58*, 322-328.
(102) Molina-Holgado, E.; Guaza, C.; Borrell, J.; Molina-Holgado, F. Effects of Cannabinoids on the Immune and Central Nervous System: Therapeutic Implications. *Biodrugs* **1999**, *12*, 317-326.
(103) Goutopoulos, A.; Markriyannis, A. From cannabis to cannabinergics: new therapeutic opportunities. *Pharmacology & Therapeutics* **2002**, *95*, 103-117.
(104) Shire, D.; Calandra, B.; RinaldiCarmona, M.; Oustric, D.; Pessegue, B.; BonninCabanne, O.; LeFur, G.; Caput, D.; Ferrara, P. Molecular cloning, expression and function of the murine CB2 peripheral cannabinoid receptor. *Biochimica Et Biophysica Acta-Gene Structure and Expression* **1996**, *1307*, 132-136.
(105) Griffin, G.; Tao, Q.; Abood, M. E. Cloning and pharmacological characterization of the rat CB_2 cannabinoid receptor. *Journal of Pharmacology and Experimental Therapeutics* **2000**, *292*, 886-894.
(106) Brown, S. M.; Wagner-Miller, J.; Mackie, K. Cloning and molecular characterization of the rat CB2 cannabinoid receptor. *Biochimica et Biophysica Acta* **2002**, *1576*, 255-264.
(107) Bouaboula, M.; Dussossoy, D.; Casellas, P. Regulation of peripheral cannabinoid receptor CB_2 phosphorylation by the inverse agonist SR 144528 - Implications for receptor biological responses. *Journal of Biological Chemistry* **1999**, *274*, 20397-20405.
(108) Lynn, A. B.; Herkenham, M. Localization of Cannabinoid Receptors and Nonsaturable High-Density Cannabinoid Binding Sites in Peripheral Tissues of the Rat: Implications for Receptor-Mediated Immune Modulation by Cannabinoids. *Journal of Pharmacology and Experimental Therapeutics* **1993**, *268*, 1612-1623.
(109) Buckley, N. E.; McCoy, K. L.; Mezey, E.; Bonner, T.; Zimmer, A.; Felder, C. C.; Glass, M.; Zimmer, A. Immunomodulation by cannabinoids is absent in mice deficient for the cannabinoid CB_2 receptor. *European Journal of Pharmacology* **2000**, *396*, 141-149.
(110) Carayon, P.; Marchand, J.; Dussossoy, D.; Derocq, J. M.; Jbilo, O.; Bord, A.; Bouaboula, M.; Galiegue, S.; Mondiere, P.; Penarier, G.; Le Fur, G.; Defrance, T.; Casellas, P. Modulation and functional involvement of CB_2 peripheral cannabinoid receptors during B-cell differentiation. *Blood* **1998**, *92*, 3605-3615.
(111) Galiegue, S.; Mary, S.; Marchand, J.; Dussossoy, D.; Carriere, D.; Carayon, P.; Bouaboula, M.; Shire, D.; Lefur, G.; Casellas, P. Expression of Central and Peripheral Cannabinoid Receptors in Human Immune Tissues and Leukocyte Subpopulations. *European Journal of Biochemistry* **1995**, *232*, 54-61.
(112) Killestein, J.; Hoogervorst, E. L. J.; Reif, M.; Blauw, B.; Smits, M.; Uitdehaag, B. M. J.; Nagelkerlen, L.; Polman, C. H. Immunomodulatory effects of orally administered cannabinoids in multiple sclerosis. *Journal of Neuroimmunology* **2003**, *137*, 140-143.

(113) Nackley, A. G.; Makriyannis, A.; Hohmann, A. G. Selective activation of cannabinoid CB_2 receptors suppresses spinal FOS protein expression and pain behaviour in a rat model of inflammation. *Neuroscience* **2003**, *119*, 747-757.
(114) New, D. C.; Wong, Y. H. BML-190 and AM251 act as inverse agonists at the human cannabinoid CB_2 receptor: signalling via cAMP and inositol phosphates. *Febs Letters* **2003**, *536*, 157-160.
(115) Griffin, G.; Atkinson, P. J.; Showalter, V. M.; Martin, B. R.; Abood, M. E. Evaluation of Cannabinoid Receptor Agonists and Antagonists Using the Guanosine-5'-*O*-(-3-[^{35}S]thio)-triphosphate Binding Assay in Rat Cerebellar Membranes. *Journal of Pharmacology and Experimental Therapeutics* **1998**, *285*, 553-560.
(116) Sim, L. J.; Selley, D. E.; Childers, S. R. In vitro autoradiography of receptor activated G proteins in rat brain by agonist-stimulated guanylyl 5'-[gamma-[^{35}S]thio]triphosphate binding. *Proceedings of the National Acadamy of Sciences* **1995**, *92*, 7242-7246.
(117) Richardson, J. D. Cannabinoids modulate pain by multiple mechanisms of action. *Journal of Pain* **2000**, *1*, 2-14.
(118) Zimmer, A.; Zimmer, A. M.; Hohmann, A. G.; Herkenham, M.; Bonner, T. Increased mortality, hypoactivity, and hypoalgesia in cannabinoid CB1 knockout mice. *Proceedings of the National Acadamy of Sciences* **1999**, *96*, 5780-5785.
(119) Calignano, A.; La Rana, G.; Giuffrida, A.; Piomelli, D. Control of Pain Initiiation by Endogenous Cannabinoids. *Nature* **1998**, *394*, 277-281.
(120) Malan, T.; Ibrahim, M.; Deng, H.; Liu, Q.; Mata, H. P.; Vanderah, T.; Porreca, F.; Makriyannis, A. CB2 cannabinoid receptor-mediated peripheral antinociception. *Pain* **2001**, *93*, 239-245.
(121) Huffman, J. W.; Liddle, J.; Yu, S.; Aung, M. M.; Abood, M. E.; Wiley, J. L.; Martin, B. R. 3-(1',1'-Dimethylbutyl)-1-deoxy-THC and Related Compounds: Synthesis of Selective Ligands for the CB_2 Receptor. *Bioorganic & Medicinal Chemistry* **1999**, *7*, 2905-2914.
(122) Aung, M. M.; Griffin, G.; Huffman, J. W.; Wu, M. J.; Keel, C.; Yang, B.; Showalter, V. M.; Abood, M. E.; Martin, B. R. Influence of the N-1 alkyl chain length of cannabimimetic indoles upon CB_1 and CB_2 receptor binding. *Drug and Alcohol Dependance* **2000**, *60*, 133-144.
(123) Mishkin, E. M.; Cabral, G. A. delta-9-THC decreases host resistance to herpes simplex virus type 2 vaginal infection in the B6C3F1 mouse. *Journal of General Virology* **1985**, *66*, 2539-2549.
(124) Kaminski, N. E.; Koh, W. S.; Yang, K. H.; Lee, M.; Kessler, F. K. Suppression of the humoral immune response by cannabinoids is partially mediated through inhibition of Adenylate Cyclase by a pertussis toxin-sensitive G-protein coupled mechanism. *Biochemical Pharmacology* **1994**, *48*, 1899-1908.
(125) Iwamura, H.; Suzuki, H.; Ueda, Y.; Kaya, T.; Inaba, T. In vitro and in vivo Pharmacological Characterization of JTE-907, a Novel Selective Ligand for Cannabinoid CB_2 Receptor. *Journal of Pharmacology and Experimental Therapeutics* **2001**, *296*, 420-425.
(126) Inaba, T.; Kaya, T.; Iwamura, H. Preparation and formulation of benzamides, cinnamides and heterocylic compounds as inflammation and allergy inhibitors; Japan Tobacco Inc, Japan: WO 97/29079, 1997.

(127) Comelli, C.; Della Valle, F.; Della Valle, M. F.; Marcolongo, G. Preparation of derivatives of alkanolamides of monocarboxylic acids and dicarboxylic acids as antagonists of the CB_2 cannabinoid receptor; Innovet Italia S.r.L, Italy: WO 0104083, 2001.
(128) Barth, F.; Millan, J.; Oustric, D.; Rinaldi, M.; Vernhet, M. Preparation and formulation of tricyclic heterocycles containing a 1-benzylpyrazole-3-carboxamide subunit for pharmaceutical use as cannabinoid receptor antagonists; Sanofi-Synthelabo, France: WO 0132629, 2001.
(129) Makriyannis, A.; Liu, Q. Preparation of pyrazole derivatives as cannabinoid receptor antagonists.; University of Connecticut, USA: WO 0129007, 2001.
(130) De Petrocellis, L.; Melck, D.; Palmisano, A.; Bisogno, T.; Laezza, C.; Bifulco, M.; Di Marzo, V. The endogenous cannabinoids inhibit human breast cancer cell proliferation. *Proceedings of the National Acadamy of Sciences* **1998**, *95*, 8375-8380.
(131) Sanchez, C.; Ceballos, M.; Gomez del Pulgar, T.; Rueda, D.; Corbacho, C.; Velasco, G.; Galve-Roperh, I.; Huffman, J. W.; Ramon y Cajal, S.; Guzman, M. Inhibition of Glioma Growth in Vivo by Selective Activation of the CB_2 Cannabinoid Receptor. *Cancer Research* **2001**, *61*, 5784-5789.
(132) McKallip, R.; Lombard, C.; Fisher, M.; Martin, B.; Ryu, S.; Grant, S.; Nagarkatti, P.; Nagarkatti, M. Targeting CB_2 cannabinoid receptors as a novel therapy to treat malignant lymphoblastic disease. *Blood* **2002**, *100*, 627-634.
(133) Jorda, M. A.; Lowenberg, B.; Delwel, R. The peripheral cannabinoid receptor CB_2, a novel oncoprotein, induces a reversible block in neutraphillic differentiation. *Blood* **2003**, *101*, 1336-1343.
(134) Khanolkar, A. D.; Palmer, S. L.; Makriyannis, A. Molecular probes for the cannabinoid receptors. *Chemistry and Physics of Lipids* **2000**, *108*, 37-52.
(135) Huffman, J. W. The search for selective ligands for the CB_2 receptor. *Current Pharmaceutical Design* **2000**, *6*, 1323-1337.
(136) Pop, E. Cannabinoids, endogenous ligands and synthetic analogues. *Current Opinion in Chemical Biology* **1999**, *3*, 418-425.
(137) Reggio, P. H. Pharmacophores for Ligand Recognition and Activation/Inactivation of the Cannabinoid Receptors. *Current Pharmaceutical Design* **2003**, *9*, 1607-1633.
(138) Huffman, J. W.; Lainton, J. A. H. Recent Developments in the Medicinal Chemistry of Cannabinoids. *Current Medicinal Chemistry* **1996**, *3*, 101-116.
(139) Reggio, P. H. Ligand-Ligand and Ligand-Receptor Approaches to Modeling the Cannabinoid CB_1 and CB_2 Receptors: Achievements and Challenges. *Current Medicinal Chemistry* **1999**, *6*, 665-683.
(140) Picone, R. P.; Fournier, D. I.; Makriyannis, A. Ligand based structural studies of the CB_1 cannabinoid receptor. *Journal of Peptide Research* **2002**, *60*, 348-356.
(141) Panico, R.; Powell, W. H.; Richer, J. C. *A Guide to IUPAC Nomenclature of Organic Compounds Recommendations 1993*; Blackwell Science, 1993; xiii.
(142) Dalzell, H. C.; Uliss, D. B.; Handrick, G. R.; Razden, R. J. Hashish. Factors Influencing Double-Bond Stability in Cannabinoids. *Journal of Organic Chemistry* **1981**, *46*, 949-953.
(143) Huffman, J. W.; Miller, J. R. A.; Liddle, J.; Yu, S.; Thomas, B. F.; Wiley, J. L.; Martin, B. R. Structure activity relationships for 1',1'-dimethylalkyl-delta^8-tetrahydrocannabinoids. *Biorganic and Medicinal Chemistry* **2003**, *11*, 1397-1410.

(144) Gareau, Y.; Dunfresne, C.; Gallant, M.; Rochette, C.; Sawyer, N.; Slipetz, D. M.; Tremblay, N.; Weech, P. K.; Metters, K. M.; Labelle, M. Structure activity relationships of Tetrahydrocannabinol analogues on human cannabinoid receptors. *Bioorganic & Medicinal Chemistry Letters* **1996**, *6*, 189-194.

(145) Charalambous, A.; Lin, S.; Marciniak, G.; Banijamali, A.; Friend, F. L.; Compton, D. R.; Martin, B. R.; Makriyannis, A. Pharmacological evaluation of halogenated delta 8-THC analogs. *Pharmacological and Biochemical Behaviour* **1991**, *40*, 509-512.

(146) Papahatjis, D. P.; Kourouli, T.; ABADJI, V.; Goutopoulos, A.; Makriyannis, A. Pharmacophoric Requirements for Cannabinoid Side Chains: Multiple Bond and C1'-substituted delta^{8}-Tetrahydrocannabinols. *Journal of Medicinal Chemistry* **1998**, *41*, 1195-1200.

(147) Papahatjis, D. P.; Nikas, S. P.; Andreou, T.; Makriyannis, A. Novel 1',1'-chain substituted delta^{8}-Tetrahydrocannabinols. *Bioorganic & Medicinal Chemistry Letters* **2002**, *12*, 3583-3586.

(148) Nadipuram, A. K.; Krishnamurthy, M.; Ferreira, A. M.; Li, W.; Moore, B. M. Synthesis and Testing of Novel Classical Cannabinoids: Exploring the Side Chain Ligand Binding Pocket of the CB_1 and CB_2 Receptors. *Bioorganic & Medicinal Chemistry* **2003**, *11*, 3121-3132.

(149) Huffman, J. W.; Yu, S. Synthesis of a Tetracyclic, Conformationally Constrained Analogue of delta^{8}-THC. *Bioorganic & Medicinal Chemistry* **1998**, *6*, 2281-2288.

(150) Khanolkar, A. D.; Lu, D.; Fan, P.; Tian, X.; Makriyannis, A. Novel Conformationally Restricted Tetracyclic Analogs of delta^{8}-Tetrahydrocannabinol. *Bioorganic & Medicinal Chemistry Letters* **1999**, *9*, 2119-2124.

(151) Krishnamurthy, M.; Ferreira, A. M.; Moore, B. M. Synthesis and testing of Novel Phenyl Substituted Side-Chain Analogues of Classical Cannabinoids. *Bioorganic & Medicinal Chemistry Letters* **2003**, *13*, 3487-3490.

(152) Song, Z. H.; Bonner, T. I. A lysine residue of the cannabinoid receptor is critical for receptor recognition by several agonists but not WIN55212-2. *Molecular Pharmacology* **1996**, *49*, 891-896.

(153) Huffman, J. W.; Yu, S.; Showalter, V. M.; Abood, M. E.; Wiley, J. L.; Compton, D. R.; Martin, B.; Bramblett, R. D.; Reggio, P. H. Synthesis and Pharmacology of a Very Potent Cannabinoid lacking a Phenolic Hydroxyl with High Affinity for the CB_2 Receptor. *Journal of Medicinal Chemistry* **1996**, *39*, 3875-3877.

(154) Tao, Q.; McAllister, S. D.; Andreassi, J.; Nowell, K. W.; Cabral, G. A.; Hurst, D. P.; Bachtel, K.; Ekman, M. C.; Reggio, P. H.; Abood, M. E. Role of a conserved lysine residue in peripheral cannabinoid receptor (CB_2): Evidence for subtype specififcity. *Molecular Pharmacology* **1999**, *55*, 605-613.

(155) Compton, D. R.; Prescott, W. R.; Martin, B. R.; Siegel, C.; Gordon, P. M.; Razaden, R. K. Synthesis and Pharmacological Evaluation of Ether and Related Analogues of delta^{8}-, delta^{9}- and delta$^{9(11)}$-Tetrahydrocannabinol. *Journal of Medicinal Chemistry* **1991**, *34*, 3310-3316.

(156) Martin, B. R.; Jefferson, R.; Winckler, R.; Wiley, J. L.; Huffman, J. W.; Crocker, P. J.; Saha, B.; Razaden, R. K. Manipulation of the Tetrahydrocannabinol Side Chain Delineates Agonists, Partial Agonists, and Antagonists. *Molecular Pharmacology* **1999**, *290*, 1065-1079.

(157) Huffman, J. W.; Bushell, S. M.; Miller, J. R. A.; Wiley, J. L.; Martin, B. 1-Methoxy-, 1-Deoxy-11-hydroxy- and 11-Hydroxy-1-methoxy-delta^8-tetrahydrocannabinols: New selective Ligands for the CB_2 receptor. *Bioorganic & Medicinal Chemistry* **2002**, *10*, 4119-4129.

(158) Melvin, L. S.; Milne, G. M.; Johnson, M. R.; Subramaniam, B.; Wilken, G. H.; Howlett, A. C. Structure-Activity Relationships for Cannabinoid Receptor-Binding and Analgesic Activity: Studies of Bicyclic Cannabinoid Analogs. *Molecular Pharmacology* **1993**, *44*, 1008-1015.

(159) Devane, W. A.; Dysarz, F. A.; Johnson, M. R.; Melvin, L. S.; Howlett, A. C. Determination and Characterization of a Cannabinoid Receptor in Rat-Brain. *Molecular Pharmacology* **1988**, *34*, 605-613.

(160) Xie, X. Q.; Melvin, L. S.; Makriyannis, A. The Conformational Properties of the Highly Selective Cannabinoid Receptor Ligand CP-55,940. *Journal of Biological Chemistry* **1996**, *271*, 10640-10647.

(161) Xie, X. Q.; Pavlopoulos, S.; DiMeglio, C. M.; Makriyannis, A. Conformational Studies on a Diastereoisomeric Pair of Tricyclic Nonclassical Cannabinoids by NMR Spectroscopy and Computer Molecular Modeling. *Journal of Medicinal Chemistry* **1998**, *41*, 167-174.

(162) Hanus, L.; Breuer, A.; Tchilibon, S.; Shiloah, S.; Goldenberg, D.; Horowitz, M.; Pertwee, R. G.; Ross, R. A.; Mechoulam, R.; E., F. HU-308: A specific agonist for CB_2, a peripheral cannabinoid receptor. *Proceedings of the National Acadamy of Sciences* **1999**, *96*, 14228-14233.

(163) Mechoulam, R.; Lander, N.; Breuer, A.; Zahalka, J. A Synthesis of the Individual, Pharmacologically Distinct, Enantiomers of a Tetrahydrocannabinol Derivative. *Tetrahedron Asymmetry* **1990**, *1*, 315-319.

(164) Huffman, J. W.; Lu, J.; Hynd, G.; Wiley, J. L.; Martin, B. R. A Pyridone Analogue of Traditional Cannabinoids. A New Class of Selective Ligands for the CB_2 Receptor. *Bioorganic & Medicinal Chemistry* **2001**, *9*, 2863-2870.

(165) Wiley, J. L.; Beletskaya, I. D.; NG, E. D.; Dai, Z.; Crocker, P. J.; Mahadevan, A.; Razaden, R. K.; Martin, B. R. Resorcinol Derivatives: A Novel Template for the Development of Cannabinoid CB_1/CB_2 and CB_2-Selective Agonists. *Journal of Pharmacology and Experimental Therapeutics* **2002**, *301*, 679-689.

(166) Mechoulam, R.; Ben-Shabat, S.; Hanus, L.; Ligumsky, M.; Kaminski, N. E.; Schatz, A. R.; Gopher, A.; Almog, S.; Martin, B. R.; Compton, D. R. Identification of an Endogenous 2-monoglyceride, present in canine gut, that binds to cannabinoid receptors. *Biochemical Pharmacology* **1995**, *50*, 83-90.

(167) Hanus, L.; Abu-Lafi, S.; Fride, E.; Breuer, A.; Vogel, Z.; Shalev, D. E.; Kustanovich, I.; Mechoulam, R. 2-Arachidonyl-glyceryl ether, an endogenous agonist of the cannabinoid CB_1 receptor. *Proceedings of the National Acadamy of Sciences* **2001**, *98*, 3662-3665.

(168) Porter, A. C.; Sauer, J. M.; Knierman, M. D.; Becker, G. W.; Berna, M. J.; Bao, J. Q.; Nomikos, G. G.; Carter, P.; Bymaster, F. P.; Leese, A. B.; Felder, C. C. Characterization of a novel endocannabinoid, virodhamine, with antagonist activity at the CB_1 receptor. *Journal of Pharmacology and Experimental Therapeutics* **2002**, *301*, 1020-1024.

(169) Huang, S. M.; Bisogno, T.; Trevisani, M.; Al-Hayani, A.; De Petrocellis, L.; Fezza, F.; Tognetto, M.; Petros, T. J.; Krey, J. F.; Chu, C. J.; Miller, J. D.; Davies, S. N.; Geppetti, P.; Walker, J. M.; Di Marzo, V. An endogenous capsaicin-like substance with high potency at recombinant and native vanilloid

VR1 receptors. *Proceedings of the National Academy of Sciences of the United States of America* **2002**, *99*, 8400-8405.
(170) Piomelli, D. The Molecular Logic of Endocannabinoid Signalling. *Nature Reviews Neuroscience* **2003**, *4*, 873-884.
(171) van der Stelt, M.; van Kuik, J. A.; Bari, M.; van Zadelhoff, G.; Leeflang, B. R.; Veldink, G. A.; Finazzi-Agro, A.; Vliegenthart, J. F. G.; Maccarrone, M. Oxygenated metabolites of anandamide and 2- arachidonoylglycerol: Conformational analysis and interaction with cannabinoid receptors, membrane transporter, and fatty acid amide hydrolase. *Journal of Medicinal Chemistry* **2002**, *45*, 3709-3720.
(172) Goutopoulos, A.; Fan, P. S.; Khanolkar, A. D.; Xie, X. Q.; Lin, S. Y.; Makriyannis, A. Stereochemical selectivity of methanandamides for the CB_1 and CB_2 cannabinoid receptors and their metabolic stability. *Bioorganic & Medicinal Chemistry* **2001**, *9*, 1673-1684.
(173) Suhara, Y.; Takayama, H.; Nakane, S.; Miyashita, T.; Waku, K.; Sugiura, T. Synthesis and biological activities of 2-arachidonoylglycerol, an endogenous cannabinoid receptor ligand, and its metabolically stable ether-linked analogues. *Chemical & Pharmaceutical Bulletin* **2000**, *48*, 903-907.
(174) Ng, E. W.; Aung, M. M.; Abood, M. E.; Martin, B. R.; Razdan, R. K. Unique analogues of anandamide: Arachidonyl ethers and carbamates and norarachidonyl carbamates and ureas. *Journal of Medicinal Chemistry* **1999**, *42*, 1975-1981.
(175) Lin, S. Y.; Khanolkar, A. D.; Fan, P. S.; Goutopoulos, A.; Qin, C.; Papahadjis, D.; Makriyannis, A. Novel analogues of arachidonylethanolamide (anandamide): Affinities for the CB_1 and CB_2 cannabinoid receptors and metabolic stability. *Journal of Medicinal Chemistry* **1998**, *41*, 5353-5361.
(176) Lan, R. X.; Liu, Q.; Fan, P. S.; Lin, S. Y.; Fernando, S. R.; McCallion, D.; Pertwee, R.; Makriyannis, A. Structure-activity relationships of pyrazole derivatives as cannabinoid receptor antagonists. *Journal of Medicinal Chemistry* **1999**, *42*, 769-776.
(177) Wiley, J. L.; Jefferson, R.; Grier, M. C.; Mahadevan, A.; Razaden, R. K.; Martin, B. R. Novel Pyrazole Cannabinoids: Insights into CB_1 Receptor Recognition and Activation. *Journal of Pharmacology and Experimental Therapeutics* **2001**, *296*, 1013-1022.
(178) Krishnamurthy, M.; Li, W.; Moore, B. M. Synthesis, biological evaluation, and structural studies on N1 and C5 substituted cycloalkyl analogues of the pyrazole class of CB_1 and CB_2 ligands. *Bioorganic & Medicinal Chemistry* **2004**, *12*, 393-404.
(179) Shim, J. Y.; Welsh, W. J.; Cartier, E.; Edwards, J. L.; Howlett, A. C. Molecular Interaction of the Antagonist SR141716 with the CB_1 Cannabinoid Receptor. *Journal of Medicinal Chemistry* **2002**, *45*, 1447-1459.
(180) Mussinu, J. M.; Ruiu, S.; Mule, A. C.; Pau, A.; Carai, M. A. M.; Loriga, G.; Murineddu, G.; Pinna, G. A. Tricyclic pyrazoles. part 1: Synthesis and biological evaluation of novel 1,4-dihydroindeno 1,2-c pyrazol-based ligands for CB_1 and CB_2 cannabinoid receptors. *Bioorganic & Medicinal Chemistry* **2003**, *11*, 251-263.
(181) Patrick, G. L. *An Introduction to Medicinal Chemsitry*; 2nd ed.; Oxford University Press, 2001.
(182) Gouldson, P.; Calandra, B.; Legoux, P.; Kerneis, A.; Rinaldi-Carmona, M.; Barth, F.; Fur, G.; Ferrara, P.; Shire, D. Mutational analysis and molecular

modelling of the antagonist SR144528 binding site on the human cannabinoid CB_2 receptor. *European Journal of Pharmacology* **2000**, *401*, 17-25.
(183) Eissenstat, M. A.; Bell, M. R.; Dambra, T. E.; Alexander, E. J.; Daum, S. J.; Ackerman, J. H.; Gruett, M. D.; Kumar, V.; Estep, K. G.; Olefirowicz, E. M.; Wetzel, J. R.; Alexander, M. D.; Weaver, J. D.; Haycock, D. A.; Luttinger, D. A.; Casiano, F. M.; Chippari, S. M.; Kuster, J. E.; Stevenson, J. I.; Ward, S. J. Aminoalkylindoles - Structure-Activity-Relationships of Novel Cannabinoid Mimetics. *Journal of Medicinal Chemistry* **1995**, *38*, 3094-3105.
(184) Huffman, J. W.; Dai, D.; Martin, B. R.; Compton, D. R. Design, Synthesis and Pharmacology of Cannabimimetic Indoles. *Bioorganic & Medicinal Chemistry Letters* **1994**, *4*, 563-566.
(185) Lainton, J. A. H.; Huffman, J. W.; Martin, B. R.; Compton, D. R. 1-Alkyl-3-(1-Naphthoyl)Pyrroles - a New Class of Cannabinoid. *Tetrahedron Letters* **1995**, *36*, 1401-1404.
(186) Kumar, V.; Alexander, M. D.; Bell, M. R.; Eissenstat, M. A.; Casiano, F. M.; Chippari, S. M.; Haycock, D. A.; Luttinger, D. A.; Kuster, J. E.; Miller, M. S.; Stevenson, J. I.; Ward, S. J. Morpholinoalkylindenes as Antinociceptive Agents - Novel Cannabinoid Receptor Agonists. *Bioorganic & Medicinal Chemistry Letters* **1995**, *5*, 381-386.
(187) Huffman, J. W. Cannabimimetic indoles, pyrroles and indenes. *Current Medicinal Chemistry* **1999**, *6*, 705-720.
(188) Wiley, J. L.; Compton, D. R.; Dai, D.; Lainton, J. A. H.; Phillips, M.; Huffman, J. W.; Martin, B. R. Structure-activity relationships of indole- and pyrrole-derived cannabinoids. *Journal of Pharmacology and Experimental Therapeutics* **1998**, *285*, 995-1004.
(189) Reggio, P. H.; Basu-Dutt, S.; Barnett-Norris, J.; Castro, M. T.; Hurst, D. P.; Seltzman, H. H.; Roche, M. J.; Gilliam, A. F.; Thomas, B. F.; Stevenson, L. A.; Pertwee, R.; Abood, M. E. The Bioactive Conformation of Aminoalkylindoles at the Cannabinoid CB_1 and CB_2 receptors: Insights Gained from (*E*) and (*Z*)-Napthylidene Indenes. *Journal of Medicinal Chemistry* **1998**, *41*, 5177-5187.
(190) Bramblett, R. D.; Panu, A. M.; Ballesteros, J. A.; Reggio, P. H. Construction of a 3D model of the cannabinoid CB1 receptor: Determination of the helix ends and helix orientation. *Life Sciences* **1995**, *56*, 1971-1982.
(191) Xie, X. Q.; Han, X. H.; Chen, J. Z.; Eissenstat, M. A.; Makriyannis, A. High-Resoltion NMR and Computer Modeling Studies of the Cannabimimetic Aminoalkylindole Prototype Win-55212-2. *Journal of Medicinal Chemistry* **1999**, *42*, 4021-4027.
(192) Huffman, J. W.; Mabon, R.; Wu, M. J.; Lu, J.; Hart, R.; Hurst, D. P.; Reggio, P. H.; Wiley, J. L.; Martin, B. R. 3-Napthoyl-1-naphthylmethanes: New Cannabimimetic Indoles Provide Evidence for Aromatic Stacking Interactions with the CB_1 Cannabinoid Receptor. *Bioorganic & Medicinal Chemistry* **2003**, *11*, 539-549.
(193) Chin, C.; Murphy, J. W.; Huffman, J. W.; Kendall, D. A. The Third Transmembrane Helix of the Cannabinoid Receptor Plays a Role in the Selectivity of the Aminoalkylindoles for CB2 Peripheral Cannabinoid Receptor. *Journal of Pharmacology and Experimental Therapeutics* **1999**, *291*, 837-844.
(194) Song, Z. H.; Slowey, C. A.; Hurst, D. P.; Reggio, P. H. The Difference between the $CB_1$and CB_2 Cannabinoid Receptors at Position 5.46 is Crucial

for the Selectivity of Win 55212-2 for CB_2. *Molecular Pharmacology* **1999**, *56*, 834-840.
(195) Gallant, M.; Dufrense, C.; Gareau, Y.; Guay, D.; Leblanc, Y.; Prasit, P.; Rochette, C.; Sawyer, N.; Slipetz, D. M.; Tremblay, N.; Metters, K. M.; Labelle, M. New Class of Potent Ligands for the Human Peripheral Cannabinoid Receptor. *Bioorganic & Medicinal Chemistry Letters* **1996**, *6*, 2263-2268.
(196) Showalter, V. M.; Compton, D. R.; Martin, B.; Abood, M. E. Evaluation of Binding in a Transfected Cell Line Expressing a Peripheral Cannabinoid Receptor (CB_2): Identification of Cannabinoid Receptor Subtype Selective Ligands. *Journal of Pharmacology and Experimental Therapeutics* **1996**, *278*, 989-999.
(197) Hynes, J.; Leftheris, K.; Wu, H.; Pandit, C.; Chen, P.; Norris, D. J.; Chen, B. C.; Zhao, R. L.; Kiener, P. A.; Chen, X. R.; Turk, L. A.; Patil-Koota, V.; Gillooly, K. M.; Shuster, D. J.; McIntyre, K. W. C-3 amido-indole cannabinoid receptor modulators. *Bioorganic & Medicinal Chemistry Letters* **2002**, *12*, 2399-2402.
(198) Makriyannis, A.; Deng, H. Preparation of CB_2 Cannabinoid Receptor Selective Cannabimimetic Aminoalkylindoles, particularly (piperidinylmethyl) and (morpholinylmethyl) indoles and their use.; University of Connecticut, USA: WO 2002/060447, 2002.
(199) Poulsen, S. A.; Milligan, G. Adenosine Receptors: New Opportunities for Future Drugs. *Bioorganic & Medicinal Chemistry* **1998**, *6*, 619-641.
(200) Macchia, M.; Salvetti, F.; Barontini, S.; Calvani, F.; Gesi, M.; Hamdan, M.; Lucacchini, A.; Pellagrini, A.; Soldani, P.; MArtini, C. Fluorescent Probes for Adenosine Receptors: Synthesis and Biology of N^6-Dansylaminoalkyl-Substituted NECA Derivatives. *Bioorganic & Medicinal Chemistry Letters* **1998**, *8*, 3223-3228.
(201) Bridges, A. J.; Moos, W. H.; Szotek, D. L.; Triverdi, B. K.; Bristol, J. A. Adensoine Ligands. *Journal of Medicinal Chemistry* **1987**, *30*, 1709-1711.
(202) Macchia, M.; Salvetti, F.; Bertini, S.; Di Bussolo, V.; Gattuso, L.; Gesi, M.; Hamdan, M.; Klotz, K. N.; Laragione, T.; Lucacchini, A.; Minutolo, F.; Nencetti, S.; Papi, C.; Tuscano, D.; Martini, C. 7-nitrobenzofurazan (NBD) derivatives of 5 '-*N*- ethylcarboxamidoadenosine (NECA) as new fluorescent probes for human A(3) adenosine receptors. *Bioorganic & Medicinal Chemistry Letters* **2001**, *11*, 3023-3026.
(203) Konig, K.; Liu, Y. G.; Sonek, G. J.; Berns, M. W.; Tromberg, B. J. Autofluorescence Spectroscopy of Optically Trapped Cells. *Photochemistry and Photobiology* **1995**, *62*, 830-835.
(204) Lorenzen, A.; Guerra, L.; Campi, F.; Lang, H.; Schwabe, U.; Borea, P. A. Thermodynamically distinct high and low affinity states of the A(1) adenosine receptor induced by G protein coupling and guanine nucleotide ligation states of G proteins. *British Journal of Pharmacology* **2000**, *130*, 595-604.
(205) Buschmann, V.; Weston, K. D.; Sauer, M. Spectroscopic Study and Evaluation of Red-Absorbing Fluorescent Dyes. *Bioconjugate Chemistry* **2003**, *40*, 10839-10848.
(206) http://www.probes.com/servlets/structure?item=10000.
(207) Briddon, S. J.; Middleton, R. J.; Kellam, B.; Hill, S. J. Characterisation of a novel fluorescent agonist for the human A(1)-adenosine receptor. *British Journal of Pharmacology* **2003**, *138*, 126P.

(208) Cordeaux, Y. Radiligand binding data for ABEA-BY 630/650: Personal Communication, Univeristy of Nottingham, 2004.
(209) Anderson, G. W.; Zimmerman, J. E.; Callahan, F. M. N-Hydroxysuccinimide Esters in Peptide Synthesis. *Journal of the American Chemical Society* **1963**, *85*, 3039.
(210) Cline, G. W.; Hanna, S. B. Kinetics and Mechanisms of the Aminolysis of N-Hydroxysuccinimide Esters in Aqeous Buffers. *Journal of Organic Chemistry* **1988**, *53*, 3583-3586.
(211) Podona, T.; Guardiola-Lemaitre, B.; Caignard, D. H.; Adam, G.; Pfeiffer, B.; Renard, P.; Guillaumet, G. 3,4-Dihydro-3-amino-2*H*-1-benzopyran Derivatives as 5-HT_{1A} Receptor Ligands and Potential Anxiolytic Agents. 1 Synthesis and Structure Activity Relationship Studies. *Journal of Medicinal Chemistry* **1994**, *37*, 1779-1793.
(212) Besson, T.; Podona, T.; Baudin, M. L.; Coudert, G.; Guillaumet, G. Fluorescent Probes for 5-HT_{1A} Receptors: Synthesis and Characterisation of 5-Methoxy-3-[*n*-propyl-(4-*n*-aminobutyl)]amino-3,4-dihydro-2*H*-1-benzopyran Derivatives. *Bioorganic & Medicinal Chemistry Letters* **1993**, *3*, 1935-1940.
(213) Berque-Bestel, I.; Soulier, J. L.; Giner, M.; Rivail, L.; Langlois, M.; Sicsic, S. Synthesis and characterization of the first fluorescent antagonists for human 5-HT4 receptors. *Journal of Medicinal Chemistry* **2003**, *46*, 2606-2620.
(214) Li, L. T.; Kracht, J.; Peng, S. Q.; Bernhardt, G.; Buschauer, A. Synthesis and pharmacological activity of fluorescent histamine H-1 receptor antagonists related to mepyramine. *Bioorganic & Medicinal Chemistry Letters* **2003**, *13*, 1245-1248.
(215) Li, L. T.; Kracht, J.; Peng, S. Q.; Bernhardt, G.; Elz, S.; Buschauer, A. Synthesis and pharmacological activity of fluorescent histamine H-2 receptor antagonists related to potentidine. *Bioorganic & Medicinal Chemistry Letters* **2003**, *13*, 1717-1720.
(216) Ilien, B.; Franchet, C.; Bernard, P.; Morisset, S.; Weill, C. O.; Bourguignon, J. J.; Hibert, M.; Galzi, J. L. Fluorescence resonance energy transfer to probe human M1 muscarinic receptor structure and drug binding properties. *Journal of Neurochemistry* **2003**, *85*, 768-778.
(217) Emmerson, P. J.; Archer, S.; ElHamouly, W.; Mansour, A.; Akil, H.; Medzihradsky, F. Synthesis and characterization of 4,4-difluoro-4-bora-3a,4a-diaza-s-indacene (BODIPY)-labeled fluorescent ligands for the mu opioid receptor. *Biochemical Pharmacology* **1997**, *54*, 1315-1322.
(218) Lakowicz, B. *Principles of Fluorescence Spectroscopy*; 2nd ed.; Plenum Publishers: New York, 1999.
(219) http://www.probes.com/handbook/sections/0104.html.
(220) Sanders, T. C.; Seto, C. T. 4-Heterocyclehexanone based inhibitors of the serine protease plasmin. *Journal of Medicinal Chemistry* **1999**, *42*, 2969-2976.
(221) Mitsunobu, O. The Use of Diethyl Azocarboxylate and Triphenylphosphine in Synthesis and Transformation of Natural Products. *Synthesis* **1981**, 1-28.
(222) Yamamoto, T.; Hori, M.; Watanabe, I.; Tsutsui, H.; Ikeda, S.; Ohtaka, H. An Acid-Catalyzed *O*,*N*-Acyl Migration and Application to the Synthesis of *N*-(4-Isopropyl-2,2-dimethyl-3-oxo-3,4-dihydro-2*H*-benzo[1,4]oxazine-6-carbonyl)guanidine Methanesulfonate (KB-R9032), a Novel Na/H Exchange Inhibitor. *Chemical & Pharmaceutical Bulletin* **1999**, *47*, 22-27.
(223) Murugesan, N.; Gu, Z.; Stein, P. D.; Bisaha, S.; Spergel, S.; Girotra, R.; Lee, V. G.; Lloyd, J.; Misra, R. N.; Schmidt, J.; Mathur, A.; Stratton, L.; Kelly, Y.

F.; Bird, E.; Waldron, T.; Liu, E. C.; Zhang, R.; Lee, H.; Serafino, R.; Abboa-Offei, B.; Mathers, P.; Giancarli, M.; Seymour, A. A.; Webb, M. L.; Moreland, S.; Barrish, J. C.; Hunt, J. T. Biphenylsulfonamide Endothelin Antagonists: Structure-Activity Relationships of a Series of Mono- and Disubstituted Analogues and Pharmacology of the Orally Active Endothelin Antagonist 2'-Amino-N- (3,4-dimethyl-5-isoxazolyl)-4'-(2-methylpropyl)[1,1'-biphenyl]-2-sulfonamide (BMS-187308). *Journal of Medicinal Chemistry* **1998**, *41*, 5198-5218.

(224) Leggett, J. D.; Aspley, S.; Beckett, S. R. G.; D'Antona, A. M.; Kendall, D. A.; Kendall, D. A. Oleamide is a Selective Endogenous Agonist of Rat and Human CB_1 Cannabinoid Receptors. *British Journal of Pharmacology* **2004**, *141*, 253-262.

(225) Batey, R. A.; Santhakumar, V.; Yoshina-Ishii, C.; Taylor, S. D. An Efficient New Protocol for the Formation of Unsymmetrical Tri and Tetrasubstituted Ureas. *Tetrahedron Letters* **1998**, *39*, 6267-6270.

(226) Miller, B. T.; Collins, T. J.; Rogers, M. E.; Kurosky, A. Peptide Biotinylation with Amine-Reactive Esters:

Differential Side Chain Reactivity. *Peptides* **1997**, *18*, 1585-1595.

(227) Oliveira, L.; Hulsen, T.; Lutje Hulsik, D.; Paiva, A. C. M.; Vriend, G. Heavier-than-air flying machines are impossible. *Febs Letters* **2004**, *564*, 269-273.

(228) Teller, D. C.; Okada, T.; Behnke, C. A.; Palczewski, K.; Stenkamp, R. E. Advances in Determination of a High-Resolution Three-Dimensional structure of Rhodopsin, a model of G-protein coupled receptors (GPCRs). *Biochemistry* **2001**, *40*, 7761-7772.

(229) Bissantz, C.; Bernard, P.; Hibert, M.; Rognan, D. Protein-Based Virtual Screening of Chemical Databases. II. Are Homology Models of G-Protein Coupled Receptors Suitable Targets? *Proteins* **2003**, *50*, 5-25.

(230) Leach, A. Chapter 10 Protein Structure Prediction, Sequence Analysis and Protein Folding. *Molecular Modelling Principles and Applications*; 2nd ed.; Pearson Eductaion, 2001.

(231) http://www.gpcr.org/articles/2002_4/index.html.

(232) Thompson, J. D.; Higgins, D. G.; Gibson, T. J. CLUSTAL W: improving the sensitivity of progressivemultiple sequence alignment through sequence weighting,position-specific gap penalties and weight matrix choice. *Nucleic Acid Research* **1994**, *22*, 4673-4680.

(233) Leach, A. Chapter 5 Energy Minimisation and Related Methods for Exploring the Energy Surface. *Molecular Modelling Principles and Applications*; 2nd ed.; Pearson Eduction, 2001.

(234) Brooks, B. R.; Bruccoleri, R. E.; Olafson, B. D.; States, D. J.; Swaminathan, S.; Karplus, M. CHARMM: A Progam for Macromolecular Energy, Minimisation, and Dynamics Calculations. *Journal of Computaional Chemistry* **1983**, *4*, 187-217.

(235) Leach, A. Chapter 7 Molecular Dynamics Simulation Methods. *Molecular Modelling Priciples and Applications*; 2nd ed.; Pearson Education, 2001.

(236) Shire, D.; Calandra, B.; Bouaboula, M.; Barth, F.; Rinaldi-Carmona, M.; Casellas, P.; Ferrara, P. Cannabinoid receptor interactions with the antagonists SR 141716A and SR 144528. *Life Sciences* **1999**, *65*, 627-635.

(237) McAllister, S. D.; Tao, Q.; Barnett-Norris, J.; Buehner, K.; Hurst, D. P.; Guarnieri, F.; Reggio, P. H.; Nowell, K. W.; Cabral, G.; Abood, M. E. A

critical role for a tyrosine residue in the cannabinoid receptors for ligand recongnition. *Biochemical Pharmacology* **2002**, *63*, 2121-2136.
(238) Rhee, M.; Nevo, I.; Bayewitch, M. L.; Zagoory, O.; Vogel, Z. Functional Role of Trytophan Residues in the Fourth Transmembrane Domain of the CB_2 Cannabinoid Receptor. *Journal Of Neurochemistry* **2000**, *75*, 2485-2491.
(239) Rhee, M. H.; Nevo, I.; Levy, R.; Vogel, Z. Role of the highly conserved Asp-Arg-Tyr motif in signal transduction of the CB2 cannabinoid receptor. *FEBS Letters* **2000**, *466*, 300-304.
(240) Feng, W.; Song, Z. H. Effects of D3.49A, R3.50A, and A6.34E Mutations on Ligand Binding and Activation of the Cannabinoid (CB2) Receptor. *Biochemical Pharmacology* **2003**, *65*, 1077-1085.
(241) Gouldson, P.; Snell, C. R.; Reynolds, C. A. A New Approach to Docking in the Beta-2-Adrenergic Receptor That Exploits the Domain Structure of G-Protein-Coupled Receptors. *Journal of Medicinal Chemistry* **1997**, *40*, 3871-3886.
(242) Xie, X. Q.; Chen, J. Z.; Billings, E. M. 3D Structural Model of the G-Protein-Coupled Cannabinoid CB_2 Receptor. *Proteins* **2003**, *53*, 307-319.
(243) Laskowski, R. A.; MacArthur, M. W.; Moss, D. S.; Thornton, J. M. PROCHECK: a program to check the stereochemical quality of protein structures. *Journal of Applied Crystallography* **1993**, *26*, 283-291.
(244) Ramachandran, G. N.; Ramakrishnan, C.; Sasiekharan, V. Stereochemistry of Polypeptide Chain Configuarations. *Journal of Molecular Biology* **1963**, *7*, 95-99.
(245) Wallace, A. C.; Laskowski, R. A.; Thornton, J. M. LIGPLOT: A program to generate schematic diagrams of protein-ligand interactions. *Protein Engineering* **1995**, *8*, 127-134.
(246) Pine, S. H. Bonding in Organic Molecules. *Organic Chemistry*; McGraw-Hill Interternational, 1987.
(247) Greene, T. W.; Wuts, P. G. *Protective Groups in Organic Synthesis*; 3rd ed.; John Wiley and Sons: New York, 1999.
(248) Clark, M. T.; Miller, D. D. 2-Fluoro and 5-Fluoro-3, 4-Dimethylphenethylamine Derived from Claisen Rearrangement Products. *Tetrahedron Letters* **1985**, *26*, 4299-4300.
(249) Williams, D. H.; Fleming, I. *Spectroscopic Methods in Organic Chemistry*; Fifth ed.; McGraw-Hill Publishing Company: London, 1995.
(250) Cainelli, G.; Contento, M.; Manescalchi, F.; Plessi, L. Catlytic Hydroxylation of Olefins by Polymer-Bound Osmium Tertroxide. *Synthesis* **1989**, *1*, 45-47.
(251) Zhou, P.; Berova, N.; Wiesler, W. T.; Nakanishi, K. Assignment of Relative and Absolute-Configuration of Acyclic Polyols and Aminopolyols by Circular-Dichroism - Trends Follow Fischer Sugar Family Tree. *Tetrahedron* **1993**, *49*, 9343-9352.
(252) DeBlasi, A.; O'Reilly, K.; Motulsky, H. J. Calculating Receptor Numbers from Binding Experiments Using the Same Compound as Radioligand and Competitor. *Trends in Pharmaceutical Sciences* **1989**, *10*, 227-229.
(253) Archer, E.; Maigret, B.; Escrieut, C.; Pradayrol, L.; Fourmy, D. Rhodopsin crystal: new template yielding realistic models of G- protein-coupled receptors? *Trends in Pharmacological Sciences* **2003**, *24*, 36-40.
(254) Wang, R.; Gao, Y.; Lai, L. LigBuilder: A Multi-Purpose Program for Structure-Based Drug Design. *Journal of Molecular Modeling* **2000**, *6*, 498–516.

(255) Kuntz, I. D.; Blaney, J. M.; Oatley, S. J.; Langridge, R.; Ferrin, T. E. A geometric approach to macromolecule-ligand interactions. *Journal of Molecular Biology* **1982**, *161*, 269-288.
(256) Goodford, P. J. A computational procedure for determining energetically favorable binding sites on biologically important macromolecules. *Journal of Medicinal Chemistry* **1985**, *28*, 849-857.
(257) Böhm, H. J. The Computer Program Ludi: A New Method for the De Novo Design of Enzyme Inhibitors. *Journal of Computer-Aided Molecular Design* **1992**, *6*, 61-78.
(258) Doughty, S. W. via a thesis Fabrizio Giordanetto, "Inhibition of Janus Kinase 2 by application of computational chemistry techniques" Queen Mary, London University, 2003, 2004.
(259) Lipinski, C. A.; Lombardo, F.; Dominy, B. W.; Feeney, P. J. Experimental and Computational Approaches to Estimate Solubility and Permeability in Drug Discovery and Development Settings. *Advanced Drug Delivery Review* **1997**, *23*, 3-25.
(260) Barnett-Norris, J.; Hurst, D. P.; Buehner, K.; Ballesteros, J. A.; Guarnieri, F.; Reggio, P. H. Agonist alkyl tail interaction with cannabinoid CB1 receptor V6.43/I6.46 groove induces a helix 6 active conformation. *International Journal of Quantum Chemistry* **2002**, *88*, 76-86.
(261) Duffy, K. J.; Darcy, M. G.; Delorme, E.; Dillon, S. B.; Eppley, D. F.; Erickson-Miller, C.; Giampa, L.; Hopson, C. B.; Huang, Y.; Keenan, R. M.; Lamb, P.; Leong, L.; Liu, N.; Miller, S. G.; Price, A. T.; Rosen, J.; Shah, R.; Shaw, T. N.; Smith, H.; Stark, K. C.; Tian, S.-S.; Tyree, C.; Wiggall, K. J.; Zhang, L.; Luengo, J. I. Hydrazinonaphthalene and Azonaphthalene Thrombopoietin Mimics Are Nonpeptidyl Promoters of Megakaryocytopoiesis. *Journal of Medicinal Chemistry* **2001**, *44*, 3730-3745.
(262) Newman, M.; Vander Zwan, M. Steric and Polar Effects in the Decarboxylation of Mercuric Salts of Unsymmetrical Aromatic 1,2-Dicarboxylic Acids (the Pesci Reaction). An Improved Procedure. *Journal of Organic Chemistry* **1973**, *38*, 319-321.
(263) Imai, K.; Uzu, S.; Kanda, S. Availability of Fluorogenic Reagents Having a Benzofurazan Structure in the Biosciences. *Analytica Chimica Acta* **1994**, *290*, 3-20.
(264) Onoda, M.; Uchiyama, S.; Santa, T.; Imai, K. The Effects of Spacer Length on the Fluorescence Quantum Yields of the Benzofurazan Compounds Bearing a Donor-Acceptor System. *Luminescence* **2002**, *17*, 11-14.
(265) Uchiyama, S.; Santa, T.; Imai, K. Study on the fluorescent 'on-off' properties of benzofurazan compounds bearing an aromatic substituent group and design of fluorescent 'on-off' derivatization reagents. *Analyst* **2000**, *125*, 1839-1845.
(266) Twenty Questions The State of GPCR Research in 2004. *Nature Reviews Drug Discovery* **2004**, *3*, 577-626.
(267) Capon, B.; Page, M. I.; Sankey, G. H. The kinetics and mechanism of the hydrolysis of 2, 3-(phenylmethylenedioxy) benzoic acid. *Journal of the Chemical Society Perkins Transactions 2* **1972**, 529-532.
(268) Borisck, K.; Diele, S.; Göring, P.; Kresse, H.; Tschiershe, C. Tailoring thermotropic cubic mesophases: amphiphilic polyhydroxy derivatives. *Journal of Materials Chemistry* **1998**, *8*, 529-544.

(269) Barton, D.; Hervé, Y.; Portier, P.; Thierry, J. Manipulation of the carboxy groups of alpha-amino acids and peptides using radical chemistry based on *N*-hydroxy-2-thiopyridone. *Tetrahedron* **1988**, *44*, 5479-5486.
(270) Clarke, B.; Graysham, R. Synthesis of 4-arylmethyl 1,2,3,-benzotriazines. *Journal of Chemical Research mini* **1981**, *10*, 3786-3795.
(271) Abadijil, V.; Lucas-Lenard, J. M.; Chin, C.; Kendall, D. A. Involvement of the carboxyl terminus of the third intracellular loop of the CB_1 receptor in constitutive activation of Gs. *Journal of Neurochemistry* **1999**, *72*, 2032-2038.